ABSTRACT

POLLOCK, JEFFREY CHARLES. The Neoproterozoic-Early Paleozoic Tectonic Evolution of the Peri-Gondwanan Margin of the Appalachian Orogen: An Integrated Geochronological, Geochemical and Isotopic Study from North Carolina and Newfoundland. (Under the direction of James Patrick Hibbard).

LAM-ICP-MS U-Pb dates are reported from more than 1000 detrital zircons from the Neoproterozoic-early Paleozoic clastic sequences of Carolinia and Avalonia. The majority of analyzed zircon grains from Carolinia are late Neoproterozoic with minor amounts of Mesoproterozoic/Paleozoic and accessory Archean grains. The overall distribution of age populations of detrital zircons is consistent with derivation from the Amazon craton and its peripheral orogenic belts on the margin of west Gondwana. The dominance of Ediacaran-early Paleozoic zircons in the Albemarle sequence suggests an underlying local protosource and deposition occurring synchronously with arc magmatism.

Neoproterozoic rocks of the type area of Avalonia are dominated by Ediacaran zircons. Early Paleozoic platform units contain an abundance of grains that have ages between 1.0-1.6 Ga, with lesser Paleoproterozoic and Archean zircons. These ages are inconsistent with recycling from underlying Neoproterozoic rocks and indicate that Avalonia's provenance is a Gondwanan craton that contains Archean, Paleo-, Meso- and Neoproterozoic rocks. These data are inconsistent with a West African provenance and suggest that Avalonia originated along the margin of the Amazon craton. The prominent change in provenance is interpreted to be related to separation of Avalonia from Gondwana during the Early Ordovician opening of the Rheic Ocean.

In central North Carolina, mafic rocks of the Stony Mountain gabbro are characterized by variable LREE enrichment, prominent negative Nb anomalies and low Nb/Th ratios; features of tholeiitic basalts in modern island-arc, subduction related lavas. Nd isotope data indicate juvenile magmas consistent with derivation from lithospheric and asthenospheric sources during decompression melting of the mantle. The Stony Mountain gabbro can be modeled as the product of 10–15% hydrous partial melting of variable mixtures of MORB- and OIB-like mantle sources overprinted by a minor subducted-slab derived hydrous fluid component. By analogy with modern settings the Stony Mountain gabbro are comparable to MORB-like to OIB-type enriched rocks from the Lau Island and Sumisu Rift and are interpreted to have formed within an evolving early Paleozoic island arc—back arc rift-basin system. The presence of an Early Cambrian arc-back arc rift system in Carolinia is broadly coeval with arc-back arc volcanism in other peri-Gondwanan blocks of the Appalachians and may be related to the early Paleozoic opening of the Rheic Ocean.

The Neoproterozoic-Early Paleozoic Tectonic Evolution of the Peri-Gondwanan Margin of the Appalachian Orogen: An Integrated Geochronological, Geochemical and Isotopic Study from North Carolina and Newfoundland

by

Jeffrey Charles Pollock

A dissertation submitted to the Graduate Faculty of
North Carolina State University
in partial fulfillment of the
requirements for the degree of
Doctor of Philosophy

Marine, Earth and Atmospheric Sciences

Raleigh, North Carolina

2007

APPROVED BY:

Dr. James Hibbard Chair of Advisory Committee	Dr. John Fountain
Dr. Brent Miller	Dr. Kevin Stewart

DEDICATION

For Mom and Dad

(who have never ceased to believe in me)

BIOGRAPHY

Jeff Pollock was born in St. John's, Newfoundland on 5 April, 1976. He graduated from Beaconsfield Catholic High School in 1994 and then enrolled at Memorial University of Newfoundland. At MUN he studied physics, psychology and geology and graduated with a Bachelor of Science (Honours) degree in 1999 with a major in earth sciences. His undergraduate research was on the tectonic setting of mélanges under the supervision of Dr. Hank Williams. After graduation he began work as a geologist in the Mineral Deposits Section of the Geological Survey of Newfoundland. In autumn 2000, he returned to Memorial University of Newfoundland to begin Masters research on the magmatic and tectonic controls of volcanogenic-hosted massive sulphide mineralization in central Newfoundland. His work was sponsored by the Geological Survey of Canada and conducted under the direction of Drs. Derek Wilton and Cees van Staal. He was awarded the degree of Master of Science in 2003 and subsequently enrolled in the doctoral program at North Carolina State University to study with Dr. Jim Hibbard. In 2007 he graduated with a Doctor of Philosophy from NC State University having completed his research on geochronology and geochemistry of peri-Gondwanan rocks of North Carolina and Newfoundland. He is employed as a Marie Curie Research Fellow at The University of Edinburgh in Scotland.

ACKNOWLEDGMENTS

First and foremost I would like to thank my supervisor, Dr. Jim Hibbard not only for providing me the chance to work with him on such a unique and innovative project, but for pushing me to further my academic career (and for putting up with a 'townie'). Jim taught me how to critically evaluate my own data, and to separate the scientific "wheat from the chaff" in order to get to the root of the underlying problem. He has been an instrumental source of information, conversation, great laughs, and wonderful memories.

I also thank the other members of my committee Drs. John Fountain, Brent Miller and Kevin Stewart, for comments and questions that have greatly improved my research and for constructive reviews of earlier drafts of this dissertation. You have been helpful in your advice, generous with your time, and accommodating with your schedules.

My research would not have been possible without the assistance from my fellow geologists who provided hours of discussion and interaction. In particular, Sean O'Brien (Geological Survey of Newfoundland), Art King and Paul Sylvester (Memorial University of Newfoundland) freely shared their knowledge of the Avalon zone in Newfoundland and were extremely supportive of this study. Phil Bradley (North Carolina Geological Survey), Chris Tacker and Trish Weaver (North Carolina Museum of Natural Science) are thanked for advice and fruitful discussions in the field. Steve Piercey (Laurentian University) gave an excellent course in lithogeochemistry and taught me the importance of quality assurance and quality control. The hospitality of Yvette Kuiper is gratefully acknowledged during my visit to Boston College.

Numerous individuals at Memorial University of Newfoundland contributed greatly to the success of this project. As always Mike Tubrett provided timely geochronology analyses and always made sure that the laser and ICP-MS ran smoothly. Michael Shaffer is thanked for running the SEM and for allowing me access at times of short notice. The exceptional assistance of Angie Paveley in the lab was vital, as were the geochemical and isotopic sample preparations by Pam King and Alain Potrel.

Many of my fellow graduate students at NC State, especially John Allen, Gordon Box and Matt Brennan, are thanked for assistance in the field, good company at the Hibernian, and the Paddy's Day parties in Raleigh. I express sincere thanks to my sister Cheryl, who came to my rescue several times in the past few years (I have not forgotten) and who seems genuinely proud to have a geologist for a brother.

The department staff in 1125 was always there when I needed something done – thank you Tammy, Connie, Sue, Paul, and especially Laura for your help in solving all the 'emergencies'. Financial support for field and analytical work was provided by a grant from the National Science Foundation and a Geological Society of America student research grant. In-kind support was provided by Memorial University of Newfoundland and the Geological Survey of Newfoundland and Labrador.

To finish I would like to extend my gratitude to Kathryn for her unwavering support, confidence, and patience throughout the entire process. Her assistance and continual encouragement during the intense final months of this effort helped guide me through this process and made it a rewarding venture. Thanks for being a part of this.

TABLE OF CONTENTS

LIST OF FIGURES

LIST OF TABLES

- Frontispiece -

View looking east from the summit of Stony Mountain, North Carolina.

"Civilization exists by geological consent, subject to change without notice."

- Will Durant -
(1885 - 1981)

INTRODUCTION

The late Neoproterozoic-early Paleozoic was characterized by dramatic changes in world-wide environmental conditions including: the rapid appearance and diversification of animal phyla, the development of multiple glaciation events at equatorial latitudes, and profound extremes in global sea level, ocean chemistry and climate (Dalziel, 1997; Hoffman and Schrag, 2002; Narbonne and Gehling, 2003). These changes are interpreted to be related to widespread orogenic activity and rifting that accompanied supercontinent assembly and dispersion. Geological evidence (Hoffman, 1991) suggests the breakup of Rodinia and opening of the Iapetus Ocean was broadly contemporaneous with Pan-African subduction-related and collisional events that resulted in the assembly of Gondwana in the late Neoproterozoic-Early Cambrian.

There is general consensus that the exotic crustal blocks along the eastern edge of the Appalachian orogen, Carolinia, Avalonia, Ganderia and Meguma, were originally located along the periphery of west Gondwana during the late Neoproterozoic and earliest Paleozoic. Such a position is consistent with paleomagnetic, faunal and isotopic data, which place these blocks at the margin of Gondwana and at considerable latitudinal distance from Laurentia (Nance and Murphy, 1994; MacNamara *et al*., 2001; Fortey and Cocks, 2002). Subsequent rifting and separation of these blocks from the margin of Gondwana in the early Paleozoic led to the formation of the Rheic Ocean (e.g. Murphy *et al*., 2006). Avalonia and Carolinia are the two largest accreted crustal blocks in the Appalachian orogen and as such the geological history of these blocks should impose significant constraints on the timing of dispersal of Gondwana and formation of the Rheic Ocean.

Considerable debate surrounds the late Neoproterozoic-early Paleozoic paleogeographical position of Carolinia and Avalonia. Some workers include Carolinia as part of Avalonia, implicitly viewing it as a composite terrane (e.g. Williams and Hatcher, 1983; Keppie and Ramos, 1999; Nance *et al*., 2002) even though a common geological history for Carolinia and Avalonia has not been explicitly demonstrated. As such, other workers have questioned this microcontinent interpretation and propose that Carolinia and Avalonia represent independent crustal blocks (Secor *et al*., 1983; Samson, 1995; Hibbard *et al*., 2007). Most early tectonic models noted overall lithologic similarities between Avalonia (including Carolinia) and Pan-African belts and therefore favoured a location adjacent to northwest Africa (Schenk, 1971; Rast and Skeehan, 1983; O'Brien *et al*., 1983; Zartman and Hermes, 1987). An Avalonia-west African connection has also been proposed by more recent workers (McNamara *et al*., 2001; Thompson *et al*., 2007) on the basis of paleomagnetic data. Although Avalonia and west Africa appear to share a similar lithotectonic history between ca. 800-600 Ma, their latest Neoproterozoic-Paleozoic tectonic evolutions diverge (Landing, 1996) which led others (Keppie *et al*., 1996; Murphy *et al*., 1996; Nance *et al*., 2002; Ingle *et al*., 2003) to propose an alternative position of Avalonia and Carolinia opposite the northern margin of Amazonia.

Despite the prominence of Carolinia and Avalonia in the Paleozoic, our understanding of such fundamental aspects of their evolution such as the timing of rifting, the nature or mode of separation and their location with respect to Gondwanan elements are all poorly constrained at best. Much of the ambiguity in the relative Neoproterozoic paleogeographic position of Carolinia and Avalonia results from the absence of useful biostratigraphic index fossils before the onset of Cambrian shelly fauna and the lack of pre-Mesozoic oceanic crust due to its destruction by the processes of subduction and obduction. Determining the location, source craton and timing and geometry of separation of Avalonia and Carolinia are fundamental to understanding the tectonic evolution of these major crustal blocks, the development of the Rheic Ocean, and the paleogeography of the early Paleozoic globe.

In order to address the lack of fundamental understanding of the timing, nature, and geometry of the Rheic Ocean this study of Carolinia and Avalonia is specifically directed at the following: (*i*) their original paleogeographic location along the Gondwanan margin by analysis of detrital zircon data from both Carolinia and Avalonia; (*ii*) their timing of rifting from Gondwana; and (*iii*) tectonic controls on provenance variations in both Carolinia and Avalonia by comparison of detrital zircon trends through time.

The following dissertation comprises three independent studies that focus mainly on Carolinia because of the lack of geochronological, geochemical and isotopic data compared to Avalonia. *Chapter one* is a systematic and comprehensive geochronological study that presents U-Pb detrital zircon data from the major lithotectonic units of Carolinia to asses the tectonic controls on their provenance and regional correlation. *Chapter two* presents and interprets a lithogeochemical and Sm-Nd isotopic dataset from early Paleozoic intrusive rocks in Carolinia to elucidate their petrogenetic evolution and to constrain the timing of rifting from Gondwana by comparison with modern and ancient analogues. *Chapter three* addresses the paleogeographical position and timing of separation of Avalonia from the margin of Gondwana by analyzing the variation in detrital zircon populations in representative samples from the clastic rocks of the type area of Avalonia in Newfoundland. In each chapter the new geochronological and geochemical data are compared with all existing geological, isotopic, faunal and stratigraphic data to construct tectonostratigraphic models for the Neoproterozoic to early Paleozoic tectonic evolution of Carolinia and Avalonia.

REFERENCES

Dalziel, I.W.D.
1997. Neoproterozoic-Paleozoic geography and tectonics; review, hypothesis, environmental speculation. Geological Society of America Bulletin, 109, p. 16-42.

Fortey, R.A. and Cocks, L.R.M.
2002. Palaeontological evidence bearing on global Ordovician-Silurian continental reconstructions. Earth Science Reviews, 61, p. 245-307.

Hoffman, P.F.
1991. Did the breakout of Laurentia turn Gondwanaland inside out?, Science, 252, p. 1409–1412.

Hoffman, P.F. and Schrag, D.P.
2002. The snowball Earth hypothesis: testing the limits of global change. Terra Nova, 14, p. 129–155.

Ingle, S., Mueller, P., Heatherington, A. and Kozuch, M.
2003. Isotopic evidence for the magmatic and tectonic histories of the Carolina terrane: implications for stratigraphy and terrane affiliation. Tectonophysics, 371, p. 187-211.

Keppie, J.D., Ramos, V.A.
1999. Odyssey of terranes in the Iapetus and Rheic oceans during the Paleozoic. *In:* Ramos, V.A., Keppie, J.D. (*eds*.), Laurentia–Gondwana Connections Before Pangea. Geological Society of America Special Paper, 336, p. 267– 276.

Keppie, J.D., Dostal, J., Murphy, J.B., and Nance, R.D.
1996. Terrane transfer between eastern Laurentia and western Gondwana in the early Paleozoic: Constraints on global reconstructions. *In:* Nance, R.D. and Thompson, M.D. (*eds*.), Avalonian and Related Peri-Gondwanan Terranes of the Circum-North Atlantic. Geological Society of America Special Paper, 304, p. 369–380.

Landing, E.
1996. Avalon: Insular continent by the latest Precambrian. *In:* Nance, R.D. and Thompson, M.D. (*eds.*) Avalonian and Related Peri-Gondwanan Terranes of the Circum-North Atlantic. Geological Society of America,Special Paper, 304, p. 29–63.

McNamara, A.K., Niocaill, C.M., van der Pluijm, B.A. and van der Voo, R.
2001. West African proximity of the Avalon terrane in the latest Precambrian. Geological Society of America Bulletin, 113, p. 1161–1170.

Murphy, J.B., Keppie, J.D., Dostal, J., and Cousins, B.L.
1996. Repeated late Neoproterozoic –Silurian lower crustal melting beneath the Antigonish Highlands, Nova Scotia: Nd isotopic evidence and tectonic interpretations. *In:*

Nance, R.D. and Thompson, M.D. (*eds*.), Avalonian and Related Peri-Gondwanan Terranes of the Circum-North Atlantic. Geological Society of America Special Paper, 304, p. 109– 120.

Murphy, J.B., Gutierrez-Alonso, G., Nance, R.D., Fernandez-Suarez, J., Keppie, J.D., Quesada, C., Strachan, R.A., and Dostal, J.
2006. Origin of the Rheic Ocean: Rifting along a Neoproterozoic suture? Geology, 34, p. 325–328.

Nance, R.D. and Murphy, J.B.
1994. Contrasting basement isotopic signatures and the palinspastic restoration of peripheral orogens: example from the Neoproterozoic Avalonian –Cadomian belt. Geology, 22, p. 617–620.

Nance, R.D., Murphy, J.B., and Keppie, J.D.
2002. A Cordilleran model for the evolution of Avalonia. Tectonophysics, 352, p. 11–31.

Narbonne, G.M. and Gehling, J.G.
2003. Life After Snowball: The Oldest Complex Ediacaran Fossils. Geology, 31, 27-30.

O'Brien, S.J., Wardle, R.J. and King, A.F.
1983. The Avalon zone: a Pan-African terrane in the Appalachian orogen of Canada. Geological Journal, 18, p. 195– 222.

Rast, N. and Skehan, J.W.
1983. The evolution of the Avalonian plate: Tectonophysics, 100, p. 257–286.

Schenk, P.E.
1971. Southeastern Atlantic Canada, northwestern Africa, and continental drift: Canadian Journal of Earth Sciences, 8, p. 1218–1251.

Secor, D.T., Samson, S., Snoke, A., and Palmer, A., 1983. Confirmation of the Carolina slate belt as an exotic terrane. Science, 221, 649–651.

Thompson, M.D., Grunow, A.M., and Ramezani, J.
2007. Late Neoproterozoic paleogeography of the Southeastern New England Avalon Zone: Insights from U-Pb geochronology and paleomagnetism. Geological Society of America Bulletin, 119, p. 681-696.

Williams, H. and Hatcher, R. D.
1983. Appalachian suspect terranes. *In:* Hatcher, R. D., Jr., Williams, H., Zietz, I. (*eds*.), Contributions to the tectonics and geophysics of mountain chains. Geological Society of America Memoir, 158, p. 33-54.

CHAPTER 1

DEPOSITIONAL AND TECTONIC SETTING OF THE NEOPROTEROZOIC-EARLY PALEOZOIC ROCKS OF CAROLINIA: EVOLUTION OF VOCLANIC ARC-RELATED SEDIMENTARY SEQUENCES BASED ON U-Pb DETRITAL ZIRCON GEOCHRONOLOGY

ABSTRACT

LAM-ICP-MS U-Pb ages of more than 500 detrital zircons from the Neoproterozoic-early Paleozoic clastic sequences of Carolinia range from ca. 530 Ma (Early Cambrian) to ca. 2600 (Archean). The majority (>80%) of analyzed zircon grains are late Neoproterozoic (Ediacaran), with minor amounts of Mesoproterozoic/Paleozoic and accessory Archean grains. The overall distribution of age populations of detrital zircons is consistent with sediment derivation from the Amazonian craton and its peripheral orogenic belts on the margin of west Gondwana. On the basis of the age of the youngest detrital zircon populations (ca. 550 Ma), the Uwharrie, Tillery, Cid and Yadkin formations are no older than Ediacaran. The minimum deposition ages of the Uwharrie and Cid formations are constrained by ages of contemporaneous volcanism (554 ± 15 Ma) and 540 ± 1.2 Ma, respectively). Thus, all units of the Albemarle sequence were deposited between ca. 554 and 528 Ma. The dominance of Ediacaran and early Paleozoic zircons in the Albemarle Group suggests an underlying local protosource for the sediments. Mesoproterozoic and older detrital grains constitute a minor component and have an age signature that suggests derivation from an adjacent Mesoproterozoic terrane. Dated samples from the Albemarle Group yield similar detrital zircon U-Pb age populations consistent with a common provenance. The results of this study illustrate that sedimentation in the Albemarle sequence is a manifestation active tectonics and was contemporaneous with felsic magmatism. These relationships suggest that magmatism, tectonism and deposition were broadly coeval and important regional-scale mechanisms consistent with formation in a late Neoproterozoic-early Paleozoic back-arc rift to back-arc basin tectonic setting.

PREAMBLE

Carolinia is located along the eastern edge of the southern Appalachian orogen and comprises one of the Neoproterozoic-early Paleozoic exotic crustal blocks that record a magmatic and tectonothermal history that predate the formation of the eastern margin of Laurentia and the Iapetus Ocean (Figure 1.1). Together with easterly terranes of the northern Appalachians (Avalonia, Ganderia and Meguma), they collectively form the peri-Gondwanan realm and resulted from Neoproterozoic subduction and arc accretion. Subsequently they experienced early Paleozoic continental rifting related to the opening and subsequent closure of the Iapetus and Rheic oceans, respectively. Numerous workers have used geological, geochemical, paleomagnetic, faunal and isotopic techniques (Secor *et al*., 1983; Ingle *et al*., 2003; Hibbard *et al*., 2002; Hibbard *et al*., 2007) to illustrate that the Neoproterozoic-early Paleozoic evolution of Carolinia was a product of protracted arc magmatism and sedimentation along an oceanic-facing margin of west Gondwana.

However, there is significant uncertainty regarding the geological history of Carolinia, specifically the age of the basement to its volcanic arc rocks, its source craton(s) in Gondwana, and the timing of its separation from this craton. In addition, the nature and timing of deposition of fundamental sequences of Carolinia are contested in the literature (e.g. Milton, 1984; Butler and Secor, 1991; Koeppen *et al*., 1995; Hibbard *et al*., 2002; Ingle *et al*., 2003).

To address these problems I initiated a systemic U-Pb detrital zircon geochronological study of Carolinia. U-Pb dating of detrital zircons from clastic sedimentary rocks is a valuable method in sedimentary provenance and crustal evolution studies because the age spectra of detrital zircons in clastic sedimentary rocks can be useful in evaluating potential source regions for the sediment by using the individual ages of detrital zircons as a proxy for their source rock. In-situ laser ablation microprobe-inductively coupled plasma-mass spectrometry (LAM-ICP-MS) analytical techniques allow for the relatively rapid acquisition of large sets of geochronological data which can be useful to determine the maximum age of deposition, identify time gaps in the geological record, define paleogeographic terranes, and interpret changes in provenance due to tectonics.

In this chapter I present new U-Pb detrital zircon geochronological data from representative samples of metaclastic sedimentary rocks throughout the North Carolina portion of Carolinia. Deposition of the units sampled spans most of the Neoproterozoic-early Paleozoic interval during which Carolinia was formed and the resulting data are used in identifying the basement source of detritus and to ascertain information about the provenance, depositional history and tectonic setting of Carolinia.

REGIONAL GEOLOGICAL SETTING

Carolinia comprises a collection Neoproterozoic-early Paleozoic magmatic arc/sedimentary terranes exposed for more than 600 km in an elongate northeast-southwest trending belt from central Virginia to Georgia. The geological and tectonic history of Carolinia is best known and described from the two largest constituents, the Carolina and Charlotte terranes (Figure 1.2) (Hibbard *et al*., 2002). Although the geological evolution is complex and only partially known, a simplified history of Carolinia, condensed from all terranes, is summarized in a tectonostratigraphic column (Figure 1.3) and subdivided into a triparite succession comprising: (*i*) an old arc phase (ca. 670 Ma) containing the oldest dated rocks in Carolinia that are preserved in the fault bounded Roanoke Rapids complex; (*ii*) an episode of younger, juvenile arc magmatism (Virgilina sequence) that formed in an open oceanic setting between 630 Ma and 610 Ma (Samson *et al*., 1995; Wortman *et al*., 2000) and overlain by younger clastic sedimentary rocks; and (*iii*) a main phase of arc magmatism and related intra-arc sedimentation in the Carolinia and Charlotte terranes that formed from ca. 575 to at least ca. 528 Ma and is best preserved in the Albemarle sequence (Hibbard *et al*., 2002).

In north-central North Carolina the Roanoke Rapids terrane comprises a fault bounded assemblage of low metamorphic-grade, mafic-ultramafic rocks (Halifax County complex) surrounded by a sequence of plutonic, felsic volcanic, metavolcanic and phyllitic volcaniclastic rocks of the Roanoke Rapids complex. Previous geochemical studies (Kite and Stoddard, 1984) interpret the Roanoke Rapids terrane to record the formation of an ophiolite complex which subsequently formed the oceanic substrate to a volcanic island arc. An isotope dilution-thermal ionization mass spectrometry (ID-TIMS) date from a granitic pluton that intrudes the Roanoke Rapids complex constrains the minimum age of island arc magmatism to 672 ± 2 Ma (Coler and Samson, 2000). ε_{Nd} data from the Roanoke Rapids complex range from 0 to -9 (Coler *et al*., 1996) which indicate that the arc was built, at least in part, on a substrate of older isotopically evolved continental crust. A period of younger magmatism is also recorded in the Roanoke Rapids terrane where a 615 ± 1 Ma metagranite intrudes volcanogenic arc-related sedimentary rocks (Coler and Samson, 2000).

This younger episode of arc activity is contemporaneous with magmatism in the Virgilina sequence, which comprises a ca. 8 km thick sequence of felsic, intermediate, and mafic metavolcanic rocks of the Hyco Formation, overlain by metasedimentary rocks of the Aaron Formation which are in turn overlain by mafic volcanic and pyroclastic rocks of the Virgilina Formation (Harris and Glover, 1988). The volcanic rocks of the Virgilina sequence are principally sub-aqueous pyroclastic-volcaniclastic rocks interpreted to have been deposited in a shallow marine environment (Glover and Sinha, 1973). ε_{Nd} data suggest that the Virgilina sequence was dominated by juvenile, mantle-derived crust and probably represents a mature arc formed on a substrate of oceanic crust (Samson *et al*., 1995). U-Pb zircon dates from plutonic and volcanic rocks suggest that the onset of subduction and initiation of magmatism began at ca. 630 Ma and continued until ca. 612 Ma (Wortman *et al*., 2000). However, clastic sedimentary rocks of the Aaron Formation are at least ca. 35 m.y. younger than the volcanic rocks of the Hyco Formation; Samson *et al*. (2001) report detrital zircons in the Aaron Formation that have ages as young as ca. 578 Ma. Thus, there is likely a hiatus within the sequence.

The Virgilina sequence is unconformably overlain by the Uwharrie Formation which forms the base of the Albemarle sequence. The Uwharrie Formation contains approximately 4.5 km of dominantly sub-aqueous felsic volcaniclastic rocks and lavas with intercalated mafic pyroclastic rocks and minor clastic sedimentary layers (Hibbard *et al*., 2002). Consistent geochemical signatures that indicate the influence of a subducting slab on magmatism imply formation in a suprasubduction zone environment (Feiss *et al*., 1993; Ingle *et al*., 2003). U-Pb geochronological data indicate that the Uwharrie Formation is Neoproterozoic or possibly earliest Cambrian; an ID-TIMS date of 551 ± 8 Ma from zircon was reported by Ingle (1999) and zircons analyzed by secondary ionization mass spectrometry (SIMS) on a sensitive high resolution ion microprobe (SHRIMP) yielded a date of 554 ± 15 Ma (Ingle *et al*., 2003).

The Uwharrie Formation is overlain by the Albemarle Group, a ca. 10 km thick sequence primarily composed of epiclastic sedimentary rocks with subordinate felsic, intermediate and mafic volcanic rocks; all of which are metamorphosed to lower greenschist facies. The Albemarle Group is subdivided into four formations, which in ascending order are the Tillery, Cid, Floyd Church and Yadkin formations. Although, it is generally accepted that the Uwharrie Formation underlies the Albemarle Group, the exact nature of this contact has been controversial. Previous workers have interpreted this contact as being either gradational (Conley, 1962; Gibson *et al*., 1984) or faulted (Feiss, 1988; Klein *et al*., 2007). Ingram (1999) shows a conformable contact between volcanic rocks of the Uwharrie Formation that are interlayered with basal sedimentary rocks of the Tillery Formation.

The Tillery Formation is dominated by laminated to thin-bedded, fine-grained epiclastic sedimentary rocks with minor lenses of conglomerate, pebbly mudstone and mafic and felsic volcanic rocks. Thin- to medium-bedded, fine-grained mudstone constitute most of the overlying Cid Formation, which contains felsic pyroclastic and epiclastic rocks of the Flat Swamp member at its top. The Floyd Church Formation comprises medium- to thick-bedded epiclastic mudstone. The overlying Yadkin Formation is dominated by fine- to medium-grained greywacke derived from an intermediate or mafic terrane with minor interbeds of andesitic basalt flows (Stromquist and Sundelius, 1969; Milton, 1984; Ingram, 1999).

Previous studies note the presence of xenocrystic zircons in volcanic and volcaniclastic rocks of the Albemarle sequence that are significantly older than the time of magmatism and deposition of the rocks (Ingle *et al*., 2003) and suggest derivation in part from Mesoproterozoic sources. It must be stressed however, that the Paleoproterozoic ages of xenocrystic zircons (Ingle *et al*., 2003) are suspect, as they are either very imprecise and/or involve long extrapolations from data plotting close to lower intercepts. Together with positive ε_{Nd} values, these data indicate that the Albemarle sequence formed upon a juvenile basement adjacent to a Mesoproterozoic terrane (Hibbard *et al*., 2007).

The age of the Albemarle Group is constrained by faunal and U-Pb isotopic data. The Ediacaran fossils *Aspidella* and *Pteridinium* are reported from the Cid and Floyd Church formations (Gibson *et al*., 1984; Weaver *et al*., 2006). Felsic to intermediate rocks from the Tillery and Cid formations yielded U-Pb zircon ages of 553 ± 20 Ma, and 547 ± 2 Ma/541 ± 2 Ma, respectively (Hibbard *et al*., 2006; Ingle *et al*., 2003), while the Yadkin Formation contains a single detrital zircon dated by ID-TIMS at 531 ± 2.5 Ma (B. Miller, personal communication, 2005). These data coupled with the ca. 554-551 Ma age of the underlying Uwharrie Formation suggest that the bulk of the Albemarle Group was deposited in a narrow time interval during the Neoproterozoic-earliest Cambrian. However, even though the Albemarle Group contains fossils, interlayed volcanic rocks and cross cutting igneous rocks, the age of deposition and internal stratigraphy of the group are contested in the literature (as discussed in Butler and Secor, 1991; Ingle, 1999; Hibbard *et al*., 2002). Fossil discoveries from the Tillery and Cid formations (Koeppen *et al*., 1995), suggest that these units are no older than Middle Ordovician and Late

Cambrian, respectively. The faunal data contradict the published geochronological data and suggest that the lower units of the Albemarle Group (Tillery and Cid formations) are younger than the overlying Floyd Church and Yadkin formations.

METHODOLOGY

Sample strategy

Single U-Pb ages from a total of 510 detrital zircon grains were obtained from six samples from clastic metasedimentary rocks throughout Carolinia in central North Carolina (Figure 1.4). The selection of individual units for analysis was based on solving specific problems, i.e. the maximum age of deposition, provenance characteristics of the sequences and/or identification of time gaps in the geological record. A sample of a low-grade quartzose metasedimentary rock from the Roanoke Rapids complex was analyzed to determine the relationship of the ca. 670 Ma old arc phase of Carolinia to the younger (ca. 630 Ma) magmatic arc sequences. A sample of the Virgilina sequence was collected from an outcrop located approximately 100 km from the locale sampled by Samson *et al*. (2001) to ascertain its provenance and to test regional correlations within the Aaron Formation. Previously reported U-Pb ages (Ingle *et al*., 2003) for the Uwharrie Formation have relatively large uncertainties and therefore a clastic rock from the Uwharrie Formation was analysed to determine the maximum age of deposition of the Albemarle sequence, and its relationship with underlying rocks of the Virgilina sequence.

The remaining three samples from the Albemarle sequence were collected from units throughout the Albemarle Group to determine temporal patterns of detrital zircon ages in the Albemarle Group and to constrain the maximum age of deposition. Additional

U-Pb geochronological data from the Tillery, Cid and Yadkin formations should also provide confirmation of their purported Neoproterozoic-Cambrian age that contradicts with the faunal evidence of Koeppen *et al*. (1995).

Analytical procedures for U-Pb geochronology

Detrital zircons were isolated from approximately 25kg of sample using a jaw crusher/Bico disc mill and concentrated using a Wilfley table, iodomethane, and a Frantz isodynamic separator at the Radiogenic Isotope Laboratory at Memorial University of Newfoundland (MUN). For each of the six samples approximately 150 zircon grains were selected from a range of non- and paramagnetic fractions in order to reduce any artificial biasing due to variations in magnetic susceptibility (Sircombe and Stern, 2002). The crystals were mounted with epoxy in 2.5 cm diameter grain mounts and ground to expose internal cross sections of the grains in order to remove the outer surfaces which are typically enriched in uranium (Krogh, 1982). All zircons were imaged with transmitted and reflected light and a scanning electron microscope. The data were acquired in back-scattered electron (BSE) mode to illuminate oscillatory zoning and inherited crystals using a FEI Quanta 400 scanning electron microscope (SEM) equipped with a solid state, twin segment backscatter electron detector. The SEM was operated under high vacuum of $<6^{-4}$ Pa with an accelerating potential of 25 keV and a beam current of 10 nA.

Isotopic data for this study were obtained at the MUN-Inco Innovation Centre using a GeoLasPro 193 nm excimer laser system attached to a Finnigan Element XR high resolution-inductively coupled plasma-mass spectrometer (ICP-MS) equipped with a dual mode secondary electron multiplier operating in both counting and analog modes. The operating ranges of these two modes allow for a large crossover range where both modes are simultaneously valid; in this range a cross-calibration is automatically performed for every spectrum acquired thereby ensuring accurate analysis. The 10 µm laser beam was focused 100–200 µm above the sample surface and fired at 10 Hz repetition rate using an energy density of 30 J/cm^2. Spot analyses were performed on homogenous BSE domains to ensure that the measured U-Pb ratios did not represent mixtures of two or more age components. Data were collected using a 30 s measurement of the gas background before the laser was switched on followed by 180 s of measurement with the laser on and zircon being ablated. During ablation the sample was mounted in a sealed sample chamber and moved beneath the laser to produce a square 40 x 40 µm pit in order to minimize the depth of ablation and consequently reduce laser-induced elemental fractionation at the ablation site. The ablated sample was flushed from the sample cell and transported to the ICP-MS using a helium carrier gas. The U, Th and Pb isotopic ratios from the zircon were acquired along with a mixed ^{203}Tl-^{205}Tl-^{209}Bi-^{233}U-^{237}Np tracer solution (concentration of 10ppb) that was nebulized simultaneously with the ablated solid sample.

Raw data were reduced using the macro-based spreadsheet program LAMdate. The ^{207}Pb/^{206}Pb, ^{208}Pb/^{206}Pb, ^{206}Pb/^{238}U and ^{207}Pb/^{235}U ratios were calculated and blank corrected for each analysis. For each analysis, time-resolved signals were obtained and studied to ensure that stable flat signal intervals were used in the age calculation. Samples exhibiting isotopic heterogeneity caused by elemental U-Pb fractionation, core-rim features, zones of high common Pb or inconsistent U-Pb and Th-Pb behaviour were rejected from the data set. Aspiration of the tracer solution allowed for a real-time instrument mass bias correction using the known isotopic ratios of the tracer solution measured while the sample was ablated; this technique is largely independent of matrix effects that can variably influence measured isotopic ratios and hence the resulting ages. The high instrumental Hg background prohibited accurate measurement of ^{204}Pb. Nonetheless the amount and composition of common-Pb present in zircons analyzed in this study represents an insignificant amount relative to the content of radiogenic Pb; as a result, no common Pb correction was applied to the data.

Accuracy and reproducibility of U-Pb analysis in the MUN laboratory are routinely monitored by measurements of natural zircon standards of known TIMS U-Pb age. To monitor the efficiency of mass bias and laser-induced fractionation, the Geostandards 91500 zircon (1065 ± 3 Ma) (Weidenbeck *et al*., 1995) and the in-house zircon standard PL (338 ± 1 Ma) (Aftalion *et al*., 1989) were analyzed before and after every eight unknowns. Residual laser-induced fractionation was typically less than 0.05%/amu based on repeat measurements of the ^{206}Pb/^{238}U ratio of the reference standards. Age determinations were calculated using the ^{238}U (1.55125×10^{-10} a^{-1}) and ^{235}U (9.8485×10^{-10} a^{-1}) decay constants and the present day ^{238}U/^{235}U ratio of 137.88 (Jaffey and others, 1971). Final ages (reported at 2σ) and Concordia diagrams were produced using the Isoplot/Ex macro (Ludwig, 1999).

For this study analysis of a minimum of 80 grains per sample (Figure 1.5) was attempted in order to achieve 95% confidence that no fraction >0.05 of the population was missed (Vermeesch, 2004). Previous studies however, have shown that dating fewer grains can still yield useful information as samples that contain as few as 45 zircons analyzed are 95% certain that no fraction >0.010 of the total population was missed (Anderson, 2004). For analyses that are concordant or overlap the Concordia curve (at 1σ errors) the Concordia age is reported because it makes optimal use of all radiogenic U/Pb and Pb/Pb ratios simultaneously and therefore is more precise than any single U-Pb or Pb-Pb age. For positively discordant analyses the low ^{207}Pb count rates in young (<1500 Ma) zircons precludes the use of $^{207}Pb/^{206}Pb$ ages and accordingly the more precise $^{206}Pb/^{238}U$ ages are preferred. The $^{206}Pb/^{238}U$ ages are also favored for slightly reversely discordant analyses. In discordant zircons older than 1.5 Ga, the $^{207}Pb/^{206}Pb$ ages are reported because they contain greater amounts of ^{207}Pb and therefore have smaller uncertainties. Reported dates are within 85%-110% concordance, where concordance is expressed as [($^{206}Pb/^{238}U$ date) / ($^{207}Pb/^{206}Pb$ date)] x 100.

Uranium concentrations in detrital zircons were calibrated using the reference zircon 91500 containing a U concentration of 80 ppm (Wiedenbeck *et al*., 1995). The unknown zircons and the calibration zircon were ablated under exactly the same conditions so no internal standard was necessary to deal with ablation yield differences. The precision in U analyses by ICP-MS, measured as percent relative standard deviation (%RSD), is typically (7-15 %).

RESULTS

The U-Pb ages for detrital zircons from all samples of Neoproterozoic-early Paleozoic clastic metasedimentary rocks of Carolinia range from Paleozoic to Archean. Analysis of the data set allows it to be divided into a series of common age groups although the age ranges and proportions of specific age intervals vary both within and between samples. The Concordia diagrams (Figure 1.6), histograms and Gaussian cumulative probability plots (Figure 1.7) show both unimodal and polymodal age spectra, indicating restricted provenance from a single terrane and a diverse provenance comprising source rocks of a range of ages, respectively.

Roanoke Rapids Terrane – Roanoke Rapids complex

The Roanoke Rapids complex was sampled from the city of Roanoke Rapids, North Carolina along the tailrace below the Roanoke Rapids dam on the southside of the Roanoke River. The analyzed sample comprises a matrix-supported, greenschist-facies metamorphosed pebbly conglomerate. The rock is composed of subangular to subrounded pebbles of quartzite, chert, granite, quartz diorite, and felsic volcanic rocks. The conglomerates locally display graded bedding and scour-and-fill structures (Parker, 1964). The Roanoke Rapids complex is the oldest dated unit in Carolinia and is constrained to the Neoproterozoic by a U-Pb TIMS age from zircon of 672 ± 2 Ma from a metamorphosed granodiorite that purportedly intrudes the complex (Coler and Samson, 2000).

A total of 80 grains were analyzed with an overwhelming dominance of Neoproterozoic ages (69 analyses or 86%) that range from 631 ± 10 Ma to 708 ± 6 Ma and form a pronounced unimodal peak on the cumulative probability curve at ca. 675 Ma. A small number (6 analyses) of older Neoproterozoic zircons yield concordant or slightly reversely discordant ages between 715 ± 12 Ma and 798 ± 24 Ma. An older Mesoproterozoic cluster comprises three concordant or nearly concordant analyses of 1065 ± 24 Ma, 1077 ± 13 Ma and 1140 ± 10 Ma which is reflected in small peaks on the cumulative probablility plot. Most of the zircons analyzed (~80%) have high (>0.80) Th/U ratios and low U (<150 ppm) concentrations similar to mafic igneous rocks.

Virgilinia sequence – Aaron Formation

The Aaron Formation comprises a ca. 1.5 km-thick sequence of coarse-grained sedimentary rocks interpreted to have been deposited by turbidity currents in a deep marine, retrogradational submarine-fan setting (Harris and Glover, 1988). The analyzed sample was collected from a roadside outcrop on a side road 3 km north of US Route 64 and consists of massive, matrix supported pebble conglomerate. The clast content is fairly constant throughout the formation. Subangular to rounded pebbles and granules of dominantly felsic volcanic, plutonic and quartz arenite clasts comprise over 90% of the coarse fraction; the groundmass consists of quartz crystals, silt and ripped-up clasts of siltstone. On the basis of provenance studies the quartzite clasts of the Aaron Formation were interpreted to be derived from erosion of continental crust that formed the basement to the Virgilina sequence (Glover and Sinha, 1973).

A late Neoproterozoic age of deposition for the Aaron Formation is constrained by faunal and radiogenic isotopic data. A Neoproterozoic Ediacaran fauna was reported from the Hyco Formation by Cloud *et al*. (1976). Tighter ages constraints are however, provided by U-Pb ages of zircon from volcanic and plutonic rocks of the Virgilina sequence. Wortman *et al*. (2000) reported a 615 +4/-2 Ma (ID-TIMS) age for the underlying Hyco Formation and a 546 +3/-2.5 Ma age for the Roxboro Granite that is intrusive into the Aaron Formation. An age of ca. 578 Ma (SHRIMP-II) from a single detrital zircon is reported from the Aaron Formation (Samson *et al*., 2001).

Analyzed zircon grains (60 analyses) within the sample all lie near or on Concordia with only five grains having a probability of concordance of greater than -0.15. The oldest zircon has a Concordia age of 2162 ± 20 Ma; whereas the youngest analysis yielded an age of 588 ± 11 Ma. The remaining analyses are separated into several groups, dominated by 29 concordant analyses (62%) that yield ages ranging from 595 ± 11 Ma to 732 ± 10 Ma and correspond to a distinct peak on the cumulative probability plot at ca. 620 Ma. A secondary peak at ca. 1200 Ma is defined by a group of 18 analyses (29%) that contain Neoproterozoic-Mesoproterozoic ages from 840 ± 45 to 1382 ± 77 Ma. Another nine grains show ages between 1491 ± 18 Ma and 1850 ± 12 Ma that corresponds to a peak on the probability curve at ca. 1650 Ma, whereas five older analyses have Paleoproterozoic ages between 1887 ± 15 Ma and 2162 ± 20 Ma. The variable Th/U ratios (0.13-1.9) and U concentrations (50-945 ppm) correspond to the complete spectrum (mafic-intermediate-felsic) of igneous rocks.

Albemarle sequence – Uwharrie Formation

The Uwharrie Formation forms the base of the Albemarle sequence and unconformably overlies the Hyco Formation. The formation is a >4 km thick dominantly bimodal volcanic sequence that consists primarily of felsic pyroclastic-volcaniclastic rocks and flows that are intercalated with subordinate mafic pyroclastic rocks and pillow lavas (Seiders, 1978; Milton, 1984). Thin bedded mafic and felsic tuff are interbedded with epiclastic very-coarse grained, granule to pebble conglomerate, which occurs at the top of the unit. A sample of this conglomerate was collected south of Yow Mill approximately 1 km from the contact with the underlying Hyco Formation. Grey to white, angular to subrounded pebbles of flow-banded rhyolite, felsite, dacite, porphyritic felsite, crystal tuff and lithic tuff predominate and are supported in a fine-grained silt matrix. Rounded clusters of coarse-grained plagioclase and quartz are locally common; mafic fragments (basalt, diorite) are rare (Harris and Glover, 1988; Ingram, 1999). Ingle *et al*. (2003) obtained a SHRIMP date of 554 ± 15 Ma for the Uwharrie Formation, which indicates a Neoproterozoic to possibly earliest Cambrian age of eruption and deposition of the formation.

All 64 analyses of zircon grains from this sample appear to overlap the Concordia curve, but six analyses are > 15% discordant and are excluded from the dataset. Of the remaining 58 analyses, the vast majority (56 analyses or 98%) have Neoproterozoic ages between 545 ± 7 Ma and 593 ± 9 Ma and form a prominent unimodal peak at ca. 560 Ma. The remaining two concordant analyses are slightly older and have ages of 665 ± 17 Ma and 685 ± 39 Ma. Th/U ratios of the zircons are typically low (<0.8) and are comparable to felsic rocks.

Albemarle Group – Tillery Formation

A sample of thin-laminated, blue to green-grey argillite with interbeds of coarse-grained siltstone and sandstone was collected from a roadside outcrop near the town of Uwharrie. Rhythmically laminated to thin-bedded siliceous siltstones are characteristic of the Tillery Formation and are locally interbedded with fine- to coarse-grained sandstone and mudstone giving the rock a ribbon-banded appearance. The rocks contain a variable composition that range from angular to subrounded grains of euhedral feldspar and quartz to coarse-grained lithic clasts composed of felsic and mafic volcanic fragments; beds show typical Bouma sequence features such as channel deposits, ripple marks, cross-bedding, grading, and parallel and low angle cross-laminations (Stromquist and Sundelius, 1969). These features and overall lithology suggest marine turbiditic sedimentation which was dominated by turbulent currents on the outer fringe or slope of a submarine fan in a large basin.

A total of 70 zircon grains were analyzed from this sample with three being discarded because they have a probability of concordance of >0.15. The remaining 67 analyses show two major groups of Neoproterozoic zircons that comprise 47 analyses (70%) and correspond to pronounced peaks on the cumulative probability curve. The major peak at ca. 550 Ma contains 26 analyses that range from 550 ± 11 Ma to 591 ± 10 Ma, whereas a secondary peak at ca. 630 Ma contain 21 grains that show ages between 598 ± 18 Ma and 698 ± 37 Ma. Two single grains have ages of 845 ± 39 Ma 1097 ± 18 Ma. The remaining 16 analyses yield older ages with major groupings in the Mesoproterozoic and Paleoproterozoic, 7 analyses that fall between 1489 ± 25 Ma and 1780 ± 14 Ma, and 5 analyses between 1984 ± 22 Ma and 2375 ± 28 Ma. The oldest grains consist of two concordant analyses with Archean ages of 2529 ± 22 Ma and 2575 ± 26 Ma. Th/U ratios are variable and range from 0.1 to 1.7 with corresponding U concentrations that are typically low and range from 38 to 558 ppm.

Albemarle Group – Cid Formation

The Cid Formation conformably overlies the Tillery Formation and is a ca. 3 km thick sequence of tuffaceous mudstone alternating rhythmically with thin interbeds of siltstone and shale (Mudstone member) overlain by ca. 750 m of felsic to intermediate volcanic rocks of the Flat Swamp member. The analyzed sample was collected north of Badin Lake in the Jacobs Creek flagstone quarry and comprises a thin laminated to thin bedded, blue-grey medium-grained greywacke. The mineralogical composition of the rock consists of angular to subrounded grains of volcanic quartz (35 to 45 percent) and sodic plagioclase (25 to 35 percent), fine-grained mica (15 to 20 percent) with trace amounts of chlorite, epidote, titanite and zircon (Stromquist and Henderson, 1985). The Mudstone member contains the Ediacaran trace fossil *Aspidella* (Hibbard *et al*., 2006: Weaver *et al*., 2006) and the Flat Swamp member has yielded U-Pb ID-TIMS dates on zircon of 547 ± 2 Ma (Hibbard *et al*., 2006) and 540 ± 1.2 Ma (Ingle *et al*., 2003).

Analysis of a total of 57 detrital zircons yielded 52 grains with >15% discordance that define a very restricted Neoproterozoic-early Paleozoic range between 539 ± 12 Ma and 568 ± 15 Ma. A minor group of four older zircons fall in the age range of 581 ± 11 Ma and 610 ± 11 Ma. The data show a single striking peak on the cumulative probability plot at 550 Ma. U concentrations of zircons are characteristically low (<150 ppm) whereas Th/U values range from 0.5 to 2.2 with a mean of 1.0.

Albemarle Group – Yadkin Formation

A sample of the Yadkin Formation was collected from an abandoned quarry on Old Mill Road, west of the city of Albemarle. The unit comprises approximately 750 m of dark-green/grey to green-black, thin- to thick bedded, poorly sorted greywacke with interbedded well-sorted quartz-rich silt and sand layers. The greywackes contain angular to rounded quartz, plagioclase, and silt- to fine-grained sand size lithic fragments in a fine-grained matrix of muscovite, chlorite, quartz and plagioclase. Internal bedding characteristics include herring-bone ripple cross-laminations, graded, flaser and lenticular bedding, and asymmetrical interference ripple marks and suggest that the Yadkin Formation represents a shoaling upward sequence in a marine basin in which deposition was controlled by waves, currents and tides in a delta top or distributary-mouth bar environment (Boggs, 1995).

Dated zircons fall on or near Concordia and range in age from 1085 ± 17 Ma to 528 ± 8 Ma. Of the total of 80 analyses, three discordant analyses were discarded. The grains are dominated (72 analyses or 93%) by a cluster of dominantly Neoproterozoic and early Paleozoic ages between 528 ± 7 Ma and 636 ± 9 Ma that show a obvious Ediacaran age peak on the cumulative probability plot at ca. 560 Ma. A secondary minor relative peak is also present at ca. 650 Ma and corresponds to a group of four analyses between 647 ± 13 Ma and 658 ± 8 Ma. Of the remaining four analyses three are Neoproterozoic at 688 ± 8 Ma, 740 ± 13 Ma and 908 ± 31 Ma; a single Mesoproterozoic grain yielded a concordant age of 1085 ± 17 Ma. The Th/U ratios of the Yadkin detrital zircons vary (0.2-1.7) with an average value of 0.7. Some zircons contain very high Th/U values (>0.8) and low U contents (<500 ppm), typical of mafic igneous rocks.

DISCUSSION

Constraints on timing of deposition

Studies on the depositional ages of sedimentary rocks using detrital heavy minerals may be facilitated by employing sampling strategies based on knowledge of the sedimentological and tectonic processes that influenced sediment transport and deposition. For many Neoproterozoic and early Paleozoic clastic metasedimentary rocks constraints on the absolute timing of deposition are difficult to establish; particularly in sequences that lack distinctive marker units, faunal data, interstratified volcanic rocks, or datable authigenic (e.g. xenotime) minerals (Bowring *et al*., 1993; McNaughton *et al*., 1999). U-Pb dates corresponding to the time of igneous crystallization of detrital zircons are commonly used as a maximum limit for the age of deposition because crystallization of the youngest detrital zircon within a sediment precedes deposition of the host sediment (Williams, 2001; Fedo *et al*., 2003; Wintsch *et al*., 2007). The maximum age of deposition of a sedimentary rock is therefore constrained to be younger than the age of the youngest detrital zircon population. However, this relationship cannot be used to constrain the minimum age of deposition, as there is no necessary relationship between the timing of zircon formation in a protosource and the age of final deposition of sediment eroded from this source.

The use of detrital zircon ages to limit the age of deposition a sedimentary rock depends both on the number of grains analyzed and on knowledge of the geology of possible source terranes. The primary factor is that the data set is large enough (i.e. $n \geq 40$) to be reasonably representative of the sample thereby decreasing the probability of missing significant fractions of the detrital age spectrum. However, even when using larger data sets ($n=50$) it is possible that potentially significant (ca. 10%), minor populations may be overlooked at the 95% confidence detection limit (Vermeesch, 2004). As such, the use of the detrital zircons in a sediment to limit the age of deposition should only be used when there is independent geological information which indicates that the youngest potential protosource contributed a significant fraction (≥10%) of the total detrital zircon content of the sediment (Anderson, 2004).

To address the ambiguity regarding the age of deposition and internal position of stratigraphic units of the Albemarle Group, the youngest zircon grains in the Tillery, Cid and Yadkin formations are compared to existing stratigraphic and high-precision U-Pb geochronological constraints. The youngest concordant zircons in the Uwharrie Formation are 545 ± 7 Ma, 545 ± 9 Ma, and 546 ± 7 Ma. Therefore, these grains have a minimum age of ca. 545 Ma, which establishes the maximum age of the original sediments in the Uwharrie Formation as latest Neoproterozoic (Figure 1.8). Geochronological data support this interpretation, as a U-Pb zircon ages of 554 ± 15 Ma (SHRIMP) and 551 ± 8 (ID-TIMS) were obtained from underlying felsic volcanic rocks of the Uwharrie Formation (Ingle, 1999; Ingle *et al*., 2003).

A date of ca. 552 Ma indicated by the youngest zircons in the Tillery Formation, 550 ± 11 Ma, 551 ± 12 Ma, 555 ± 11 Ma, and 555 ± 8 Ma, is interpreted as a maximum age of deposition for the clastic sediments of the unit. The minimum age of deposition of the Tillery Formation is constrained by the age of felsic volcanism in the overlying Cid Formation. The Tillery Formation was therefore deposited later than the ~552 Ma minimum age of detrital zircons but before 547 ± 2 Ma, the U-Pb zircon date obtained on a dacite flow from the Flat Swamp member (Hibbard *et al*., 2006).

The dates obtained for the youngest zircons in the Cid Formation (ca. 540 Ma) overlap within uncertainty with a younger 540 ± 1.2 Ma age for the Flat Swamp member (Ingle *et al*., 2003). These data suggest that sedimentation was coeval with magmatism and that the ca. 540 Ma age of the youngest zircon therefore approximates the depositional age of the Cid Formation. Assuming a conformable contact between the Flat Swamp member and overlying Yadkin Formation, the youngest zircons in the Yadkin

Formation (528 ± 8 Ma, 533 ± 10 Ma, 538 ± 11 Ma, and 541 ± 16 Ma) establish both a maximum age of ca. 528 Ma for the Yadkin Formation and a minimum age for the Cid Formation. Obviously, it is impossible for the Cid Formation to have been deposited prior to 540 Ma, thus deposition of the sedimentary protolith to the Cid Formation must have occurred during the ca. 12 m.y. time interval available between 540 and 528 Ma.

It should be noted, however, that the minimum ages of detrital zircons suggests sedimentation for the entire Uwharrie-Albemarle sequence between ca. 555-528 Ma, a time interval that is approximately equivalent to the analytical error obtained from the individual zircon analyses. Taking into account these uncertainties, the detrital zircon data suggests a relatively short time span between local magmatism, uplift, erosion and deposition of the clastic sedimentary precursors to the Uwharrie-Albemarle sequence. The previous age assignments of Middle Ordovician and Late Cambrian for the Tillery and Cid formations, respectively, of Koeppen *et al*. (1995) are opposed (but not disproved) by these new isotopic data that support a latest Neoproterozoic (Ediacaran) to Early Cambrian depositional age. These ages are also compatible with the presence of the Ediacaran fossil *Aspidella* in the Cid Formation (Weaver *et al*., 2006).

Provenance

Determining the provenance of metasedimentary rocks is important because knowledge of the nature, age and source(s) of detrital zircons have significant implications for the tectonic and paleogeographic evolution of ancient orogens (e.g. Cawood *et al*., 2003; Wintsch *et al*., 2007). In order to place constraints on the Neoproterozoic-early Paleozoic evolution of Carolinia and its surrounding source regions, it is necessary to compare the detrital zircon age spectra from Carolinia with that from cratons with known and distinct ages of its constituent zircon generating terranes. This method however, requires a prior knowledge of the age distributions of these potential provenances and crustal blocks. Complexities in natural processes such as differences in zircon fertility in protosource rocks, mineral density fractionation during transport, sedimentary recycling and loss of zircons due to mechanical abrasion can affect the zircon content of the sample and therefore illustrate the inherent limitations in provenance analysis. Nonetheless, most studies of provenance analysis can be solved by analyzing a sufficient amount of zircon grains (ca. 60-70) in order to detect age populations that have low abundances in the sediment, and visually comparing these data to the ages of rocks in potential protosource terranes.

Paleomagnetic, faunal, isotopic and geological data support the premise that Carolinia was positioned along the margin of west Gondwana in the Neoproterozoic-early Paleozoic (Secor *et al*., 1983; Samson *et al*., 1990; Ingle *et al*., 2003; Hibbard *et al*., 2007). However, its precise position with respect to other peri-Gondwanan terranes and its source craton(s) in Gondwana are unconstrained. The ages of detrital zircons presented in Table 1.1 allow some inferences about provenance and timing of assembly of the various terranes present in Carolinia. The late Archean, early Paleoproterozoic to late Mesoproterozoic and Neoproterozoic detrital zircons in Carolinia indicate a varied provenance. A comparison between the U-Pb detrital zircon ages from Carolinia and the age of tectonothermal and magmatic events in potential source areas is shown in Figure 1.9. Although most potential source areas contain late Neoproterozoic, Paleoproterozoic and Archean rocks suggesting several possible sources, there are several distinct differences in the ages of these tectonothermal and magmatic events within the principal lithotectonic units recognized along the margins of west Gondwana and Laurentia.

Archean, Paleo- and Mesoproterozoic zircons— Archean detritus is rare in the rocks analyzed from Carolinia. The oldest detrital zircons in Carolinia are obtained from the Tillery Formation and comprise only two Neoarchean zircons, which correspond to the timing of crust formation (2.5-2.8 Ga) in the central-Amazon craton (Sadowski and Bettencourt, 1996). Early Mesoproterozoic and Paleoproterozoic (1400-2500 Ma) zircons comprise only a minor (5-20%) component in three samples, but the number of Proterozoic (and Archean) grains may be slightly under represented because discordant grains were discarded from the data set and not included in the cumulative probability plots. Nonetheless, these ages correspond to Ventuari–Tapajós and Rio Negro–Jurena orogens of Amazonia (Tassinari *et al*., 2000). The ca. 2.10-1.87 Ga Ventuari–Tapajós tectonic province records an arc-continent collision and shows widespread calc-alkaline arc magmatism represented by the Cuiú–Cuiú complex (ca. 2.10-1.92 Ga) followed by generation of post-tectonic calc-alkaline to subalkaline plutonic suites of the Parauari magmatic event between ca. 1.88-1.87 Ga (Juliani *et al*., 2002). The Rio Negro–Juruena orogen was formed in two distinct tectonomagmatic events caused by the accretion of juvenile material to the Amazon craton and formation of the Alto Jauru terrane at 1.80–1.75 Ga. which was followed by intrusion of rapakivi granite suites of the Serra da Providência Intrusive Suite between 1606 and 1532 Ma (Geraldes *et al*., 2001).

Late Mesoproterozoic-early Neoproterozoic zircons—Detrital zircons with ages between 900 Ma to 1500 Ma comprise a small but significant number of detrital grains in four of the analyzed samples. These Proterozoic age clusters correspond to successive episodes of magmatism, metamorphism, and deformation between 1550 and 970 Ma in the Rondônia–San Ignacio and Sunsás–Aguapeí provinces in the southwestern Amazon craton (Bettencourt *et al*., 1999). Rocks representing the Cachoeirinha magmatic event consist of calc-alkaline plutons that have U-Pb zircon ages from 1560 to 1540 Ma and are interpreted as the roots of a continental margin arc built upon basement comprised of the Rio Negro–Juruena province. Widespread 1520–1310 Ma magmatism in Rondônia is interpreted to represent anorogenic magmatism, related to subduction and continental margin collapse during the final stages of the Rondônian–San Ignacio orogeny (Sadowski and Bettencourt, 1996). The Rondônia–San Ignacio province was intruded by a variety of late Mesoproterozoic (1.3–1.0 Ga) granitic plutons (Bettencourt *et al*., 1999; Geraldes, 2000).

There is ample evidence of ca. 1000 Ma orogenesis in the Amazon craton manifested as deformation, metamorphism and plutonism in the Sunsás orogeny. Magmatic rocks of the Sunsás orogeny are represented in the Amazon craton by voluminous rapakivi and AMGC magmatic suites with associated subordinate mafic plutonic and intermediate to felsic volcanic rocks, intruded in several distinct episodes between 1080–1075 Ma and 995–950 Ma (Sadowski and Bettencourt, 1996; Dall'Agnol *et al*., 1999) and related to the collision of Amazonia with southern Laurentia (Hoffman, 1991; Dalziel, 1997). However, some of the Proterozoic and Archean ages also correspond to the Eburnian (1900–2200 Ma) and Liberian (>2500 Ma) orogenic events of the West African craton (Nance and Murphy, 1996). This part of Gondwana, however, contains only minor occurrences of early Neoproterozoic magmatism (ca. 1000 Ma, de

Witt *et al*., 2005) and no record of a Mesoproterozoic orogenic event thereby negating a West African provenance for Carolinia.

On a broad scale, there is a remarkable correspondence between the orogenic events in Amazonia and the geological history along the eastern and southern margins of Laurentia and Baltica. Archean to early Neoproterozoic rocks are present in Laurentia and correspond with Archean cratons (North Atlantic, Superior) welded by Paleoproterozoic orogens (1.8-1.6 Ga; Torngat, New Quebec, Makkovik, Ketilidian) which are in turn overprinted by Rigolet, Ottawan, and Shawinigan orogenesis (1200-980 Ma) (Gower and Krogh, 2002). However, these Laurentian terranes are unlikely sources for the Carolinian rocks several reasons: (1) the presence of 1600-1520 Ma zircons in the analyzed samples is inconsistent with a Laurentian source. Although 1600-1520 Ma magmatism and orogenesis are common within Amazonia, rocks of this age are noticeably absent from the Paleoproterozoic orogens of Laurentia (Gower and Krogh, 2002); (2) the samples from Carolinia contain no zircons with ages between 1700-1630 Ma that correspond to the Labradorian or Svencofennian orogenies in Laurentia and Baltica (Van Schmus *et al*., 1993; Rivers, 1997) whereas Amazonia lacks any magmatic activity between 1700–1630 Ma and contains no evidence for orogenesis during this period; and (3) a link between Carolinia and Amazonia is also consistent with "Acado-Baltic" fossils (Samson *et al*., 1990) that are considered exotic to Laurentia and similar to Gondwanan faunas.

Late Neoproterozoic-early Paleozoic zircons—The largest age population (>75%) common to all analyzed samples spans the late Neoproterozoic (Ediacaran) and early Paleozoic (Cambrian). The distribution of ages ranges from ca. 670 Ma to 530 Ma, with most zircons falling in a fairly restricted time interval between ca. 610 Ma and 550 Ma. Rocks of this age range occur within peri-Gondwanan arc systems from Carolinia that record the history of Neoproterozoic magmatic arc/sedimentary terranes and their ensuing Paleozoic evolution.

The peak of detrital zircon ages at ca. 670 Ma, corresponds with plutonic rocks of the Roanoke Rapids complex (672 ± 2 Ma U-Pb zircon ID-TIMS, Coler and Samson, 2000). The spread of detrital zircon ages from the Roanoke Rapids and Aaron Formation samples that range from 630 and 600 Ma, with a pronounced peak at ca. 620 Ma, overlaps the age range (633 and 612 Ma) of arc magmatic rocks of the Virgilina sequence (Wortman *et al*., 2000). This span also is coeval with a phase of granitoid intrusion in the Roanoke Rapids complex at ca. 615 Ma (Coler and Samson, 2000).

The continuous span of detrital zircon ages between ca. 570 to 540 Ma closely corresponds with vestiges of Ediacaran-Early Cambrian rocks of the Albemarle sequence. These rocks not only include the Uwharrie, Tillery, and Cid formations but the the Morrow Mountain rhyolite, which is intrusive into each of these formations (Ingram, 1999) and is dated by U-Pb ID-TIMS on zircon at 539 ± 6 Ma (Ingle *et al*., 2003). Ediacaran-Early Cambrian zircons could also be derived from felsic volcanic rocks of the Persimmon Fork Formation in the South Carolina sequence, which is along strike of and considered equivalent to the Albemarle sequence and has a range of U-Pb ages between 580–545 Ma (Barker *et al*., 1998).

Ediacaran to Early Cambrian detrital zircons in the analyzed samples also overlap with another episode of widespread magmatism in Carolinia, in the Charlotte terrane. The Charlotte terrane is dominated by plutonic rocks that were intruded into a suite of principally metaigneous rocks in two major magmatic pulses: ca. 570 Ma and ca. 540-530 Ma. The best evidence for this magmatism is preserved in the Means Crossroads complex which contains foliated metadiorites that intrude deformed mafic volcanic rocks and are dated by U-Pb zircon (ID-TIMS) at 579 ± 4 and 571 ± 16 Ma (Dennis and Wright, 1997). Syn- and post-tectonic dioritic phases of this complex yield U-Pb zircon ages of 538 ± 5 and 535 ± 4 Ma, respectively.

The close correspondence of detrital zircon ages between all samples from Carolinia, albeit in varying proportions in each unit, including large late Neoproterozoic and Paleozoic age populations as well as very few Mesoproterozoic and Paleoproterozoic grains, suggests an overall common provenance for all of these rocks. The detrital zircon ages older than ca. 700 Ma can be correlated with Ventuari–Tapajós, Rio Negro–Jurena, Rondônia and Sunsás orogenic sources that are characteristic of the Archean Amazon craton and its peripheral Proterozoic orogenic belts. The younger late Neoproterozoic and Paleozoic age population, on the other hand, are consistent with derivation from the plutonic and volcanic rocks from Carolinia that have stratigraphic links to rocks with faunal, isotopic and tectonomagmatic features (Hibbard *et al*., 2002) that are characteristic of a peri-Gondwanan setting. Collectively, the data support the interpretation that the rocks of Carolinia formed adjacent to the Amazonian margin of west Gondwana.

Tectonic setting

Most paleogeographical reconstructions (e.g. Nance and Murphy, 1994; Keppie *et al*., 1996; Dalziel, 1997; Cocks and Torsvik, 2002) show the Amazonian margin of west

Gondwana facing an open ocean during most of the Neoproterozoic and early Paleozoic. The igneous and sedimentary rocks of Carolinia that record this evolution, have been interpreted as episodic (ca. 670–540 Ma) Neoproterozoic subduction followed by early Paleozoic sedimentation and accretion to Laurentia in the early to middle Paleozoic. The U-Pb detrital zircon data presented herein concerning provenance and ages of deposition of these sediments constrain plate tectonic scenarios for the Neoproterozoic to early Paleozoic history of Carolinia and may provide important constraints on the tectonic history of other peri-Gondwanan terranes in the Appalachian orogen.

The abundant ca. 670 Ma age detritus in the Roanoke Rapids complex is consistent with derivation from the underlying felsic to intermediate volcanic–plutonic rocks that are interpreted to record island arc magmatism at 672 ± 2 Ma (U-Pb zircon; Coler and Samson, 2000). The high Th/U ratios and low U contents in the detrital zircons, however, are comparable to mafic igneous rocks and suggest significant input from the mafic–ultramafic ophiolitic rocks of the terrane. The ca. 1050 Ma detrital zircons are here interpreted to be derived from the basement to the Roanoke Rapids volcanic arc; this interpretation is compatible with ε_{Nd} data that illustrate that the felsic rocks are variably influenced by isotpically evolved (Proterozoic) continental crust or sedimentary rocks derived from such a Proterozoic crust (Coler and Samson, 2000). The presence of detrital grains with ages between 640 and 630 Ma indicates that deposition of the sedimentary rocks of the Roanoke Rapids complex postdates the arc magmatism by ca. 30-40 m.y. and therefore requires the sedimentary rocks to lie unconformably or be faulted upon the underlying volcanic-plutonic rocks.

A post ca. 630 Ma sedimentary sequence in the Roanoke Rapids terrane corresponds in age to volcanic rocks in the Virgilina sequence. Felsic metavolanic rocks of the Hyco Formation and associated plutonic rocks indicate a ca. 20 m.y. period of arc magmatism between ca. 633 Ma and ca. 612 Ma. Although the Virgilina sequence developed above a subduction zone on the Gondwanan margin, the basement upon which the arc was developed is nowhere exposed. As a result, the nature of this substrate has been characterized indirectly from the crustally-derived felsic volcanic rocks that represent melt fractions extracted from the basement. The sequence exhibits highly positive ε_{Nd} values and model ages that are relatively close to crystallization ages of the rocks (Samson *et al*., 1995) which implies that the Virgilina sequence is composed of juvenile, largely mantle-derived crust and does not contain a significant component of mid-Proterozoic or older recycled material.

This interpretation is in contrast to Glover and Sinha (1973) who interpreted the significant quantities of felsic plutonic rocks and the presence of quartz arenite clasts in overlying Aaron Formation to indicate that the basement to the Virgilina sequence is some form of continental crust. The detrital zircons from the Aaron Formation consist dominantly of grains with ages equivalent to the Virgilina sequence (630-610 Ma), which is consistent with interpretation of the volcanic rocks of the Hyco Formation as the principal source for the conglomerates of the Aaron Formation. The presence of detrital zircons in the Aaron Formation that are much younger than the Hyco Formation however, implies a significant interval between eruption of the Hyco volcanics and deposition of the Aaron conglomerates. The age of the youngest detrital zircon from the Aaron Formation analyzed in this study at ca. 588 Ma corresponds within error to the youngest detrital zircon age (ca. 578 Ma) reported by Samson *et al*. (2001) and confirms that the maximum time of deposition of the formation is approximately 35 m.y. after the ca. 615 Ma minimum age of the Hyco Formation. Thus, the detrital zircon ages imply a disconformable relationship between the two formations and preclude a direct relationship between the Aaron Formation and the basement to the Virgilina sequence. The presence of significant detrital zircons with Paleoproterozoic to early Neoproterozoic ages in the Aaron Formation is inconsistent with recycling of such zircons from the underlying Neoproterozoic sedimentary and volcanic units. Thus, their presence in the Aaron Formation implies incorporation of Mesoproterozoic and Paleoproterozoic continental cratonic rocks from the distant Gondwanan orogenic hinterland.

A maximum age of ca. 578 Ma for the Aaron Formation is also critical to constraining the age of the Neoproterozoic deformational events in Carolinia. The age of the Virgilina orogeny was previously bracketed between the 612 +5/-2 Ma age of the youngest pre-deformation pluton and the 551 ± 8 Ma age for the unconformably overlying Uwharrie Formation (Wortman *et al*., 2000; Ingle *et al*., 2003). The Virgilina sequence is folded into a series of tight to close, northeast plunging folds which is attributed to the Virgilina deformation (Harris and Glover, 1988). The single ca. 588 Ma grain identified in the Aaron Formation therefore provides a maximum limit of the timing of this deformation. This limit can be constrained even younger by using the ca. 578 Ma age (Samson *et al*., 2001). The Uwharrie Formation is undeformed by this event and is inferred to lie unconformably upon the Aaron Formation. Thus, the timing of Virgilina deformation is constrained to a ca. 25 m.y. period between 578 Ma and 554 Ma.

The timing of this deformation event is contemporaneous with a folding, faulting and foliation deformational event in the western portion of the Charlotte terrane (Dennis and Wright, 1997). U-Pb ages from mafic metavolcanic rocks that are intruded by granodiorite and diorite plutons of the Means Crossroads complex, bracket the age of deformation between ca. 580 to 538 Ma (Dennis and Wright, 1997). This Neoproterozoic deformation has been variously attributed to either: (1) rifting of the Virgilina arc and opening of a back-arc basin that subsequently led to subsidence and submergence of the Virgilina sequence (Feiss *et al*., 1993); or (2), arc-arc collision that was ultimately responsible for amalgamation of the Charlotte and Carolina terranes (Dennis and Shervais, 1996; Barker *et al*., 1998; Hibbard and others, 2002).

Given that the presence of Mesoproterozoic and Paleoproterozoic detrital zircons in the Aaron and Tillery formations implies exposure of older rocks of the cratonic hinterland, the merger of the Carolina and Charlotte terranes, as suggested in the arc-arc collision model of Dennis and Shervais (1996) is best for explaining the variation in detrital zircon ages. The termination of convergence in a Moluccan Sea-style arc-arc collision in the late Neoproterozoic (578-554 Ma) provides both a mechanism for exposing older cratonic rocks from either a frontal thrust sheet or from the hinterland with the development of a varied topography with significant relief and a switch from localized to extensive transverse drainage systems.

The clastic rocks of the Uwharrie Formation and Albemarle Group contain a narrower range of detrital zircon populations than underlying rocks. The Uwharrie, Tillery, Cid, and Yadkin formations all contain Ediacaran zircons. Although these units have a similar provenance, indicating a potential spatial relationship with, and derivation from a common protosource, the time of deposition varies based on constraints from the age of the youngest detrital zircon population. The Uwharrie Formation contains abundant zircons that are coeval with the late Neoproterozoic depositional age (ca. 545 Ma) of the unit and the age of the Flat Swamp member of the Cid Formation. These data suggest that deposition occurred synchronously with magmatism in a tectonically active volcanic arc environment (Figure 1.10).

The overlying Tillery Formation is dominated by the same Ediacaran zircon population which suggests either a common protosource or recycling of sediment. However, the presence of detrital age peaks in the Tillery Formation in the Mesoproteorozoic, Paleoproterozoic and Archean indicates that the Tillery Formation also sourced a different and significantly older protolith. The juvenile Nd isotopic character and absence of U-Pb zircon inheritance (Mueller *et al*., 1996; Ingle *et al*., 2003) in plutonic rocks of Carolinia argue against an older continental crustal basement beneath the Albemarle sequence. Thus, the Tillery Formation was in all probability built upon a juvenile basement, but derived in part from an adjacent composite terrane of dominantly Mesoproterozoic rocks with lesser quantities of Paleoproterozoic and Archean rocks.

Similarly, the paucity of detritus of Mesoproterozoic (and older) age in the Cid and Yadkin formations and the overwhelming dominance of latest Neoproterozoic age zircons is consistent with a common protosource. However, the dates obtained for the youngest zircons in these formations are similar to the age of interstratified volcanic rocks, which suggests that deposition occurred proximal to volcanic sources with the absence of older rocks.

Although there are several possible subduction-related tectonic settings for the Albemarle Group, including a forearc, foreland, or successor basin, there is, no direct evidence that the Albemarle Group formed in any of these settings. First, sedimentary facies in the Albemarle Group are inconsistent with deposition in a forearc basin, principally the absence of thick conglomerate sequences and rapid lateral and vertical facies changes. Second, the Albemarle Group is unlike typical foreland basin successions, which are dominated by coarsening-upwards sequences dominated by alluvial rocks derived from adjacent fold-thrust belts. Third, the age of deposition of the Albemarle Group is not compatible with formation in a successor basin as such a basin would have to form as a post-collisional sequence during the terminal stages of Appalachian orogenesis rather than a subduction-related succession in the late Neoproterozoic-early Paleozoic that is established by detrital zircon data. The lateral and vertical consistency of siltstone-dominated facies, proximal turbidites and thick debris flows, local sources for detritus suggested by detrital zircon ages, and contemporaneous tholeiitic igneous activity are consistent with deposition in an active plate margin setting in an arc-rift or back-arc basin.

Most tectonic models for back-arc basins mechanically link subduction-related extension with rifting of the magmatic arc and the initiation of sea-floor spreading behind the arc (Karig, 1975; Jordan, 1995). In actively spreading back-arc basins simple proximity suggests that adjacent volcanic rocks of the active volcanic arc should dominate the sources of detritus deposited in the back arc. However, some workers have shown that detrital zircons can be transported considerable distances in fluviatile environments (Rainbird *et al*. 2001), implying laterally extensive drainage systems that can cross structural barriers and extend into the orogenic hinterland providing a mechanism for transporting distal cratonic sediment sources. In addition, the enhanced relief which results from block faulting accompanying arc rifting can expose rocks of the underlying basement and thus provide another source of detritus. However, the extent to which of these processes is the dominant factor in providing detritus to the back arc basin in all probability relates to: (*i*) differences in pre-existing basin shape and size; (*ii*) provenance pathways and topographic confinement; (*iii*) extrabasinal tectonic activity; (*iv*) rates of subsidence; (*v*) changes in sea-level; and (*vi*) variations in rate of erosion and accumulation of sediment related to latitude.

Existing geological, geochemical and isotopic data (Samson *et al*., 1995; Wortman *et al*., 2000; Hibbard *et al*., 2002; Ingle *et al*., 2003) and geochronological data presented here illustrate that the Albemarle sequence records a complex and episodic history of Neoproterozoic-early Paleozoic arc magmatism and sedimentation. Interpretation of the Albemarle sequence as having formed in an arc-rift – back-arc basin setting is also supported by new geochemical and isotopic data (Chapter 2). Examples of modern back-arc basins that may be an acceptable analogue for the Albemarle sequence are the Sea of Japan, Okinawa trough and Lau Basin. It should be noted however, that there are problems in comparisons between ancient rocks and those in modern settings including: (*i*) the complex interaction of volcanic, sedimentary, tectonic and surface processes, which leads to a variety of sediment types; (*ii*) the poor preservation of ancient back-arc basins that results from subduction or incorporation of the basin into orogenic belts; and (*iii*) the need for detailed geochemical and isotopic data to isolate and identify the type of ancient tectonic basins. Although each of the modern back-arc basins have individual characteristics and display a variety of sediment types and sources, they all record the initiation of the basin by rifting of continental crust, and deep-marine sedimentation of detritus derived for the most part from the magmatic arc. As a result it is proposed that these modern analogues constitute an acceptable model for the Neoproterozoic-early Paleozoic tectonic development of the Albemarle sequence.

CONCLUSIONS

The results of this study impose important constraints on the paleotectonic relationships between clastic sequences in Carolinia, namely their sediment sources, depositional and tectonic histories. The conclusions are as follows:

1) Detrital zircons in clastic sedimentary rocks from Carolinia yield broadly similar detrital zircon U-Pb age populations containing accessory Archean, and Paleoproterozoic, minor Mesoproterozoic and early Neoproterozoic, and major Neoproterozoic-early Paleozoic zircons. These data are consistent with a common provenance and derivation from the Amazon craton and its peripheral orogenic belts on the margin of west Gondwana.

2) An age population ca. 630 Ma in the Roanoke Rapids sample implies that sedimentation is approximately 40 m.y. younger than previously considered and consequently the sedimentary rocks of the Roanoke Rapids terrane must lie unconformably or faulted upon the Roanoke Rapids complex.

3) A minimum age of ca. 588 Ma for detrital zircons in the Aaron Formation is within error of the previously reported maximum age of the Aaron Formation and thus constrains the timing of the Virgilina deformation to ca. 35 m.y. period

between ca. 578 Ma and the ca. 554-545 Ma age of the overlying Uwharrie Formation.

4) The ca. 545 Ma age of the youngest zircons in the Uwharrie Formation is coeval with magmatism in the Cid Formation and suggest several phases of rapid volcanism contemporaneous with sedimentation of the Tillery and Cid formations in a tectonically active environment.

5) The dominance of Ediacaran and early Paleozoic zircons in the Albemarle Group suggests an underlying local protosource for the original sediments. However, the presence of Mesoproterozoic and older detrital grains in one of the samples is most easily explained by exposure and erosion of an adjacent Mesoproterozoic terrane.

6) The presence of large populations of detrital zircons that have ages comparable to the inferred age of deposition of Uwharrie and Cid formations suggests that the detritus is dominated by first-cycle material and that any input from reworking of older Proterozoic sedimentary is minimal.

7) The ages of detrital zircons and underlying igneous rocks (ca. 552 Ma) in the Tillery Formation constrain its depositional age to be Ediacaran or possibly early Paleozoic. An early Paleozoic age for the deposition of the Cid Formation is also suggested by its youngest detrital zircons and contemporaneous volcanic rocks (ca. 540 Ma). Thus, the Albemarle Group is suggested to have been deposited during a relatively short time (ca. 20 m.y.) during the latest Neoproterozoic (Ediacaran) to Early Cambrian.

8) The clastic sedimentary rocks of the Albemarle Group are interpreted to represent deposition associated with Ediacaran-Early Cambrian back-arc rifting and basin generation within the Carolinia. It is speculated that Neoproterozoic subduction represented by the Albemarle sequence was disrupted by subduction hinge retreat, migration of arc magmatism, and the onset of back-arc extension. The spatial association of sedimentary sequences and volcanic rocks coupled with the ages of detrital zircons that are similar to the age of volcanism suggests that magmatism, tectonism and deposition were broadly coeval and is consistent with formation in an active tectonic setting, interpreted to be an arc-rift to back-arc basin environment.

REFERENCES

Aftalion, M., Bowes, D.R., and Vrana, S.
1989. Early Carboniferous U–Pb zircon age of garnetiferous, hyperpotassic granulites, Blanský les massif, Czechoslovakia. Neues Jahrbuch fur Mineralogie, Monatshefte, 4, p. 1452-1455.

Anderson, T.
2004. Detrital zircons as tracers of sedimentary provenance: limiting conditions from statistics and numerical simulation. Chemical Geology, 216, p. 249-270.

Barker, C., Secor Jr., D.T., Pray, J., and Wright, J.
1998. Age and deformation of the Long town meta granite, South Carolina Piedmont: a possible constraint on the origin of the Carolina terrane. Journal of Geology 106, p. 713-725.

Bettencourt, J.S., Tosdal, R.M., Leite, W.B., and Payolla, B.L.
1999. Mesoproterozoic rapakivi granites of the Rondônia Tin Province, southwestern border of the Amazon Craton, Brazil: I-reconnaissance U-Pb geochronology and regional implications. Precambrian Research, 95, p. 41-67.

Boggs, S.
1995. Principles of Sedimentology and Stratigraphy, 2nd ed., Pearson-Prentice Hall.

Bowring, S.A., Grotzinger, J.P., Isachsen, C.E., Knoll, A.H., Pelechaty, S.M., and Kolosov, P.
1993. Calibrating rates of early Cambrian evolution. Science, 261, p. 1293-1298.

Butler, J.R. and Secor Jr., D.T.
1991. The central Piedmont. *In:* Horton, W., Zullo, V. (*eds.*). The Geology of the Carolinas. Univ. of Tennessee Press, Knoxville, TN, p. 59-78.

Cawood, P.A., Nemchin, A.A., Smith, M. and Loewy, S.
2003. Source of the Dalradian Supergroup constrained by U–Pb dating of detrital zircon and implications for the East Laurentian margin. Journal of the Geological Society, London, 160, p. 231-246.

Cocks, L.R.M. and Torsvik, T.H.
2002. Earth geography from 500 to 400 million years ago. A faunal and palaeomagnetic review. Journal of the Geological Society of London. 159, p. 631-644.

Coler, D. and Samson, S.
2000. Characterization of the Spring Hope and Roanoke Rapids terranes, southern Appalachians: a U–Pb geochronolgic and Nd isotopic study. Geological Society of America Abstracts with Programs 32 (1), A-11-A-12.

Coler, D., Samson, S., and Stoddard, E.
1996. Terrane correlation and characterization in the southern Appalachians: isotopic investigation. EOS 77, p. 290.

Conley, J.F.
1962. Road Log of the Geology of Moore County, N.C, Carolina Geological Society Guidebook, 6 p.

Dall'Agnol, R., Costi, H.T., Leite, A.A., Magalhaes, M.S., and Teixeira, N.P.
1999. Rapakivi granites from Brazil and adjacent areas. Precambrian Research. 95, p. 9-39.

Dalziel, I.W.D.
1997. Neoproterozoic-Paleozoic geography and tectonics; review, hypothesis, environmental speculation. Geological Society of America Bulletin, 109, p. 16-42.

Dennis, A. and Shervais, J.
1996. The Carolina terrane in northwestern South Carolina: insights into the development of an evolving island arc. *In:* Nance, D., Thompson, M. (*eds.*), Avalonian and Related Peri-Gondwanan Terranes of the Circum-North Atlantic. Geological Society of America Special Paper, 304, p. 237– 256.

de Wit, M.J., Bowring, S., Dudas, F., and Kamga, G.
2005. The great Neoproterozoic central Saharan Arc and the amalgamation of the North African Shield. Geolgoical Association of Canada, Abstracts with programs.

Dennis, A.J. and Wright, J.E.
1997. The Carolina terrane in northwestern South Carolina, USA: age of deformation and metamorphism in an exotic arc. Tectonics, 16, p. 460– 473.

Fedo, C.M., Sircombe, K.N., and Rainbird, R.H.
2003. Detrital zircon analysis of the sedimentary record. Reviews in Mineralogy and Geochemistry, 53, p. 277-303.

Feiss, G., Vance, K., Wesolowski, D.
1993. Volcanic rock-hosted gold and base-metal mineralization associated with Neoproterozoic–Early Paleozoic back-arc extension in the Carolina terrane, southern Appalachian Piedmont. Geology, 21, 439-442.

Fullagar, P., Goldberg, S., and Butler, R.
1997. Nd and Sr isotopic characterization of crystalline rocks from the southern Appalachian Piedmont and Blue Ridge, North and South Carolina. *In:* Sinha, K., Whalen, J., Hogan, J. (*eds*.), The Nature of Magmatism in the Appalachian Orogen. Geological Society of America Memoir, 191, p. 165-179.

Gibson, G., Teeter, S., and Fedonkin, M.
1984. Ediacarian fossils from the Carolina slate belt, Stanly County, North Carolina. Geology, 12, p. 387-390.

Glover, L. and Sinha, A.
1973. The Virgilina deformation, a late Precambrian to Early Cambrian (?) orogenic event in the central Piedmont of Virginia and North Carolina. American Journal of Science, 273, p. 234-251.

Geraldes, M.,Van Schmus, W.R., Condie, K.C., Bell, S., Teixeira, W., and Babinski, M.
2001. Proterozoic geologic evolution of the SW part of the Amazonian Craton in Mato Grosso state, Brazil. Precambrian Research, 111, p. 91–128

Geraldes, M.C.
2000. Geoquımica e Geocronologia dos plutons granıticos Mesoproterozo icos do SW do Estado de Mato Grosso (SW do Crato Amazonico). Universidade de Sao Paulo, Sao Paulo-SP, Brazil, 185 p.

Gower, C.F. and Krogh, T.E.
2002. A U–Pb geochronological review of the Proterozoic history of the eastern Grenville Province. Canadian Journal of Earth Sciences, 35, p. 795-829.

Harris, C. and Glover, L.
1988. The regional extent of the ca. 600 Ma Virgilina deformation: implications for stratigraphic correlation in the Carolina terrane. Geological Society of America Bulletin, 100, p. 200-217.

Hibbard, J.
2000. Docking Carolina: Mid Paleozoic accretion in the southern Appalachians. Geology, 28, p. 127-130.

Hibbard, J. and Samson, S.
1995. Orogenesis exotic to the Iapetan cycle in the southern Appalachians. *In:* Hibbard, J., van Staal, C., Cawood, P. (*eds.*), Current Perspectives in the Appalachian–Caledonian Orogen. Geological Association of Canada Special Paper, 41, p. 191–205.

Hibbard, J.P., van Staal, C.R., and Miller, B.V.
2007. Links between Carolinia, Avalonia and Ganderia in the Appalachian peri-Gondwanan realm. Geological Society of America, Special Paper.

Hibbard, J.P., Stoddard, E.F., Secor, D.T. and Dennis, A.J.
2002. The Carolina Zone: overview of Neoproterozoic to early Paleozoic peri-Gondwanan terranes along the eastern flank of the southern Appalachians. Earth Science Reviews, 57, p. 299-339.

Hibbard, J.P., McMenamin, M.A.S., Pollock, J.C., Weaver, P.G., Tacker, R.C., Miller., B.V., Samson, S.D. and Secor, D.T.
2006. Significance of a new Ediacaran fossil find in the Carolina Terrane of North Carolina. Geological Society of America, Abstracts with Programs, Northeast Section, 38, p. 91.

Hoffman, P.F.
1991. Did the breakout of Laurentia turn Gondwanaland inside out? Science, 252, p. 1409–1412.

Ingle, S.
1999. Age and tectonic significance of the Uwharrie Formation and Albemarle Group, Carolina slate belt. Unpublished MS thesis, University of Florida, Gainesville, FL, 96 p.

Ingle-Jenkins, S., Mueller, P. and Heatherington, A.
1999. Evidence for Mesoproterozoic basement in the Carolina and other southern Appalachian terranes. Geological Society of America, Abstracts with Programs, 27, p. 397.

Ingle, S., Mueller, P.A., Heatherington, A.L. and Kozuch, M.
2003. Isotopic evidence for the magmatic and tectonic histories of the Carolina Terrane: implications for stratigraphy and terrane affiliation. Tectonophysics, 371, p. 187-211.

Ingram, S.
1999. Geology of the northern half of the Morrow Mountain Quadrangle North Carolina: a revision of the Albemarle Group. Unpublished M.Sc. Thesis, North Carolina State University, Raleigh, 109 p.

Jaffey, A.H., Flynn, K.F., Glendenin, L.E., Bentley, W.C., and Essling, A.M.
1971. Precision measurement of half-lives and specific activities of 235U and 238U. Phys. Rev. C4, p. 1889–1906.

Juliani, C., Correa-Silva, R.H., Monteiro, L.V.S., Bettencourt, J.S., and Nunes, C.M.D.
2002. The Batalha Au-granite system-Tapajo´s Gold Province, Amazonian craton, Brazil: hydrothermal alteration and regional implications. Precambrian Research, 119, p. 225-256.

Jordan, T.E.
1995. Retroarc foreland and related basins. In Busby, C. J., and Ingersoll, R. V., eds. Tectonics of sedimentary basins. Cambridge, Mass., Blackwell Science, p. 331–362.

Karig, D.E.
1975. Basin genesis in the Philippine Sea. In Ingle, J. C, Jr., Karig, D. E., *et al*., Init. Repts. DSDP, 31: Washington (U.S. Govt. Printing Office), p. 857-879.

Keppie, D., Dostal, J., Murphy, B., and Nance, D.
1996. Terrane transfer between eastern Laurentia and western Gondwana in the early Paleozoic: constraints on global reconstructions. *In:* Nance, D., Thompson, M. (*eds.*), Avalonian and Related Peri-Gondwanan Terranes of the Circum-North Atlantic. Geological Society of America Special Paper, 304, p. 369-380.

Kite, L. and Stoddard, E.
1984. The Halifax County complex: oceanic lithosphere in the eastern North Carolina Piedmont. Geological Society of America Bulletin, 95, p. 422–432.

Klein, T.L., Cunningham, C.G., Logan, M.A.V., and Seal, R.R.
2007. The Russell Gold Deposit, Carolina Slate Belt, North Carolina. Economic Geology, 102, p. 239-256.

Krogh, T.E.
1982. Improved accuracy of U–Pb zircon ages by the creation of a more concordant system using an air abrasion technique. Geochimica et Cosmochimica Acta, 46, p. 637–649.

Ludwig, K. R.
1999. Isoplot/Ex 2.01: a Geochronological Toolkit for Microsoft Excel. Berkeley Geochronology Center, Berkeley, CA.

McNaughton, N.J., Rasmussen, B., and Fletcher, I.R.
1999. SHRIMP uranium-lead dating of diagenetic xenotime in siliciclastic sedimentary rocks. Science, 285, p. 78-80.

Milton, D.
1984. Revision of the Albemarle Group, North Carolina. U.S. Geological Survey Bulletin 1537-A, A69–A72.

Mueller, P., Kozuch, M., Heatherington, A., Wooden, J., Offield, T., Koeppen, R., Klein, T. and Nutman, A.
1996. Evidence for Mesoproterozoic basement in the Carolina terrane and speculation on its origins. *In:* Nance, D. & Thompson, M. (*eds.*), Avalonian and Related Peri-Gondwanan Terranes of the Circum-North Atlantic. Geological Society of America Special Paper, 304, p. 207-217.

Nance, R.D. and Murphy, J.B.
1994. Contrasting basement isotopic signatures and the palinspastic restoration of peripheral orogens: Example from the Neoproterozoic Avalonian-Cadomian belt: Geology, 22, p. 617–620.

Nance, R.D. and Murphy, J.B.
1996. Basement isotopic signatures and Neoproterozoic paleogeography of Avalonian-

Cadomian and related terranes in the circum–North Atlantic. *In:* Nance, R.D., and Thompson, M.D., (*eds*.), Avalonian and related peri-Gondwanan terranes of the circum–North Atlantic: Geological Society of America Special Paper 304, p. 333–346.

Murphy, J.B., Gutierrez-Alonso, G., Nance, R.D., Fernandez-Suarez, J., Keppie, J.D., Quesada, C., Strachan, R.A., and Dostal, J.
2006. Origin of the Rheic Ocean: Rifting along a Neoproterozoic suture? Geology, 34, p. 325-328.

Nance, R.D., Murphy, J.B., and Keppie, J.D.
2002. A Cordilleran model for the evolution of Avalonia. Tectonophysics, 352, p. 11-31.

O'Brien, S.J., O'Brien, B.H., Dunning, G.R., and Tucker, R.D.
1996. Late Neoproterozoic Avalonian and related peri-Gondwanan rocks of the Newfoundland Appalachians. *In:* Nance, R.D. & Thompson, M.D. (*eds*.) Avalonian and Related Peri-Gondwanan Terranes of the Circum-North Atlantic. Geological Society of America, Special Paper, 304, p. 9-28.

Offield, T., Kunk, M., Koeppen, R.
1995. Style and age of deformation, Carolina slate belt, central North Carolina. Southeastern Geology, 35, p. 59-77.

Pimentel, M.M. and Fuck, R.A.
1992. Neoproterozoic crustal accretion in central Brazil. Geology, 20, p. 375– 379.

Rainbird, R.H., Hamilton, M.A., and Young, G.M.
2001. Detrital zircon geochronology and provenance of the Torridonian, NW Scotland. Journal of the Geological Society. 158, p. 15-27.

Rivers, T.
1997. Lithotectonic elements of the Grenville Province: review and tectonic implications. Precambrian Research, 86, p. 117–154.

Sadowski, G.R. and Bettencourt, J.S.
1996. Mesoproterozoic tectonic correlations between eastern Laurentia and the western border of the Amazon craton: Precambrian Research, 76, p. 213–227,

Samson, S.D.
1995. Is the Carolina terrane part of Avalon? *In:* Current Perspective in the Appalachian-Caledonian Orogen, Hibbard, J.P., van Staal, C.R. and Cawood, P. (*eds*.), Geological Association of Canada, Special Paper 41, p. 253-264.

Samson, S., Hibbard, J., and Wortman, G.
1995. Nd isotopic evidence for juvenile crust in the Carolina terrane, southern Appalachians. Contributions to Mineralogy and Petrology, 121, p. 171-184.

Secor, D.T., Samson, S., Snoke, A., and Palmer, A.
1983. Confirmation of the Carolina slate belt as an exotic terrane. Science, 221, p. 649–651.

Seiders, V.M.
1981. Geologic map of the Asheboro, North Carolina and adjacent areas. United States Geological Survey, Map I-1314.

Sircombe K.N., Stern R.A.
2002. An investigation of artificial biasing in detrital zircon U-Pb geochronology due to magnetic separation in sample preparation. Geochimica Et Cosmochimica Acta, 66, 13, p. 2379-2397.

Stromquist, A.A. and Sundelius, H.W.
1969. Stratigraphy of the Albemarle Group of the Carolina Slate Belt in Central North Carolina. U. S. Geological Bulletin, 1274-B.

Stromquist, A.A. and Henderson, J.R.
1985. Geologic and geophysical maps of south-central North Carolina. United States Geological Survey, Map I-1400.

Tassinari, C.C.G., Bettencourt, J.S., Geraldes, M.C., Macambira, M.J.B., and Lafon, J.M.
2000. The Amazonian Craton. *In:* Cordani, U.G., Milani, E.J., Thomaz Filho, A., Campos, D.A. (*eds*.) 2000. Tectonic Evolution of South America. Ac. Bras. Cienc. etc. Rio de Janeiro, p. 41-96.

Van Schmus, W.R., Bickford, M.E., Sims, P.K., Anderson, R.R., Shearer, C.K., and Treves, S.B.
1993. Proterozoic geology of the western midcontinent basement. *In:* Reed Jr., J.C., Bickford, M.E., Houston, R.S., Link, P.K., Rankin, D.W., Sims, P.K., Van Schmus, W.R. (*eds*.), Precambrian: Conterminous US Boulder, Colorado, Geological Society of America, The Geology of North America, C-2, p. 239–259.

Vermeesch, P.
2004. How many grains are needed for a provenance study? Earth and Planetary Science Letters, 224, p. 441-451.

Weaver, P.G., McMenamin, M.A.S., and Tacker, R.C.
2006. Paleoenvironmental and paleobiogeographic implications of a new Ediacaran body fossil from the Neoproterozoic Carolina Terrane, Stanley County, North Carolina. Precambrian Research, 150, p. 123-135.

Wiedenbeck, M., Allé, P., Corfu, F., Griffin, W.L., Meier, M., Oberli, F., von Quadt, A., Roddick, J.C., and Spiegel, W.
1995. Three natural zircon standards for U–Th–Pb, Lu–Hf, trace element and REE analysis. Geostandards Newsletters, 19, p. 1-23.

Williams, I. S.
2001. Response of detrital zircon and monazite, and their U-Pb isotopic systems, to regional metamorphism and host-rock partial melting, Cooma Complex, southeastern Australia. Australian Journal of Earth Sciences, 48, p. 557-580.

Wintsch, R.P., Aleinikoff, J.N., Walsh, G.J., Bothner, W.A., Hussey, II, A.M., and Fanning, C.M.
2007. Shrimp U-Pb evidence for a Late Silurian age of metasedimentary rocks in the Merrimack and Putnam-Nashoba terranes, eastern New England. American Journal of Science. 307, p. 119-167.

Wortman, G., Samson, S.D. and Hibbard, J.P.
2000. Precise U-Pb zircon constraints on the earliest magmatic history of the Carolina Terrane. Journal of Geology, 108, p. 321-338.

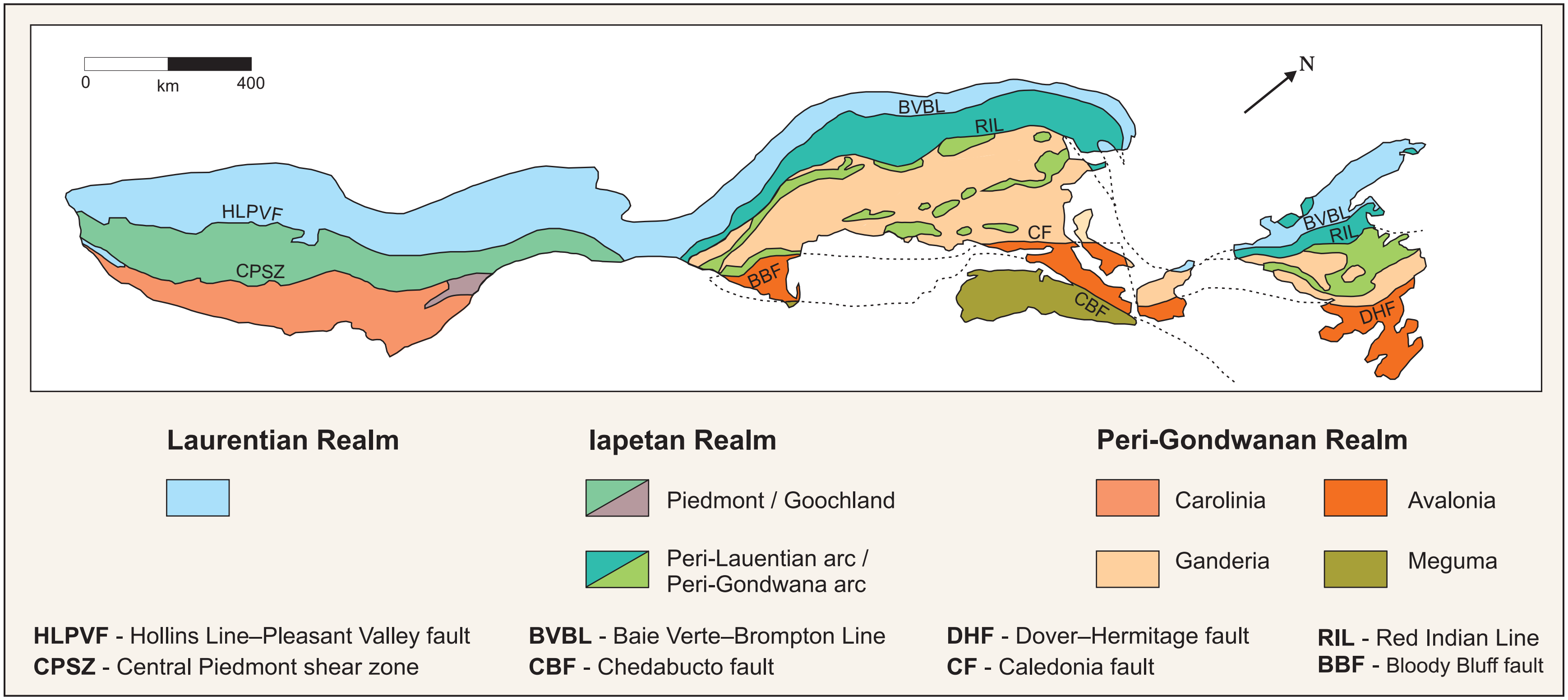

Figure 1.1. Regional geological setting of the Appalachian orogen with the distribution of peri-Gondwanan crustal blocks (modified after Hibbard *et al*., 2007).

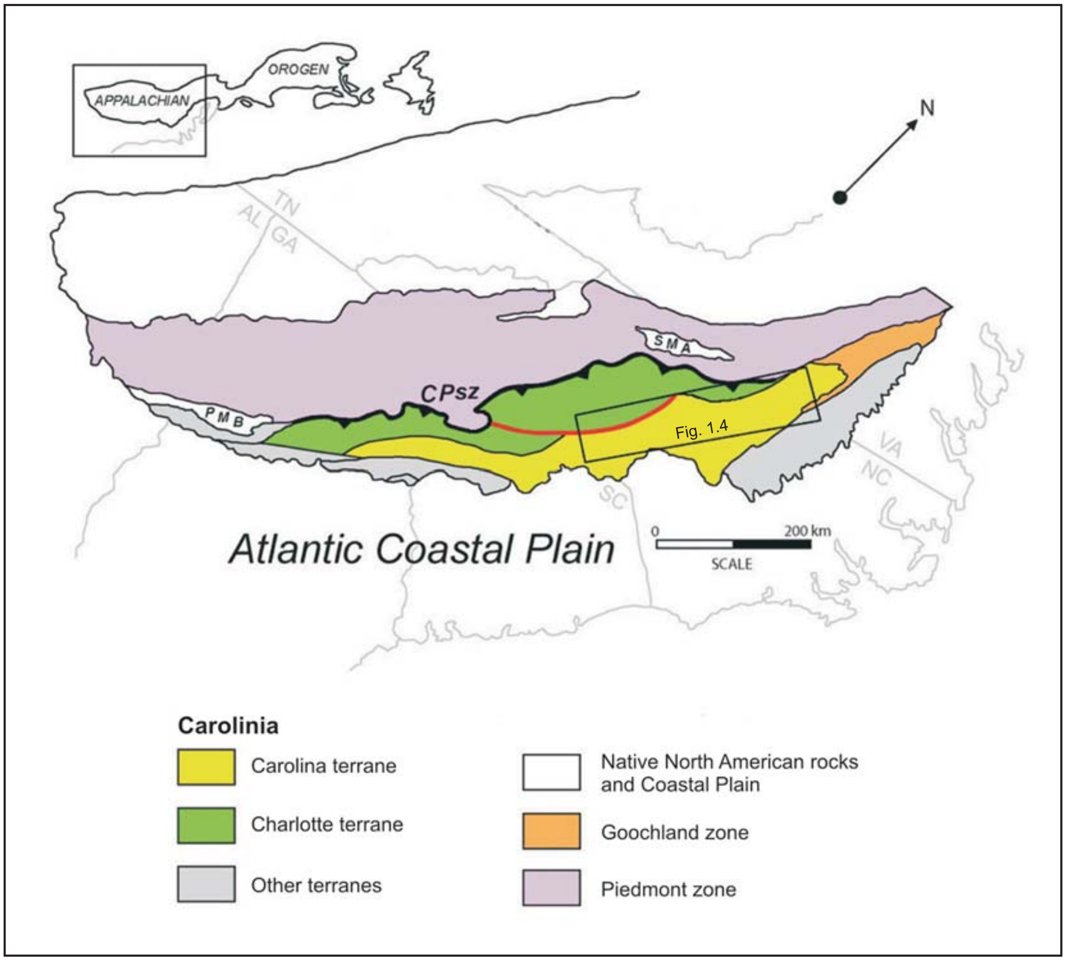

Figure 1.2. Distribution of the major tectonic elements of Carolinia and adjoining terranes (modified after Hibbard *et al*., 2002).

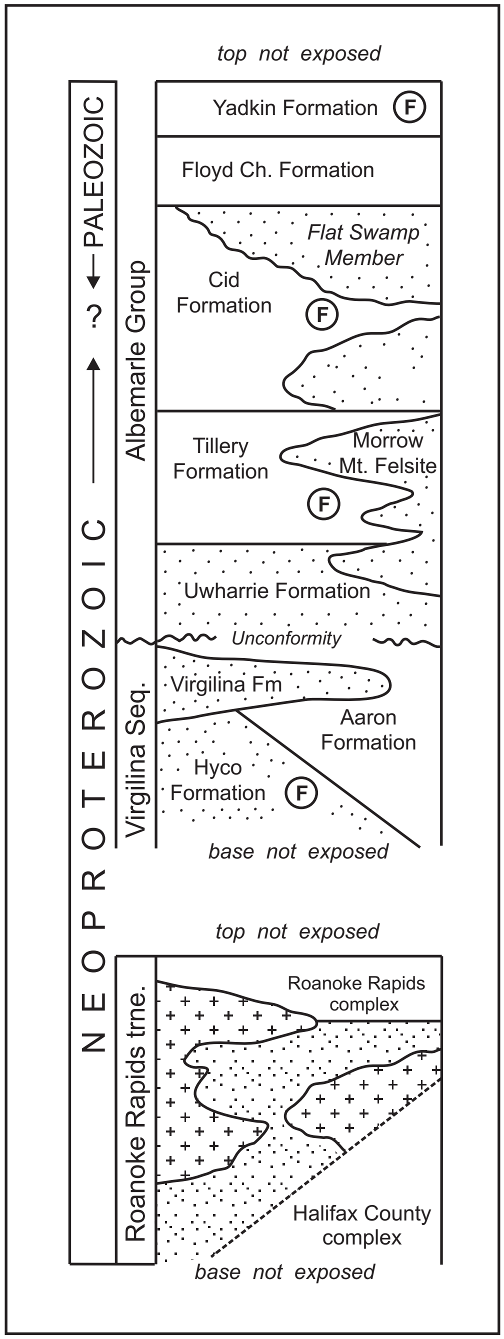

Figure 1.3. Neoproterozoic-Paleozoic stratigraphic chart for the area of study in Carolinia.

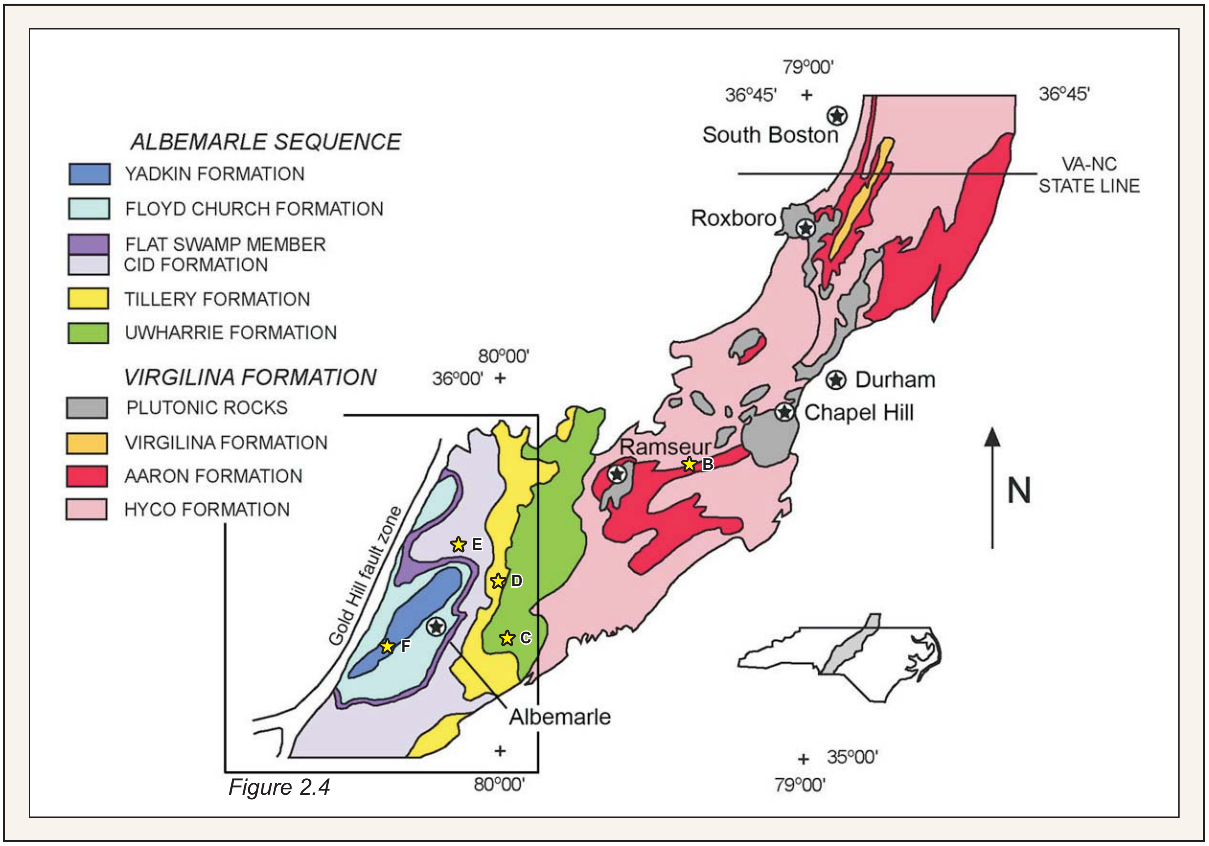

Figure 1.4. Location map of detrital zircon samples.

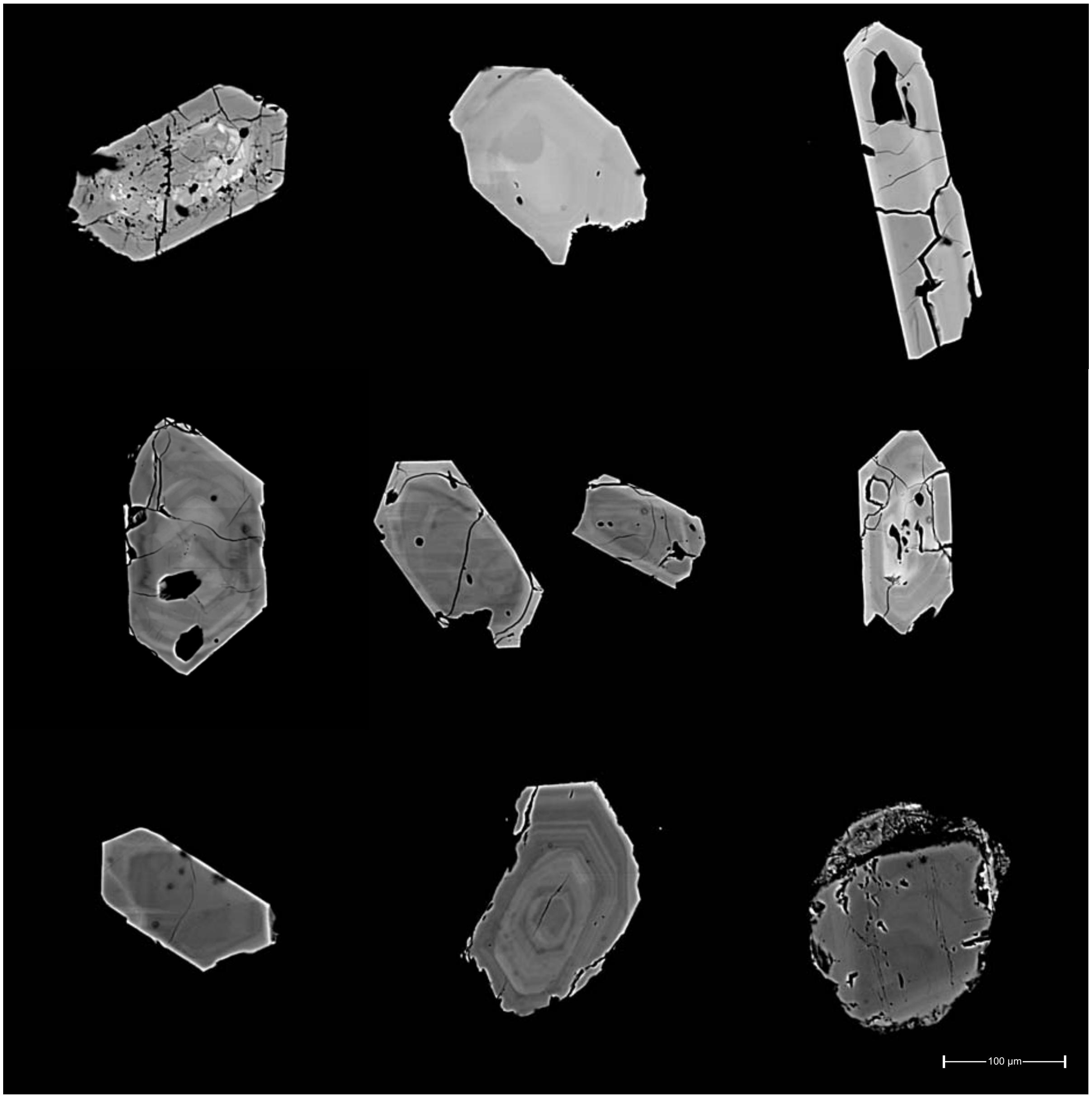

Figure 1.5. Back-scatter electron-scanning electron microscope images of typical zircons from Carolinia.

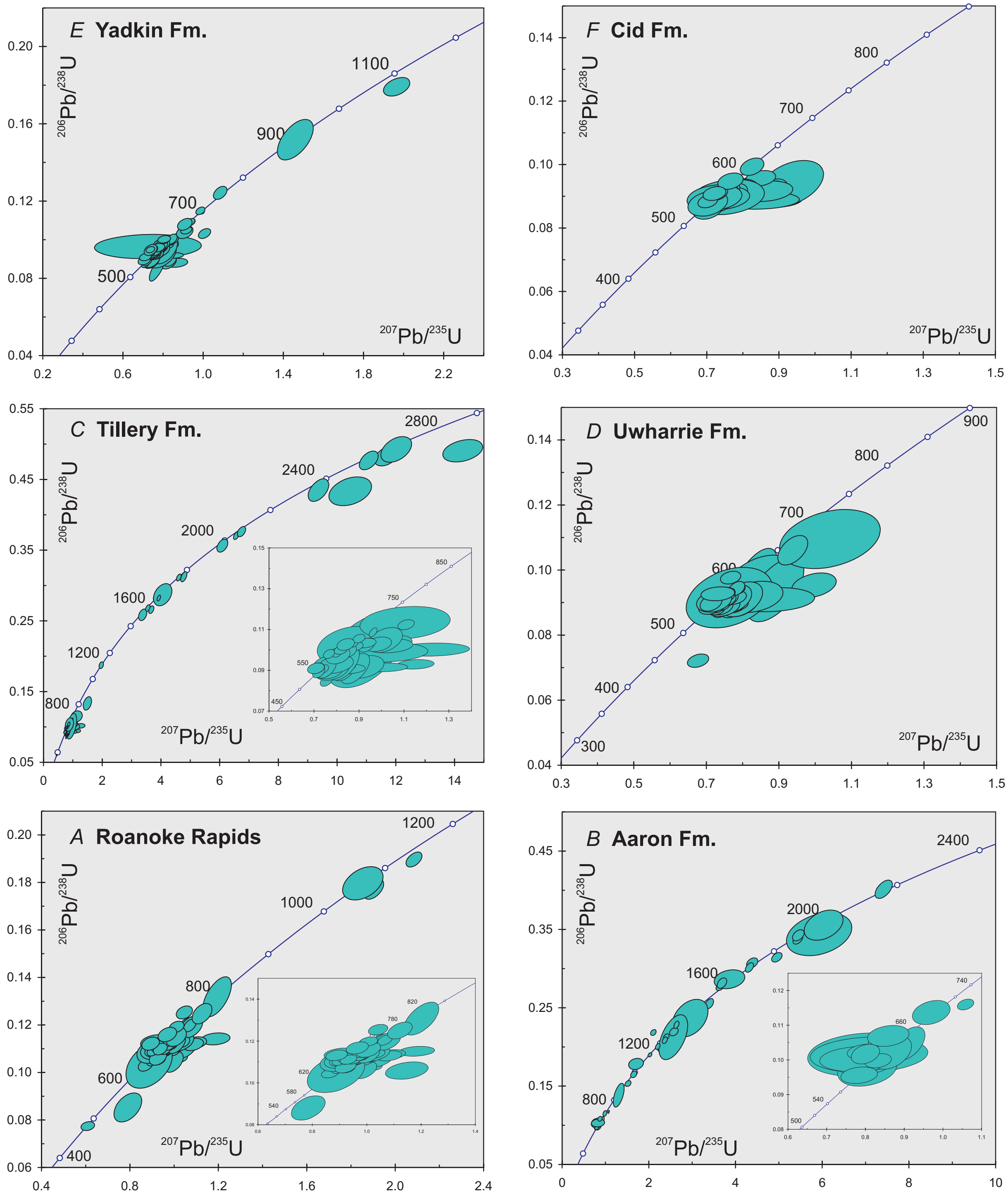

Figure 1.6. U-Pb Concordia diagrams of dated samples; ellipses are 1σ uncertainties.

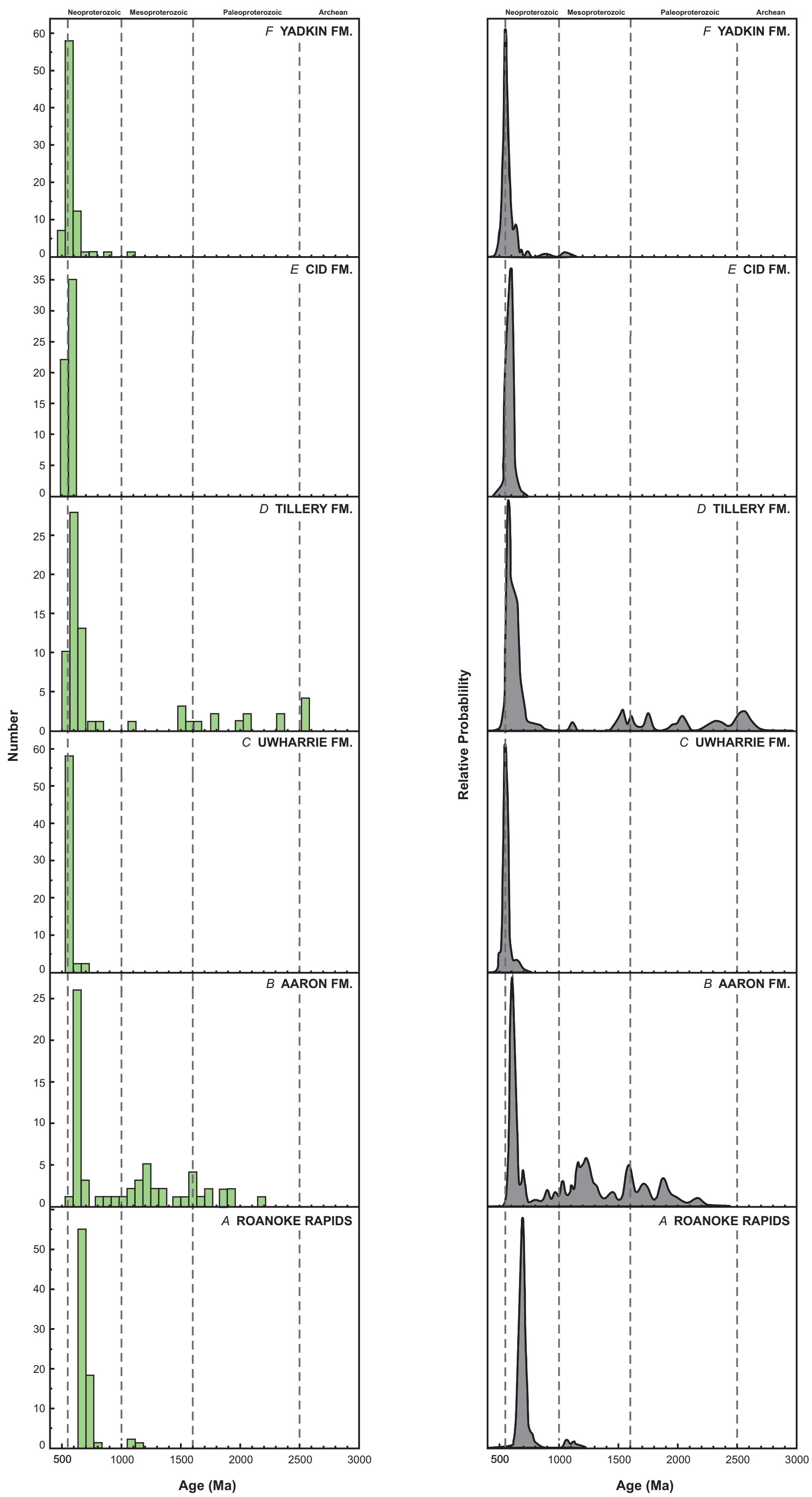

Figure 1.7. Histograms and Gaussian cumulative probability curves for analyzed samples. Only analyses within +0.15/-0.10 concordance are plotted.

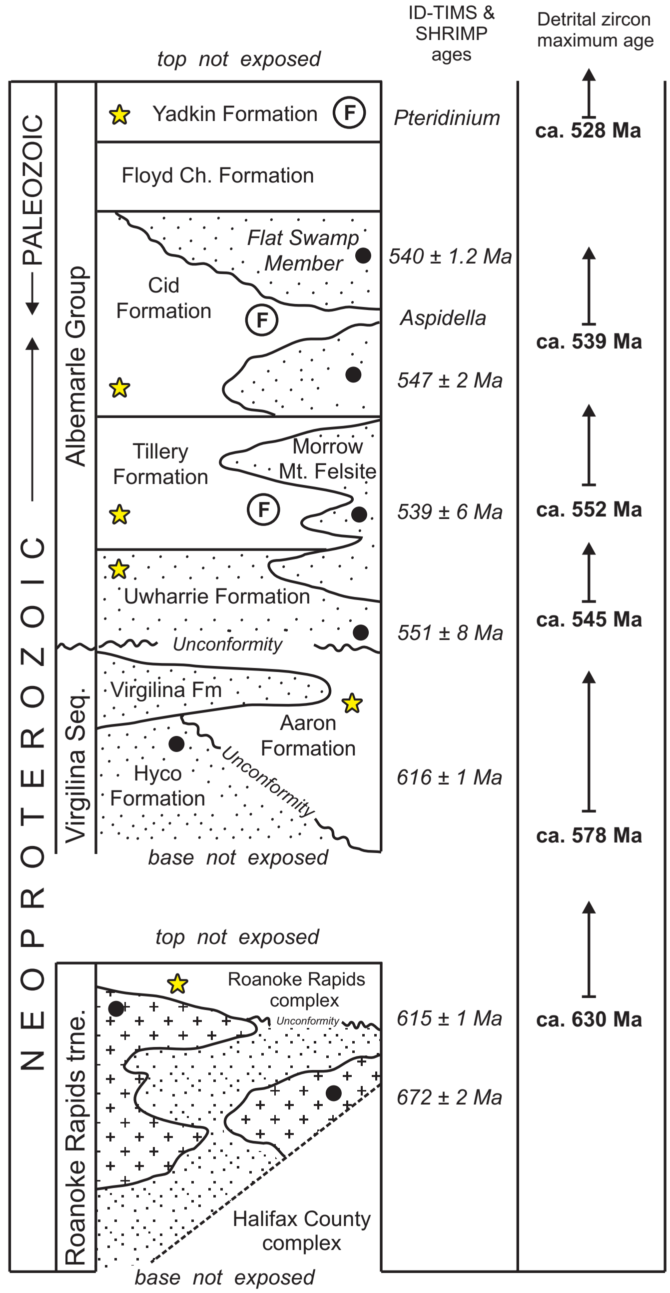

Figure 1.8. Correlation chart showing stratigraphic ranges of dated units from Carolinia. The maximum age of deposition indicated by U-Pb data suggest that the Uwharrie and Cid formations are time equivalent units and that the Aaron Formation and Roanoke Rapids complex unconformably overly underlying units.

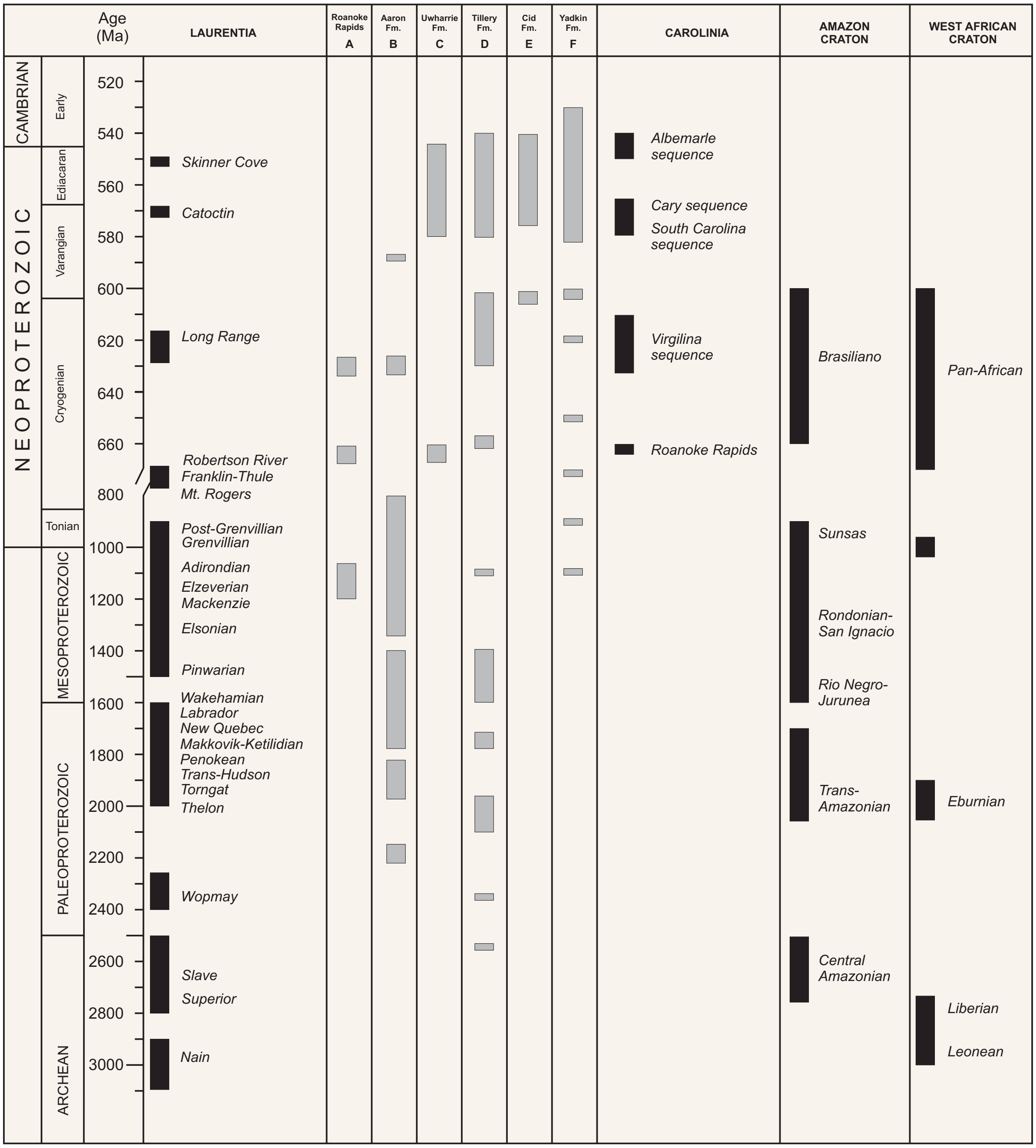

Figure 1.9. Comparison chart of detrital zircon ages from Neoproterozoic-early Paleozoic sequences of Carolinia and ages of magmatic, metamorphic and orogenic events in Laurentia (Hoffman, 1988; Gower and Krogh, 2002), Amazon craton (Sadowski and Bettencourt, 1996; Geraldes *et al*., 2001) and northwest Africa (Rocci *et al*., 1991; de Witt *et al*., 2005).

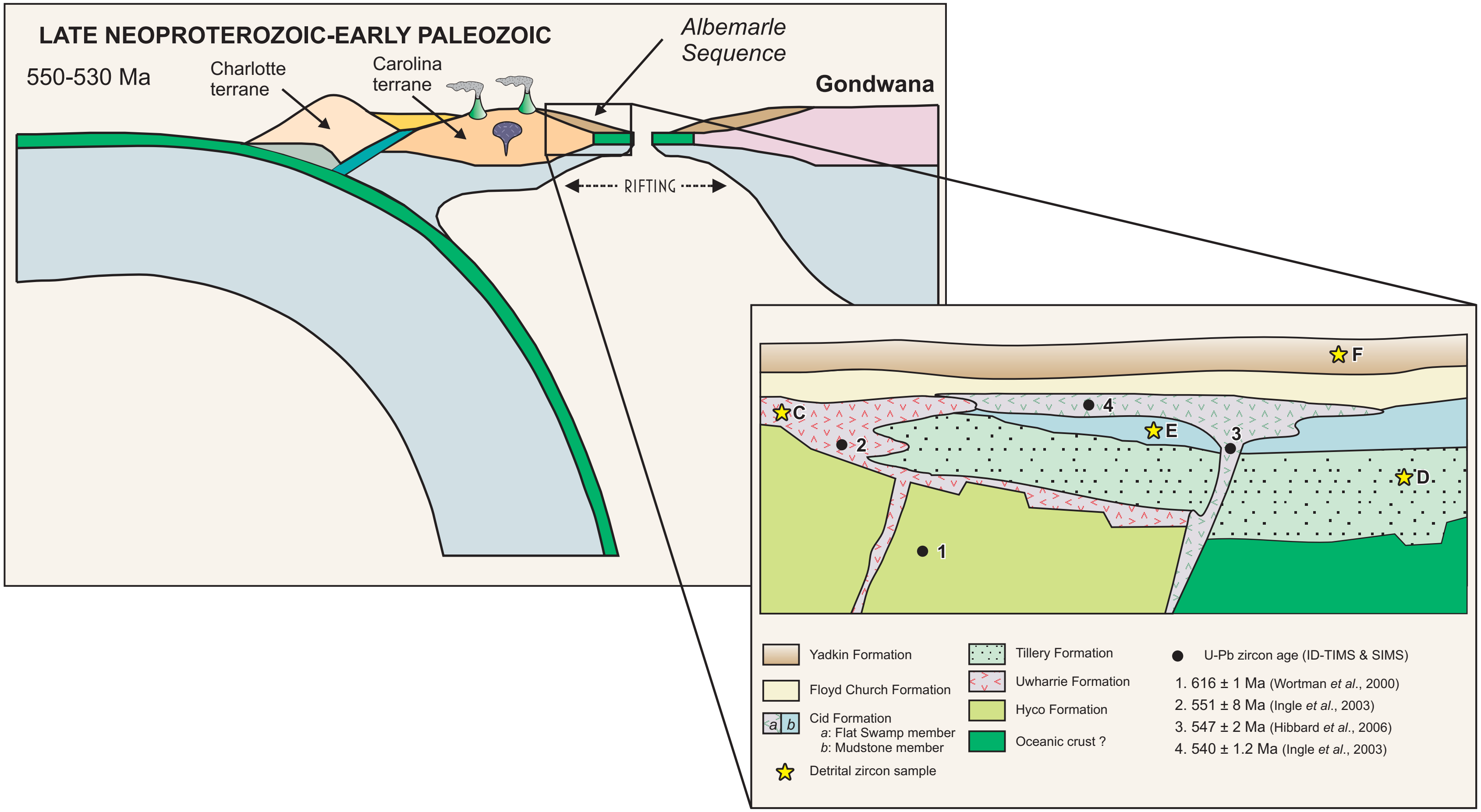

Figure 1.10. Schematic tectonic diagram for the proposed tectonic setting of the Albemarle sequence. Inset shows idealized cross-section through the Albemarle sequence showing infilling history of the proposed back arc basin. The Uwharrie Formation was emplaced on a faulted topography of the Hyco Formation proximal to an active volcanic edifice with possible hydrothermal activity. Volcaniclastic turbidites (Tillery Formation) abruptly appear in the basin, reflecting quiescence and erosion of a large stratovolcano, coupled with a shift to a more distal and more diverse source area. The Cid, Floyd Church, and Yadkin formations are marked by a change from epiclastic turbidites to felsic explosive volcanism with increasing periods of quiescence.

Table 1.1. U-Pb isotopic data of LAM ICP-MS analysis of detrital zircons.

Roanoke Rapids (36 28.763 N, 77 39.516 E)

	CONCORDIA COLUMNS					2 σ %	2 σ %							AGES Ma						
					I N T E R C E P T V A L U E S															
file	207/235	7/5 err	206/238	6/8 err	Rho	207/235	206/238	7/5 age	1σ	6/8 age	1σ	207/206	7/6 err	207/206	7/6 age	1σ	Th232 ppm	U238 ppm	Th/U	Concordance
my18a88	1.1866	0.0540	0.1138	0.0021	0.20	9.10	3.68	794.4	25.1	694.5	12.1	0.0772	0.0012	3.16	1126.0	31.4	81	72	1.117	62
my18a143	0.7873	0.0515	0.0848	0.0050	0.45	13.09	11.77	589.6	29.3	524.9	29.7	0.0671	0.0006	1.84	841.7	19.1	182	186	0.977	62
my18a11	1.0252	0.0285	0.1057	0.0016	0.27	5.56	3.04	716.5	14.3	647.7	9.4	0.0720	0.0008	2.09	985.3	21.3	97	112	0.870	66
my18a76	1.0415	0.0478	0.1100	0.0036	0.36	9.17	6.63	724.7	23.8	672.5	21.2	0.0705	0.0012	3.32	943.4	34.0	44	57	0.774	71
my18a111	1.0965	0.0401	0.1122	0.0020	0.24	7.31	3.52	751.7	19.4	685.3	11.4	0.0711	0.0010	2.88	960.3	29.5	118	129	0.914	71
my18a90	1.0847	0.0377	0.1114	0.0022	0.28	6.94	3.89	745.9	18.3	681.1	12.6	0.0694	0.0010	2.86	911.0	29.4	75	78	0.967	75
my18a50	0.9971	0.0350	0.1040	0.0035	0.48	7.02	6.75	702.3	17.8	637.9	20.5	0.0674	0.0006	1.83	849.4	19.0	230	366	0.628	75
my18a158	1.0339	0.0255	0.1109	0.0015	0.27	4.94	2.71	720.9	12.7	677.9	8.7	0.0680	0.0006	1.89	869.8	19.6	71	98	0.723	78
my18a101	0.9412	0.0240	0.1033	0.0022	0.41	5.10	4.23	673.5	12.5	633.7	12.8	0.0654	0.0006	1.79	788.7	18.8	122	123	0.985	80
my18a148	0.9938	0.0298	0.1091	0.0021	0.32	5.99	3.82	700.6	15.2	667.7	12.1	0.0665	0.0007	2.03	822.0	21.2	103	90	1.150	81
my18a119	0.9068	0.0478	0.1036	0.0037	0.34	10.54	7.16	655.4	25.4	635.7	21.7	0.0645	0.0006	1.74	757.3	18.4	111	152	0.730	84
my18a42	0.8848	0.0866	0.1028	0.0080	0.40	19.58	15.61	643.5	46.7	630.7	46.9	0.0640	0.0007	2.15	742.4	22.7	157	167	0.940	85
my18a77	0.9286	0.0263	0.1051	0.0020	0.33	5.65	3.72	666.9	13.8	644.3	11.4	0.0644	0.0006	1.75	755.5	18.5	342	164	2.081	85
my18a155	1.0244	0.0342	0.1119	0.0031	0.41	6.67	5.48	716.1	17.1	683.9	17.8	0.0656	0.0006	1.80	793.2	18.9	136	279	0.489	86
my18a10	0.9504	0.0343	0.1103	0.0021	0.27	7.21	3.88	678.3	17.8	674.3	12.4	0.0652	0.0008	2.54	780.0	26.7	100	113	0.883	86
my18a120	1.0166	0.0575	0.1128	0.0037	0.29	11.31	6.50	712.2	29.0	688.9	21.2	0.0656	0.0009	2.61	794.9	27.4	90	83	1.077	87
my18a131	0.9941	0.0291	0.1141	0.0017	0.26	5.86	2.99	700.8	14.8	696.8	9.9	0.0659	0.0007	2.06	803.3	21.6	60	78	0.764	87
my18a23	0.8964	0.0431	0.1062	0.0029	0.28	9.63	5.48	649.8	23.1	650.8	17.0	0.0640	0.0007	2.21	742.4	23.3	88	100	0.886	88
my18a52	0.8878	0.0186	0.1043	0.0014	0.33	4.19	2.78	645.2	10.0	639.3	8.4	0.0635	0.0004	1.38	723.5	14.7	103	184	0.557	88
my18a67	0.9670	0.0329	0.1109	0.0025	0.34	6.81	4.58	686.9	17.0	678.0	14.7	0.0647	0.0005	1.58	765.4	16.7	148	224	0.659	89
my18a146	0.9639	0.0255	0.1089	0.0020	0.35	5.30	3.72	685.3	13.2	666.5	11.8	0.0642	0.0005	1.50	747.2	15.8	244	166	1.466	89
my18a73	0.8680	0.0266	0.1025	0.0020	0.32	6.13	3.95	634.5	14.5	629.1	11.8	0.0629	0.0006	1.77	704.2	18.9	100	123	0.814	89
my18a20	1.0541	0.0374	0.1181	0.0038	0.45	7.10	6.41	730.9	18.5	719.8	21.8	0.0658	0.0005	1.41	801.5	14.8	229	305	0.752	90
my18a160	1.1935	0.0526	0.1315	0.0069	0.60	8.82	10.52	797.6	24.4	796.4	39.4	0.0686	0.0008	2.33	886.2	24.0	112	96	1.173	90
my18a30	0.9506	0.0439	0.1102	0.0032	0.31	9.23	5.80	678.4	22.8	673.6	18.6	0.0642	0.0007	2.14	746.6	22.6	234	210	1.114	90
my18a121	0.8974	0.0253	0.1064	0.0019	0.31	5.63	3.48	650.3	13.5	651.9	10.8	0.0633	0.0006	1.76	718.9	18.7	93	113	0.826	91
my18a63	0.9643	0.0272	0.1107	0.0020	0.32	5.64	3.60	685.5	14.0	676.7	11.6	0.0641	0.0005	1.63	743.7	17.2	110	133	0.825	91
my18a113	0.9212	0.0209	0.1078	0.0017	0.36	4.53	3.22	663.0	11.0	659.8	10.1	0.0635	0.0004	1.32	724.8	14.0	150	161	0.929	91
my18a32	0.9126	0.0418	0.1080	0.0030	0.30	9.15	5.47	658.5	22.2	661.2	17.2	0.0635	0.0007	2.19	726.3	23.2	189	165	1.148	91
my18a61	0.9014	0.0232	0.1050	0.0021	0.40	5.15	4.07	652.5	12.4	643.7	12.5	0.0629	0.0004	1.29	706.0	13.7	241	364	0.661	91
my18a51	0.8998	0.0570	0.1085	0.0041	0.30	12.66	7.63	651.6	30.4	663.8	24.1	0.0636	0.0006	1.84	726.9	19.5	97	181	0.538	91
my18a79	1.0755	0.0418	0.1189	0.0038	0.41	7.78	6.41	741.4	20.5	724.1	22.0	0.0655	0.0009	2.78	790.9	29.2	43	52	0.837	92
my18a39	0.9455	0.0259	0.1083	0.0021	0.35	5.48	3.83	675.8	13.5	662.8	12.1	0.0634	0.0006	1.78	721.2	18.9	160	243	0.660	92
my18a139	0.9119	0.0236	0.1065	0.0017	0.32	5.18	3.28	658.1	12.5	652.3	10.2	0.0630	0.0005	1.64	709.1	17.4	103	137	0.750	92
my18a161	0.9882	0.0171	0.1118	0.0012	0.31	3.47	2.17	697.8	8.8	683.1	7.0	0.0639	0.0005	1.45	737.1	15.3	123	135	0.916	93
my18a100	0.9587	0.0225	0.1104	0.0015	0.28	4.70	2.67	682.6	11.7	675.1	8.6	0.0635	0.0005	1.63	726.0	17.2	122	115	1.060	93
my18a151	1.0049	0.0238	0.1153	0.0020	0.36	4.73	3.39	706.3	12.0	703.4	11.3	0.0644	0.0006	1.92	753.4	20.3	58	72	0.812	93
my18a44	0.9110	0.0533	0.1091	0.0034	0.26	11.69	6.18	657.6	28.3	667.5	19.6	0.0632	0.0007	2.25	713.8	24.0	98	124	0.787	94
my18a136	0.9152	0.0575	0.1122	0.0027	0.19	12.56	4.81	659.8	30.5	685.6	15.7	0.0637	0.0007	2.31	731.9	24.4	48	71	0.680	94
my18a62	0.9716	0.0291	0.1126	0.0018	0.27	5.99	3.28	689.3	15.0	688.0	10.7	0.0638	0.0006	1.88	734.4	19.9	127	134	0.942	94
my18a87	1.9032	0.0372	0.1769	0.0035	0.51	3.91	3.99	1082.2	13.0	1050.1	19.3	0.0768	0.0003	0.89	1115.7	8.9	83	613	0.136	94
my18a33	0.9025	0.0299	0.1088	0.0022	0.30	6.62	3.97	653.1	15.9	665.8	12.6	0.0629	0.0006	1.92	705.0	20.4	156	176	0.890	94
my18a14	0.9537	0.0302	0.1122	0.0020	0.28	6.34	3.50	680.0	15.7	685.5	11.4	0.0635	0.0006	1.86	724.8	19.7	119	143	0.832	95
my18a89	0.9599	0.0256	0.1120	0.0017	0.28	5.33	2.95	683.3	13.2	684.6	9.6	0.0634	0.0004	1.41	723.1	15.0	120	125	0.956	95
my18a57	1.0075	0.0298	0.1182	0.0024	0.34	5.92	4.04	707.6	15.1	720.2	13.8	0.0645	0.0006	1.74	759.6	18.4	89	96	0.927	95
my18a56	1.0699	0.0222	0.1195	0.0022	0.45	4.15	3.72	738.7	10.9	727.6	12.8	0.0646	0.0005	1.55	761.6	16.3	199	162	1.229	96

Table 1.1. (continued)

my18a24	0.9454	0.0209	0.1099	0.0015	0.32	4.43	2.80	675.7	10.9	672.0	8.9	0.0627	0.0005	1.75	699.4	18.6	103	145	0.711	96
my18a86	0.9762	0.0260	0.1149	0.0018	0.30	5.33	3.17	691.6	13.4	701.4	10.5	0.0636	0.0006	1.77	728.5	18.8	136	113	1.202	96
my18a22	2.0872	0.0295	0.1895	0.0026	0.49	2.82	2.74	1144.6	9.7	1118.5	14.1	0.0784	0.0003	0.67	1157.4	6.6	485	530	0.916	97
my18a144	0.9245	0.0321	0.1057	0.0026	0.35	6.94	4.85	664.7	16.9	647.9	15.0	0.0618	0.0005	1.78	668.9	19.0	115	114	1.013	97
my18a07	0.9526	0.0244	0.1119	0.0018	0.32	5.11	3.25	679.4	12.7	683.6	10.5	0.0629	0.0006	1.86	703.8	19.8	33	71	0.465	97
my18a40	0.9009	0.0214	0.1086	0.0017	0.32	4.76	3.05	652.2	11.5	664.5	9.6	0.0623	0.0005	1.67	682.9	17.8	231	240	0.963	97
my18a147	1.0444	0.0210	0.1124	0.0017	0.38	4.01	3.06	726.1	10.4	686.8	10.0	0.0629	0.0006	1.83	704.9	19.5	100	98	1.019	97
my18a29	1.0083	0.0348	0.1119	0.0035	0.45	6.90	6.26	708.0	17.6	683.6	20.3	0.0628	0.0007	2.10	701.5	22.4	88	110	0.799	97
my18a149	1.0146	0.0157	0.1158	0.0012	0.33	3.10	2.07	711.2	7.9	706.1	6.9	0.0635	0.0004	1.28	724.5	13.6	148	212	0.696	97
my18a133	0.9885	0.0258	0.1150	0.0017	0.28	5.21	2.93	698.0	13.2	701.6	9.7	0.0633	0.0006	1.88	718.0	20.0	48	74	0.648	98
my18a68	0.9896	0.0243	0.1128	0.0020	0.37	4.91	3.60	698.5	12.4	689.0	11.8	0.0629	0.0005	1.60	704.5	17.1	137	168	0.819	98
my18a167	0.9864	0.0202	0.1109	0.0013	0.29	4.10	2.39	696.9	10.3	677.8	7.7	0.0625	0.0005	1.57	692.6	16.8	102	101	1.010	98
my18a114	0.9970	0.0248	0.1131	0.0025	0.45	4.98	4.46	702.3	12.6	690.5	14.6	0.0629	0.0005	1.74	704.9	18.5	77	95	0.810	98
my18a66	0.9809	0.0198	0.1109	0.0017	0.37	4.03	3.01	694.1	10.1	677.9	9.7	0.0625	0.0005	1.53	691.4	16.3	224	156	1.440	98
my18a21	0.9280	0.0231	0.1107	0.0017	0.31	4.97	3.09	666.6	12.2	676.9	9.9	0.0625	0.0005	1.57	690.3	16.7	102	127	0.802	98
my18a46	0.9558	0.0226	0.1093	0.0017	0.34	4.72	3.18	681.1	11.7	668.6	10.1	0.0622	0.0005	1.67	679.9	17.9	209	182	1.147	98
my18a96	0.9764	0.0184	0.1107	0.0015	0.36	3.77	2.67	691.8	9.4	677.0	8.6	0.0624	0.0005	1.55	688.2	16.6	102	126	0.803	98
my18a09	0.9296	0.0194	0.1090	0.0015	0.34	4.17	2.82	667.4	10.2	666.9	8.9	0.0621	0.0005	1.61	675.9	17.2	116	119	0.971	99
my18a159	0.9978	0.0253	0.1130	0.0020	0.34	5.07	3.47	702.7	12.8	690.2	11.3	0.0627	0.0006	1.86	696.9	19.9	88	106	0.832	99
my18a65	1.0009	0.0317	0.1137	0.0025	0.35	6.33	4.43	704.3	16.1	694.5	14.6	0.0626	0.0006	1.88	695.7	20.1	107	91	1.173	100
my18a13	0.9111	0.0183	0.1119	0.0012	0.27	4.01	2.20	657.7	9.7	683.9	7.1	0.0623	0.0005	1.48	684.5	15.8	128	140	0.915	100
my18a137	1.8549	0.0753	0.1794	0.0058	0.40	8.12	6.43	1065.2	26.8	1063.6	31.5	0.0747	0.0004	1.01	1060.4	10.2	104	297	0.352	100
my18a64	0.9479	0.0367	0.1123	0.0021	0.24	7.75	3.67	677.0	19.2	686.3	11.9	0.0622	0.0007	2.12	682.6	22.7	85	145	0.585	101
my18a25	0.9241	0.0234	0.1105	0.0019	0.34	5.06	3.46	664.5	12.3	675.5	11.1	0.0619	0.0005	1.66	669.6	17.8	99	104	0.945	101
my18a75	1.0078	0.0372	0.1145	0.0032	0.38	7.39	5.60	707.8	18.8	699.0	18.6	0.0625	0.0006	1.94	689.7	20.7	116	115	1.010	101
my18a41	0.9352	0.0256	0.1095	0.0020	0.33	5.48	3.60	670.4	13.4	669.7	11.5	0.0613	0.0005	1.71	651.3	18.4	223	201	1.109	103
my18a80	1.0100	0.0279	0.1188	0.0019	0.29	5.53	3.26	708.9	14.1	723.8	11.2	0.0626	0.0006	2.07	696.0	22.0	83	87	0.950	104
my18a124	1.1251	0.0371	0.1244	0.0036	0.43	6.59	5.71	765.4	17.7	755.9	20.4	0.0635	0.0005	1.67	726.1	17.7	126	113	1.116	104
my18a54	0.9677	0.0338	0.1156	0.0025	0.31	6.99	4.38	687.3	17.4	705.0	14.6	0.0618	0.0006	2.08	668.5	22.3	60	64	0.931	105
my18a55	1.0450	0.0296	0.1249	0.0022	0.32	5.67	3.57	726.4	14.7	758.8	12.8	0.0629	0.0007	2.16	704.1	23.0	58	70	0.838	108

Table 1.1. (continued)

Aaron Formation (35 45.480 N, 79 33.414 E)

	CONCORDIA COLUMNS					2 σ %	2 σ %						AGES Ma							
					INTERCEPT VALUES															
file	207/235	7/5 err	206/238	6/8 err	Rho	207/235	206/238	7/5 age	1σ	6/8 age	1σ	207/206	7/6 err	207/206	7/6 age	1σ	Th232 ppm	U238 ppm	Th/U	Concordance
fe19A43	0.8136	0.0242	0.0993	0.0017	0.28	5.94	3.33	604.4	13.5	610.6	9.7	0.0612	0.0006	1.93	646.2	20.7	289	275	1.050	94
fe21A65	3.3824	0.0827	0.2542	0.0053	0.43	4.89	4.19	1500.3	19.2	1460.2	27.3	0.0956	0.0021	4.33	1539.8	40.8	47	131	0.361	95
fe21A27	4.9469	0.0961	0.3137	0.0050	0.41	3.88	3.21	1810.3	16.4	1758.7	24.7	0.1133	0.0007	1.29	1852.5	11.8	190	168	1.130	95
fe19A23	1.2896	0.1014	0.1370	0.0124	0.57	15.72	18.04	841.1	45.0	827.7	70.0	0.0677	0.0057	12.15	858.8	115.0	0	2	0.126	96
fe19A53	0.8043	0.0627	0.0972	0.0040	0.26	15.59	8.21	599.3	35.3	597.7	23.4	0.0604	0.0011	3.58	617.8	38.4	56	61	0.907	97
fe21A41	2.9421	0.3367	0.2359	0.0197	0.36	22.89	16.67	1392.8	86.7	1365.1	102.5	0.0892	0.0043	9.71	1409.5	93.0	101	518	0.195	97
fe19A05	2.3547	0.0420	0.2051	0.0028	0.38	3.57	2.70	1229.0	12.7	1202.5	14.8	0.0818	0.0005	1.14	1241.4	11.2	112	373	0.301	97
fe19A28	2.3722	0.0466	0.2113	0.0032	0.38	3.93	2.99	1234.3	14.0	1235.5	16.8	0.0832	0.0004	0.99	1274.1	9.8	263	572	0.460	97
fe21A47	2.2363	0.0350	0.1968	0.0029	0.47	3.13	2.95	1192.5	11.0	1158.0	15.6	0.0798	0.0011	2.77	1191.1	27.4	151	346	0.436	97
fe19A25	2.5482	0.2717	0.2112	0.0234	0.52	21.32	22.15	1285.9	77.7	1235.1	124.5	0.0828	0.0011	2.67	1265.3	26.0	34	96	0.355	98
fe19A09	5.9234	0.6176	0.3431	0.0223	0.31	20.85	12.98	1964.7	90.6	1901.3	106.8	0.1190	0.0015	2.37	1941.8	21.0	37	50	0.745	98
fe19A59	1.7747	0.0307	0.1747	0.0025	0.41	3.46	2.85	1036.3	11.2	1037.9	13.6	0.0747	0.0004	1.18	1059.4	12.0	163	547	0.298	98
fe21A42	6.0223	0.3679	0.3547	0.0159	0.37	12.22	8.96	1979.1	53.2	1956.9	75.6	0.1220	0.0040	6.63	1985.6	59.0	174	358	0.486	99
fe21A19	0.8328	0.0235	0.1001	0.0014	0.25	5.65	2.87	615.1	13.0	614.9	8.4	0.0605	0.0006	2.03	622.2	21.8	224	324	0.691	99
fe19A19	2.3875	0.0526	0.2118	0.0032	0.34	4.41	2.98	1238.8	15.8	1238.6	16.8	0.0823	0.0007	1.70	1253.0	16.8	61	134	0.458	99
fe21A36	2.3557	0.0483	0.2075	0.0035	0.41	4.10	3.36	1229.3	14.6	1215.5	18.6	0.0813	0.0014	3.46	1228.2	34.0	76	183	0.415	99
fe21A68	5.4301	0.0961	0.3366	0.0052	0.44	3.54	3.11	1889.6	15.2	1870.4	25.3	0.1153	0.0015	2.65	1884.5	23.9	432	420	1.028	99
fe21A54	3.9969	0.0752	0.2856	0.0044	0.41	3.76	3.07	1633.6	15.3	1619.7	22.0	0.1004	0.0016	3.18	1630.8	29.5	128	193	0.665	99
fe19A58	0.7931	0.0228	0.0970	0.0019	0.34	5.74	3.91	592.9	12.9	597.0	11.1	0.0598	0.0005	1.54	595.9	16.5	336	853	0.394	100
fe19A37	0.8308	0.0247	0.0983	0.0016	0.28	5.95	3.35	614.0	13.7	604.4	9.7	0.0600	0.0007	2.22	602.6	23.5	276	382	0.723	100
fe21A51	2.0135	0.0355	0.1887	0.0022	0.33	3.52	2.31	1120.1	11.9	1114.1	11.8	0.0765	0.0012	3.27	1107.2	32.6	121	215	0.564	101
fe19A45	3.8156	0.0522	0.2810	0.0033	0.43	2.73	2.34	1596.0	11.0	1596.5	16.6	0.0978	0.0005	1.14	1583.1	10.7	120	234	0.512	101
fe19A24	0.8095	0.0245	0.0995	0.0017	0.28	6.05	3.36	602.2	13.7	611.5	9.8	0.0601	0.0007	2.47	606.0	26.9	124	156	0.793	101
fe19A26	0.7818	0.0495	0.0982	0.0018	0.15	12.67	3.70	586.5	28.2	603.8	10.6	0.0598	0.0025	7.34	597.8	75.6	307	270	1.137	101
fe19A21	0.7846	0.0848	0.1002	0.0030	0.14	21.61	6.05	588.1	48.2	615.3	17.8	0.0602	0.0010	2.98	609.1	31.1	292	373	0.783	101
fe19A57	4.3763	0.1054	0.3062	0.0053	0.36	4.82	3.47	1707.9	19.9	1722.1	26.2	0.1044	0.0008	1.59	1704.6	14.7	78	91	0.854	101
fe21A22	1.0589	0.0173	0.1159	0.0013	0.34	3.27	2.23	733.3	8.5	707.1	7.5	0.0626	0.0004	1.32	694.4	14.0	342	663	0.516	102
fe21A26	3.6241	0.0738	0.2754	0.0034	0.31	4.07	2.49	1554.8	16.2	1568.3	17.4	0.0956	0.0009	1.79	1539.2	16.8	99	158	0.626	102
fe19A56	2.5659	0.0785	0.2182	0.0043	0.32	6.12	3.90	1291.0	22.3	1272.2	22.5	0.0821	0.0009	2.12	1248.3	20.4	34	57	0.597	102
fe21A43	7.4153	0.1639	0.4006	0.0096	0.54	4.42	4.78	2162.8	19.8	2171.8	44.1	0.1321	0.0025	3.74	2125.8	32.7	76	116	0.659	102
fe21A63	5.4414	0.1099	0.3417	0.0059	0.43	4.04	3.45	1891.4	17.3	1894.9	28.3	0.1134	0.0022	3.79	1854.3	34.3	65	67	0.979	102
fe19A14	0.8338	0.0205	0.1004	0.0016	0.32	4.91	3.09	615.7	11.3	616.9	9.1	0.0600	0.0006	1.85	602.3	20.0	262	412	0.637	102
fe21A67	4.3103	0.0762	0.3004	0.0049	0.46	3.53	3.28	1695.3	14.6	1693.1	24.5	0.1012	0.0016	3.24	1646.8	30.1	143	292	0.491	103
fe19A13	2.1932	0.0479	0.1992	0.0031	0.36	4.36	3.15	1178.9	15.2	1170.8	16.9	0.0776	0.0005	1.32	1137.7	13.1	81	182	0.444	103
fe19A27	3.8525	0.2928	0.2855	0.0101	0.23	15.20	7.05	1603.8	61.3	1619.1	50.5	0.0971	0.0016	3.14	1569.3	29.0	39	59	0.672	103
fe19A33	1.6364	0.0593	0.1638	0.0036	0.30	7.24	4.35	984.3	22.8	978.0	19.7	0.0707	0.0009	2.42	947.7	24.4	82	96	0.856	103
fe19A06	2.6249	0.0523	0.2272	0.0039	0.43	3.98	3.43	1307.6	14.6	1320.0	20.5	0.0834	0.0006	1.38	1278.1	13.5	72	248	0.291	103
fe19A36	0.9115	0.0347	0.1046	0.0040	0.50	7.60	7.57	657.8	18.4	641.4	23.1	0.0604	0.0006	2.01	617.7	21.7	1084	945	1.147	104
fe21A12	0.8432	0.0495	0.1021	0.0023	0.19	11.74	4.55	620.9	27.3	626.5	13.6	0.0600	0.0009	2.65	602.0	27.9	796	889	0.895	104
fe21A21	0.8002	0.0390	0.1022	0.0019	0.19	9.76	3.66	596.9	22.0	627.2	10.9	0.0600	0.0009	2.86	602.5	29.9	268	315	0.851	104
fe21A07	0.7929	0.1169	0.1014	0.0052	0.17	29.48	10.15	592.8	66.2	622.8	30.1	0.0598	0.0013	4.38	596.7	47.2	102	94	1.086	104
fe19A12	1.5036	0.0593	0.1519	0.0032	0.26	7.89	4.16	931.9	24.1	911.7	17.7	0.0681	0.0010	2.77	870.7	28.6	125	64	1.940	105
fe21A20	0.7837	0.0389	0.0955	0.0020	0.21	9.92	4.10	587.6	22.1	587.9	11.5	0.0588	0.0010	3.02	560.4	31.4	218	181	1.206	105
fe19A44	0.8926	0.0133	0.1038	0.0013	0.41	2.98	2.47	647.7	7.1	636.5	7.5	0.0600	0.0003	1.12	603.4	12.1	389	653	0.595	106
fe21A62	3.6732	0.0913	0.2805	0.0056	0.40	4.97	3.98	1565.6	19.8	1594.0	28.1	0.0941	0.0022	4.76	1509.3	45.0	72	108	0.664	106
fe19A46	0.8571	0.0170	0.1045	0.0015	0.36	3.97	2.89	628.6	9.3	640.8	8.8	0.0600	0.0005	1.73	604.1	18.8	315	312	1.008	106

Table 1.1. (continued)

fe21A53	1.6935	0.1428	0.1771	0.0059	0.20	16.87	6.68	1006.1	53.8	1051.3	32.4	0.0712	0.0051	14.34	963.8	146.4	169	114	1.474	109
fe21A18	0.8339	0.0219	0.1052	0.0013	0.24	5.25	2.52	615.8	12.1	645.1	7.7	0.0595	0.0006	1.85	585.4	19.8	237	333	0.711	110
fe19A47	0.8666	0.0206	0.1031	0.0016	0.32	4.76	3.03	633.7	11.2	632.4	9.1	0.0591	0.0004	1.39	572.4	14.9	345	615	0.561	110
fe19A35	0.8479	0.0295	0.1042	0.0016	0.22	6.95	3.11	623.5	16.2	638.7	9.4	0.0591	0.0011	3.43	572.2	35.7	220	259	0.848	112
fe19A10	0.8680	0.0417	0.1020	0.0039	0.40	9.61	7.64	634.5	22.7	626.2	22.8	0.0587	0.0008	2.82	556.9	30.8	156	180	0.866	112
fe19A55	0.9700	0.0401	0.1136	0.0029	0.30	8.27	5.03	688.5	20.7	693.8	16.5	0.0603	0.0010	3.07	614.6	32.3	66	80	0.823	113
fe21A38	0.8686	0.0233	0.1076	0.0015	0.26	5.36	2.75	634.8	12.6	658.6	8.6	0.0587	0.0016	5.46	556.1	59.5	135	190	0.713	118
fe19A22	0.8321	0.0285	0.0997	0.0017	0.25	6.86	3.39	614.8	15.8	612.5	9.9	0.0576	0.0008	2.51	515.3	26.9	121	128	0.943	119
fe21A52	0.7996	0.0301	0.1016	0.0023	0.30	7.53	4.58	596.6	17.0	623.8	13.6	0.0576	0.0022	7.67	512.7	84.3	221	153	1.450	122
fe19A11	0.8091	0.1247	0.1014	0.0043	0.14	30.83	8.38	601.9	70.0	622.7	24.9	0.0562	0.0010	3.18	460.8	33.7	148	139	1.059	135
fe21A49	2.0910	0.0525	0.2172	0.0032	0.29	5.02	2.92	1145.8	17.2	1266.8	16.8	0.0700	0.0017	4.86	929.6	49.9	46	102	0.449	136
fe21A11	0.8586	0.0439	0.1068	0.0025	0.23	10.23	4.68	629.4	24.0	654.4	14.6	0.0554	0.0010	3.24	427.9	34.9	62	67	0.931	153

Table 1.1. (continued)

Uwharrie Formation (53 33.081 N, 79 44.083 E)

	CONCORDIA COLUMNS					2 σ %	2 σ %	AGES Ma												
					INTERCEPT VALUES															
file	207/235	7/5 err	206/238	6/8 err	Rho	207/235	206/238	7/5 age	1σ	6/8 age	1σ	207/206	7/6 err	207/206	7/6 age	1σ	Th232 ppm	U238 ppm	Th/U	Concordance
my11a43	0.8769	0.0117	0.0903	0.0008	0.35	2.67	1.85	639.3	6.3	557.5	4.9	0.0641	0.0005	1.60	744.8	17.0	598	607	0.985	75
my11a33	0.8810	0.0959	0.0907	0.0031	0.15	21.77	6.73	641.5	51.8	559.6	18.0	0.0737	0.0012	3.34	1032.0	33.8	478	403	1.188	54
my11a143	0.8896	0.0640	0.0936	0.0080	0.60	14.38	17.17	646.1	34.4	577.0	47.4	0.0645	0.0008	2.42	759.5	25.5	68	133	0.507	76
my11a147	0.8399	0.0431	0.0912	0.0016	0.17	10.26	3.47	619.1	23.8	562.8	9.4	0.0659	0.0015	4.50	803.9	47.1	195	258	0.755	70
my11a41	0.8316	0.0648	0.0915	0.0040	0.28	15.58	8.68	614.5	35.9	564.5	23.5	0.0661	0.0008	2.51	810.6	26.3	113	168	0.671	70
my11a160	1.0408	0.1136	0.1093	0.0074	0.31	21.83	13.61	724.3	56.5	668.7	43.2	0.0647	0.0007	2.16	763.8	22.8	115	187	0.614	88
my11a126	0.7912	0.0426	0.0895	0.0033	0.35	10.77	7.47	591.8	24.1	552.4	19.8	0.0645	0.0008	2.40	759.3	25.3	231	313	0.737	73
my11a34	0.7709	0.0244	0.0877	0.0016	0.29	6.32	3.69	580.3	14.0	541.9	9.6	0.0617	0.0006	1.93	664.5	20.6	124	174	0.714	82
my11a121	0.7742	0.0299	0.0885	0.0029	0.42	7.71	6.52	582.2	17.1	546.8	17.1	0.0628	0.0009	2.81	702.8	29.9	66	112	0.587	78
my11a40	0.7611	0.0238	0.0874	0.0013	0.24	6.25	2.96	574.6	13.7	540.4	7.7	0.0631	0.0007	2.31	710.5	24.6	100	157	0.637	76
my11a113	0.7957	0.0484	0.0907	0.0044	0.40	12.17	9.76	594.4	27.4	559.8	26.2	0.0637	0.0011	3.30	731.7	35.0	89	170	0.527	77
my11a137	0.8441	0.0848	0.0951	0.0076	0.40	20.09	15.93	621.4	46.7	585.3	44.6	0.0641	0.0009	2.85	746.3	30.2	97	155	0.624	78
my11a104	0.7787	0.0298	0.0894	0.0024	0.35	7.65	5.31	584.7	17.0	552.1	14.1	0.0623	0.0008	2.55	685.0	27.2	99	173	0.570	81
my11a56	0.7837	0.0248	0.0900	0.0013	0.23	6.34	2.92	587.6	14.1	555.7	7.8	0.0633	0.0007	2.20	718.0	23.3	130	171	0.760	77
my11a60	0.7914	0.0185	0.0913	0.0013	0.31	4.68	2.90	592.0	10.5	563.5	7.8	0.0612	0.0004	1.41	645.6	15.2	133	187	0.710	87
my11a155	0.7523	0.0185	0.0881	0.0021	0.48	4.91	4.70	569.6	10.7	544.5	12.3	0.0603	0.0004	1.24	612.8	13.4	213	385	0.552	89
my11a100	0.7572	0.0470	0.0891	0.0019	0.17	12.41	4.16	572.4	27.1	550.0	11.0	0.0659	0.0013	3.90	802.8	40.8	115	190	0.603	69
my11a72	0.7404	0.0206	0.0876	0.0020	0.40	5.56	4.49	562.7	12.0	541.1	11.7	0.0599	0.0004	1.18	599.8	12.7	515	526	0.980	90
my11a57	0.7523	0.0123	0.0887	0.0009	0.30	3.26	1.97	569.5	7.1	547.8	5.2	0.0609	0.0004	1.33	635.2	14.3	161	244	0.661	86
my11a105	0.7740	0.0415	0.0909	0.0036	0.37	10.72	7.96	582.0	23.8	560.6	21.4	0.0612	0.0008	2.56	645.0	27.5	66	107	0.616	87
my11a163	0.9377	0.0336	0.1058	0.0037	0.49	7.17	7.07	671.7	17.6	648.4	21.8	0.0633	0.0005	1.69	718.4	17.9	59	309	0.190	90
my11a35	0.7464	0.0368	0.0885	0.0025	0.28	9.86	5.61	566.1	21.4	546.7	14.7	0.0628	0.0007	2.38	703.1	25.4	90	139	0.647	78
my11a64	0.7429	0.0247	0.0883	0.0020	0.33	6.64	4.45	564.1	14.4	545.7	11.6	0.0600	0.0005	1.73	602.2	18.8	77	119	0.641	91
my11a32	0.7642	0.0196	0.0904	0.0011	0.23	5.12	2.37	576.4	11.3	557.8	6.3	0.0616	0.0006	1.89	659.5	20.2	148	250	0.594	85
my11a165	0.7737	0.0296	0.0913	0.0018	0.26	7.64	3.95	581.9	16.9	563.3	10.7	0.0634	0.0007	2.09	722.2	22.1	186	253	0.736	78
my11a51	0.8284	0.0531	0.0965	0.0082	0.66	12.82	17.01	612.7	29.5	593.6	48.2	0.0595	0.0005	1.58	586.3	17.2	157	221	0.710	101
my11a117	0.7650	0.0179	0.0909	0.0016	0.37	4.68	3.43	576.9	10.3	560.8	9.2	0.0591	0.0005	1.76	571.9	19.1	197	224	0.878	98
my11a55	0.7431	0.0111	0.0889	0.0009	0.33	3.00	1.99	564.2	6.5	549.3	5.2	0.0595	0.0004	1.19	586.9	12.9	145	241	0.603	94
my11a42	0.7280	0.0176	0.0875	0.0013	0.31	4.83	2.95	555.4	10.3	540.8	7.7	0.0603	0.0004	1.48	614.0	16.0	153	230	0.665	88
my11a54	0.7624	0.0978	0.0913	0.0076	0.33	25.67	16.71	575.4	56.4	563.1	45.0	0.0603	0.0006	2.02	614.0	21.8	110	173	0.632	92
my11a83	0.7574	0.0138	0.0909	0.0012	0.37	3.63	2.70	572.5	7.9	560.6	7.2	0.0590	0.0004	1.36	567.4	14.9	108	185	0.582	99
my11a140	0.7419	0.0229	0.0896	0.0020	0.37	6.19	4.53	563.5	13.4	553.0	12.0	0.0597	0.0004	1.49	593.9	16.2	189	328	0.577	93
my11a116	0.7313	0.0169	0.0886	0.0016	0.40	4.62	3.69	557.3	9.9	547.1	9.7	0.0587	0.0004	1.49	554.9	16.3	126	178	0.710	99
my11a150	0.7526	0.0235	0.0907	0.0017	0.30	6.25	3.74	569.8	13.6	559.5	10.0	0.0606	0.0005	1.76	624.0	18.9	229	325	0.705	90
my11a133	0.7857	0.0172	0.0938	0.0014	0.33	4.38	2.91	588.7	9.8	578.1	8.1	0.0594	0.0005	1.74	580.2	18.9	94	168	0.558	100
my11a111	0.7827	0.0188	0.0941	0.0018	0.39	4.81	3.79	587.0	10.7	579.5	10.5	0.0600	0.0005	1.50	603.2	16.2	85	168	0.506	96
my11a85	0.7527	0.0162	0.0913	0.0014	0.36	4.30	3.07	569.8	9.4	563.0	8.3	0.0585	0.0004	1.29	548.8	14.1	188	208	0.902	103
my11a87	0.7448	0.0150	0.0907	0.0011	0.29	4.03	2.32	565.2	8.7	559.6	6.2	0.0584	0.0005	1.77	545.0	19.3	59	88	0.672	103
my11a91	0.7234	0.0182	0.0887	0.0012	0.27	5.02	2.73	552.7	10.7	547.6	7.2	0.0604	0.0005	1.57	617.7	16.9	133	169	0.783	89
my11a71	0.7543	0.0205	0.0919	0.0020	0.40	5.44	4.38	570.7	11.9	566.5	11.9	0.0585	0.0004	1.43	547.9	15.6	98	172	0.572	103
my11a125	0.7394	0.0137	0.0908	0.0013	0.40	3.72	2.95	562.1	8.0	560.0	7.9	0.0595	0.0004	1.42	584.3	15.4	89	153	0.581	96
my11a172	0.7359	0.0242	0.0905	0.0014	0.24	6.58	3.19	560.0	14.2	558.4	8.5	0.0631	0.0006	1.86	712.6	19.7	98	160	0.615	78
my11a67	0.7304	0.0240	0.0900	0.0015	0.26	6.56	3.41	556.8	14.1	555.8	9.1	0.0593	0.0004	1.35	579.9	14.7	229	212	1.079	96
my11a53	0.7109	0.0207	0.0883	0.0017	0.33	5.83	3.83	545.3	12.3	545.3	10.0	0.0595	0.0004	1.33	585.1	14.4	178	262	0.677	93
my11a70	0.7436	0.0139	0.0916	0.0009	0.26	3.75	1.97	564.5	8.1	565.3	5.3	0.0594	0.0004	1.34	581.4	14.5	84	164	0.511	97
my11a50	0.7189	0.0170	0.0892	0.0012	0.28	4.72	2.68	550.0	10.0	551.0	7.1	0.0595	0.0004	1.27	585.6	13.7	235	299	0.787	94

Table 1.1. (continued)

my11a84	0.7109	0.0174	0.0884	0.0015	0.36	4.90	3.49	545.3	10.3	546.3	9.2	0.0573	0.0005	1.58	501.8	17.3	74	142	0.524	109
my11a61	0.7102	0.0261	0.0884	0.0019	0.29	7.34	4.31	544.9	15.5	546.0	11.3	0.0597	0.0005	1.72	591.5	18.6	80	114	0.706	92
my11a141	0.7243	0.0207	0.0900	0.0018	0.36	5.71	4.06	553.2	12.2	555.5	10.8	0.0581	0.0004	1.26	532.7	13.8	166	277	0.600	104
my11a124	0.7310	0.0175	0.0907	0.0015	0.34	4.78	3.27	557.2	10.2	559.8	8.8	0.0589	0.0005	1.76	563.4	19.2	78	126	0.615	99
my11a75	0.7186	0.0216	0.0898	0.0014	0.27	6.01	3.21	549.8	12.8	554.2	8.5	0.0586	0.0005	1.57	552.4	17.1	99	155	0.641	100
my11a171	0.7101	0.0186	0.0890	0.0014	0.31	5.24	3.21	544.8	11.1	549.4	8.5	0.0588	0.0004	1.45	558.6	15.8	105	172	0.611	98
my11a136	0.7205	0.0396	0.0902	0.0028	0.28	10.99	6.13	550.9	23.4	556.7	16.4	0.0594	0.0005	1.66	581.4	18.0	124	189	0.653	96
my11a102	0.7462	0.0195	0.0928	0.0014	0.29	5.23	3.01	566.0	11.4	572.0	8.2	0.0599	0.0005	1.66	600.0	18.0	113	166	0.683	95
my11a123	0.7221	0.0140	0.0906	0.0014	0.39	3.88	3.06	551.9	8.3	559.3	8.2	0.0583	0.0004	1.46	541.8	15.9	123	185	0.668	103
my11a142	0.7117	0.0251	0.0896	0.0021	0.33	7.07	4.60	545.8	14.9	553.2	12.2	0.0581	0.0005	1.70	534.5	18.6	96	165	0.581	104
my11a152	0.7308	0.0382	0.0925	0.0018	0.18	10.45	3.81	557.0	22.4	570.2	10.4	0.0611	0.0007	2.45	641.4	26.3	111	140	0.793	89
my11a154	0.7666	0.0230	0.0974	0.0016	0.28	6.01	3.33	577.8	13.2	599.4	9.5	0.0591	0.0006	2.10	571.5	22.9	43	76	0.570	105

Table 1.1. (continued)

Tillery Formation (35 23.688 N, 80 00.904 E)

	CONCORDIA COLUMNS					2 σ %	2 σ %						AGES Ma							
					INTERCEPT VALUES															
file	207/235	7/5 err	206/238	6/8 err	Rho	207/235	206/238	7/5 age	1σ	6/8 age	1σ	207/206	7/6 err	207/206	7/6 age	1σ	Th232 ppm	U238 ppm	Th/U	Concordance
my15a58	0.9190	0.0752	0.0915	0.0046	0.31	16.38	10.03	661.8	39.8	564.2	27.1	0.0712	0.0014	3.98	964.0	40.6	172	250	0.687	59
my16b26	1.0655	0.0576	0.1032	0.0029	0.26	10.81	5.68	736.5	28.3	633.1	17.1	0.0706	0.0011	3.22	945.7	32.9	282	558	0.506	67
my16b37	1.4744	0.1159	0.1315	0.0078	0.38	15.72	11.85	920.0	47.5	796.5	44.4	0.0809	0.0011	2.64	1219.2	25.9	53	429	0.124	65
my15a51	1.0357	0.0856	0.1019	0.0029	0.17	16.53	5.70	721.8	42.7	625.4	17.0	0.0740	0.0016	4.30	1042.2	43.4	348	232	1.502	60
my15a76	0.8819	0.0534	0.0906	0.0061	0.56	12.11	13.49	642.0	28.8	559.0	36.1	0.0686	0.0014	3.94	885.9	40.7	210	259	0.810	63
my15a56	0.8189	0.0191	0.0866	0.0015	0.37	4.68	3.47	607.4	10.7	535.4	8.9	0.0649	0.0006	1.72	770.0	18.1	330	436	0.758	70
my16b17	0.8348	0.0404	0.0899	0.0043	0.49	9.67	9.50	616.3	22.3	554.7	25.3	0.0624	0.0009	2.87	688.5	30.6	27	48	0.560	81
my15a32	1.0165	0.0634	0.1047	0.0050	0.39	12.48	9.64	712.2	31.9	641.8	29.5	0.0687	0.0014	4.04	890.4	41.8	42	47	0.895	72
my15a52	0.8402	0.0722	0.0905	0.0021	0.13	17.19	4.57	619.2	39.8	558.3	12.2	0.0705	0.0022	6.10	943.4	62.5	170	199	0.856	59
my15a47	0.9856	0.0487	0.1026	0.0029	0.29	9.89	5.68	696.5	24.9	629.5	17.0	0.0715	0.0009	2.58	972.5	26.3	114	113	1.013	65
my16b06	1.1092	0.0300	0.1122	0.0020	0.34	5.41	3.65	757.8	14.4	685.3	11.9	0.0686	0.0008	2.39	885.9	24.7	56	75	0.750	77
my15a55	1.1047	0.1646	0.1131	0.0066	0.19	29.80	11.61	755.6	79.4	690.9	38.0	0.0743	0.0016	4.42	1048.4	44.6	98	195	0.503	66
my16b36	0.7539	0.0227	0.0845	0.0022	0.43	6.01	5.15	570.5	13.1	523.1	12.9	0.0628	0.0005	1.69	701.6	18.0	125	199	0.628	75
my16b38	0.9251	0.1420	0.0994	0.0149	0.49	30.69	29.93	665.1	74.9	611.0	87.2	0.0661	0.0009	2.62	810.5	27.4	137	152	0.903	75
my15a43	0.7739	0.0384	0.0869	0.0015	0.18	9.93	3.48	582.0	22.0	537.0	9.0	0.0671	0.0011	3.30	840.3	34.4	136	172	0.788	64
my15a89	0.8304	0.0461	0.0919	0.0028	0.27	11.11	6.01	613.9	25.6	566.9	16.3	0.0674	0.0009	2.58	850.0	26.8	125	128	0.978	67
my16b27	0.7893	0.0490	0.0884	0.0022	0.20	12.43	4.91	590.8	27.8	545.9	12.9	0.0667	0.0012	3.46	828.1	36.1	70	110	0.637	66
my15a54	14.2789	0.5602	0.4898	0.0130	0.34	7.85	5.31	2768.4	37.2	2570.0	56.3	0.2215	0.0011	1.04	2991.8	8.3	130	491	0.265	86
my15a63	0.8354	0.0336	0.0933	0.0020	0.27	8.06	4.29	616.6	18.6	575.1	11.8	0.0646	0.0011	3.33	761.3	35.1	102	167	0.610	76
my15a75	0.8327	0.0562	0.0932	0.0068	0.54	13.50	14.67	615.1	31.1	574.6	40.3	0.0627	0.0007	2.32	696.9	24.7	70	108	0.649	82
my15a35	10.4342	0.5967	0.4323	0.0168	0.34	11.44	7.75	2474.1	53.0	2316.2	75.4	0.1670	0.0020	2.44	2528.0	20.5	27	200	0.134	92
my15a31	0.9336	0.0305	0.1022	0.0028	0.42	6.54	5.50	669.6	16.0	627.0	16.4	0.0650	0.0005	1.54	775.2	16.2	192	203	0.946	81
my16b07	0.9318	0.0363	0.1032	0.0019	0.24	7.79	3.74	668.6	19.1	632.9	11.3	0.0658	0.0009	2.68	799.3	28.1	160	248	0.643	79
my15a68	0.7784	0.0650	0.0905	0.0046	0.31	16.69	10.22	584.5	37.1	558.5	27.3	0.0641	0.0007	2.28	744.6	24.1	143	217	0.658	75
my16b29	0.8134	0.0212	0.0939	0.0020	0.41	5.20	4.22	604.4	11.8	578.7	11.7	0.0603	0.0005	1.66	615.7	17.9	179	191	0.935	94
my15a53	0.7505	0.0169	0.0883	0.0016	0.40	4.51	3.56	568.5	9.8	545.3	9.3	0.0600	0.0006	1.88	603.8	20.4	151	148	1.019	90
my15a74	0.7651	0.0528	0.0897	0.0034	0.27	13.79	7.54	577.0	30.3	554.0	20.0	0.0638	0.0009	2.93	734.7	31.0	147	124	1.189	75
my15a07	0.7542	0.0220	0.0890	0.0020	0.39	5.83	4.59	570.7	12.7	549.5	12.1	0.0588	0.0005	1.86	558.1	20.3	82	129	0.635	98
my16b28	0.8864	0.0262	0.1015	0.0018	0.29	5.91	3.47	644.5	14.1	623.3	10.3	0.0638	0.0005	1.46	733.8	15.5	417	425	0.981	85
my15a42	0.7769	0.0241	0.0916	0.0027	0.48	6.20	5.89	583.7	13.8	564.8	15.9	0.0604	0.0004	1.41	617.2	15.2	208	211	0.988	92
my15a19	0.9626	0.0146	0.1085	0.0018	0.54	3.04	3.31	684.6	7.6	663.8	10.4	0.0621	0.0003	1.06	676.8	11.3	325	356	0.914	98
my15a12	0.7511	0.0231	0.0893	0.0023	0.41	6.15	5.09	568.8	13.4	551.6	13.5	0.0589	0.0005	1.84	563.6	20.0	76	109	0.697	98
my15a20	3.6503	0.0710	0.2648	0.0045	0.44	3.89	3.43	1560.6	15.5	1514.6	23.1	0.1016	0.0004	0.81	1653.2	7.5	307	393	0.782	92
my16b13	0.7861	0.0728	0.0929	0.0039	0.22	18.52	8.29	589.0	41.4	572.5	22.7	0.0629	0.0007	2.12	705.5	22.5	156	225	0.691	81
my15a33	0.8531	0.0287	0.0991	0.0025	0.38	6.73	5.06	626.4	15.7	609.3	14.7	0.0619	0.0005	1.50	669.0	16.1	93	121	0.772	91
my15a73	0.7422	0.0235	0.0888	0.0022	0.39	6.34	4.99	563.7	13.7	548.5	13.1	0.0602	0.0005	1.65	611.6	17.8	141	190	0.743	90
my15a36	0.7355	0.0151	0.0884	0.0017	0.47	4.11	3.87	559.8	8.8	546.2	10.1	0.0593	0.0004	1.25	576.4	13.5	146	243	0.600	95
my15a14	0.7470	0.0163	0.0898	0.0014	0.35	4.36	3.04	566.5	9.5	554.1	8.1	0.0591	0.0005	1.59	571.6	17.3	110	163	0.673	97
my15a69	9.3628	0.2843	0.4341	0.0130	0.49	6.07	5.99	2374.2	27.9	2324.2	58.4	0.1553	0.0006	0.83	2405.3	7.0	58	166	0.351	97
my15a79	4.7631	0.0819	0.3115	0.0060	0.56	3.44	3.83	1778.4	14.4	1747.9	29.3	0.1095	0.0004	0.80	1791.2	7.3	66	224	0.294	98
my15a30	11.6759	0.3315	0.4827	0.0113	0.41	5.68	4.70	2578.8	26.6	2538.9	49.3	0.1759	0.0006	0.71	2614.8	5.9	160	317	0.505	97
my16b16	0.7523	0.0373	0.0910	0.0041	0.45	9.91	8.98	569.6	21.6	561.2	24.1	0.0583	0.0004	1.27	542.3	13.9	221	305	0.726	103
my15a88	4.0430	0.2577	0.2859	0.0128	0.35	12.75	8.95	1642.9	51.9	1620.9	64.2	0.1042	0.0007	1.43	1700.5	13.1	92	126	0.727	95
my16b19	6.0783	0.1535	0.3555	0.0076	0.42	5.05	4.28	1987.1	22.0	1960.9	36.2	0.1220	0.0007	1.15	1985.9	10.2	87	80	1.083	99
my15a11	3.3625	0.1184	0.2573	0.0067	0.37	7.04	5.23	1495.7	27.6	1476.2	34.5	0.0975	0.0007	1.40	1576.6	13.1	87	125	0.691	94
my15a45	6.5540	0.0797	0.3695	0.0045	0.51	2.43	2.46	2053.2	10.7	2026.9	21.4	0.1263	0.0004	0.63	2047.5	5.6	314	425	0.738	99

Table 1.1. (continued)

my15a08	3.9118	0.0474	0.2810	0.0033	0.48	2.42	2.32	1616.1	9.8	1596.5	16.4	0.0989	0.0004	0.84	1602.6	7.8	119	161	0.739	100
my16b15	0.8773	0.0169	0.1030	0.0016	0.40	3.85	3.06	639.5	9.1	632.2	9.2	0.0610	0.0003	1.03	640.5	11.0	227	298	0.761	99
my16b25	6.7359	0.1136	0.3752	0.0058	0.46	3.37	3.09	2077.3	14.9	2053.8	27.2	0.1292	0.0006	0.87	2086.4	7.7	186	106	1.755	98
my15a24	0.7429	0.0178	0.0904	0.0017	0.39	4.79	3.72	564.1	10.4	558.0	9.9	0.0601	0.0004	1.33	606.7	14.4	309	307	1.006	92
my15a30	12.0097	0.4311	0.4920	0.0150	0.42	7.18	6.09	2605.2	33.6	2579.3	64.7	0.1767	0.0006	0.72	2622.1	6.0	158	311	0.510	98
my16b04	0.8997	0.0221	0.1054	0.0018	0.34	4.92	3.35	651.5	11.8	645.9	10.3	0.0602	0.0005	1.66	611.3	18.0	99	131	0.755	106
my15a13	11.0685	0.2617	0.4764	0.0107	0.47	4.73	4.49	2528.9	22.0	2511.4	46.7	0.1674	0.0006	0.71	2531.8	5.9	206	456	0.453	99
my15a40	3.5363	0.0556	0.2669	0.0040	0.47	3.15	2.96	1535.4	12.5	1525.0	20.1	0.0942	0.0004	0.80	1512.8	7.6	84	197	0.427	101
my16b18	0.8057	0.0443	0.0970	0.0033	0.31	10.99	6.87	600.1	24.9	597.0	19.6	0.0597	0.0009	2.87	591.1	31.1	13	47	0.282	101
my15a87	0.8567	0.1170	0.1019	0.0077	0.28	27.30	15.18	628.3	64.0	625.4	45.3	0.0635	0.0006	1.86	725.2	19.7	505	406	1.244	86
my15a64	4.5918	0.0604	0.3100	0.0041	0.50	2.63	2.63	1747.8	11.0	1740.5	20.0	0.1065	0.0004	0.70	1741.1	6.4	165	264	0.625	100
my15a25	0.7202	0.0225	0.0890	0.0024	0.42	6.25	5.30	550.8	13.3	549.7	14.0	0.0588	0.0004	1.44	559.6	15.6	219	238	0.921	98
my15a41	1.9435	0.0660	0.1858	0.0040	0.31	6.80	4.28	1096.2	22.8	1098.6	21.6	0.0759	0.0006	1.48	1092.6	14.8	92	90	1.018	101
my15a18	0.8010	0.0158	0.0979	0.0014	0.37	3.94	2.88	597.4	8.9	602.3	8.3	0.0607	0.0004	1.35	627.8	14.6	159	282	0.562	96
my15a29	0.8185	0.0243	0.0998	0.0018	0.31	5.93	3.65	607.2	13.6	613.4	10.7	0.0604	0.0006	1.97	618.8	21.2	70	66	1.066	99
my15a44	0.8404	0.0319	0.1025	0.0024	0.30	7.60	4.63	619.4	17.6	628.8	13.9	0.0612	0.0005	1.64	646.2	17.6	62	130	0.473	97
my15a15	0.4240	0.0093	0.0585	0.0010	0.39	4.37	3.42	358.9	6.6	366.3	6.1	0.0530	0.0003	1.20	327.3	13.6	42	452	0.093	112
my15a09	0.7085	0.0311	0.0908	0.0022	0.27	8.78	4.80	543.9	18.5	560.3	12.9	0.0579	0.0006	2.06	527.3	22.6	88	88	0.998	106
my15a09	0.7074	0.0311	0.0908	0.0022	0.27	8.78	4.80	543.2	18.5	560.1	12.9	0.0579	0.0006	2.06	524.7	22.6	88	88	0.998	107
my15a85	0.7661	0.0203	0.0978	0.0018	0.35	5.31	3.73	577.5	11.7	601.3	10.7	0.0577	0.0006	2.11	519.3	23.1	21	38	0.555	116

Table 1.1. (continued)

Cid Formation (35 31.739 N, 80 06.305 E)

	CONCORDIA COLUMNS					2 σ %	2 σ %				AGES Ma									
					I N T E R C E P T V A L U E S															
file	207/235	7/5 err	206/238	6/8 err	Rho	207/235	206/238	7/5 age	1σ	6/8 age	1σ	207/206	7/6 err	207/206	7/6 age	1σ	Th232 ppm	U238 ppm	Th/U	Concordance
my23a147	0.9076	0.0519	0.0913	0.0030	0.29	11.43	6.55	655.8	27.6	563.1	17.7	0.0743	0.0013	3.54	1049.1	35.7	24	36	0.679	54
my23a155	0.9330	0.0736	0.0937	0.0060	0.40	15.77	12.72	669.2	38.6	577.6	35.1	0.0705	0.0010	2.75	944.3	28.1	367	177	2.072	61
my23a153	0.8470	0.0898	0.0885	0.0022	0.12	21.21	5.05	623.0	49.4	546.5	13.2	0.0784	0.0026	6.64	1158.3	65.9	107	103	1.037	47
my23a135	0.8815	0.0341	0.0922	0.0025	0.35	7.74	5.43	641.8	18.4	568.3	14.8	0.0667	0.0008	2.49	828.6	25.9	57	79	0.718	69
my23a76	0.8755	0.0360	0.0917	0.0024	0.32	8.23	5.25	638.6	19.5	565.4	14.2	0.0676	0.0009	2.73	855.9	28.3	136	106	1.289	66
my23a30	0.8556	0.0394	0.0904	0.0017	0.21	9.22	3.83	627.7	21.6	558.0	10.2	0.0712	0.0011	3.21	964.2	32.7	104	103	1.009	58
my23a98	0.8644	0.0603	0.0913	0.0026	0.21	13.94	5.77	632.5	32.8	563.4	15.6	0.0737	0.0010	2.68	1034.2	27.1	59	70	0.843	54
my23a125	0.7850	0.0222	0.0877	0.0017	0.34	5.65	3.84	588.3	12.6	542.1	10.0	0.0615	0.0006	1.95	656.6	20.9	55	74	0.745	83
my23a142	0.7765	0.0220	0.0883	0.0018	0.36	5.66	4.12	583.5	12.6	545.5	10.8	0.0603	0.0007	2.32	615.3	25.0	66	78	0.843	89
my23a121	0.7648	0.0167	0.0877	0.0011	0.30	4.37	2.59	576.7	9.6	541.7	6.7	0.0618	0.0006	1.94	666.0	20.8	133	128	1.040	81
my23a65	0.8479	0.0350	0.0954	0.0020	0.26	8.25	4.24	623.5	19.2	587.4	11.9	0.0621	0.0009	2.98	679.1	31.9	45	54	0.835	86
my23a49	0.7575	0.0207	0.0878	0.0016	0.33	5.47	3.63	572.6	12.0	542.2	9.4	0.0614	0.0004	1.46	652.6	15.6	838	537	1.561	83
my23a157	0.7651	0.0310	0.0885	0.0031	0.44	8.09	7.10	576.9	17.8	546.8	18.6	0.0600	0.0006	1.83	602.8	19.7	293	218	1.348	91
my23a115	0.7628	0.0199	0.0892	0.0017	0.37	5.22	3.88	575.7	11.5	550.7	10.2	0.0595	0.0005	1.65	587.0	17.9	197	182	1.081	94
my23a159	0.7704	0.0505	0.0900	0.0045	0.38	13.10	9.91	580.0	29.0	555.2	26.4	0.0590	0.0006	1.99	567.6	21.4	117	135	0.869	98
my23a99	0.7608	0.0289	0.0891	0.0028	0.41	7.61	6.20	574.5	16.7	550.0	16.3	0.0596	0.0006	2.15	588.3	23.3	86	87	0.992	93
my23a32	0.7893	0.0430	0.0918	0.0027	0.27	10.90	5.90	590.8	24.4	566.1	16.0	0.0597	0.0006	2.05	591.7	21.9	92	119	0.771	96
my23a39	0.7630	0.0230	0.0895	0.0018	0.33	6.04	3.96	575.7	13.3	552.8	10.5	0.0602	0.0007	2.17	612.0	23.4	83	94	0.885	90
my23a148	0.7610	0.0278	0.0894	0.0032	0.49	7.31	7.12	574.6	16.0	552.1	18.8	0.0594	0.0004	1.47	580.3	15.9	416	274	1.516	95
my23a137	0.7713	0.0348	0.0909	0.0025	0.30	9.03	5.45	580.5	20.0	560.6	14.6	0.0603	0.0008	2.54	615.1	27.4	58	68	0.850	91
my23a86	0.7423	0.0254	0.0882	0.0017	0.29	6.85	3.95	563.7	14.8	544.9	10.3	0.0589	0.0007	2.26	564.4	24.3	71	85	0.838	97
my23a28	0.7414	0.0274	0.0881	0.0022	0.33	7.38	4.94	563.2	16.0	544.4	12.9	0.0599	0.0007	2.15	600.0	22.7	370	258	1.434	91
my23a100	0.7563	0.0841	0.0895	0.0045	0.23	22.25	10.15	571.9	48.6	552.8	26.9	0.0600	0.0011	3.66	602.8	39.1	86	93	0.928	92
my23a133	0.7539	0.0342	0.0894	0.0029	0.35	9.08	6.39	570.5	19.8	551.8	16.9	0.0594	0.0005	1.84	582.1	20.0	252	218	1.159	95
my23a112	0.7476	0.0338	0.0889	0.0023	0.28	9.05	5.12	566.8	19.6	549.0	13.5	0.0589	0.0009	2.99	563.5	32.2	37	50	0.737	97
my23a134	0.7251	0.0207	0.0868	0.0018	0.36	5.72	4.16	553.6	12.2	536.6	10.7	0.0598	0.0005	1.56	596.5	16.9	161	138	1.168	90
my23a74	0.7567	0.0339	0.0899	0.0024	0.30	8.96	5.43	572.1	19.6	554.7	14.4	0.0601	0.0007	2.34	607.4	25.3	88	115	0.770	91
my23a130	0.7687	0.0363	0.0911	0.0023	0.27	9.44	5.10	579.0	20.8	561.9	13.7	0.0600	0.0007	2.24	603.7	24.1	90	93	0.960	93
my23a63	0.7525	0.0205	0.0896	0.0018	0.37	5.45	4.05	569.7	11.9	552.9	10.7	0.0600	0.0005	1.76	602.2	19.0	119	160	0.742	92
my23a95	0.7397	0.0357	0.0885	0.0029	0.33	9.64	6.45	562.2	20.8	546.8	16.9	0.0587	0.0009	3.04	554.7	33.1	33	52	0.629	99
my23a152	0.7467	0.0581	0.0892	0.0030	0.22	15.56	6.72	566.3	33.8	550.8	17.7	0.0597	0.0015	4.67	593.0	49.3	189	135	1.401	93
my23a64	0.7717	0.0154	0.0917	0.0015	0.42	3.98	3.38	580.7	8.8	565.8	9.1	0.0602	0.0004	1.21	610.7	13.1	657	427	1.537	93
my23a71	0.7589	0.0249	0.0906	0.0019	0.32	6.57	4.20	573.4	14.4	559.3	11.2	0.0601	0.0006	1.89	606.8	20.2	135	158	0.854	92
my23a165	0.7483	0.1397	0.0898	0.0129	0.38	37.34	28.73	567.2	81.1	554.4	76.3	0.0599	0.0004	1.50	600.8	16.3	1253	560	2.240	92
my23a24	0.7331	0.0378	0.0884	0.0031	0.34	10.30	7.10	558.4	22.1	546.2	18.6	0.0602	0.0008	2.54	610.3	27.4	33	55	0.598	90
my23a40	0.7409	0.0244	0.0893	0.0021	0.35	6.60	4.59	562.9	14.3	551.2	12.1	0.0581	0.0007	2.27	533.4	24.8	56	65	0.867	103
my23a87	0.7019	0.0336	0.0856	0.0025	0.30	9.56	5.78	539.9	20.0	529.4	14.7	0.0581	0.0009	2.93	534.5	31.7	36	50	0.733	99
my23a146	0.7341	0.0311	0.0895	0.0025	0.33	8.47	5.51	558.9	18.2	552.4	14.6	0.0598	0.0007	2.18	597.4	23.5	265	196	1.356	92
my23a52	0.7291	0.0163	0.0890	0.0015	0.37	4.47	3.32	556.0	9.6	549.9	8.8	0.0576	0.0005	1.64	514.5	18.0	113	208	0.544	107
my23a72	0.7259	0.1437	0.0891	0.0076	0.22	39.60	17.04	554.2	84.6	550.3	44.9	0.0589	0.0010	3.44	565.1	37.5	117	114	1.027	97
my23a38	0.7258	0.0251	0.0893	0.0020	0.32	6.91	4.46	554.1	14.7	551.1	11.8	0.0586	0.0007	2.30	553.3	25.1	94	92	1.017	100
my23a75	0.7082	0.0301	0.0876	0.0022	0.30	8.51	5.12	543.7	17.9	541.1	13.3	0.0592	0.0006	2.08	576.2	22.4	163	163	0.998	94
my23a96	0.7034	0.0360	0.0872	0.0021	0.23	10.22	4.76	540.8	21.4	538.7	12.3	0.0596	0.0008	2.45	589.7	26.3	102	113	0.899	91
my23a54	0.8252	0.0267	0.0991	0.0022	0.34	6.48	4.46	611.0	14.9	609.1	13.0	0.0597	0.0004	1.46	591.9	15.8	223	256	0.872	103
my23a166	0.7342	0.0299	0.0903	0.0021	0.28	8.14	4.57	559.0	17.5	557.5	12.2	0.0604	0.0005	1.61	618.6	17.4	444	332	1.336	90
my23a167	0.7253	0.0373	0.0896	0.0031	0.33	10.29	6.84	553.8	22.0	553.4	18.1	0.0594	0.0006	2.01	581.5	21.8	68	78	0.861	95

Table 1.1. (continued)

my23a25	0.7206	0.0622	0.0893	0.0034	0.22	17.27	7.53	551.0	36.7	551.2	19.9	0.0583	0.0010	3.38	541.2	36.3	30	50	0.592	102
my23a29	0.7018	0.0451	0.0874	0.0032	0.28	12.87	7.30	539.8	26.9	540.3	18.9	0.0586	0.0008	2.78	552.9	30.3	61	70	0.865	98
my23a44	0.7274	0.0240	0.0907	0.0019	0.31	6.59	4.10	555.0	14.1	559.6	11.0	0.0601	0.0008	2.69	608.4	29.1	45	64	0.715	92
my23a83	0.7651	0.0292	0.0945	0.0021	0.29	7.62	4.43	577.0	16.8	582.2	12.3	0.0583	0.0006	2.00	540.0	21.8	118	128	0.921	108
my23a43	0.7018	0.0226	0.0882	0.0017	0.29	6.43	3.79	539.8	13.5	544.8	9.9	0.0600	0.0006	1.93	604.0	20.8	249	187	1.327	90
my23a156	0.7202	0.0258	0.0906	0.0018	0.27	7.17	3.93	550.8	15.2	559.1	10.5	0.0590	0.0005	1.74	568.1	18.9	104	167	0.624	98

Table 1.1. (continued)

Yadkin Formation (35 19.259 N, 80 19.844 E)

	CONCORDIA COLUMNS					2 σ %	2 σ %				AGES Ma									
					I N	T E	R C	E P	T	V A	L U	E S								
file	207/235	7/5 err	206/238	6/8 err	Rho	207/235	206/238	7/5 age	1σ	6/8 age	1σ	207/206	7/6 err	207/206	7/6 age	1σ	Th232 ppm	U238 ppm	Th/U	Concordance
my10b135	1.0382	0.0366	0.0921	0.0013	0.21	7.05	2.92	723.0	18.2	568.1	7.9	0.0782	0.0012	3.05	1151.7	30.3	319	339	0.942	49
my10b62	0.8408	0.0292	0.0839	0.0045	0.77	6.95	10.64	619.6	16.1	519.1	26.5	0.0649	0.0011	3.53	769.5	37.1	192	218	0.883	67
my11a24	0.8486	0.0474	0.0855	0.0019	0.20	11.18	4.49	623.9	26.1	528.7	11.4	0.0762	0.0017	4.38	1100.9	43.8	382	298	1.282	48
my10b93	0.8079	0.0341	0.0854	0.0029	0.40	8.44	6.67	601.3	19.2	528.5	16.9	0.0658	0.0011	3.49	800.5	36.6	669	519	1.288	66
my10b119	0.8170	0.0266	0.0864	0.0024	0.42	6.50	5.52	606.3	14.8	534.1	14.1	0.0699	0.0008	2.18	925.9	22.4	616	467	1.320	58
my10b122	0.9894	0.0247	0.1007	0.0021	0.42	5.00	4.22	698.4	12.6	618.6	12.4	0.0721	0.0006	1.56	987.4	15.9	153	229	0.670	63
my11a19	0.8376	0.0374	0.0892	0.0012	0.15	8.93	2.74	617.8	20.7	550.7	7.2	0.0675	0.0014	4.26	854.5	44.3	51	87	0.584	64
my11a12	0.7514	0.0319	0.0821	0.0052	0.75	8.48	12.75	569.0	18.5	508.8	31.2	0.0675	0.0008	2.37	852.4	24.6	1010	1127	0.896	60
my10b75	0.7804	0.0207	0.0879	0.0029	0.62	5.31	6.54	585.7	11.8	543.3	17.0	0.0615	0.0004	1.27	656.7	13.6	285	274	1.040	83
my10b64	0.7981	0.0228	0.0902	0.0020	0.40	5.72	4.52	595.8	12.9	556.9	12.1	0.0626	0.0005	1.51	693.4	16.1	102	140	0.727	80
my10b179	0.7467	0.0297	0.0868	0.0032	0.46	7.96	7.38	566.3	17.3	536.6	19.0	0.0610	0.0007	2.19	640.8	23.6	153	273	0.561	84
my10b160	0.7439	0.0209	0.0866	0.0020	0.40	5.63	4.50	564.7	12.2	535.6	11.6	0.0617	0.0005	1.62	662.2	17.3	130	148	0.877	81
my10b120	0.7954	0.0152	0.0914	0.0012	0.35	3.82	2.66	594.2	8.6	564.1	7.2	0.0616	0.0005	1.60	659.9	17.2	139	195	0.713	85
my10b95	0.8225	0.0202	0.0948	0.0025	0.54	4.92	5.32	609.4	11.3	583.8	14.8	0.0627	0.0004	1.16	698.8	12.4	376	778	0.483	84
my10b140	0.7843	0.0184	0.0914	0.0014	0.33	4.68	3.07	587.9	10.5	563.6	8.3	0.0620	0.0005	1.62	674.2	17.3	149	245	0.609	84
my11a18	0.7702	0.0635	0.0901	0.0059	0.40	16.49	13.15	579.9	36.4	555.9	35.0	0.0618	0.0009	2.92	667.6	31.2	240	305	0.787	83
my10b170	0.8175	0.0341	0.0944	0.0027	0.35	8.35	5.77	606.7	19.1	581.7	16.0	0.0626	0.0004	1.38	693.4	14.7	343	361	0.951	84
my10b44	1.9569	0.0537	0.1781	0.0040	0.41	5.49	4.52	1100.8	18.5	1056.7	22.0	0.0794	0.0004	0.89	1183.3	8.8	439	336	1.306	89
my10b22	0.7828	0.0180	0.0915	0.0016	0.38	4.59	3.47	587.1	10.2	564.2	9.4	0.0607	0.0004	1.47	628.1	15.8	349	490	0.711	90
my10b74	0.7906	0.0531	0.0923	0.0060	0.49	13.44	13.06	591.5	30.1	569.2	35.6	0.0643	0.0010	3.24	751.1	34.2	341	199	1.717	76
my10b63	0.7661	0.0182	0.0901	0.0019	0.46	4.75	4.32	577.5	10.5	555.8	11.5	0.0596	0.0003	1.07	589.6	11.6	240	392	0.611	94
my10b106	0.8888	0.0353	0.1015	0.0027	0.34	7.95	5.36	645.7	19.0	623.1	15.9	0.0638	0.0006	1.80	734.6	19.0	84	127	0.661	85
my11a27	0.8145	0.0174	0.0948	0.0014	0.35	4.27	3.00	605.0	9.7	584.1	8.4	0.0615	0.0005	1.55	656.6	16.6	63	132	0.480	89
my10b42	0.8980	0.0227	0.1025	0.0016	0.32	5.05	3.21	650.7	12.1	629.0	9.6	0.0629	0.0005	1.66	703.4	17.6	195	223	0.875	89
my11a11	0.7206	0.0343	0.0864	0.0031	0.38	9.52	7.22	551.0	20.3	534.3	18.5	0.0605	0.0005	1.76	622.9	19.0	151	164	0.915	86
my10b54	0.7769	0.0306	0.0921	0.0027	0.37	7.87	5.83	583.7	17.5	567.7	15.8	0.0602	0.0005	1.80	611.5	19.5	100	147	0.680	93
my10b180	0.7855	0.0161	0.0931	0.0016	0.41	4.09	3.34	588.6	9.1	573.7	9.2	0.0594	0.0004	1.38	580.0	15.0	68	118	0.570	99
my11a17	0.7206	0.0358	0.0871	0.0034	0.39	9.94	7.75	551.0	21.1	538.1	20.0	0.0596	0.0004	1.36	587.5	14.7	239	305	0.784	92
my10b166	0.7618	0.0215	0.0911	0.0024	0.46	5.65	5.16	575.0	12.4	562.0	13.9	0.0587	0.0004	1.33	554.2	14.5	151	187	0.806	101
my10b49	0.7478	0.0289	0.0899	0.0021	0.31	7.74	4.73	566.9	16.8	554.8	12.6	0.0615	0.0008	2.73	656.0	29.2	38	51	0.755	85
my10b168	0.8203	0.0213	0.0970	0.0019	0.37	5.18	3.88	608.2	11.9	596.6	11.1	0.0590	0.0005	1.73	567.0	18.9	104	92	1.127	105
my10b59	0.8267	0.0272	0.0976	0.0019	0.30	6.59	3.89	611.8	15.1	600.5	11.2	0.0628	0.0005	1.58	699.9	16.8	221	192	1.149	86
my10b29	0.7353	0.0145	0.0892	0.0011	0.32	3.95	2.51	559.6	8.5	550.5	6.6	0.0589	0.0005	1.65	564.1	18.0	56	91	0.615	98
my10b104	0.7396	0.0260	0.0896	0.0021	0.33	7.03	4.66	562.1	15.2	553.2	12.4	0.0608	0.0005	1.60	633.4	17.3	241	238	1.014	87
my11a14	0.6900	0.0154	0.0847	0.0015	0.39	4.46	3.50	532.8	9.2	524.3	8.8	0.0591	0.0004	1.35	572.0	14.7	176	352	0.498	92
my10b167	0.7499	0.0212	0.0907	0.0017	0.34	5.65	3.82	568.2	12.3	559.6	10.2	0.0600	0.0005	1.58	602.7	17.1	74	145	0.511	93
my10b40	0.7572	0.0160	0.0915	0.0012	0.31	4.23	2.59	572.4	9.3	564.3	7.0	0.0599	0.0005	1.61	599.3	17.5	67	142	0.469	94
my10b125	0.8251	0.0221	0.0979	0.0021	0.41	5.35	4.39	610.9	12.3	602.3	12.6	0.0612	0.0004	1.29	646.3	13.9	148	260	0.569	93
my10b45	0.9215	0.0189	0.1068	0.0015	0.33	4.10	2.75	663.1	10.0	654.2	8.5	0.0625	0.0005	1.48	691.2	15.8	87	159	0.550	95
my10b25	0.7272	0.0109	0.0887	0.0009	0.34	3.01	2.03	554.9	6.4	547.9	5.3	0.0587	0.0003	0.94	557.2	10.3	322	332	0.972	98
my10b16	0.7369	0.0159	0.0897	0.0017	0.45	4.32	3.88	560.6	9.3	553.9	10.3	0.0605	0.0003	1.14	622.8	12.3	433	551	0.785	89
my10b155	0.9181	0.0185	0.1067	0.0017	0.40	4.02	3.19	661.3	9.8	653.8	9.9	0.0611	0.0003	1.10	642.6	11.8	143	243	0.586	102
my10b159	0.7330	0.0158	0.0894	0.0014	0.35	4.32	3.03	558.3	9.3	551.9	8.0	0.0588	0.0004	1.34	557.9	14.6	186	226	0.824	99
my10b98	0.7076	0.0106	0.0870	0.0010	0.39	3.00	2.33	543.3	6.3	537.9	6.0	0.0587	0.0003	1.04	555.0	11.3	219	363	0.604	97
my10b112	0.7242	0.0136	0.0887	0.0011	0.32	3.77	2.39	553.1	8.0	548.1	6.3	0.0600	0.0004	1.45	604.5	15.7	73	150	0.485	91
my10b132	0.7018	0.0206	0.0866	0.0024	0.47	5.87	5.57	539.8	12.3	535.4	14.3	0.0587	0.0002	0.82	555.0	9.0	189	605	0.312	96

Table 1.1. (continued)

my11a07	0.7284	0.0269	0.0893	0.0018	0.27	7.39	3.92	555.6	15.8	551.5	10.4	0.0604	0.0006	2.07	617.8	22.3	84	110	0.770	89
my11a20	0.7194	0.0154	0.0885	0.0015	0.40	4.29	3.43	550.3	9.1	546.4	9.0	0.0585	0.0004	1.31	547.3	14.3	337	295	1.143	100
my10b99	0.7519	0.0204	0.0917	0.0014	0.28	5.43	3.08	569.3	11.8	565.3	8.3	0.0602	0.0005	1.77	611.3	19.1	55	95	0.582	92
my10b08	0.7257	0.0131	0.0891	0.0014	0.44	3.61	3.17	554.0	7.7	550.3	8.4	0.0586	0.0003	1.15	552.2	12.6	178	237	0.752	100
my10b139	0.7785	0.0267	0.0943	0.0021	0.33	6.85	4.48	584.6	15.2	581.1	12.4	0.0605	0.0006	1.85	622.3	19.9	97	201	0.484	93
my10b86	1.4461	0.0744	0.1503	0.0088	0.57	10.29	11.67	908.3	30.9	902.7	49.2	0.0755	0.0005	1.38	1083.1	13.8	565	1046	0.540	83
my11a23	0.7697	0.0266	0.0937	0.0023	0.36	6.91	4.97	579.6	15.3	577.5	13.7	0.0588	0.0006	2.08	560.5	22.6	66	87	0.752	103
my10b77	0.7180	0.0176	0.0887	0.0016	0.37	4.89	3.62	549.5	10.4	547.7	9.5	0.0598	0.0003	1.00	594.9	10.8	308	550	0.559	92
my10b115	0.8984	0.0211	0.1059	0.0023	0.47	4.70	4.43	650.8	11.3	649.2	13.7	0.0615	0.0003	0.91	657.2	9.8	218	377	0.578	99
my10b129	0.7408	0.0133	0.0912	0.0010	0.31	3.59	2.19	562.9	7.7	562.4	5.9	0.0602	0.0004	1.42	609.7	15.4	176	228	0.771	92
my10b11	0.7292	0.0218	0.0901	0.0021	0.40	5.98	4.75	556.1	12.8	555.9	12.6	0.0591	0.0004	1.51	571.4	16.4	113	150	0.752	97
my10b96	0.8919	0.0298	0.1057	0.0026	0.37	6.68	4.93	647.4	16.0	647.5	15.2	0.0596	0.0006	2.08	590.7	22.6	79	87	0.902	110
my10b149	0.7117	0.0101	0.0884	0.0011	0.42	2.83	2.38	545.8	6.0	546.2	6.2	0.0585	0.0003	0.88	550.2	9.7	145	441	0.329	99
my10b181	0.9692	0.0188	0.1127	0.0016	0.38	3.88	2.92	688.1	9.7	688.7	9.5	0.0621	0.0003	1.06	676.9	11.4	177	207	0.858	102
my10b05	0.7282	0.0215	0.0902	0.0016	0.30	5.91	3.54	555.5	12.6	556.6	9.4	0.0593	0.0005	1.76	578.3	19.2	79	134	0.589	96
my10b81	0.7299	0.0270	0.0904	0.0019	0.28	7.39	4.12	556.5	15.8	557.7	11.0	0.0606	0.0005	1.78	625.9	19.2	92	119	0.777	89
my10b84	0.7744	0.0347	0.0950	0.0028	0.33	8.95	5.83	582.3	19.8	584.9	16.3	0.0603	0.0004	1.27	613.9	13.7	183	351	0.520	95
my10b127	0.7363	0.0225	0.0914	0.0016	0.28	6.12	3.42	560.2	13.2	563.7	9.2	0.0598	0.0004	1.42	595.6	15.4	168	236	0.712	95
my10b175	0.7349	0.0288	0.0912	0.0018	0.25	7.85	3.94	559.4	16.9	562.9	10.6	0.0599	0.0007	2.36	601.0	25.5	69	108	0.639	94
my10b61	0.7690	0.0271	0.0946	0.0022	0.34	7.06	4.73	579.2	15.6	582.9	13.2	0.0594	0.0004	1.41	582.3	15.3	72	169	0.426	100
my10b151	0.7163	0.0106	0.0894	0.0010	0.38	2.96	2.25	548.5	6.3	552.1	6.0	0.0585	0.0002	0.80	546.8	8.8	155	466	0.332	101
my11a10	1.0689	0.0290	0.1222	0.0029	0.44	5.42	4.77	738.2	14.2	743.1	16.7	0.0630	0.0004	1.35	709.0	14.4	112	133	0.845	105
my10b176	0.6858	0.0249	0.0864	0.0018	0.28	7.27	4.09	530.3	15.0	534.5	10.5	0.0601	0.0005	1.53	606.9	16.5	57	227	0.252	88
my10b43	0.7902	0.0159	0.0969	0.0012	0.30	4.03	2.43	591.3	9.0	596.3	6.9	0.0595	0.0005	1.63	584.3	17.7	174	133	1.313	102
my10b91	0.7536	0.0301	0.0933	0.0019	0.26	7.98	4.13	570.3	17.4	575.2	11.4	0.0603	0.0005	1.71	615.8	18.4	46	138	0.334	93
my10b71	0.7163	0.0178	0.0903	0.0014	0.31	4.97	3.06	548.5	10.5	557.5	8.2	0.0588	0.0004	1.36	559.0	14.8	134	175	0.764	100
my10b103	0.7353	0.0172	0.0924	0.0016	0.36	4.69	3.40	559.7	10.1	569.7	9.3	0.0591	0.0006	1.99	571.8	21.7	81	104	0.773	100
my10b128	0.7294	0.0128	0.0921	0.0010	0.30	3.51	2.13	556.2	7.5	567.8	5.8	0.0601	0.0004	1.21	608.9	13.0	188	219	0.860	93
my11a28	0.7850	0.0261	0.0978	0.0016	0.25	6.65	3.32	588.4	14.9	601.7	9.5	0.0600	0.0007	2.33	603.5	25.2	95	87	1.095	100
my10b02	0.6914	0.0243	0.0884	0.0016	0.26	7.03	3.67	533.7	14.6	546.4	9.6	0.0592	0.0006	2.15	573.6	23.4	55	128	0.427	95
my10b150	0.7186	0.0275	0.0922	0.0025	0.35	7.66	5.38	549.8	16.3	568.3	14.6	0.0586	0.0005	1.65	552.0	18.0	153	168	0.907	103
my10b19	0.7172	0.0180	0.0922	0.0014	0.29	5.02	2.94	549.0	10.6	568.8	8.0	0.0577	0.0005	1.70	518.2	18.6	66	82	0.811	110
my10b76	0.6864	0.2216	0.0920	0.0051	0.09	64.58	11.17	530.7	133.5	567.1	30.3	0.0627	0.0012	3.73	699.3	39.7	80	204	0.390	81

CHAPTER 2

GEOCHEMISTRY AND TECTONIC SIGNIFICANCE OF THE STONY MOUNTAIN GABBRO, NORTH CAROLINA: IMPLICATIONS FOR THE EARLY PALEOZOIC EVOLUTION OF CAROLINIA

ABSTRACT

Carolinia comprises a collection of Neoproterozoic-early Paleozoic magmatic arc and sedimentary terranes that were amalgamated and accreted to Laurentia in the early to middle Paleozoic. In central North Carolina, mafic rocks of the Stony Mountain gabbro intrude sub-aqueous volcanic and sedimentary rocks and submarine epiclastic sedimentary rocks of the Albemarle Group. The age of the Stony Mountain gabbro is constrained to the Early Cambrian-Middle Ordovician. Field relations indicate that the gabbro represents the final phase of magmatism following the eruption and deposition of the Neoproterozoic-earliest Cambrian Albemarle Group, yet the gabbro pre-dates regional metamorphism and tectonism related to the Late Ordovician accretion of Carolinia to Laurentia.

On a Hughes diagram, the Stony Mountain gabbro rocks display a moderate degree of scatter and plot near or in the igneous spectrum suggesting that the alkali elements have not been significantly altered by regional metamorphism. All rocks have sub-alkaline basaltic compositions, variable TiO_2*, MgO and Ni/Cr values. Mg# values range from 80-50 and imply that the rocks span the range from primitive to more evolved. Primitive mantle-normalized rare earth element patterns are characterized by variable LREE enrichment with moderate sloping extended REE patterns. On tectonic discrimination diagrams the rocks have a geochemical signature typical of island-arc tholeiitic basalt. The degree of LREE enrichment, prominent negative Nb anomalies and Nb/Th ratios are all features of low-K to medium-K tholeiitic basalts in modern island-arc, subduction related lavas.*

The Nd isotope data are dominated by juvenile compositions that are consistent with derivation from lithospheric and asthenospheric sources during decompression melting of the mantle. The Stony Mountain gabbro records subduction zone magmatism in an island arc setting and can be modeled as the product of ~10–15% hydrous partial melting of variable mixtures of MORB- and OIB-like mantle sources overprinted by a minor subducted-slab derived hydrous fluid component. By analogy with modern settings the rocks of the Stony Mountain gabbro are comparable to MORB-like to OIB-type enriched rocks from the Lau Island and Sumisu Rift and are interpreted to have formed within an evolving early Paleozoic island arc—back arc rift-basin system. The presence of an Early Cambrian arc-back arc rift system in Carolinia is broadly coeval with arc-back arc volcanism in other peri-Gondwanan blocks of the Appalachians and may be related to the Early Paleozoic opening of the Rheic Ocean.

PREAMBLE

Carolinia comprises several late Neoproterozoic-Early Cambrian composite arc magmatic and sedimentary sequences that record a long and complex paleotectonic history (Figure 2.1). Faunal, isotopic, paleomagnetic and detrital mineral data (Hibbard *et al*., 2002; Ingle *et al*., 2003 and references therein) indicate that Carolinia formed during the late Neoproterozoic along the margin of west Gondwana; however, several fundamental aspects of its early Paleozoic tectonic evolution are poorly known. Although paleomagnetic data and regional, foliation-forming tectonothermal events constrain the accretion of Carolinia to eastern Laurentia during the Late Ordovician-Early Silurian (Hibbard, 2000), the timing and nature of separation of Carolinia from Gondwana related to opening of the Rheic Ocean, has hitherto remained elusive.

Neoproterozoic-early Paleozoic felsic volcanic rocks of the Albemarle sequence are widespread throughout Carolinia in North Carolina and exhibit strong evidence for formation in subduction zone setting with the possible incorporation of evolved continental material (e.g. Ingle *et al*., 2003). Mafic plutonic rocks of the Stony Mountain gabbro occur throughout the Albemarle sequence, but there is a paucity of geochemical and isotopic data for these intrusive rocks that can be used to constrain their petrogenetic history and paleotectonic setting of formation. As such the geochemical, isotopic, petrological and tectonic relationships between intrusive and extrusive phases of the Albemarle sequence remained unknown.

In an effort to address these unresolved questions, I initiated a lithogeochemical and isotopic study of the Stony Mountain gabbro and present new data that document the youngest known arc-related magmatism in Carolinia. The geochemical data provided in this chapter imply that intrusive mafic rocks of the Stony Mountain gabbro record derivation from variably enriched mantle sources within an ensimatic volcanic arc rift—back arc-basin setting associated with rifting of Carolinia and separation from Gondwana during inception of the Rheic Ocean in the Early Cambrian. The combined geochemical and isotopic dataset presented herein aims to: (*i*) document the geochemical signatures of mafic plutonic rocks of the Stony Mountain gabbro; (ii) provide insights into its magmatic origins and petrogenesis; (*ii*) determine the relative roles of mantle and/or continental crust during formation of mafic intrusive rocks of the Stony Mountain gabbro; (*iii*) elucidate the paleotectonic setting of Carolinia to compare to possible modern and ancient analogues; and (*iv*) ascertain the significance of the style of magmatism in the tectonic evolution of Carolinia with respect to opening of the Rheic Ocean.

REGIONAL GEOLOGY

Carolinia comprises a collection Neoproterozoic-early Paleozoic magmatic arc/sedimentary terranes that extend from central Virginia southwest to Alabama (Figure 2.2). In North Carolina, the tectonomagmatic and depositional history of Carolinia is best known in the Carolina terrane. The Carolina terrane comprises a tripartite succession of typically low-grade volcanic-plutonic and marine siliciclastic rocks formed in three distinct time intervals: (*i*) Pre-600 Ma rocks of the Virgilina sequence record a juvenile, felsic volcanic-dominated magmatic arc generated on an oceanic substrate; (*ii*) this was followed by deposition of magmatic-siliciclastic rocks of the Albemarle sequence between 590-550 Ma; and (*iii*) post-550 Ma magmatic and depositional events of the

Albemarle Group, which is characterized by juvenile felsic volcanism and associated epiclastic rocks with subsequent plutonism.

In central North Carolina, the Carolina terrane is composed of lower-greenschist grade igneous and associated sedimentary rocks of the Virgilina sequence, Uwharrie Formation and Albemarle Group (Figure 2.3). The Neoproterozoic (633 to 612 Ma; Wortman *et al*., 2000) Virgilina sequence is dominated by subaqueous volcanic rocks and turbidites that are unconformably overlain by the Uwharrie Formation, a collection of mainly subaqueous felsic volcaniclastic and sedimentary rocks that have yielded U-Pb zircon ages of 551 ± 8 Ma (Ingle, 1999) and 554 ± 15 Ma (Ingle *et al*., 2003). The Uwharrie Formation is overlain by the Albemarle Group, a sequence of submarine epiclastic sedimentary rocks with minor felsic and mafic volcanic rocks. Structurally, from lowest to highest, the group includes: *i*) Tillery Formation, comprising thin-bedded fine-grained clastic sedimentary rocks with minor felsic and mafic volcanic rocks; *ii*) Cid Formation, a sequence of fine-grained sedimentary rocks with substantially more felsic and mafic volcanic rocks than the Tillery Formation; *iii*) Floyd Church Formation, comprising medium-bedded fine-grained epiclastic rocks; and *iv*) Yadkin Formation, composed dominantly of greywacke derived from a mafic source (Hibbard *et al*., 2002).

The age of the Albemarle Group is constrained by faunal and geochronological controls to the late Neoproterozoic-earliest Cambrian. The Ediacaran trace fossils *Pteridinium* and *Aspidella* are reported from the Floyd Church Formation and Cid Formation, respectively (Weaver *et al*., 2006; Hibbard *et al*., 2006). Ingle *et al*. (2003) obtained a U-Pb zircon ages of 554 ± 15 Ma for the Uwharrie Formation and 540.6 ± 1.2 Ma for the Flat Swamp member of the Cid Formation; the latter unit has also yielded zircon from rhyolite flows that have been dated by U-Pb (zircon) ID-TIMS at 547 ± 2 Ma (Hibbard *et al*., 2006). The maximum age of the Yadkin Formation is constrained to the Early Cambrian from a detrital zircon dated by U-Pb ID-TIMS at ca. 531 Ma (B. Miller personal communication, 2005).

In central North Carolina (Figure 2.4), the Stony Mountain gabbro occurs as numerous irregular stocks of gabbro that are exposed in outcrops along hilltops, ridges and lake shorelines. The contacts of most of the intrusions are not well exposed; however, local intrusive contacts are present in the Tillery Formation and large gabbro bodies are present in the Uwharrie Formation and all units of the Albemarle Group (Seiders, 1981). Geophysical data (Stromquist and Henderson, 1985) indicate that the gabbro is present in the limbs of large scale upright folds as northeast-striking and west dipping, sill-like bodies that vary in size from 1 metre to several hundred metres in thickness.

The Stony Mountain gabbro consists of equigranular, medium- to course-grained, dark green to greenish-grey gabbro. The rock contains predominantly (ca. 50%) of subhedral to euhedral plagioclase that is variably saussuritized and in places completely altered to sericite and epidote. Mafic minerals clinopyroxene, amphibole and biotite comprise about 35% of the rock and are variably altered to pleochroic colourless to pale green chlorite and actinolite. The cores of augite crystals are replaced by green-brown and pleochroic hornblende. Hornblende also occurs as poikilitic crystals that enclose aggregates of alteration minerals and plagioclase crystals and is typically altered. Minor amounts of anhedral quartz occur interstitial to the plagioclase and mafic minerals. Pyrite and opaque minerals occur as accessory minerals in the groundmass.

Stratigraphic relationships indicate that intrusion of the Stony Mountain gabbro occurred after deposition of the early Paleozoic Yadkin Formation (ca. 531 Ma; B.Miller personal communication, 2005; Chapter 1) but before a Late Ordovician (ca. 456 Ma) tectonothermal event responsible for upright folding and greenschist facies metamorphism in the Albemarle sequence (Offield *et al*., 1995) that has been interpreted (Hibbard, 2000) to be related to the accretion of Carolinia to eastern Laurentia. Thus, the age of the Stony Mountain gabbro is constrained to the Early Cambrian-Late Ordovician.

LITHOGEOCHEMISTRY

The analysis of trace and rare earth element geochemical data is a valuable tool in understanding and interpreting the petrology and petrogenesis of igneous rocks (e.g. Swinden *et al*., 1990; Jenner, 1996; Piercey *et al*., 2001). The purpose of this geochemical investigation is primarily directed toward solving petrogenetic and tectonic, rather than alteration-related, problems. Magmatic rock geochemical signatures, through comparison of geochemical data with those in modern environments, can provide insight into the paleotectonic setting, and therefore allows a reconstruction of the early Paleozoic tectonic evolution of Carolinia.

Analytical techniques

Representative gabbro samples (n=24) from the Stony Mountain gabbro were collected for whole-rock geochemical analysis. All samples have been metamorphosed to lower greenschist facies during regional metamorphism and where possible, samples with excessive alteration, veining, or weathering were discarded. Pearce (1987) and MacLean and Barrett (1993) have demonstrated that the alkali-elements (Na, K, Ca), SiO_2 and the low field strength elements (LFSE: Rb, Ba, U, Cs, Sr) are mobile under these metamorphic conditions which restricts their use in elucidating petrogenetic processes. However, thorium, by definition a LFSE is considered to be immobile during alteration and low-grade metamorphism (Jenner, 1996). The rare earth elements (REE), high field strength elements (HFSE: P, Ti, Y, Zr, Nb, Hf, Ta), transition elements (Te-Sc, V, Cr, Co, Ni) and major element Al_2O_3 are considered to be immobile under low-grade alteration and metamorphic conditions. The exception however is Eu, which can be very mobile under most hydrothermal conditions (Rollinson, 1993).

Analyses of major-element oxides (recalculated to an anhydrous total of 100%) and selected trace elements (Rb, Sr, Zr, Y, Nb, K, Ti) were performed on pressed powder pellets using X-Ray Fluorescence (XRF) spectrometry at the Department of Earth Sciences, Memorial University of Newfoundland. Analytical procedures, precision, accuracy and limits of detection are described by Longerich (1995). The REE and Th were determined by Na_2O_2 sinter dissolution, followed by solution and inductively-coupled plasma mass-spectrometry (ICP-MS) using the method of Longerich *et al.* (1990). The internal check of Zr and Hf analyzed by XRF and ICP-MS indicates that there were no dissolution problems associated with the Na_2O_2 sinter. Precision in trace element analyses by XRF and ICP-MS, measured as percent relative standard deviation (% RSD), is observed as mainly excellent to good (0-7% RSD); accuracy measured as percent relative difference (% RD) from IGRM standards is generally less than 8%.

Alteration and element mobility

To assess the degree of silica and alkali-element mobility during hydrothermal alteration all samples are plotted on a total alkalies versus silica plot (Figure 2.5). The samples exhibit a large degree of scatter in SiO_2 that is most likely the result of silica mobility during hydrothermal alteration. Silica concentration generally decreases with hydrothermal alteration; in least altered rocks however, there is no correlation between SiO_2 content and indices of alteration (e.g. Ishikawa alteration index and Al_2O_3/Na_2O) suggesting that these rocks have largely retained their primary igneous SiO_2 contents.

To asses the degree of spilitisation and K-metasomatism, rocks are plotted (Figure 2.6) on a K_2O+Na_2O vs $K_2O/(K_2O+Na_2O)$ diagram of Hughes (1973). Most of the samples lie within or near the igneous spectrum field suggesting that these easily mobilized elements have not been significantly altered by regional metamorphism. This alteration is also unlikely to have significantly fractionated the immobile trace elements because there is no correlation between them and the Al_2O_3/Na_2O alteration index. Coish (1977), Coish *et al*. (1983) and Alt and Emmermann (1985) suggest that in rocks altered under low water/rock ratios, changes in the MgO/FeO ratio are considered to be small to negligible, thereby allowing this ratio to be used as an indication of primary igneous processes and differentiation index.

Geochemical characteristics

The rocks of the Stony Mountain gabbro are characterized by basaltic affinities (Zr/TiO_2 <0.1) and non-alkalic ratios (Nb/Y <0.8) (Figure 2.7) with variable but typically high MgO (8-20%), Ni (12-433 ppm) and Cr (16-1366 ppm) concentrations. The HFSE contents (Nb, Zr, Hf, Ga, Y) are low to moderate and are also reflected in Nb/La and Zr/La values and are characteristic of arc-related volcanic rocks. These rocks have major element compositions of high-Fe to high-Mg tholeiitic basalt (Fe + Ti – Al – Mg cation plot of Jensen, 1976; Figure 2.8), which is also reflected in V, TiO_2 and P_2O_5 concentrations which show a positive correlation with decreasing Mg#, suggesting incompatibility of all these elements during fractionation. In contrast, compatible elements Ni, Cr, and Sc exhibit a negative trend with Mg# (Figure 2.9), which is consistent with continued fractional crystallization involving olivine and pyroxene. Mg# [Mg/(Mg+Fe)] range from 80-50 and imply that the rocks span the range from primitive to more evolved. The rocks have Ni concentrations between 10–100 ppm, which is typical for island arc tholeiites with these MgO contents (Gill, 1981). Many of the samples however, contain high Ni and MgO contents, and high Cr/Ni values (>3); features that are characteristics of boninites. The high MgO (>10), high Ni (>350 ppm), high Cr (>1000 ppm) and low SiO_2 (<45%) in the samples with high Mg# (>70) suggest that these rocks are primary magma melts from the mantle that have not undergone significant high-level fractionation after segregation from their source.

Primitive mantle extended REE patterns (Figure 2.10) illustrate the variety of REE patterns in the Stony Mountain intrusive suite. The data are characterised by an enrichment of the LFSE relative to the most incompatible HFSE and a depletion in Nb relative to La and Th, resulting in negative Nb anomalies (Nb/Nb* ~ 0.8). The data also show negative Zr and Hf anomalies relative to Sm and Nd, flat HREE patterns and differences in overall abundances relative to Mg#. The LREE enriched patterns ($[La/Yb]_n$ ~ 2.0-2.5) are also reflected in other ratios of more/less incompatible elements, namely Th/La, Ti/V, Zr/Y and Nb/Zr and are similar to that found in low-K to medium-K tholeiites in modern arc settings (Figure 2.11). The samples have essentially parallel patterns with the least primitive samples (lowest Mg#) having the higher element abundances, which is compatible with a suite generated by low-pressure fractional crystallization of olivine + plagioclase ± clinopyroxene phases. The relatively flat HREE patterns preclude garnet as a refractory mineral phase in the source and indicate melting occurred at relatively shallow (<50 km) depths.

Rocks of the Stony Mountain gabbro are plotted on a series of discrimination diagrams (Figure 2.12) using incompatible immobile trace elements to interpret the tectonic setting in which they formed. The low TiO_2 contents are reflected on the Ti–V plot (Figure 2.12a) of Shervais (1982), as all of the rocks plot in the normal island arc tholeiite (IAT) field and define a trend with chondritic Ti/V ratios (~15) with the least fractionated samples plotting at lower absolute abundances. On a ternary plot (Figure 2.12b) of Nb-Y-Zr (Meschede, 1986) most of the samples plot in the IAT field with one sample plotting away from the Zr apex outside the volcanic arc basalt field and in the E-MORB field. Most samples plot (Figure 2.12c) in the VAB field on a Nb–Hf–Th plot (Wood, 1980) and are displaced towards the Th apex, reflecting their negative Nb anomalies and higher Th/Nb ratios.

To discriminate between arc and non-arc rocks the samples were plotted (Figure 2.12d) on Swinden *et al.*'s (1989) plot of Nb/Th versus Y. The Stony Mountain samples have a clear arc geochemical signature and suggest derivation from a relatively refractory source. Although tectonic discrimination diagrams using highly incompatible immobile trace elements suggest an arc-related origin for the rocks of the Stony Mountain gabbro, ratios using the less incompatible elements (Zr, Ti, Y) indicate a non-arc origin in some of the samples (Figure 2.13). Plots involving Th, however, suggest an island arc-related setting or contamination by continental crust.

Sm-Nd ISOTOPIC SYSTEMATICS

The Samarium-Neodymium isotopic composition was determined for two samples of the Stony Mountain gabbro to elucidate the relative roles of mantle and continental crust and to provide constraints on modelling the processes involved in the petrogenetic history. The samples were processed and analysed at the Radiogenic Isotope Facility at Memorial University of Newfoundland. For each sample, the measured and calculated initial ratios (at t=500 Ma) are given with ε_{Nd} and T_{DM} model ages that are calculated according to the model of DePaolo (1988) using linear evolution for a mantle separated from the CHUR at 4.55 Ga and having a present day $\varepsilon_{Nd} = +10$. The data are listed in Table 2.2. Full details regarding analytical procedures, accuracy, and precision are given in Appendix 2.A.

The two samples analyzed have $\varepsilon_{Nd}500= +2.6$ and +3.4 and T_{DM} = 1.5-1.6 Ga which is similar to previously reported data for the Uwharrie Formation and Albemarle Group (Mueller *et al*., 1996; Hibbard *et al*., 2007). These data are consistent with a source dominated by juvenile material with long-term LREE depletion which is interpreted to be depleted mantle (Figure 2.14) and also indicate that an older, highly evolved crustal component is not present. However, these samples have $^{147}Sm/^{144}Nd$ ratios less than that expected for depleted mantle and element ratios interpreted to reflect the mantle source of the Stony Mountain gabbro (i.e. Zr/Nb) suggest that these rocks were derived from melting a mixed depleted mantle with a more enriched mantle component. On a plot of $^{147}Sm/^{144}Nd$ vs ε_{Nd} (Figure 2.15), the rocks plot slightly below the field for mixing of depleted and fertile mantle which is consistent with incompatible element abundances that indicate an older LREE-enriched component was present during magma genesis. This component may be either a crustal source, recycled juvenile crustal material or a time-integrated, LREE-enriched source of unknown origin in the mantle.

In order to quantify the potential contribution of these source components, I have attempted to model the processes involved in the petrogenesis of the Stony Mountain gabbro using the method of Swinden (1987) and the mixing equations of Langmuir *et al*. (1978). The approach has been to utilize a minimum number of hypothetical sources to calculate a partial melting-mixing model that corresponds to the observed isotopic and geochemical compositions. Although the generation of a single precise model for the petrogenesis of the Stony Mountain gabbro is limited because only one isotopic system is used, the aim is to construct a geologically compatible model by which the observed compositions could be derived and that illustrates possible mechanisms of magma genesis. Previous studies from the Cordillera (Piercey *et al*., 2003) and Appalachians (Swinden *et al*., 1990; MacLachlan and Dunning, 1998) have demonstrated the usefulness of this method in interpreting the petrogenesis of ancient magmatic rocks.

Generation of the Stony Mountain gabbro can be modeled as resulting from simple melting/mixing processes between a dominantly MORB-like depleted mantle (DM) source and a minor enriched ocean island basalt (OIB) component that has LREE-enrichment (low $^{147}Sm/^{144}Nd$) but positive ε_{Nd} values (long-term LREE-depletion). Although, the $^{147}Sm/^{144}Nd$ concentrations can be generated from simple partial melting of this mixed mantle source, the assumed $\varepsilon_{Nd}t$ of this component (estimated to range from +4 to +7) is too high to account for the observed isotopic compositions. In order to generate $\varepsilon_{Nd}t$ in the range +2 to +3 from DM/OIB, mixing with an old LREE-enriched component is required. This could be a subduction-related component that was in equilibrium with juvenile material such as subducted oceanic crust with little or no pelagic sediment; however, incompatible element abundances (e.g. Nb/Th, Ti/V) suggest that this component is best interpreted as LREE-enriched hydrous fluids related to subduction and derived from the downgoing oceanic slab. Despite the uncertainties in the composition and nature of these sources the petrogenesis of the Stony Mountain gabbro is best explained using a simple two-component mixing model that consists of 10% partial melting of a mixed source comprising 99% DM (with lesser amounts of OIB) and 1% of a slab-derived crustal component.

DISCUSSION

Petrogenesis

Deciphering the origin of mafic magmatism of the Stony Mountain gabbro requires distinguishing between mantle source features versus superimposed features related to fractional crystallization and other open-system processes (e.g. crustal contamination). To examine the composition of the mantle wedge and the role of mantle source depletion or enrichment prior to subduction, it is necessary to examine the systematics of immobile, incompatible trace elements that are not affected by crustal contamination and slab metasomatism and are therefore considered to reflect the composition of the original mantle. In particular, the elements Zr, Hf, Y, Ti, Sc, Ga, and

HREE are conservative with respect to the mantle source (i.e. they are not affected by subduction) and their geochemical behaviour is determined solely by the composition of the mantle and the various processes of partial melting, mixing and fractional crystallization that occur during magma generation (Woodhead *et al*., 1993; Pearce and Peate, 1995).

Bivariant plots of Zr and Ti vs. Nb (normalized to Yb) in the Stony Mountain gabbro (Figure 2.16) plot in the non-arc MORB field that extends from average N-MORB to more enriched (E-MORB) compositions; this linear array indicates the occurrence of both incompatible element depleted (Nb/Yb ratios < average N-MORB) and moderately enriched (Nb/Yb ratios > N-MORB) pre-metasomatic mantle sources. Although previous workers (Stern, 1981; Morris and Hart, 1983; Foley and Wheller, 1990) have suggested that mixing of enriched-mantle sources with partial melts of depleted mantle in the presence of residual mineral phases is capable of producing the complete spectrum of geochemical compositions in island arc magmas, the LFSE enrichment and depletion in HREE and Y in the Stony Mountain gabbro are inconsistent with residual minor phases controlling the incompatible element contents of arc magmas. Although the Nd isotope data indicate that the Stony Mountain gabbro magmas are a mixture of MORB-like and OIB-type enriched source, chondrite normalized LREE and MREE abundances are greater than that interpolated for the mantle and therefore indicate the presence of an additional component during magma generation.

The LFSE enriched REE patterns, low abundances of HFSE and prominent negative Nb and Ti anomalies are similar to tholeiitic basalts formed in modern arc environments (e.g Tonga, Aleutian arcs) (Gill, 1981; Pearce and Peate, 1995 and references therein). Negative Nb anomalies are common features of rocks associated with subduction zones, due to the influx of LFSE into the mantle source regions from the subducted slab (Kay, 1980). This observation suggests the additional component in the generation of the Stony Mountain gabbro is related to subduction and is in all probability an aqueous fluid derived from dehydration and partial melting of the downgoing oceanic crust. Although negative Nb and LFSE-enriched compositions are features of the upper continental crust, plots of conservative (Nb-La-Yb) and non-conservative (Th) elements together with εNd data argue against significant crustal contamination and suggest the presence of a subducted slab component during formation of these rocks in a volcanic arc environment. The Th-Nb-Yb systematics (Figure 2.16) indicate that most samples are displaced to higher Th/Yb ratios than MORB and have undergone significant Th enrichment. The high Th/Nb ratios are inversely proportional with high La/Sm ratios, which is inconsistent with crustal contamination and suggests the input of Th from subduction-zone fluids in the mantle wedge (Figure 2.17).

Tectonic setting

The goal of this geochemical and isotopic study is to ultimately determine the tectonic environment of formation of the Stony Mountain gabbro and thus to provide constraints on the nature of the early Paleozoic history of Carolinia. Although the geochemical and isotopic data presented herein allow for an interpretation of the source region and petrogenetic history of the Stony Mountain gabbro, they do not provide direct evidence for its geological and tectonic history and therefore any interpretation of the paleotectonic evolution of Carolinia must depend on comparisons between the relationships displayed by similar rocks in modern analogues and ancient correlatives.

Rocks with tholeiitic affinities and OIB signatures are found in a variety of tectonic settings including continental arc rifts (Goodfellow *et al*. 1995), oceanic hot spots related to mantle plumes (Leitch and Davies, 2001) and volcanic arc rift settings (van Staal *et al*. 1991; Shinjo *et al*. 1999). The geochemical and geological features of the Stony Mountain gabbro are consistent with formation within an Early Cambrian ensimatic island arc-arc rift basin. The HFSE-depleted signatures coupled with negative Nb anomalies on primitive mantle extended REE diagrams and degree of LREE enrichment ($[La/Yb]n \sim 2.0\text{-}2.5$) are similar to low-K to medium-K tholeiitic rocks in modern island arc settings (Gill, 1981).

The LREE-enriched patterns and positive εNd of the Stony Mountain gabbro indicate mixing between mantle and slab-derived crustal sources. Conservative element ratios of less/more incompatibility reflect the geochemical diversity of the mantle source prior to the effects of subduction and indicate that the Stony Mountain gabbro magmas contain variable mixtures of depleted lithospheric (N-MORB) mantle and enriched (OIB-like) asthenospheric mantle sources. These data are similar to interpreted athenospheric mantle derived mafic rocks in the modern Okinawa Trough back-arc basin (Shinjo *et al*. 1999) and back-arc basin basalts in the Ordovician Bathurst Mining camp (van Staal *et al*. 1991).

Mantle wedge enrichment is recognized as a feature of many island arc systems. In the modern environment, island arc volcanic rocks with enriched mantle compositions are often formed during and immediately after arc rifting which is usually related to the early stages of back-arc spreading (Pearce and Peate, 1995). The rocks of the Stony Mountain gabbro are interpreted as the products of a volcanic arc rifting event, with the magmas forming as a result of decompression partial melting of a mixture of depleted lithospheric and enriched asthenospheric mantle sources. There are several examples of similar arc-rift rocks in the modern environment that span all stages of arc rifting, notably the Lau Islands, Sumisu Rift in the Izu-Ogasawara arc, and the northern Marianas (Volcano arc).

The Lau Islands represent one of the most thoroughly studied arc-backarc systems (Hawkins *et al*., 1994; Pearce *et al*., 1994) and record the changing volcanic activity in a Cenozoic arc to back arc transition and contain a record of Lau arc volcanism prior to, during, and following arc rifting (Gill, 1984). There is evidence that the mantle was depleted prior to rifting and that the rifting event that caused the remnant arc to move away from the subduction zone caused enriched OIB-like magmas to erupt in this remnant arc. An example of an arc that is currently undergoing rifting is found in the Sumisu Rift in the Izu-Ogasawara arc, where isotope and trace element data are consistent with mixing of an E-MORB mantle source and an N-MORB subduction-affected source (Hochstaedter *et al*., 1990). The enriched rocks of the Volcano arc in the northern Mariana Islands are located where the arc is starting to reform following arc rifting (Lin *et al*., 1990). Isotopic data also suggest a two-component mixing between a MORB like, subduction-affected source and a source similar to that of ocean-island basalts (OIB). Each of these volcanic arc systems record the transition from island arc volcanism to intra arc rifting, leading to the eventual inception of a back arc basin. The central region of the Vanuatu arc however, preserves a different type of arc rifting that resulted from collision of an older arc edifice with the modern arc. The ongoing collision of the Vanuatu arc with an Eocene arc complex resulted in a major compositional change in source regions during the past 2 m.y. This collision is interpreted to have caused an influx of fertile mantle from the back-arc region into the mantle wedge as recorded in the geochemical change from a Pacific-MORB and sediment, subduction-derived Pb to Indian-MORB mantle-derived Pb signature (Laporte & Briqueu, 1993; Pearce and Peate, 1995). In each of these examples mantle enrichment is considered to be related to arc rifting which causes new, fertile mantle to invade the mantle wedge by the addition of small volumes of asthenospheric melts.

Similar ranges of MORB-like to OIB-type enriched rocks have also been reported from ancient volcanic rocks interpreted to have formed in intra-arc rift-backarc basinal environments. The Yukon-Tanana terrane of the Canadian Cordillera has many similarities to the Early Cambrian arc in Carolinia. It comprises Late Devonian (365-50 Ma) mafic metavolcanic rocks that were the products of partial melting of mixtures of asthenospheric and lithospheric mantle due to arc rifting and separation of the Yukon-Tanana terrane from the North American craton coeval with the formation of a backarc basin inboard of this arc system (Piercey *et al.*, 2001; Piercey *et al.*, 2004). In terms of geochemistry and geodynamic setting, the best analogues to the arc in Carolinia are found in the Ganderian margin of the Appalachians in the Tetagouche Group in New Brunswick and Wild Bight Group in Newfoundland (van Staal *et al.*, 1991; Swinden *et al.*, 1990) which record extension and rifting of the Popelogan-Victoria arc system in the Middle Ordovician forming the Tetagouche-Exploits marginal basin (van Staal, 1994; MacLachlan and Dunning, 1998). Although there are several differences between each of these modern and ancient arc systems and Carolinia, they are presently the best geodynamic analogue and accordingly support an Early Cambrian arc-rift to back-arc basin setting for Carolinia.

Implications for the tectono-magmatic evolution of Carolinia

The inferred age, trace element, and isotopic characteristics of the Stony Mountain gabbro indicate that subduction-related arc magmatism in Carolinia did not terminate with deposition of the late Neoproterozoic-Early Cambrian volcanic sequences of the Carolina terrane, but that island arc magmatism continued into the Early Cambrian. Integration of new geochemical and isotopic data with existing geological and geochronological evidence allows proposal of a revised Neoproterozoic-Early Cambrian tectonic history of Carolinia involving the transition from an arc to a backarc rift. Between 633 - 612 Ma an arc system (Virgilina arc), represented by dominantly sub-aqueous felsic to intermediate pyroclastic rocks of the Virgilina sequence, developed in along the ocean facing margin of west Gondwana (Figure 2.18). The primitive ε_{Nd} signatures and Neoproterozoic T_{DM} ages suggest that this mature arc system is composed of juvenile, largely mantle-derived crust built on a basement of oceanic crust (Kozuch, 1994; Samson *et al*., 1995). The overlying sedimentary-volcanic rocks of the Albemarle sequence indicate that subduction and arc magmatism continued into at least the Early Cambrian (ca. 535 Ma). Nd isotopic signatures (Hibbard *et al*., 2007) suggest that these arc magmas were derived from melting of the older juvenile basement sources. Geochronological data from inherited zircons (Ingle *et al*., 2003) in contemporaneous volcanic and volcaniclastic rocks are consistent with variable mixing of a sedimentary component with a composition similar to that of the alleged Mesoproterozoic basement to Carolinia (e.g., Mueller *et al*., 1996). Continued subduction of the Carolinia arc probably resulted in slab rollback on the Gondwanan margin and led to the development of an extensional tectonic regime which was accompanied by rising geotherms that promoted decompression melting in the upwelling asthenospheric mantle and the initiation of a back arc rift. In the proposed model initial magmatism in the rift formed as low-degree partial melts of N-MORB-type lithospheric mantle which when mixed with upwelling enriched (OIB-like) asthenospheric mantle resulted in the hybrid E-MORB signatures seen in the Stony Mountain gabbro. The petrogenesis of these rocks cannot be modeled by two-component mixing of MORB-type and OIB-like mantle and therefore they require the addition of a high LFSE/HFSE component which in all likelihood was a hydrous fluid derived from the subducting slab and transferred to the subarc mantle wedge. The presence of an Early Cambrian arc-rifting event in Carolinia has previously been proposed on the basis of whole rock $\delta^{18}O$ isotopic data (Feiss *et al*., 1993) and the presence of tectonothermal events (Hibbard and Samson, 1995; Dennis and Wright, 1997; Wortman *et al*., 2000) interpreted to be related to intra-arc transtension (Harris and Glover, 1988).

Rifting of Carolinia and opening of Rheic Ocean

A wealth of geological, isotopic, paleomagnetic and paleotological data indicate that the Rheic Ocean formed in the Late Cambrian-Early Ordovician by the rifting of peri-Gondwanan terranes from the northern margin of Gondwana (van Staal *et al*., 1998; Murphy *et al*., 2006). Although Carolinia comprises the second largest peri-Gondwanan block in the Appalachian-Caledonian orogen, evidence for the timing of rifting of Carolinia and the nature or mode of its opening have received little attention in the literature. The lack of data with respect to Carolinia is critical as precise constraints on the timing of continental rifting and initiation of sea-floor spreading are necessary for paleogeographic reconstructions of the Neoproterozoic-early Paleozoic earth.

Presently, most models (e.g. Keppie *et al*., 2003; Murphy *et al*., 2006) for rifting of Carolinia from Gondwana are based on the conventional correlation of Carolinia with the northern Appalachian terrane of Avalonia which is generally accepted to have rifted from Gondwana in the Early Ordovician (Prigmore *et al*., 1997; Cocks and Torsvik, 2002; Murphy *et al*., 2006). The presence in both of Neoproterozoic felsic-dominated magmatic-sedimentary sequences has led many workers (e.g. Williams & Hatcher, 1983; Nance *et al*., 2002; Ingle *et al*., 2003) to consider these two first-order crustal blocks as representing portions of a single peri-Gondwanan microcontinent. This microcontinent model implies that the Rheic Ocean opened as a single major seaway with Avalonia/Carolinia at its leading margin. However, on the basis of their detailed lithotectonic records, Secor *et al*. (1983), Samson (1995), Hibbard *et al*. (2002) and Hibbard *et al*. (2007) showed that Carolinia and Avalonia have distinct faunal, paleomagnetic, isotopic, and tectonothermal histories in the late Neoproterozoic-early Paleozoic and therefore likely represent separate independent crustal blocks.

The data require substantial revision of extant tectonic models for the early Paleozoic history of the Appalachian peri-Gondwanan realm. The recognition of rocks of island-arc affinity with enriched mantle compositions of the Stony Mountain gabbro support an Early Cambrian arc rift to back-arc basin setting for Carolinia and thereby provide a mechanism for the initiation of the Rheic Ocean (Figure 2.18). Geological, geochemical and isotopic data suggest that the Neoproterozoic-Early Cambrian evolution of Carolinia was the result of arc magmatism related to subduction in the Tornqvist Sea/Iapetus Ocean on the margin of west Gondwana. In Carolinia, this magmatism is represented by the rocks of the ca. 633 to 612 Ma Virgilina sequence and overlying ca. 551 to 554 Ma Uwharrie Formation and is accompanied by a thick succession of marine volcaniclastic sedimentary rocks of the Albermarle Group that formed proximal to the active arc (Chapter 1). After ca. 528 Ma (youngest date for detrital zircons of the Yadkin Formation), it is proposed that arc volcanism was disrupted as the arc underwent extension and rifted forming an ensimatic back-arc marginal basin, (the initiation of the Rheic Ocean) between the active arc and Gondwana. The tholeiitic magmas of the Stony Mountain gabbro from this study record the initiation of this arc-rifting event and formed as a result of hydrous partial melting of a mixed lithospheric/asthenospheric mantle source that was contaminated by an incompatible element-enriched aqueous fluid from the subducting oceanic lithosphere.

Temporal correlatives of this early Paleozoic arc in Carolinia occur in the peri-Gondwanan crustal block of Ganderia in Maine, New Brunswick and Newfoundland. These sequences include Late Neoproterozoic (ca. 565 Ma) arc plutonic and volcanic rocks and Lower Cambrian (ca. 514 Ma) volcanic rocks which have been interpreted as remnants of a Ganderian arc/back arc sequence (Colman-Sadd *et al*., 1992; Jenner and Swinden, 1993), termed the Penobscot complex (van Staal *et al*., 1998). van Staal (2007) suggested that an overall westward younging of the Cambrian arc volcanic rocks in the

Penobscot complex (Rogers *et al*., 2006) implied that it formed above an east-dipping subduction zone beneath Gondwana.

Although the actual mechanism of the rift to drift transition is uncertain, it is suggested that arc rifting of the Carolina arc may have been in response to, or induced, the initial opening of the Rheic Ocean between the rifted Carolinian microcontinent and cratonic northern Gondwana. The rapid Late Cambrian opening of the Rheic Ocean was probably achieved by slab rollback of the subducting oceanic plate and was synchronous with a polarity flip and initiation of subduction along the northern margin of Iapetus. The increasing slab pull forces in Iapetus together with slab roll back beneath the arc in the Rheic Ocean are responsible for the transfer of Carolinia from Gondwana longitudinally into and across the contracting Iapetus Ocean from which it was accreted to Laurentia in the Late Ordovician. This model is analogous to the movement of the Cimmerian microcontinent across Paleo-Tethys and opening of Neo-Tethys in the Cenozoic (Stampfli and Borel, 2002). However, Keppie *et al*. (2003) proposed an alternate scenario in which the transition from arc to rift geodynamic setting in Carolinia occurred by the replacement of subduction by transform faulting as a result of ridge–trench collision where the trench is replaced by a transform fault as the ridge is overridden leading to a switch from arc to rift magmatism. As the ridge–trench–transform triple point migrates this triple point became unstable leading to extension and the separation of Carolinia in a manner similar to the modern opening of the Gulf of California (*i.e.*, a “Baja-type” model).

CONCLUSIONS

The geochemical and isotopic data presented in this study illustrate that the Stony Mountain Gabbro records episodic early Paleozoic arc-rift magmatism on the continental margin of west Gondwana that are interpreted to represent magmatism associated with Early Cambrian ensimatic back-arc rifting and basin generation. Early Cambrian subduction in Carolinia was most likely disrupted by subduction hinge retreat of the oceanic slab, migration of arc magmatism, and the onset of back-arc extension. Partial melting and generation of the studied gabbros was probably driven by extension-related emplacement at mid-crustal levels of mafic mantle-derived magmas. However, the paucity of Late Cambrian-Ordovician rocks in Carolinia means that there are insufficient data to constrain many of the aspects of this back-arc basin and therefore many features of the early Paleozoic evolution of Carolinia remain equivocal.

The volcanic and epiclastic rocks of the Albemarle sequences were interpreted previously to represent a volcanic arc built in proximity to ca. 1.0 Ga Gondwanan continental margin (Hibbard *et al*., 2002; Ingle *et al*., 2003). The geochemical and isotopic data presented herein support and refine this model with the recognition that younger arc magmatism formed due to rifting of the Carolina arc during the opening of a back-arc marginal basin. Decompression melting of the mantle associated with arc-rifting resulting in melting and the formation of the Stony Mountain gabbro. Nd isotope data are consistent with magma derivation entirely from melting of variable mantle sources. It is proposed herein that continued rifting led to seafloor spreading in the back arc between the rifted Carolinian microcontinent and northern Gondwana which led to the initiation of the Rheic Ocean. This model implies that the Carolinian microcontinent defined the boundary between the expanding Rheic Ocean to the south and the contracting Iapetus Ocean in the north. Expansion of the Rheic Ocean coupled was synchronous with the continued closure of Iapetus which ultimately led to the accretion of Carolinia to the eastern Laurentian margin in the Middle Ordovician.

Neoproterozoic-early Paleozoic (ca. 570-540 Ma) arc-related rocks are widespread throughout the peri-Gondwanan margin of Gondwana as temporal correlatives of the Carolina arc are found throughout the northern Appalachian peri-Gondwanan terrane of Ganderia. It is evident from the timing of magmatism in Carolinia and Ganderia that arc rifting and initiation of the Rheic Ocean and subsequent accretion to Laurentia was diachronous along the northern margin of Gondwana. By 455 Ma, Carolinia was extensively deformed and metamorphosed due to its docking to Laurentia, whereas Ganderia, was still an independent microcontinent until its Early Silurian accretion to Laurentia (van Staal *et al*., 1998; Pollock *et al*., 2007). Although both Carolinia and Ganderia share common features in their first order geological and tectonic characteristics, it remains to be seen if they represent two independent peri-Gondwanan microcontinents or diverse tectonic regimes within a single crustal block.

REFERENCES

Alt, J.C. and Emmermann, R.
1985. Geochemistry of hydrothermally altered basalts: Deep Sea Drilling Project Hole 504B, Leg 83. Initial Reports, Deep Sea Drilling Project, 83, p. 249-262.

Barth, M.G., McDonough, W.F. and Rudnick, R.L.
2000. Tracking the budget of Nb and Ta in the continental crust. Chemical Geology, 165, p. 33-41.

Cocks, L.R.M. and Torsvik, T.H.
2002. Earth geography from 500 to 400 million years ago. A faunal and palaeomagnetic review. Journal of the Geological Society of London, 159, p. 631-644.

Coish, R.A.
1977. Ocean floor metamorphism in the Betts Cove ophiolite, Newfoundland. Contributions to Mineralogy and Petrology, 60, p. 255-270.

Coish, R.A., Hickey, R. and Frey, F.A.
1983. Rare earth element geochemistry of the Betts Cove ophiolite, Newfoundland: complexities in ophiolite formation. Geochemica et Cosmochemica Acta, 46, p. 2117-2134.

Colman-Sadd, S.P., Dunning, G.R., and Dec, T.
1992. Dunnage-Gander relationships and Ordovician orogeny in central Newfoundland; a sediment provenance and U/Pb age study. American Journal of Science, 292, p. 317-355.

Dennis, A.J., Wright, J.E.
1997. The Carolina terrane in northwestern South Carolina, USA: age of deformation and metamorphism in an exotic arc. Tectonics 16, p. 460-473.

DePaolo, D.J.
1981. Neodymium isotopes in the Colorado Front Range and crust–mantle evolution in the Proterozoic. Nature, 291, p. 193–196.
1988. Neodymium isotope geochemistry-an introduction, Springer, 187 p.

Feiss, G., Vance, K., Wesolowski, D.
1993. Volcanic rock-hosted gold and base-metal mineralization associated with Neoproterozoic–Early Paleozoic back-arc extension in the Carolina terrane, southern Appalachian Piedmont. Geology, 21, p. 439– 442.

Foley, S.F. and Wheller, G.E.
1990. Parallels in the origin of the geochemical signatures of island arc volcanics and continental potassic igneous rocks: the role of residual titanates. Chemical Geology, 85, p. 1-18.

Fullagar, P., Goldberg, S., Butler, R.
1997. Nd and Sr isotopic characterization of crystalline rocks from the southern Appalachian Piedmont and Blue Ridge, North and South Carolina. *In*: Sinha, K., Whalen, J., Hogan, J. (*eds.*), The Nature of Magmatism in the Appalachian Orogen. Geological Society of America Memoir, 191, p. 165– 179.

Gill, J.B.
1981. Orogenic Andesites and Plate Tectonics. Springer-Verlag, Berlin, 390 p.
1984. Sr-Pb-Nd isotopic evidence that both MORB and OIB sources contribute to oceanic island arc magma sources in Fiji. Earth and Planetary Science Letters, 68, p. 443-58

Goodfellow, W.D., Cecile, M.P., and Leybourne, M.I.
1995. Geochemistry, petrogenesis, and tectonic setting of lower Paleozoic alkalic and potassic volcanic rocks, Northern Canadian Cordilleran Miogeocline. Canadian Journal of Earth Sciences, 32, p. 1236–1254.

Harris, C. and Glover, L.
1988. The regional extent of the ca. 600 Ma Virgilina deformation: implications for stratigraphic correlation in the Carolina terrane. Geological Society of America Bulletin, 100, p. 200– 217.

Hawkins, J.W., Bloomer, S.H., Evans, C.A., and Melchoir, J.T.
1994. Evolution of intra-oceanic arc-trench systems. Tectonophysics, 102, p. 175–205.

Hawkesworth C J, Hergt JM, Ellam RM, McDermott F.
1991. Element fluxes associated with subduction related magmatism. Philosophical Transactions Royal Society London, 335, p. 393-405.

Hibbard, J.
2000. Docking Carolina: Mid Paleozoic accretion in the southern Appalachians. Geology, 28, p. 127-130.

Hibbard, J. and Samson, S.
1995. Orogenesis exotic to the Iapetan cycle in the southern Appalachians. *In:* Hibbard, J., van Staal, C., Cawood, P. (*eds.*), Current Perspectives in the Appalachian–Caledonian Orogen. Geological Association of Canada Special Paper, 41, p. 191–205.

Hibbard, J.P., van Staal, C.R., and Miller, B.V.
2007. Links between Carolinia, Avalonia and Ganderia in the Appalachian peri-Gondwanan realm. Geological Society of America, Special Paper.

Hibbard, J.P., Stoddard, E.F., Secor, D.T. and Dennis, A.J.
2002. The Carolina Zone: overview of Neoproterozoic to early Paleozoic peri-Gondwanan terranes along the eastern flank of the southern Appalachians. Earth Science Reviews, 57, p. 299-339.

Hibbard, J.P., McMenamin, M.A.S., Pollock, J.C., Weaver, P.G., Tacker, R.C., Miller., B.V., Samson, S.D. and Secor, D.T.
2006. Significance of a new Ediacaran fossil find in the Carolina Terrane of North Carolina. Geological Society of America, Abstracts with Programs, Northeast Section, 38, p. 91.

Hochstaedter A.G., Gill J.B., and Morris J.D.
1990. Volcanism in the Sumisu Rift, II. Subduction and non-subduction related components. Earth and Planetary Science Latters, 100, p. 195-209.

Hughes, C.J.
1973. Spilites, keratophyres and the igneous spectrum. Geological Magazine, 109, p. 503-527.

Ingle-Jenkins, S., Mueller, P. and Heatherington, A.
1999. Evidence for Mesoproterozoic basement in the Carolina and other southern Appalachian terranes. Geological Society of America, Abstracts with Programs, 27, p. 397.

Ingle, S., Mueller, P.A., Heatherington, A.L. and Kozuch, M.
2003. Isotopic evidence for the magmatic and tectonic histories of the Carolina Terrane: implications for stratigraphy and terrane affiliation. Tectonophysics, 371, p. 187-211.

Ingram, S.
1999. Geology of the northern half of the Morrow Mountain Quadrangle North Carolina: a revision of the Albemarle Group. Unpublished M.Sc. Thesis, North Carolina State University, Raleigh, 109 p.

Jenner, G.A.
1996. Trace element geochemistry of igneous rocks: geochemical nomenclature and analytical geochemistry. *In:* Trace Element Geochemistry of Volcanic Rocks: Applications for Massive Sulphide Exploration, Wyman, D.A. (*ed.*), Geological Association of Canada, Short Course Notes, 12, p. 51-77.

Kay, R.W.,
1980. Volcanic arc magma genesis: Implications for element recycling in the crust-upper mantle system, Journal of Geology, 88, p. 497-522.

Keppie, J.D., Nance, R.D., Murphy, J.B., and Dostal, J.
2003. Tethyan, Mediterranean, and Pacific analogues for the Neoproterozoic-Paleozoic birth and development of peri-Gondwanan terranes and their transfer to Laurentia and Laurussia: Tectonophysics, 365, p. 195–219.

Kozuch, M.
1994. Age, isotopic, and geochemical characterization of the Carolina slate and Charlotte belts: Implications for stratigraphy and petrogenesis. Unpublished MS thesis, University of Florida, Gainesville, FL, 115 p.

Langmuir, C.H., Vocke, R.D. Jr., Hanson, G.H., and Hart S.R.
1978. A general mixing equation with applications to Icelandic basalts. Earth and Planetary Science Letters, 37, p. 380-392.

Laporte, C. and Briqueu, L.
1993. Spatial and temporal magmatic evolution of the New Hebrides arc: Pb, Sr and Nd isotopic evidence from the coexistence of two mantle components beneath the arc. Terra Abstracts. 5, p. 582.

Leitch, A.M. and Davies, G.F.
2001. Mantle plumes and flood basalts: Enhanced melting from plume ascent and an eclogite component. Journal of Geophysical Research, 106, p. 2047–2059

Lin, P.N., Stem, R.J., Morris, J., and Bloomer, S.H.
1990. Nd- and Sr-isotopic compositions of lavas from the northern Mariana and southern Volcano arcs: implications for the origin of island arc melts. Contributions to Mineralogy and Petrology, 105, p. 381- 92.

Longerich, H.P.
1995. Analysis of pressed powder pellets of geological samples using wavelength-dispersive X-ray fluorescence spectrometry. X-ray Spectrometry, 24, p. 123-136.

Longerich, H.P., Jenner, G.A., Fryer, B.J. and Jackson, S.E.
1990. Inductively coupled plasma mass spectrometric analysis of geological samples: case studies. Chemical Geology, 83, p. 105-118.

MacLachlan K. and Dunning, G.
1998. U-Pb ages and tectonomagmatic relationships of early Ordovician low-Ti tholeiites, boninites and related plutonic rocks in central Newfoundland, Canada. Contributions to Mineralogy and Petrology, 133, p. 235-258.

MacLean, W.H. and Barrett, T.J.
1993. Lithogeochemical techniques using immobile elements. Journal of geochemical Exploration, 48, p. 109-133.

Meschede, M.
1986. A method for discrimination between different types of mid-ocean ridge basalts and continental tholeiites with the Nb-Zr-Y diagram. Chemical Geology, 56, p. 207-218.

Morris, J.D. and Hart, S.R.
1983. Isotopic and incompatible element constraints on the genesis of island arc volcanics from Cold Bay and Amak Island, Aleutians, and implications for mantle structure. Geoehimica et Cosmochimica Acta, 47, p. 2015-2030.

Mueller, P., Kozuch, M., Heatherington, A., Wooden, J., Offield, T., Koeppen, R., Klein, T. and Nutman, A.
1996. Evidence for Mesoproterozoic basement in the Carolina terrane and speculation on its origins. *In:* Nance, D. and Thompson, M. (*eds.*), Avalonian and Related Peri-Gondwanan Terranes of the Circum-North Atlantic. Geological Society of America Special Paper, 304, p. 207-217.

Murphy, J.B., Gutierrez-Alonso, G., Nance, R.D., Fernandez-Suarez, J., Keppie, J.D., Quesada, C., Strachan, R.A., and Dostal, J.
2006. Origin of the Rheic Ocean: Rifting along a Neoproterozoic suture? Geology, 34, p. 325-328.

Nance, R.D., Murphy, J.B. and Keppie, J.D.
2002. A Cordilleran model for the evolution of Avalonia. Tectonophysics, 352, p. 11-31.

O'Brien, S.J., O'Brien, B.H., Dunning, G.R., and Tucker, R.D.
1996. Late Neoproterozoic Avalonian and related peri-Gondwanan rocks of the Newfoundland Appalachians. *In:* Nance, R.D. & Thompson, M.D. (*eds.*) Avalonian and Related Peri-Gondwanan Terranes of the Circum-North Atlantic. Geological Society of America, Special Paper, 304, p. 9-28.

Offield, T., Kunk, M., Koeppen, R.
1995. Style and age of deformation, Carolina slate belt, central North Carolina. Southeastern Geology, 35, p. 59-77.

Pearce, J.A.
1983. Role of the sub-continental lithosphere in magma genesis at active continental margins. *In:* C.J. Hawkesworth and M.J. Norry (*eds.*) Continental Basalts and Mantle Xenoliths, Nantwich, UK: Shiva, p. 230-49.
1987. An expert system for the tectonic characterisation of ancient volcanic rocks. Journal of Volcanological and Geothermal Research, 44, p. 189-229.
1996. A user's guide to basalt discrimination diagrams. *In:* Trace Element Geochemistry of Volcanic Rocks: Applications for Massive Sulphide Exploration, Wyman, D.A. (*ed.*), Geological Association of Canada, Short Course Notes, 12, p. 79–113.

Pearce, J.A. and Cann, J.R.
1973. Tectonic setting of basic volcanic rocks determined using trace element analyses. Earth and Planetary Science Letters, 19, p. 290–300.

Pearce, J.A. and Peate, D.W.
1995. Tectonic implications of the composition of volcanic arc magmas. Annual Reviews in Earth and Planetary Science, 23, p. 251–285.

Pearce, J.A., Harris, N.B.W., and Tindle, A.G.
1984. Trace element discrimination diagrams for the tectonic interpretation of granitic rocks. Journal of Petrology, 25, p. 956-983.

Piercey, S.J., Paradis, S., Murphy, D.C., and Mortensen, J.K.
2001. Geochemistry and paleotectonic setting of felsic volcanic rocks from the Finlayson Lake volcanic-hosted massive sulfide (VHMS) district,Yukon, Canada. Economic Geology, 96, p. 1877-1905.

Piercey,S.J., Mortensen, J.K., Murphy, D.C., Paradis, S. and Creaser, R.A.
2002. Geochemistry and tectonic significance of alkalic mafic magmatism in the Yukon–Tanana terrane, Finlayson Lake region, Yukon. Canadian Journal of Earth Sciences, 39, p. 1729–1744.

Piercey, S.J., Mortensen, J.K., and Creaser, R.A.
2003. Neodymium isotope geochemistry of felsic volcanic and intrusive rocks from the Yukon-Tanana Terrane in the Finlayson Lake Region, Yukon, Canada. Canadian Journal of Earth Sciences, 40, p. 77-97.

Piercey, S.J., Murphy, D.C., Mortensen, J.K., and Creaser, R.A.
2004. The Mid-Paleozoic Initiation of the Northern Cordilleran Marginal Back-Arc Basin: Geological, Geochemical and Neodymium Isotopic Evidence from the Oldest Mafic Magmatic Rocks in Yukon-Tanana Terrane, Finlayson Lake district, Southeast Yukon, Canada. Geological Society of America Bulletin, 116, p. 1087-1106.

Prigmore, J.K., Butler, A.J., and Woodcock, N.H.
1997. Rifting during separation of eastern Avalonia from Gondwana; evidence from subsidence analysis. Geology, 25, p. 203-206.

Rollinson, H.
1993. Using Geochemical Data: Evaluation, Presentation, Interpretation, Longman, 352 p.

Rogers, N., van Staal., C.R., McNicoll., V, Pollock, J., Zagorevski, A. and Whelan, J.
2006. Neoproterozoic and Cambrian arc magmatism along the eastern margin of the Victoria Lake Supergroup: A remnant of Ganderian basement in central Newfoundland? Precambrian Research, 147, p. 320-341.

Samson, S.D.
1995. Is the Carolina terrane part of Avalon? *In:* Current Perspective in the Appalachian-Caledonian Orogen, Hibbard, J.P., van Staal, C.R. and Cawood, P. (*eds.*), Geological Association of Canada, Special Paper 41, p. 253-264.

Samson, S., Hibbard, J., and Wortman, G.
1995. Nd isotopic evidence for juvenile crust in the Carolina terrane, southern Appalachians. Contributions to Mineralogy and Petrology, 121, p. 171-184.

Secor, D.T., Samson, S., Snoke, A., and Palmer, A.
1983. Confirmation of the Carolina slate belt as an exotic terrane. Science, 221, p. 649–651.

Seiders, V.M.
1981. Geologic map of the Asheboro, North Carolina and adjacent areas. United States Geological Survey, Map I-1314.

Shervais, J.W., 1982. Ti-V plots and the petrogenesis of modern and ophiolitic lavas. Earth and Planetary Science Letters, 59, p. 101-118.

Shinjo, R., Chung, S.L., Kato, Y., and Kimura, M.
1999. Geochemical and Sr-Nd isotopic characteristics of volcanic rocks from the Okinawa Trough and Ryukyu Arc: Implications for the evolution of a young, intracontinental back arc basin, Journal of Geophysical Research, 104, p. 591-608.

Steiger, R.H. and Jäger, E.
1977. Subcommission on geochronology: convention on the use of decay constants in geo- and cosmochronology. Earth and Planetary Science Letters, 36, p. 359–362.

Stromquist, A.A. and Henderson, J.R.
1985. Geologic and geophysical maps of south-central North Carolina. United States Geological Survey, Map I-1400.

Stampfli, G.M. and Borel, G.D.
2002. A plate tectonic model for the Paleozoic and Mesozoic constrained by dynamic plate boundaries and restored synthetic oceanic isochrons. Earth and Planetary Science Letters, 196, p. 17-33.

Stern, R.J.
1981. A common mantle source for western Pacific island arc and "hotspot" magmas: implications for layering in the upper mantle. Carnegie Institute of Washington Yearbook, 80, p. 455-461.

Stern, R.A., Syme, E.C., Bailes, A.H., and Lucas, S.B.
1995. Paleoproterozoic (1.90–1.86 Ga) arc volcanism in the Flin Flon Belt, Trans-Hudson Orogen, Canada. Contributions to Mineralogy and Petrology, 119, p. 117–141.

Sun, S-S. and McDonough, W.F.
1989. Chemical and isotopic systematics of oceanic basalts: implications for mantle composition and processes. *In:* Magmatism in the ocean basins, Saunders, A.J. and Norry, M.J. (*eds.*), Geological Society Special Publication (London), 42, p. 313-345.

Swinden, H.S.
1987. Ordovician volcanism and mineralization in the Wild Bight Group, central Newfoundland: a geological, petrological, geochemical and isotopic study. Unpublished PhD thesis, Memorial University of Newfoundland, St. John's, Newfoundland.

Swinden, S.H., Jenner, G.A., Kean, B.F., and Evans, D.T.W.
1989. Volcanic rock geochemistry as a guide for massive sulphide exploration in central Newfoundland. Newfoundland Department of Mines and Energy, Geological Survey Branch, Report 89-1, p. 201–219.

Swinden, H.S., Jenner, G.A., Fryer, B.J., Hertogen, J. and Roddick, J.C.
1990. Petrogenesis and paleotectonic history of the Wild Bight Group, an Ordovician rifted island arc in central Newfoundland. Contributions to Mineralogy and Petrology, 105, p. 219-241.

Taylor, S.R. and McLennan, S.M.
1985. The continental crust: Its composition and evolution. Oxford, Blackwell Scientific Publications, 312 p.

van Staal, C.R.
1994. The Brunswick subduction complex in the Canadian Appalachians: record of the Late Ordovician to Late Silurian collision between Laurentia and the Gander margin of Avalon: Tectonics, 13, p. 946-962.

van Staal, C.R., Winchester, J. A. & Bédard, J.H.
1991. Geochemical variations in Middle Ordovician volcanic rocks of the northern Miramichi Highlands and their tectonic significance. Canadian Journal of Earth Sciences, 28, p. 1031-1049.

van Staal, C.R., Sullivan, R.W. and Whalen, J.B.
1996. Provenance and tectonic history of the Gander Margin in the Caledonian/Appalachian Orogen: implications for the origin and assembly of Avalonia. *In:* Avalonian, related peri-Gondwanan terranes of the circum-North, Atlantic, Nance, R.D. and Thompson, M.D. (*eds.*), Geological Society of America Special Paper, 304, p. 347–367.

van Staal, C.R., Dewey, J.F., Mac Niocaill, C. and McKerrow, W.S.,
1998. The Cambrian–Silurian tectonic evolution of the northern Appalachians and British Caledonides: history of a complex, west and southwest Pacific-type segment of Iapetus. *In:* Lyell: the Past is the Key to the Present, Blundell, D.J., Scott, A.C. (*eds.*), Geological Society, London, Special Publication, 143, p. 199–242.

Weaver, S. D., Saunders, A. D. Pankhurst, R. J., and Tarney, J.
1979. A geochemical study of magmatism associated with the initial stages of back-arc spreading: the Quaternary volcanics of Bransfield Strait, from South Shetland Islands. Contributions to Mineralogy and Petrology, 68, p. 151–169.

Weaver, P.G., McMenamin, M.A.S. and Tacker, R.C.
2006. Paleoenvironmental and paleobiogeographic implications of a new Ediacaran body fossil from the Neoproterozoic Carolina Terrane, Stanley County, North Carolina. Precambrian Research, 150, p. 123-135.

Williams, H. and Hatcher, R.D.
1983. Appalachian suspect terranes. *In:* Contributions to the tectonics and geophysics of mountain chains, Hatcher, R.D., Williams, H. and Zeitz, I. (*eds.*), Geological Society of America, Memoir 158, p. 33-54.

Winchester, J.A. and Floyd, P.A.
1977. Geochemical discrimination of different magma series and their differentiation products using immobile elements. Chemical Geology, 20, p. 325–343.

Wood, D.A.
1980. The application of a Th-Hf-Ta diagram to problems of tectonomagmatic classification and to establishing the nature of crustal contamination of basaltic lavas of the British Tertiary Volcanic Province. Earth and Planetary Science Letters, 50, p. 11-30.

Woodhead, J.D. , Eggins, S., and Gamble, J.
1993. High field strength and transition element systematics in island arc and back-arc basin basalts: evidence for multi-phase melt extraction. Earth and Planetary Science Letters, 114, p. 491-504.

Wortman, G., Samson, S.D. and Hibbard, J.P.
2000. Precise U-Pb zircon constraints on the earliest magmatic history of the Carolina Terrane. Journal of Geology, 108, p. 321-338.

APPENDIX 2.A

Samarium-Neodymium isotope analysis

Selected samples were analyzed for Sm-Nd isotopes in the Radiogenic Isotope Laboratory Memorial University of Newfoundland. Approximately 0.1 g of rock powder was dissolved in Savilex Teflon beakers using a mixture of concentrate HF – HNO_3 acids. A mixed $^{150}Nd/^{149}Sm$ spike was added to each sample prior to acid digestion. Both sample and spike were weighed on a high-precision balance. After five days of digestion, the solution was evaporated to dryness and then taken up in 6 N HCl acid for two days. The solution was then dried and taken up in 2.5N HCl and loaded on cationic exchange chromatography using AG50W – X8 resin to collect the REE fractions. The REE fractions were then purified and Sm and Nd were isolated using a secondary column loaded with Eichrom Ln resin. All reagents were purified in order to insure a low contamination level. The measured total chemical blanks ranged between 40 and 90 pg and are considered negligible. Sm and Nd concentrations and Nd isotopic compositions were analyzed using a Finnigan MAT262V thermal ionization mass spectrometer. Neodymium and Sm ratios were measured using simultaneous Faraday multi-collection routines. Nd isotopic ratios were normalized to $^{146}Nd/^{144}Nd = 0.7219$. The reported values were not adjusted to an external standard, as the Jndi-1 isotopic standard was used for the first time during the course of the present study. Two runs of this standard yielded a mean value of 0.512127 ± 0.00014 in agreement with the database on the same material. The certified value of this standard is 0.512115 ± 7. The in-run precisions on Nd isotopic ratio are given at 95% confidence level. Errors on Nd isotopic compositions are <0.002% and errors on the $^{147}Sm/^{144}Nd$ ratio are estimated to be lower than 0.1%. The ε_{Nd}

values were calculated using $^{147}Sm/^{144}Nd$ = 0.1967 and $^{143}Nd/^{144}Nd$ = 0.512638 values for the present day chondrite uniform reservoir (CHUR). ^{147}Sm decay constant is 6.54 x 10^{-12}/yr (Steiger and Jäger, 1977). T_{DM} was calculated with respect to the depleted mantle model of De Paolo (1981).

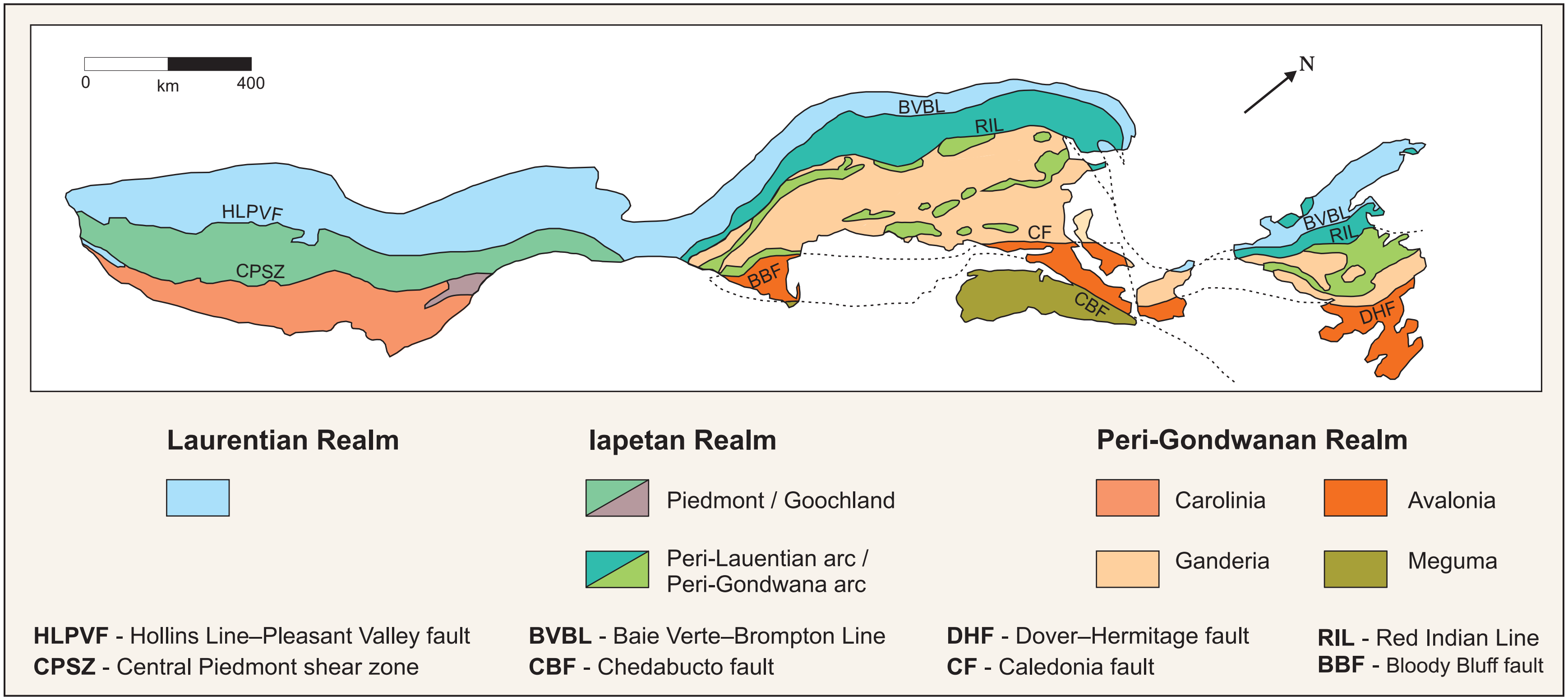

Figure 2.1. Simplified geological map of the Appalachian orogen with the distribution of the tectonostratigraphic zones and major tectonic elements discussed in text (modified after Hibbard *et al*., 2007).

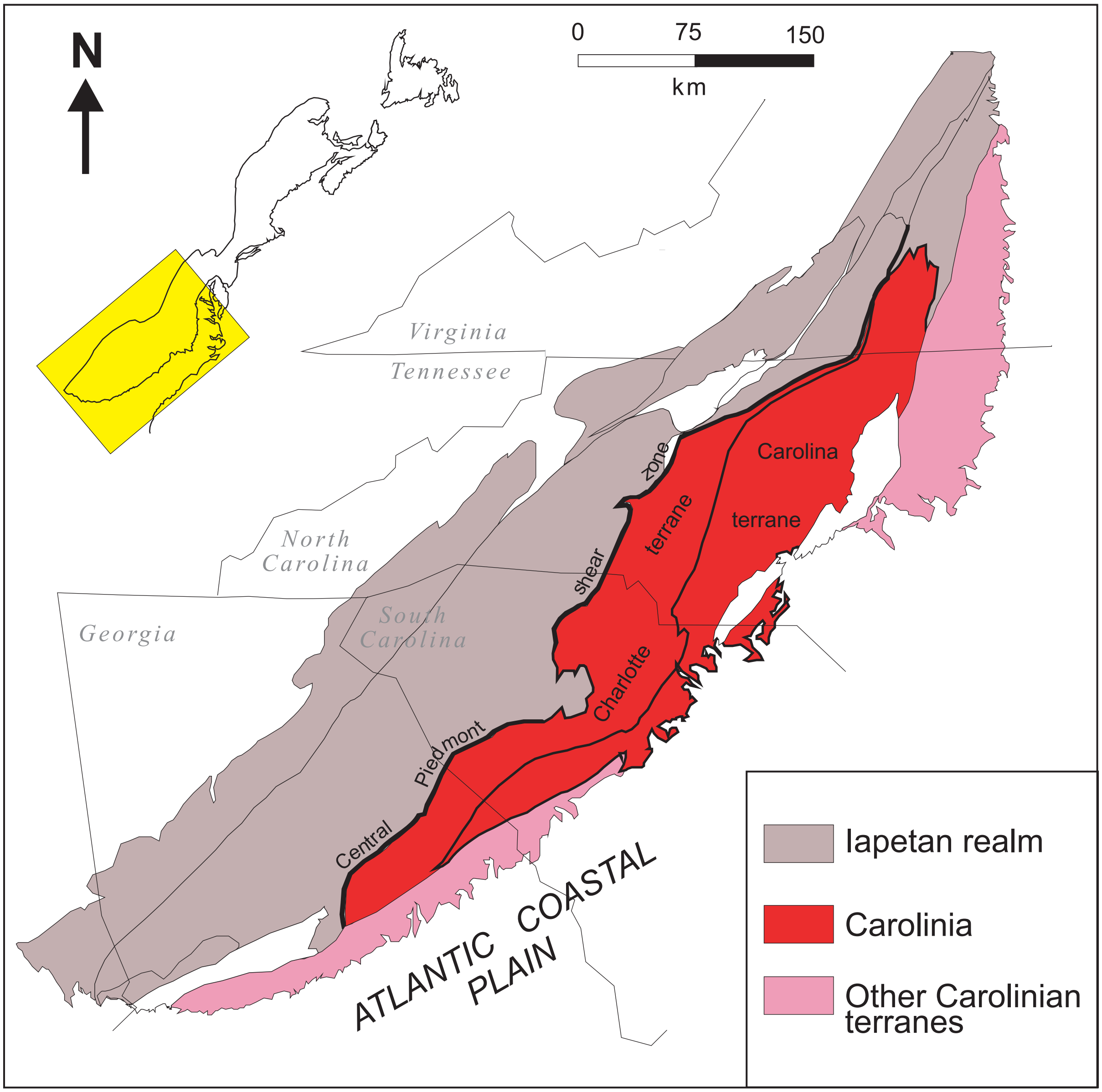

Figure 2.2. Major tectonic elements of the southern Appalachians and Carolinia (modified after Hibbard *et al.*, 2007).

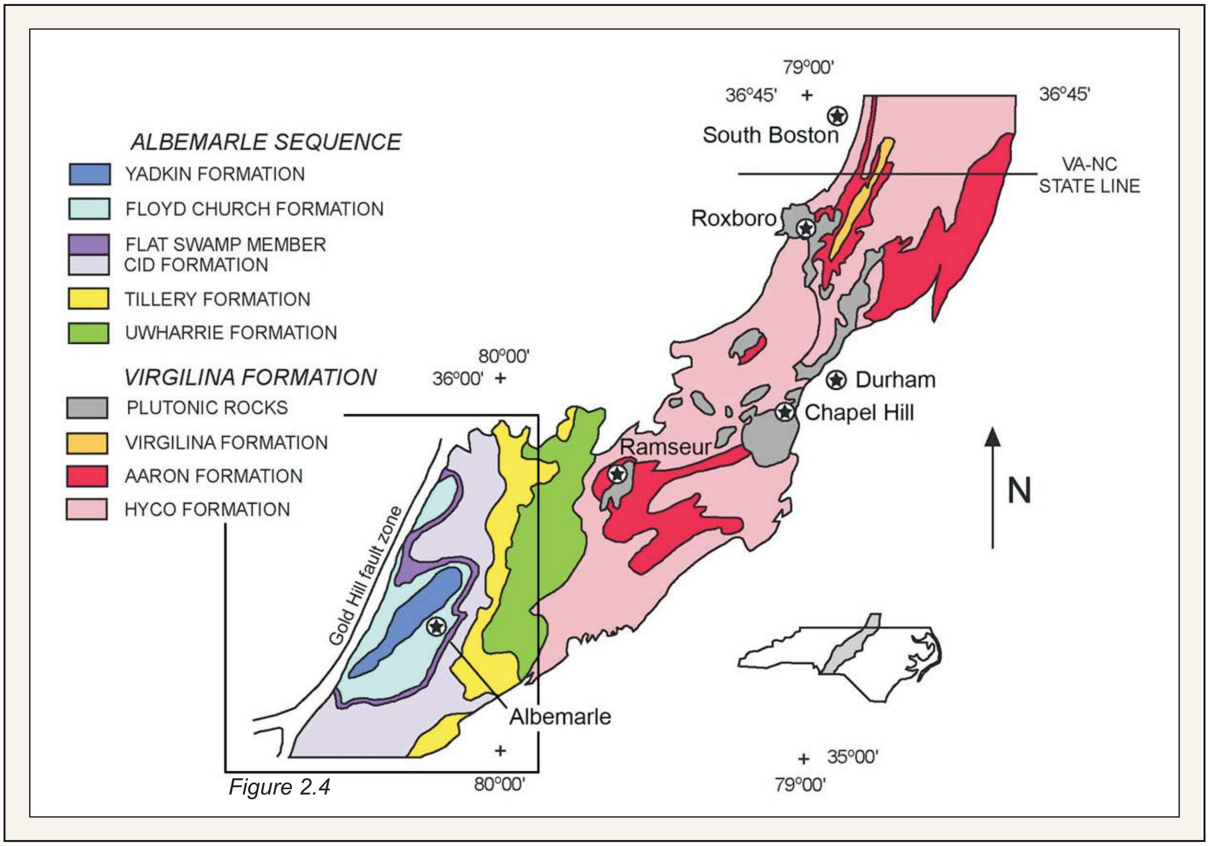

Figure 2.3. Simplified geology of Carolinia (Hibbard *et al*., 2002).

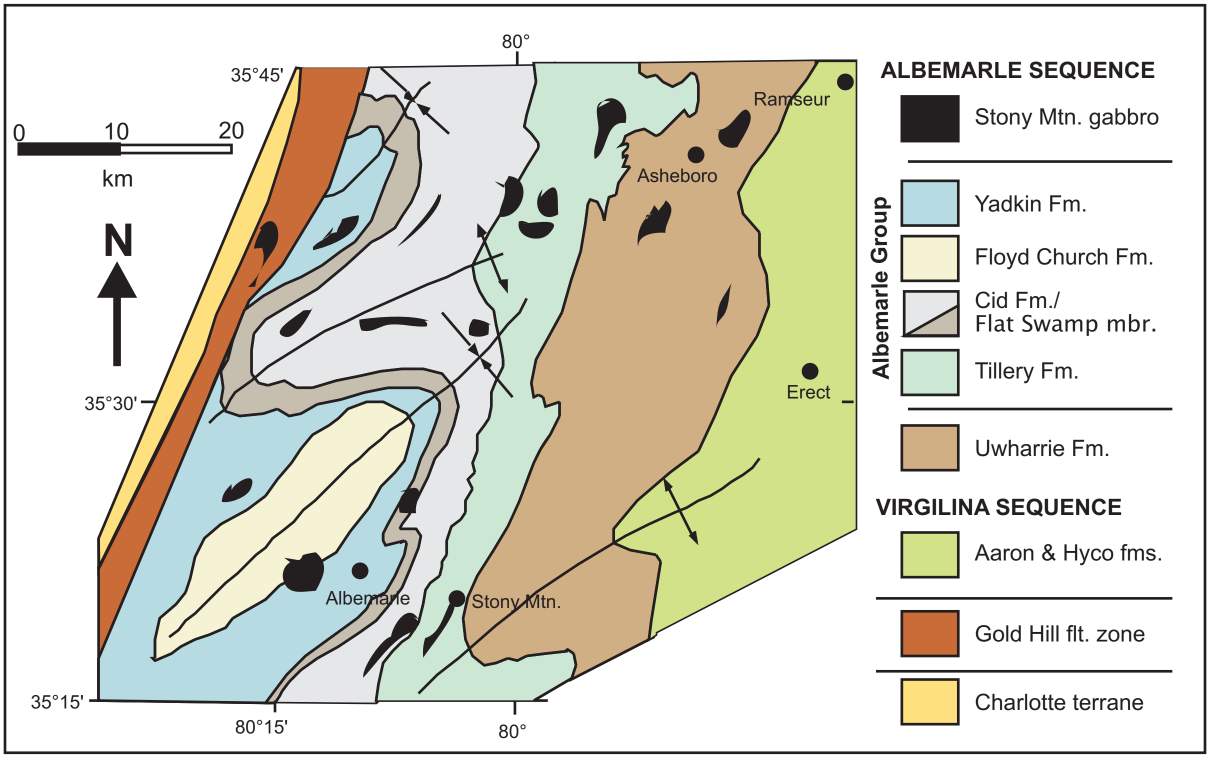

Figure 2.4. Geology of the Albemarle and Virgilina sequences in central North Carolina.

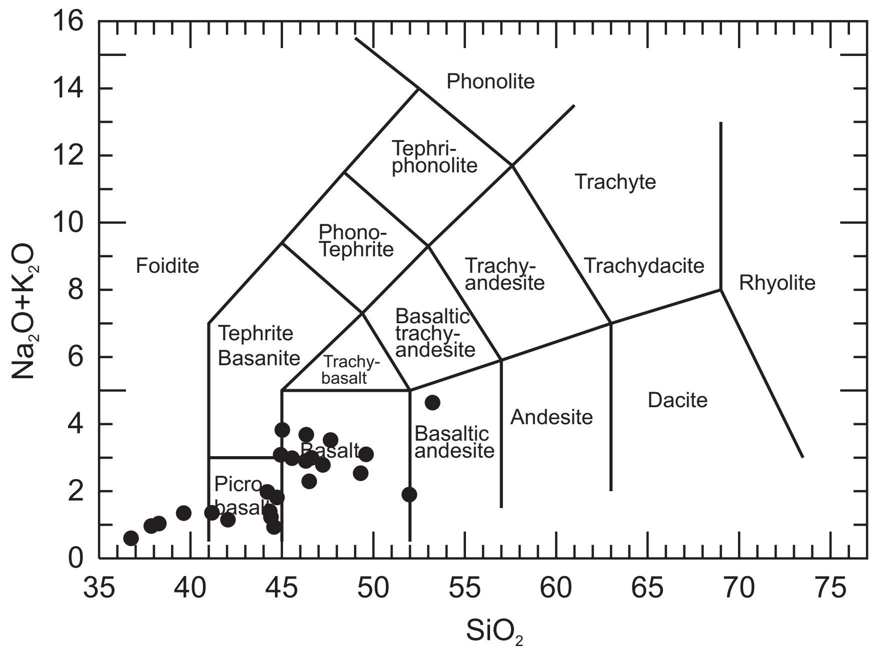

Figure 2.5. Total alkalies (Na_2O+K_2O) versus SiO_2 plot.

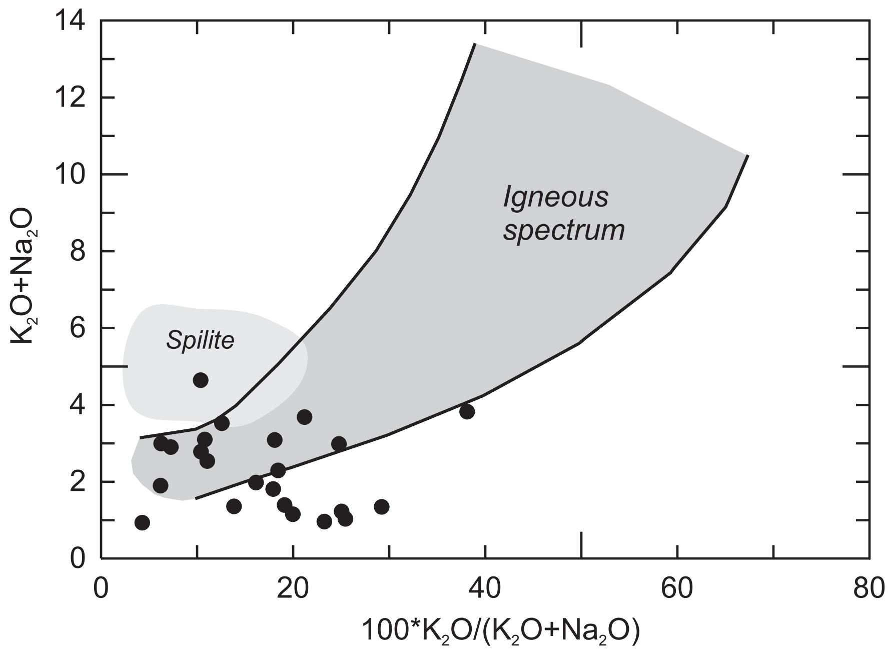

Figure 2.6. Modified Hughes (1973) plot illustrating Na and K changes during alteration of the Stony Mountain gabbro.

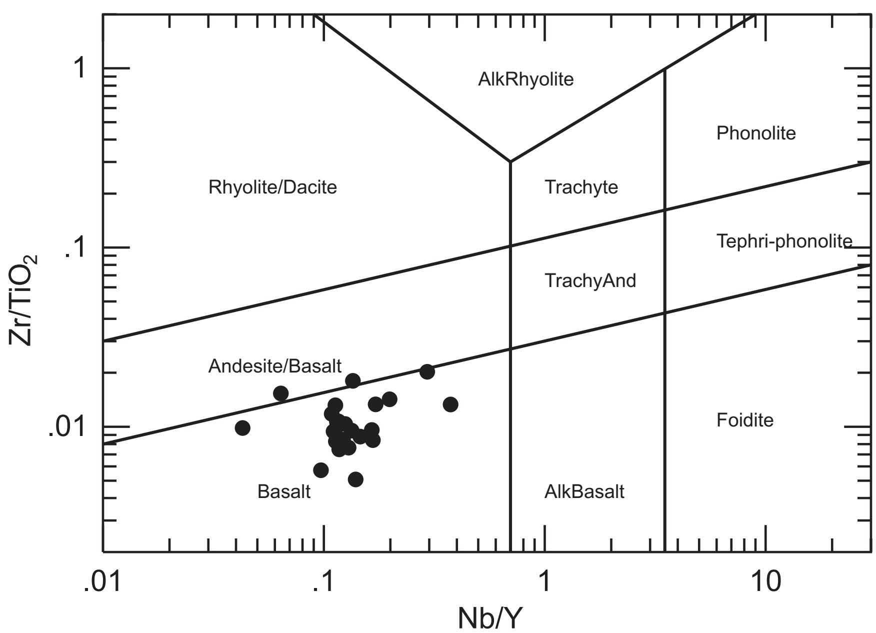

Figure 2.7. Lithology and subdivision into alkaline and subalkaline rocks using modified Winchester and Floyd (1977) Zr/TiO_2 vs Nb/Y plot of Pearce (1996).

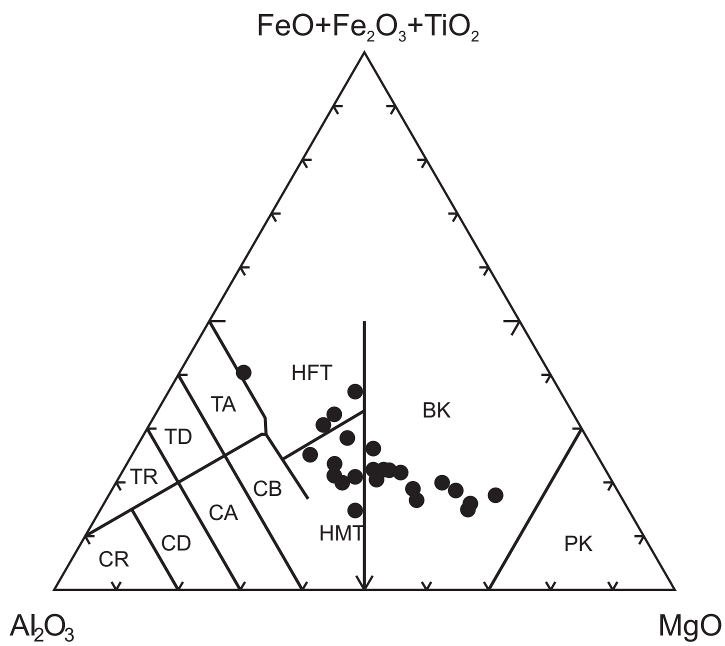

Figure 2.8. AFM ternary (cation percent) plot. HFT=high Fe tholeiite; HMT=high Mg tholeiite; BK=basaltic komatiite; PK=peridotitic komatiite; T=tholeiite; C=calc-alkaline, (A=andesite, B=basalt, D=dacite, R=rhyolite).

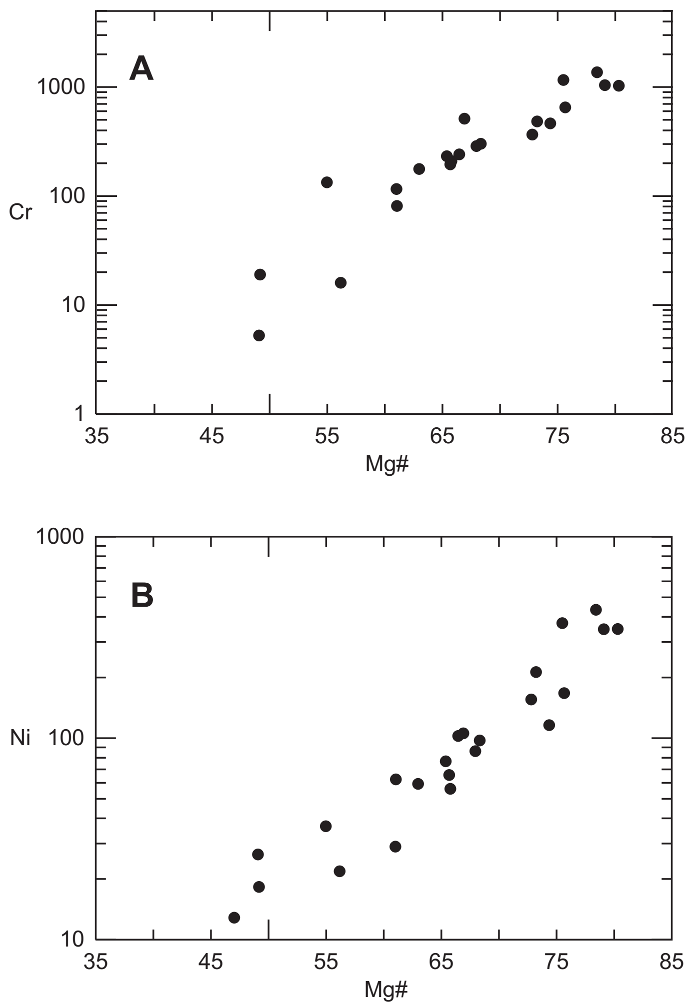

Figure 2.9. A) Log Cr vs Mg#; B) Log Ni vs Mg#.

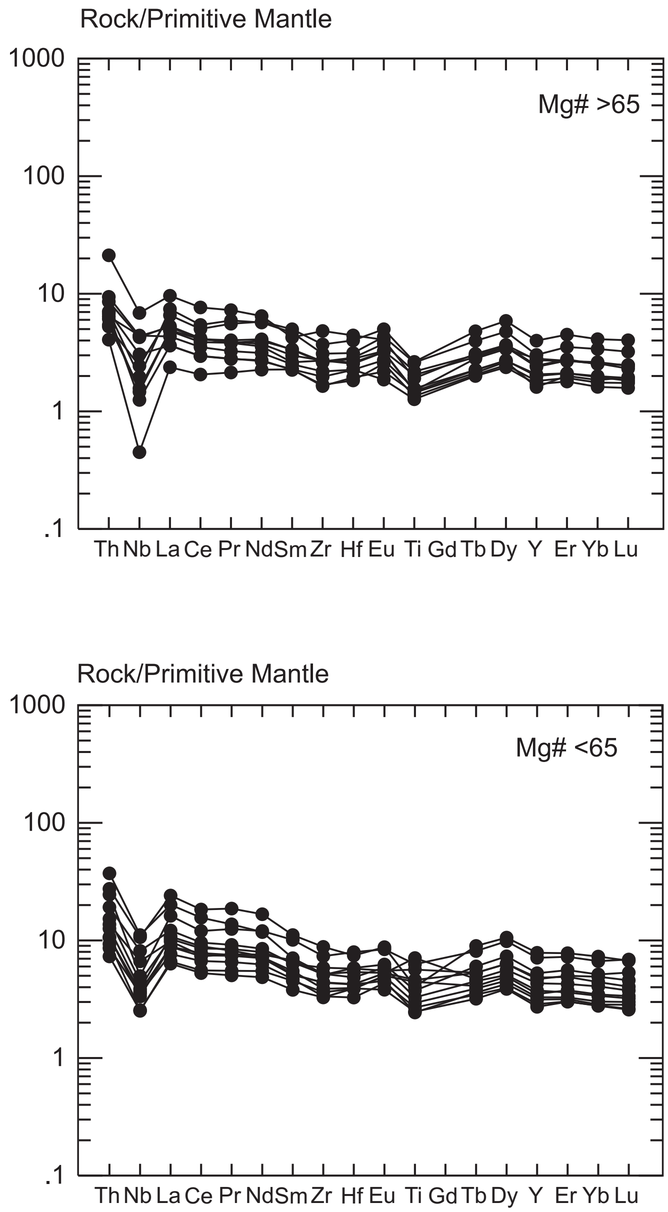

Figure 2.10. Primitive mantle normalized extended REE patterns showing the variation in trace element abundances at different Mg#. Primitive mantle normalizing values from Swinden *et al*. (1989).

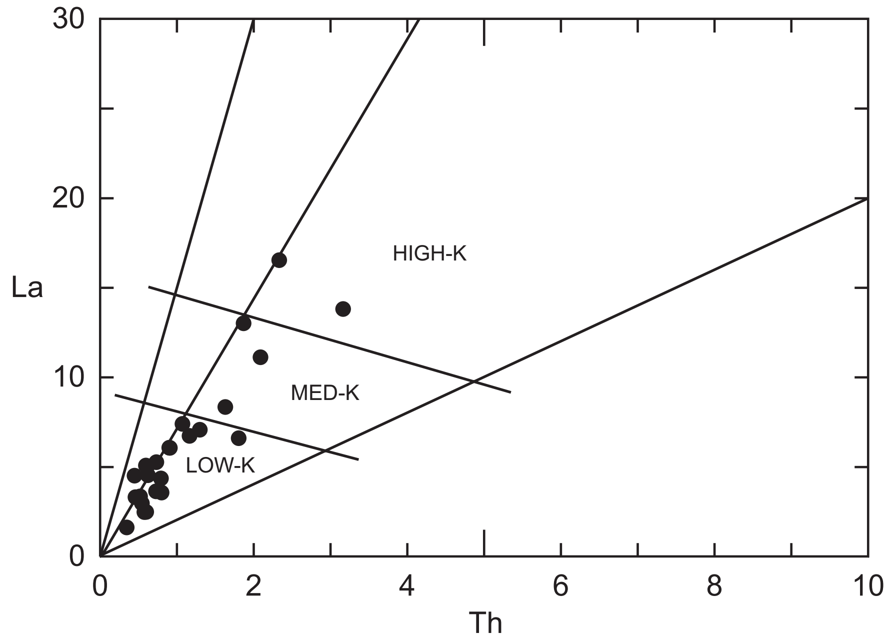

Figure 2.11. Th vs La discrimination diagram of low-, medium-, and high-K orogenic rocks (Gill, 1981).

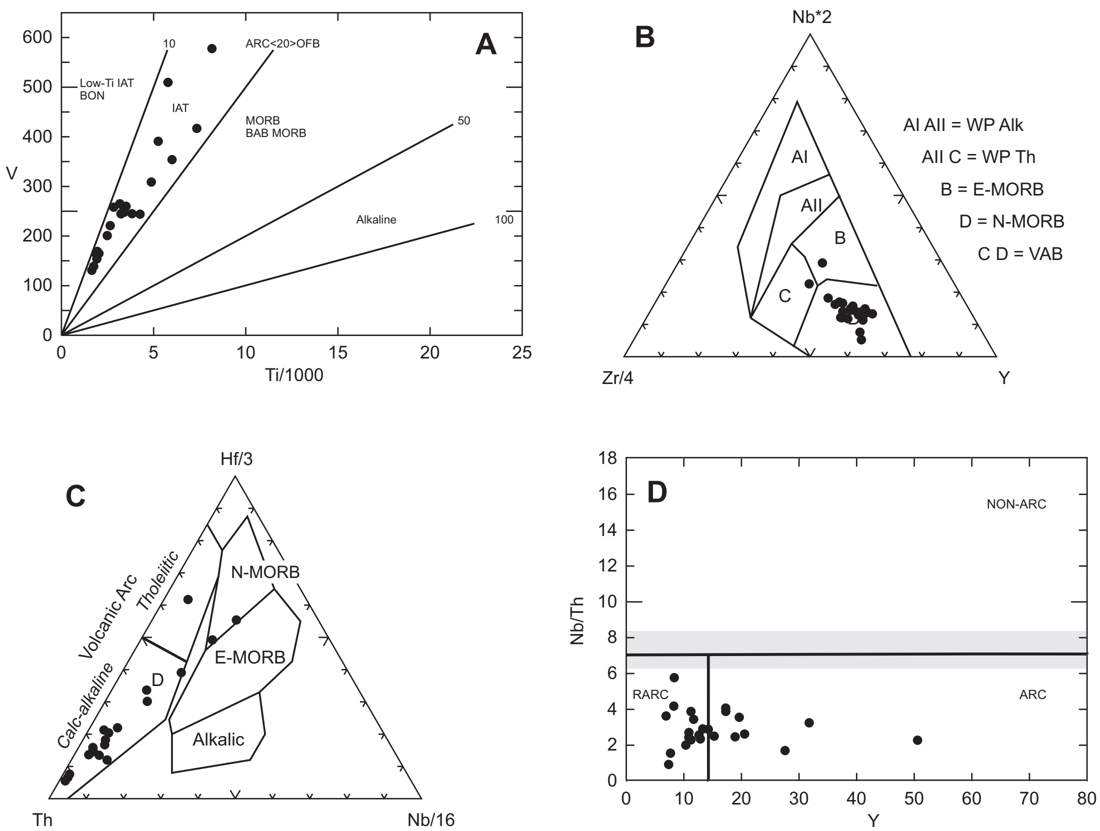

Figure 2.12. Tectonic discrimination diagrams. (A) Ti vs V plot of Shervais (1982); (B) Nb-Zr-Y plot, with fields defined by Meschede (1986); (C) Hf-Nb-Th plot, with fields defined by Wood (1980); (D) Nb/Th vs Y diagram of Swinden *et al*. (1990) separating arc, non-arc and refractory arc magmatic rocks.

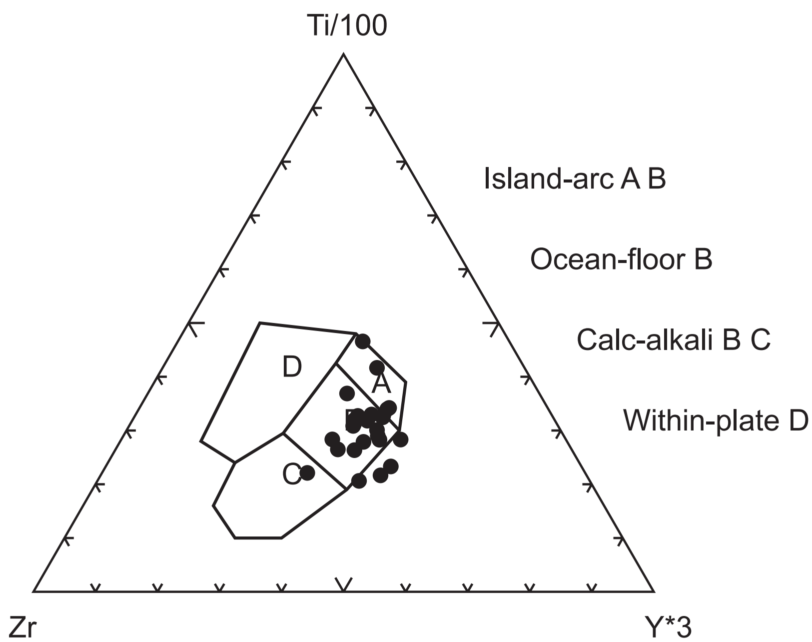

Figure 2.13. Ti-Zr-Y diagram of Pearce and Cann (1973).

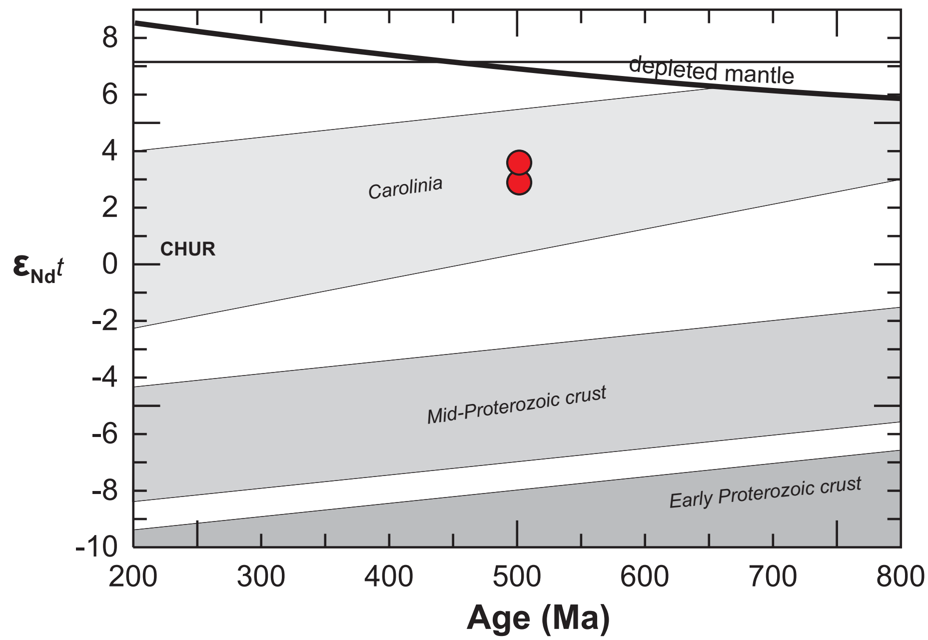

Figure 2.14. Plot of εNd vs age for samples of the older portion of the Stony Mountain gabbro. The high positive εNd of the rocks indicate that they cannot contain a large proportion of early to mid-Proterozoic crust. CHUR =Chondrite uniform reservoir, or bulk Earth. Fields from Samson *et al*. (1995) and Hibbard *et al*. (2007).

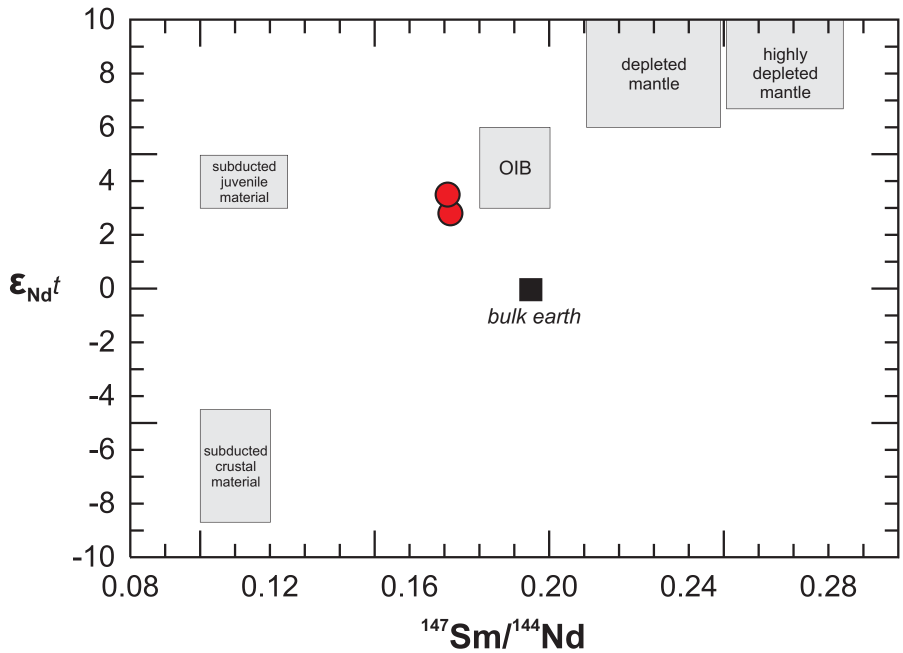

Figure 2.15. Plot of εNd vs $^{147}Sm/^{144}Nd$ for mafic rocks from the Stony Mountain gabbro, showing the various mantle and subduction components interpreted to be involved in generating these rocks. To produce the observed compositions requires mixing a depleted mantle source with an older LREE-enriched source. Fields from Swinden *et al*. (1990).

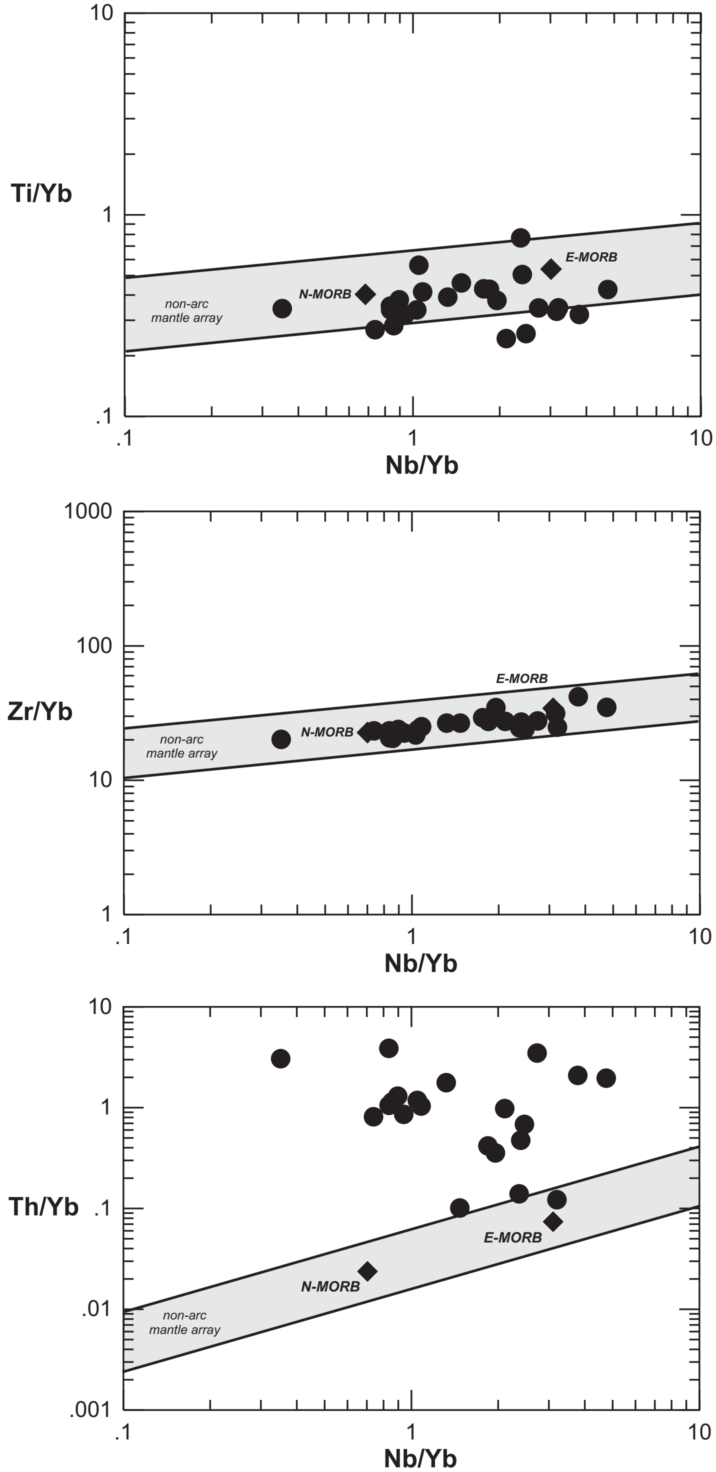

Figure 2.16. Trace element plots of Ti & Zr/Yb vs Nb/Yb and Th/Yb vs Nb/Yb (modified after Pearce and Peate, 1995) used to distinguish between conservative behaviour (e.g. Ti and Zr) and nonconservative (e.g. Th) behaviour.

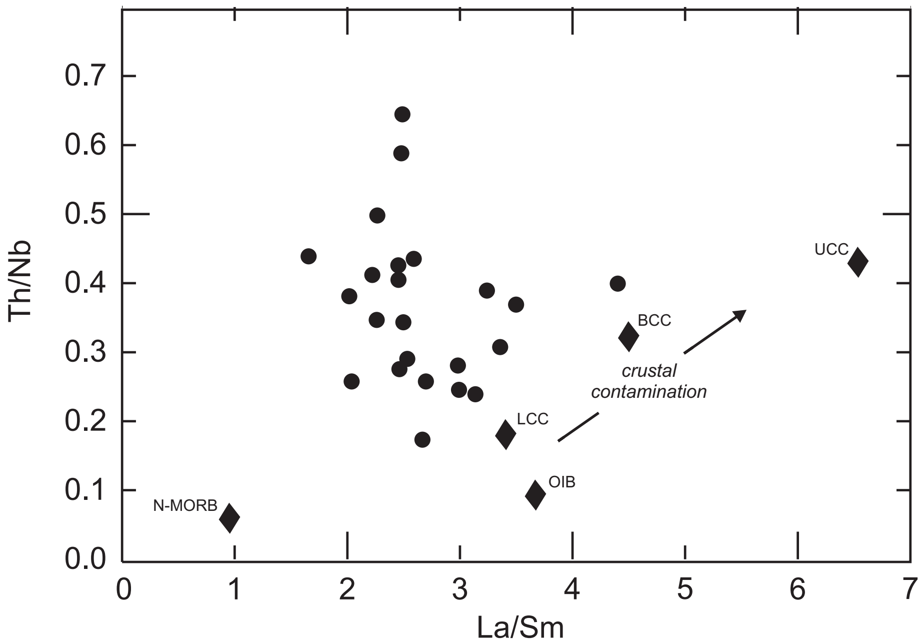

Figure 2.17. Trace element plot of Th/Nb vs La/Sm. The increase in Th/Nb at a constant La/Sm value is inconsistent with the rocks having experienced crustal contamination. N-MORB=normal mid-ocean ridge basalt; OIB=ocean island basalt; LCC=lower continental crust; BCC=bulk continental crust; UCC=upper continental crust.

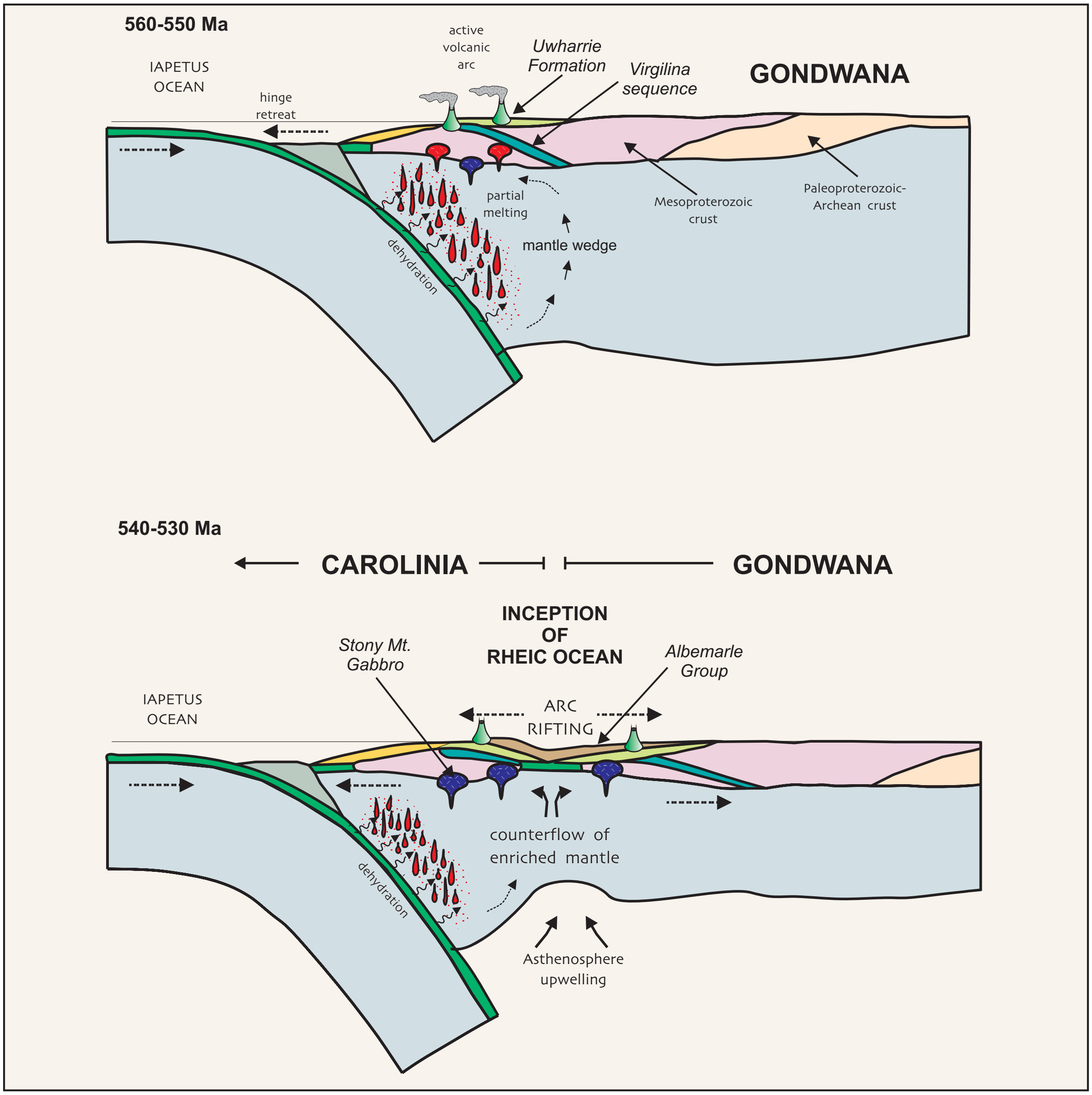

Figure 2.18. Summary of the late Neoproterozoic-early Paleozoic tectonostratigraphic evolution of Carolinia. Arc magmatism within the Uwharrie Formation is disrupted by rapid hinge retreat of the subducting oceanic plate leading to rifting of the arc and the subsequent formation of a back-arc rift/basin. Within this basin sedimentation was dominated by deep marine, arc-derived turbidites and felsic volcanic rocks of the Albemarle Group. Decompression melting during extension led to the generation of basaltic melts derived from depleted and enriched mantle that led to the formation of the Stony Mountain gabbro.

Table 2.1. Geochemical data for rocks from the Stony Mountain gabbro.

Sample	SiO2	TiO2	Al2O3	Fe2O3	MnO	MgO	CaO	Na2O	K2O	P2O5	S	Cr	Ni	Cl	Sc	V	Cu
289	44.33	0.34	12.89	9.79	0.16	15.34	11.31	1.13	0.27	0.05	92.08	651.33	167.32	56.33	34.30	164.50	33.77
290	49.30	1.22	12.51	13.11	0.23	8.48	8.74	2.26	0.28	0.17	77.16	15.85	21.86	39.15	43.73	417.27	117.33
291	37.86	0.32	11.48	12.44	0.19	19.33	7.78	0.74	0.22	0.06	107.70	1161.16	372.45	37.99	24.50	169.23	64.45
292	44.40	0.41	12.74	11.02	0.17	14.87	10.72	0.92	0.31	0.11	51.60	366.11	155.59	95.87	27.31	201.20	65.97
293	46.33	0.88	13.68	15.06	0.24	7.35	4.77	2.90	0.78	0.27	58.47	19.30	18.28	87.17	37.37	391.45	97.93
294	45.55	1.54	10.92	17.54	0.27	7.85	8.21	2.25	0.74	0.12	60.12	-4.78	12.86	59.57	45.67	1300.67	93.12
295	44.73	0.32	16.10	8.12	0.15	11.87	11.93	1.49	0.32	0.07	62.02	463.64	116.00	40.08	35.77	153.63	37.72
296	45.02	0.71	13.48	12.50	0.21	12.49	6.49	2.37	1.46	0.28	63.44	241.49	102.51	51.88	28.13	243.67	58.36
297	39.62	0.27	11.50	10.12	0.15	20.80	8.46	0.95	0.39	0.05	57.52	1027.14	348.28	55.40	29.68	130.58	32.89
298	44.93	0.58	13.45	12.02	0.20	11.44	8.47	2.53	0.56	0.15	42.61	232.25	76.75	48.53	33.93	259.57	67.67
299	47.66	0.64	14.40	10.94	0.18	10.56	9.29	3.08	0.44	0.17	102.49	195.43	65.60	142.32	34.28	244.89	63.46
300	38.27	0.29	10.75	10.56	0.17	20.14	9.15	0.77	0.26	0.04	55.39	1039.87	347.15	44.73	32.25	139.45	41.40
301	46.49	0.53	15.63	11.23	0.18	9.64	9.54	1.87	0.42	0.15	46.16	177.27	59.29	78.15	27.22	265.45	94.33
302	49.60	1.00	13.43	10.45	0.18	8.25	9.99	2.77	0.33	0.19	89.47	115.54	28.97	58.99	41.32	353.52	106.98
201	51.97	1.36	12.26	14.91	0.20	7.25	7.21	1.78	0.12	0.26	61.97	5.25	26.46	41.50	40.26	577.80	298.14
203	53.23	1.55	12.87	15.00	0.23	2.13	5.96	4.16	0.48	0.72	74.20	-6.83	-0.89	34.07	36.42	46.84	247.05
204	47.24	0.81	14.83	11.83	0.19	7.29	9.62	2.50	0.29	0.17	47.67	133.30	36.57	39.11	39.45	308.79	89.15
205	36.74	0.31	9.63	12.91	0.18	23.65	8.00	0.15	0.45	0.05	56.72	1366.70	433.54	14.80	22.21	164.74	15.94
206	46.62	0.54	15.42	10.52	0.18	10.20	9.13	2.81	0.19	0.10	52.91	209.25	56.02	16.15	35.31	244.75	99.81
207	41.18	0.57	12.14	11.57	0.19	11.80	10.90	1.17	0.19	0.14	94.54	513.05	105.73	19.27	37.90	248.18	78.49
208	46.30	0.96	11.89	12.86	0.18	10.16	8.91	2.69	0.21	0.14	269.00	81.04	62.45	42.27	55.87	509.54	702.50
209	42.05	0.44	11.24	12.30	0.20	16.96	9.32	0.92	0.23	0.08	1045.63	483.45	212.69	9.38	38.93	221.06	81.07
210	44.57	0.56	12.23	12.01	0.19	13.06	10.81	0.90	0.04	0.12	50.84	301.76	97.39	61.31	41.00	253.35	122.07
211	44.20	0.47	13.89	11.33	0.19	12.12	10.17	1.66	0.32	0.10	39.25	287.56	86.18	47.31	45.12	258.09	81.28

Table 2.1. (continued)

Sample	Zn	Ga	As	Rb	Sr	Y	Zr	Nb	Ba	Ce	Pb	Th	U	Y	Zr	Nb	Ba
289	28.15	10.10	0.72	6.87	206.37	9.10	20.02	0.39	115.51	3.44	2.90	0.12	-2.18	8.33	24.44	3.15	78.00
290	47.07	19.45	40.73	7.19	303.85	21.31	61.76	3.55	164.46	44.37	7.67	1.15	-2.13	19.61	65.69	5.81	128.85
291	39.13	10.11	18.75	9.24	137.53	12.77	25.63	1.44	122.65	34.10	4.01	0.86	-0.28	11.23	30.28	3.11	79.98
292	33.12	13.77	-6.91	7.29	267.28	12.39	50.32	3.64	110.18	21.21	4.31	2.70	-0.78	10.89	54.08	4.89	89.14
293	73.18	15.44	0.90	19.12	203.90	35.76	94.67	4.84	262.27	49.05	8.56	3.52	0.29	31.75	98.70	7.59	303.31
294	60.96	17.23	-0.56	28.37	241.59	19.67	46.79	2.74	241.29	50.29	6.83	0.28	1.29	17.27	49.22	4.74	199.56
295	23.05	13.79	5.51	8.43	300.08	9.38	25.60	1.61	117.56	62.22	4.47	-0.72	-0.71	8.25	30.29	3.04	96.68
296	52.58	14.42	12.92	51.51	300.02	17.07	56.71	6.40	200.32	39.18	7.23	3.27	-1.97	15.27	58.23	7.92	183.96
297	27.47	9.97	2.53	16.07	140.13	7.74	19.42	0.84	106.21	40.69	3.76	2.77	1.06	6.92	22.01	2.17	98.83
298	44.79	14.08	19.48	11.68	328.21	13.06	35.27	1.50	279.10	18.49	6.36	0.57	1.68	11.70	37.50	2.52	269.13
299	40.26	14.54	3.61	8.51	382.88	14.95	41.03	1.74	186.26	15.78	5.33	-1.35	0.97	13.28	43.47	2.62	213.64
300	26.19	11.11	10.51	10.11	147.76	8.25	18.11	1.03	63.45	28.41	2.68	-0.91	-1.22	7.68	18.79	0.89	67.44
301	39.57	17.13	0.66	10.13	301.38	14.30	45.14	2.84	156.34	15.87	6.79	0.50	0.96	12.63	48.90	2.75	142.17
302	33.29	17.37	-3.93	6.00	241.10	21.97	57.51	3.62	187.81	12.96	4.11	0.22	-1.74	18.90	58.04	3.21	191.54
201	43.09	15.66	27.05	1.38	207.88	32.44	77.64	4.34	37.48	54.61	4.07	3.41	-0.86	27.56	82.28	3.55	48.61
203	82.43	21.32	14.84	12.21	214.24	64.59	142.58	4.12	237.82	67.23	8.42	4.68	0.99	50.58	134.52	4.26	190.11
204	39.69	14.79	2.90	7.04	289.77	23.93	51.85	2.74	96.53	31.95	5.57	2.17	-0.71	20.54	56.95	2.38	92.26
205	30.38	8.43	1.83	27.14	79.49	7.33	13.97	0.86	74.64	12.42	3.53	2.79	3.20	7.36	18.35	0.32	62.63
206	45.23	14.11	-2.22	6.68	318.87	12.41	28.43	1.81	59.26	30.85	10.66	2.44	-0.61	11.23	36.68	1.82	84.39
207	32.12	15.24	-0.85	4.72	238.62	18.15	32.24	2.01	186.85	42.31	5.62	2.31	2.47	17.28	41.54	1.74	155.22
208	42.04	16.44	2.17	3.17	247.26	15.98	33.02	1.55	95.97	-10.48	4.10	2.02	2.99	14.24	40.63	1.79	113.75
209	35.96	13.63	-7.62	5.66	275.06	10.88	22.38	1.33	70.34	24.49	4.06	4.85	1.24	10.34	29.22	1.04	73.68
210	38.14	14.62	-4.98	1.17	290.87	13.74	28.02	1.56	7.21	12.90	1.87	1.76	1.73	12.87	34.60	1.40	27.45
211	31.48	16.42	-4.52	6.34	255.59	11.13	21.66	1.44	108.20	15.02	2.95	1.62	-1.03	10.86	29.75	1.12	130.28

Table 2.1. (continued)

Sample	La	Ce	Pr	Nd	Sm	Eu	Gd 160	Tb	Dy	Ho	Er	Tm	Yb	Lu	Hf	Ta	Th
289	2.98	6.58	0.90	4.23	1.12	0.46	1.48	0.24	1.61	0.34	1.01	0.15	0.98	0.14	0.70	0.09	0.55
290	8.35	17.92	2.53	11.47	2.80	0.93	3.49	0.57	3.76	0.82	2.40	0.35	2.42	0.34	1.78	0.25	1.63
291	3.58	7.66	1.08	5.06	1.33	0.54	1.84	0.30	2.02	0.43	1.29	0.19	1.26	0.17	0.80	0.08	0.80
292	6.61	14.32	2.00	8.73	1.89	0.68	2.16	0.33	2.19	0.44	1.28	0.19	1.29	0.18	1.37	0.20	1.80
293	16.54	34.30	5.15	22.56	4.93	1.47	5.89	0.97	6.29	1.29	3.74	0.55	3.60	0.50	2.30	0.27	2.33
294	6.74	13.95	2.05	9.53	2.25	0.89	3.05	0.51	3.35	0.70	2.05	0.30	2.00	0.28	1.31	0.19	1.16
295	3.64	7.82	1.05	4.82	1.16	0.54	1.48	0.24	1.61	0.33	1.01	0.14	0.96	0.13	0.78	0.14	0.73
296	13.82	29.20	3.79	15.89	3.14	0.99	3.38	0.49	3.03	0.60	1.73	0.26	1.67	0.24	1.50	0.31	3.16
297	2.49	5.53	0.77	3.61	1.01	0.31	1.28	0.22	1.41	0.28	0.86	0.12	0.80	0.12	0.70	0.09	0.60
298	5.27	12.49	1.81	8.43	2.08	0.73	2.31	0.37	2.35	0.49	1.45	0.20	1.37	0.19	1.01	0.11	0.73
299	6.08	14.60	2.08	9.71	2.43	0.83	2.66	0.42	2.71	0.55	1.57	0.23	1.49	0.22	1.22	0.12	0.90
300	2.49	5.52	0.77	3.67	1.00	0.43	1.29	0.22	1.48	0.31	0.92	0.13	0.86	0.13	0.57	0.07	0.58
301	7.41	16.66	2.26	9.86	2.29	0.76	2.47	0.39	2.54	0.51	1.52	0.21	1.41	0.21	1.30	0.17	1.07
302	7.08	15.97	2.33	10.74	2.88	0.89	3.47	0.57	3.78	0.78	2.35	0.33	2.18	0.30	1.66	0.20	1.30
201	11.13	22.51	3.46	16.24	4.49	1.41	5.51	0.88	5.86	1.18	3.48	0.50	3.28	0.51	2.46	0.26	2.09
203	13.02	30.03	4.96	25.88	7.87	2.38	10.17	1.66	10.80	2.18	6.34	0.89	5.76	0.89	4.01	0.22	1.87
204	6.07	13.73	2.10	10.24	3.01	1.05	3.87	0.65	4.37	0.90	2.68	0.39	2.53	0.40	1.80	0.15	0.91
205	1.63	3.85	0.59	3.05	1.01	0.37	1.38	0.23	1.57	0.33	0.96	0.14	0.91	0.14	0.60	0.03	0.35
206	4.36	9.87	1.39	6.57	1.68	0.64	2.11	0.35	2.30	0.48	1.45	0.21	1.38	0.19	1.21	0.12	0.79
207	4.51	9.39	1.54	7.81	2.21	0.84	3.01	0.52	3.50	0.73	2.16	0.31	2.02	0.30	1.24	0.09	0.45
208	4.54	10.41	1.52	7.41	2.01	0.84	2.63	0.44	2.93	0.60	1.81	0.26	1.71	0.25	1.20	0.10	0.62
209	3.36	7.68	1.11	5.53	1.48	0.55	1.91	0.31	2.10	0.43	1.30	0.19	1.25	0.18	0.86	0.07	0.52
210	5.08	10.16	1.63	7.68	2.07	0.72	2.50	0.43	2.84	0.58	1.69	0.25	1.67	0.24	0.97	0.10	0.60
211	3.32	7.25	1.06	5.36	1.49	0.63	1.95	0.33	2.14	0.45	1.33	0.19	1.25	0.18	0.88	0.07	0.46

Table 2.2. Nd- and Sm-isotope data for the Stony Mountain gabbro whole-rock samples.

Sample	Nd (ppm)	Sm (ppm)	147Sm/144Nd	143Nd/144Nd	2σ	εNd(0)	εNd(500)	T De Paolo	TDM2
305	3.771	1.071	0.1717	0.512691	5	1.4	2.6	1200	1666
208	7.242	2.047	0.1709	0.512728	5	2.2	3.4	1051	1504

TDM2 calculated using a linear evolution for a mantle separated from the CHUR at 4.55Ga and having a present day Epsilon value of +10

CHAPTER 3

EARLY ORDOVICIAN RIFTING OF AVALONIA FROM GONDWANA: U-Pb DETRITAL ZIRCON CONSTRAINTS FROM NEWFOUNDLAND

ABSTRACT

Avalonia is the largest accreted peri-Gondwanan crustal block in the Appalachian orogen and comprises a collection of late Neoproterozoic volcano-sedimentary sequences that are overlain by a Cambrian-Ordovician shale-rich platformal sedimentary succession. U-Pb ages of detrital zircons from Neoproterozoic-early Paleozoic rocks from the type area of Avalonia contain varied zircon populations. The oldest analyzed samples from the Conception Group are dominated by zircons that fall in the 570-620 Ma range and contain a significant detrital component generated by erosion of coeval igneous rocks formed in main phase of magmatic arc activity. Overlying samples from the arc-platform transition sequence, Cuckold and Crown Hill formations, are dominated by Ediacaran populations with ages between 600 and 650 Ma and are interpreted to be derived from the underlying the calc-alkaline plutonic rocks (the Holyrood and Simmons Brook intrusive suites) of the main Avalonian arc.

Early Paleozoic platform units are dominated by ca. 620 Ma zircons with an abundance of grains that have ages between 1.0-1.6 Ga, with lesser Paleoproterozoic and Archean zircons. These ages are inconsistent with recycling from underlying Neoproterozoic rocks and indicate significant difference in provenance from the underlying Avalonian sequences. The range of detrital zircon ages, combined with isotopic, paleomagnetic, sedimentological and fossil data, indicate that Avalonia's provenance is a Gondwanan craton that contains Archean, Paleo-, Meso- and Neoproterozoic rocks. These data are inconsistent with a West African provenance and suggest that Avalonia originated along the margin of the Amazon craton.

The rapid influx of Proterozoic and Archean detritus in the upper sequences of the Avalonian platform suggest a major change in tectonic regime to expose older material that is temporally consistent with Avalonian basement. The prominent change in provenance is interpreted to be related to separation of Avalonia from Gondwana during the Early Ordovician opening of the Rheic Ocean. The Arenig Redmans Formation is interpreted to represent the rift-drift transition of the Rheic Ocean, which imposes important constraints on the paleotectonic evolution of Avalonia.

PREAMBLE

Avalonia is the largest accreted peri-Gondwanan crustal block in the Appalachian-Caledonian orogen and comprises Neoproterozoic-early Paleozoic magmatic arc and sedimentary cover sequences that can be traced from the British Caledonides in England southwest to Rhode Island (Figure 3.1). Lithostratigraphic, isotopic, faunal, and paleomagnetic data indicate that Avalonia records a Neoproterozoic tectonomagmatic history that predates opening of the Iapetus Ocean and is considered to have formed as a Neoproterozoic arc-related terrane along an active margin of Gondwana (O'Brien *et al*., 1996; Murphy *et al*., 1999; Nance *et al*., 2002). Sometime between the latest Neoproterozoic and Middle Ordovician Avalonia rifted and separated from Gondwana as a microcontinent where it constituted the boundary between the expanding Rheic Ocean to the south and the contracting Iapetus Ocean to the north (van Staal *et al*., 1998; Murphy *et al*., 2006). Despite its prominence in Paleozoic paleogeography, our understanding of such fundamental aspects of Avalonia such as the precise timing of rifting and separation, its source area(s) in Gondwana, and its geometry and relationship with respect to other peri-Gondwanan terranes are poorly constrained. The resolution of these uncertainties bears directly upon our understanding of the timing and nature of opening and the geometry of the Rheic Ocean.

In an attempt to resolve these problems, a U-Pb geochronological study was conducted on detrital zircon grains in clastic sedimentary rocks from the major lithotectonic units of the type area of Avalonia, the Avalon Peninsula of eastern Newfoundland. Recent advances in high-frequency sampling have led to improved resolution of sediment provenance studies which is critical to understanding the paleotectonic evolution of the major Neoproterozoic-early Paleozoic continents.

Despite its low abundance in sediments and sedimentary rocks, zircon is a common detrital constituent in many sedimentary rocks because it occurs in a complete spectrum of igneous rock types and is one of the few primary igneous minerals that can survive the highest grades of metamorphism and partial melting as well as abrasion during fluvial transport and hence can survive in the crust almost indefinitely (Mezger and Krögstad, 1997).

Previous studies have shown that single grain detrital zircon geochronology is a useful method of dating and tracing crustal processes because it can provide information that can be used to: (*i*) assist stratigraphic correlation of monotonous sedimentary sequences that lack distinctive marker units (Samson *et al*., 2005); (*ii*) determine a maximum limit for the age of deposition of a stratigraphic succession (Barr *et al*., 2003); (*iii*) determine time gaps in the geological record (Davis, 2002); (*iv*) fingerprint source areas with distinct zircon age populations (Murphy *et al*., 2004; Cawood *et al*., 2003); and (*v*) constrain the timing of tectonic processes on a orogenic scale (Cawood and Nemchin, 2001; Pollock *et al*., 2007). The ability to utilize zircon to interpret the provenance history of a sedimentary sequence requires that the depositional age of the sequence to be analysed be constrained by either faunal and/or high precision ID-TIMS data and that the source area(s) of this sequence have a well-defined and distinct U-Pb age signature.

This study is the first zircon provenance analysis of Neoproterozoic-early Paleozoic rocks from the type area of Avalonia in Newfoundland. In this chapter I demonstrate the ability of U-Pb detrital zircon geochronology to address two critical problems in Avalonia: (*i*) the timing of rifting of Avalonia from Gondwana; and (*ii*) the provenance and ultimate source craton in Gondwana of Avalonian sedimentary sequences.

REGIONAL GEOLOGICAL SETTING

On the island of Newfoundland, the type area of Avalonia comprises Neoproterozoic (ca. 760-540 Ma), largely juvenile, low-grade arc-related volcano-sedimentary sequences and associated plutonic rocks that experienced a prolonged tectonic history before deposition of a terminal Neoproterozoic-early Paleozoic cover of fine-grained platformal sedimentary rocks that contain Acado-Baltic faunas (O'Brien *et al*., 1996; Landing, 1996; Kerr *et al*., 1995). The general evolution of Avalonia (Figure 3.2) indicates a protracted and episodic geological history of tectonomagmatic and depositional events that define a quadruplex succession comprising: (*i*) early phases of arc- and rift-related magmatism between 760 and 670 Ma; (*ii*) a main phase (635-570 Ma) of arc volcanism with coeval sedimentary succession dominated by volcanogenic turbidites and cogenetic plutons; (*iii*) rift-related intracontinental volcanism and interlayered clastic sedimentation that records the transition from an arc to a platform without collision between 570-545 Ma; and (*iv*) deposition of a Cambrian-Ordovician shale-rich platformal sedimentary succession (Nance *et al*., 2002).

Remnants of the early arc-related magmatic activity are preserved in three distinct intervals at ca. 760, 730 and 685-670 Ma. On the Burin Peninsula, a fault-bounded, mixed assemblage of sedimentary and rift-related volcanic rocks and gabbro of the Burin

Group is analogous to basalts and mafic intrusive complexes in modern ocean basins and immature island arcs and are interpreted to represent an incomplete ophiolite sequence (Strong and Dostal, 1980). An ID-TIMS age of 763 ± 2 Ma from zircon dates this gabbroic succession (Krogh *et al*., 1988). Vestiges of the ca. 730 Ma arc are preserved along the southern shore of Conception Bay at Chapel Cove. The Hawke Hills tuff (O'Brien *et al*., 2001) comprises a subaerial felsic to mafic volcanic sequence that is intruded by 630-640 Ma plutonic rocks and unconformably overlain by Neoproterozoic marine siliciclastic rocks of the Conception Group. The Hawk Hills tuff has traditionally been included with the younger Harbour Main Group; however, a U-Pb age from a felsic volcanic tuff sampled immediately below the sub-Conception Group unconformity yields a date of 729 ± 7 Ma (Israel, 1998), thereby negating any correlation with the younger volcanic arc sequences. On the Connaigre Peninsula, early arc rocks are represented by low-grade calc-akaline rhyolite flows and pyroclastic rocks of the Tickle Point Formation have yielded a 682.8 ± 1.6 Ma U-Pb zircon age (Swinden & Hunt, 1991). Prior to the deposition of younger Neoproterozoic rocks, the Tickle Point Formation was intruded by granite and gabbro of the Furby's Cove Intrusive Suite; U-Pb zircon analysis on granite from the suite indicates an intrusive age of 673 ± 3 Ma (O'Brien *et al*., 1996).

The main phase of Avalonian magmatism records volcanism and plutonism and coeval sedimentation in arc-related and arc-adjacent basins following an apparent hiatus of approximately 40 m.y. between deposition of the youngest early arc sequences and the main phase. Main phase volcanic successions are defined by the widespread occurrence of low metamorphic grade felsic to mafic submarine to subaerial volcanic rocks that are several kilometres thick and formed between 635-565 Ma. West to east, these rocks include the Marystown, Love Cove and Harbour Main groups which have calk-alkaline to transitional and island arc (arc-rift) tholeiitic affinities. Radiogenic isotopic analysis of these rocks yield the following U-Pb ages: 631 ± 2 Ma, 606 +3.7/-2.9 Ma and 589.5 ± 3 Ma for the Harbour Main Group, and 608 +20/-7 Ma for the Marystown Group (Krogh *et al*., 1988; O' Brien *et al*., 1996). These sequences are intruded by calk-alkaline plutonic complexes shortly after their eruption, of which the Holyrood and Simmonds Brook intrusive suites have both been dated at 620 ± 2 Ma (Krogh *et al*., 1988; O'Brien *et al*., 1995). Sm-Nd and Pb isotopic characteristics and ages of xenocrystic zircons indicate that this main phase is juvenile, but erupted on some form of ca. 1.0-1.2 Ga continental crust (Kerr *et al*., 1995).

These arc-related magmatic rocks are spatially associated with thick successions of coeval marine siliciclastic rocks dominated by volcanogenic turbidites that were deposited in intra-arc, interarc, and back-arc basins proximal to active volcanic arcs. The Conception, Connaigre Bay and Connecting Point groups are 4-5 km thick sedimentary successions that are dominated by low-grade, fine-grained siliceous volcaniclastic and epiclastic sedimentary rocks. Basal interfingering of the Conception Group with the Harbour Main Group and volcanic rocks at the base of the Connaigre Bay Group (dated at 626 ± 3 Ma) indicate that deposition commenced ca. 630-620 Ma upon a basement substrate of 685-670 Ma volcanic and plutonic rocks. In the upper part of the Conception Group, the Drook and Mistaken Point formations contain the Ediacaran index fossil *Charnia* on the upper surfaces of bedding planes that are generally overlain by thin layers of tuff dated at 565 ± 3 Ma (G. Dunning *in* Benus, 1988), indicating that deposition of these epiclastic successions continued for at least 50 m.y. In the southwest Avalon

Peninsula, a bimodal volcanic succession, the ca. 575 Ma Bull Arm Formation and 580-565 Ma migmatites and calc-alkaline, volcanic (Long Harbour Group) and intrusive (Louil Hills granite) complexes occur stratigraphically above the Connecting Point and Connaigre Bay groups (O'Brien *et al*., 1996).

The ca. 570 Ma change to bimodal igneous activity is coeval with the cessation of arc-related magmatism and is interpreted to be related to the termination of subduction and the transition to an extensional or transtensional regime (Murphy and Nance, 1989). This transition is accompanied by clastic sedimentation in pull-apart basins that first produced thin-bedded, deltaic sandstones and shales (St. John's Group) that pass upwards to fluvial and alluvial facies sedimentary rocks (Signal Hill Group) without significant disconformity (O'Brien *et al*., 1996). Although sedimentation, which continued until the terminal Neoproterozoic, was accompanied by deformation and metamorphism expressed as local thrust faulting, gentle folding and low-grade (prehnite-pumpellyite) regional metamorphism (Calon, 2001), there is no evidence for major regional orogenesis and crustal shortening.

The arc-platform transition rocks are overlain by an undeformed, siliciclastic-dominated late Neoproterozoic-early Paleozoic platform sequence. In the latest Neoproterozoic-Early Cambrian, deposition was dominated by quartz arenite transgressive successions (Chapel Island and Random formations) which pass conformably upward into Middle to Late Cambrian shale and limestone sequences (Bonavista Group) locally accompanied by eruption of alkalic mafic volcanics (Greenough and Papezik, 1986). The top of the Avalonian platform is represented by the Early Ordovician Bell Island and Wabana groups, which record tidal-dominated sedimentation of micaceous sandstone, siltstone, oolitic hematite and quartz arenite (Ranger *et al*., 1984; Brenchly *et al*., 1993).

SAMPLE SELECTION

U-Pb ages were obtained from single detrital zircon grains from seven samples of Neoproterozoic-early Paleozoic rocks from eastern Newfoundland in an attempt to constrain the tectonic evolution of Avalonia (Figure 3.3). Two samples were collected from the main phase of arc volcanism (635-570 Ma); two samples from the arc-platform transition (590-545 Ma); and three samples from the Paleozoic platform sequence (Figure 3.4). However, a sample from the Middle Cambrian Kellys Island Formation of the Bell Island Group did not yield enough zircons and therefore was not analyzed. Each sample consisted of ca. 40 kg of rock that comprised several subsamples collected at varying stratigraphic locations from a single continuous outcrop. This method greatly reduces any potential natural bias that may result from variations due to the inherent complexity of sedimentary systems. Previous studies have shown that a single lithostratigraphic unit may contain a diverse zircon population as significant variations can exist in zircon age distributions at different geographic locations at the same stratigraphic level from the same formation (DeGraaff-Surpless *et al*., 2003), while other workers showed that mixed detrital zircon age distributions may occur throughout the vertical section (Sircombe *et al*., 2001).

Main Arc Phase

Conception Group – Mall Bay Formation

A sample of a thick-laminated, grey to green siltstone argillite was collected from the lower Conception Group along the eastern shore of Holyrood Bay. At this location the Conception Group comprises ca. 700 m of rhythmically interbedded fine-grained siliceous sandstone, siltstone and mudstone that show typical Bouma sequence features such as sole marks, rip-up clasts, grading, parallel- and crosslaminations and structureless mudstone. These features and overall lithology suggest that deposition was controlled by turbidity currents in a deep marine environment (O'Brien *et al*., 1996). The consistency of Conception Group stratigraphy over the entire Avalon Peninsula (Williams *et al*., 1995) invites correlation of the sampled unit with the Mall Bay Formation (Williams and King, 1979) which therefore provides an age constraint on the timing of deposition. A maximum age is provided by a U-Pb date of 606 + 3.7/-2.9 Ma from the Harbour Main Group which unconformably underlies the Conception Group below the basal Mall Bay Formation (Krogh *et al*., 1988). On the southern Avalon Peninsula, the Mall Bay Formation is conformably overlain by glaciogenic rocks of the Gaskiers Formation (Williams and King, 1979; Myrow and Kaufmann, 1999). Lithostratigraphic correlation of the Avalonian successions of Boston Bay and Newfoundland (Narbonne and Gehling, 2003) suggests an upper limit on the deposition of the Mall Bay Formation as the correlative of the Gaskiers Formation in the Boston basin, the Squantum Member diamictite of the Roxbury Formation is dated as 595.5 ± 2 Ma (Thomson and Bowring, 2000).

Conception Group – Briscal Formation

The Briscal Formation was sampled on the southern Avalon Peninsula from well exposed outcrops on Portugal Cove Brook. At this location the formation consists of 1200 m of coarse-grained, thick-bedded (1-2 m) grey-green sandstone turbidites containing pyroclastic and epiclastic detritus interpreted to have been deposited in a deep marine environment (Williams and King, 1979). The Briscal Formation conformably overlies the Drook Formation and is in turn conformably overlain by the Mistaken Point Formation. A late Neoproterozoic age of deposition is suggested for the sequence as all three formations contain the Ediacaran fauna *Charnia masoni* (Narbonne and Gehling, 2003) and a minimum age of deposition is constrained by a date of 565 ± 3 Ma from a volcanic tuff in the Mistaken Point Formation (G. Dunning *in* Benus, 1988).

Arc-Platform Transition

Signal Hill Group – Cuckold Formation (Cape Spear member)

The Cuckold Formation was collected from the type section of the Cape Spear member at Cape Spear National Park and represents the most easterly onshore formation on the North American continent. The unit comprises approximately 250 m of gently westward dipping, matrix supported, pebble to cobble conglomerates that contain predominantly sub-angular red to purple clasts of rhyolite, rhyolite porphyry, ignimbrite and coarse-grained granitoid. Beds in the middle of the formation contain distinctive exotic clasts of quartz-sericite schist, quartzite, vein-quartz and other low-grade metamorphic rocks that locally form less than 25 percent of the coarse fraction and have been interpreted by King (1990) to indicate a sialic basement source. Diffuse interbeds of pebbly sandstone show large scale trough crossbeds with a unimodal paleoflow to the south-southwest (King, 1990).

At Flatrock the Cape Spear Member is disconformably overlain by grey conglomerate of the Flat Rock Cove Formation which was deposited in response to east-vergent thrusting (Rice, 1996). The recognition of this contact as a composite progressive unconformity related to faulting (Calon, 2001) indicates that the Cuckold Formation represents a sedimentary succession deposited syntectonically during the earliest phase of deformation. The youngest rocks of the Flat Rock Cove Formation overlie Conception Group strata with angular unconformity and constrain the age of faulting and deposition of the Signal Hill Group to the latest Neoproterozoic Avalonian Orogeny (Anderson *et al*., 1975).

Musgravetown Group – Crown Hill Formation

The Crown Hill Formation was sampled for analysis from the community of Tickle Cove on the Bonavista Peninsula and comprises a red to maroon pebble to cobble conglomerate that commonly shows medium to large scale trough crossbeds. On the basis of similar facies and overall stratigraphy, O'Brien and King (2005) have correlated this unit with the Cuckold Formation of the Signal Hill Group on the Avalon Peninsula. On the Bonavista Peninsula the Crown Hill Formation is conformably overlain by the earliest Cambrian Random Formation.

Fluvial and alluvial facies developed within molasse-like rocks of the Cuckold and Crown Hill formations are characteristic of braided river deposits interpreted to have developed in response to major uplift of Avalonia related to the Avalonian Orogeny (King, 1990).

Platform

Random Formation

The Random Formation is a distinctive unit of orthoquartzite, sandstone and shale that locally attains thicknesses of up to 400 m and is exposed across the entire western half of Avalonia in Newfoundland (Walcott, 1900; Landing, 1996). A sample of two interbedded rock types of the Random Formation was collected from a 90 m thick section at Keels on the Bonavista Peninsula; a thick- to very thick-bedded, white coarse-grained crossbedded quartzarenite with lenses and thin beds of quartz granule conglomerate from the base of the formation and a dark grey micaceous siltstone that occurs ca. 30 m higher in the stratigraphic sequence. Facies analysis suggest deposition under macrotidal conditions in an open marine environment (Hiscott, 1982). The age of the Random Formation is earliest Cambrian (Brasier *et al*., 1994). On the Burin Peninsula the Random Formation conformably overlies the Chapel Island Formation which contains the global stratotype section and point for the Neoproterozoic-Cambrian boundary at Fortune Head; elsewhere in eastern Newfoundland, the Random Formation underlies all exposed fossiliferous Cambrian strata in Avalonia.

Bell Island Group – Redmans Formation

This sample was collected from the type section of the Redmans Formation at Redmans Head on the northeast shore of Bell Island. The rock is a medium-grained, white to grey thin- to medium-bedded quartzarenite with minor thin silty interbeds. Most of the sandstones display trough and herringbone cross-bedding, mega ripple marks and channel and scour surfaces (Ranger *et al*., 1984); all features associated with tidal sand wave or barrier island deposits generated by transgression and regression (Brenchly *et al*., 1993). The Redmans Formation conformably overlies the Beach Formation and is inturn conformably overlain by the Ochre Cove Formation. Rare inarticulate brachiopods (van Ingen, 1914) and abundant trace fossils in all formations of the Bell Island Group indicate deposition of the Redmans Formation during the Arenig (Ranger *et al*., 1984).

ANALYTICAL METHODS

All samples were processed at the Radiogenic Isotope Laboratory at Memorial University of Newfoundland. Zircons were extracted using a jaw crusher and Bico disc mill and concentrated using a Wilfley table, iodomethane, and a Frantz isodynamic separator. For each sample approximately 150 zircon grains were selected from various non- and paramagnetic fractions and mounted in 2.5 cm diameter epoxy grain mounts. The crystals were polished to expose even surfaces at the cores of the grains in order to remove the outer surfaces which are typically enriched in uranium (Krogh, 1982) and imaged with transmitted and reflected light and a scanning electron microscope in back-scattered electron mode to illuminate oscillatory zoning and inherited crystals.

Analyses within selected zircon crystals were performed using a GeoLasPro 193 nm excimer laser coupled to a Finnigan Element XR high resolution-inductively coupled plasma-mass spectrometer (ICP-MS) equipped with a dual mode SEM and Faraday detector. During ablation, the sample was mounted in an airtight sample chamber and moved beneath the stationary laser to produce a square pit measuring 40 x 40 x 15 μm. The ablated sample was flushed from the sample cell and transported to the ICP-MS using a helium carrier gas. The U, Th and Pb isotopic ratios were acquired for ca. 180 s, along with a Tl/Bi/Np tracer solution that was nebulized simultaneously with the ablated solid sample.

Raw data were downloaded to a PC for processing using an in-house spreadsheet-utility program (LAMdate). The $^{207}Pb/^{206}Pb$, $^{208}Pb/^{206}Pb$, $^{206}Pb/^{238}U$ and $^{207}Pb/^{235}U$ ratios were calculated and blank corrected for each analysis. Aspiration of the Tl/Bi/Np tracer solution allowed for a real-time instrument mass bias correction using the known isotopic ratios of the tracer solution measured while the sample was ablated; this technique is largely independent of matrix effects that can variably influence measured isotopic ratios and hence the resulting ages. The high instrumental Hg background prohibited accurate measurement of ^{204}Pb. Nonetheless the amount and composition of common-Pb present in zircons analyzed represents an insignificant amount relative to the content of radiogenic Pb; hence, no common Pb correction was applied to the data. Most LAM analyses are accurate enough to solve most problems of provenance without applying a common Pb correction (e.g. Cox *et al*., 2003; Murphy *et al*., 2004).

Accuracy and reproducibility of U-Pb analysis in the MUN laboratory are routinely monitored by measurements of natural in-house zircon standards of known TIMS U-Pb age. To monitor the efficiency of mass bias and laser-induced fractionation, the zircon standards 91500 and PL were analyzed before and after every eight unknowns. Residual laser-induced fractionation was typically less than 0.05%/amu based on repeat measurements of the $^{206}Pb/^{238}U$ ratio of the reference standard. Age determinations were calculated using the ^{238}U (1.55125*10^{-10} a^{-1}) and ^{235}U (9.8485*10^{-10} a^{-1}) decay constants and the present day ^{238}U/^{235}U ratio of 137.88 (Jaffey and others, 1971). Final ages and Concordia diagrams were produced using the Isoplot/Ex macro (Ludwig, 1999) in conjunction with the LAMdate spreadsheet program (Košler and others, 2002).

U-Pb RESULTS

A total of 502 detrital zircon grains (Figure 3.5) from seven sedimentary rocks were analysed. Analysis of a minimum of 80 grains per sample were attempted to achieve 95% confidence that no fraction >0.05 of the population was missed. Concordance was calculated by using ^{207}Pb/^{206}Pb, ^{206}Pb/^{238}U, and ^{207}Pb/^{235}U ratios and is expressed as [(^{206}Pb/^{238}U date) / (^{207}Pb/^{206}Pb date)] x 100. Analyses that are concordant or overlap Concordia (at 1σ errors) are reported using the Concordia age. This method is favored because it makes optimal use of all radiogenic U/Pb and Pb/Pb ratios simultaneously and therefore is more precise than any single U-Pb or Pb-Pb age. No attempt was made to interpret inheritance or Pb-loss in grains with ≥20% discordance or ≥10% reverse discordance and these ages were excluded from the dataset. For positively discordant analyses (i.e. concordance < 100) the low ^{207}Pb count rates in zircons younger than 1.5 Ga precludes the use of ^{207}Pb/^{206}Pb ages and accordingly the more precise ^{206}Pb/^{238}U ages are preferred. The ^{206}Pb/^{238}U ages are also favored for reversely discordant analyses. In discordant zircons older than 1.5 Ga, the ^{207}Pb/^{206}Pb ages are reported as the ^{207}Pb/^{206}Pb ages are less sensitive to Pb-loss and because they contain higher amounts of ^{207}Pb and therefore have smaller uncertainties. The data are presented in Table 3.1 and plotted on Concordia diagrams (Figure 3.6), histograms and Gaussian cumulative probability curves

(Figure 3.7) to display both ages and associated errors. All ages are reported at the 2σ confidence level.

Main arc phase

The Mall Bay Formation is characterized by Neoproterozoic zircons (61 analyses) that show one major cluster between 690 ± 22 Ma and 580 ± 8 Ma. Four older Meso- and Paleoproterozoic components are present as individual analyses of 1244 ± 17, 1427 ± 18, 1634 ± 15, and 1795 ± 30 Ma. The detrital zircon age distribution of the Briscal Formation of the Conception Group is similar to the Mall Bay Formation and dominated by a zircon population that constitutes >90% of analyses and comprises Ediacaran zircons that span the age from 570 to 620 Ma. However, in the Briscal Formation this main group is separated by a gap of 100 Ma from an older Neoproterozoic component that is present in two analyses of 727 ± 10 Ma and 728 ± 8 Ma. A single zircon grain yielded a Mesoproterozoic age of 1390 ± 30 Ma. Cumulative probability plots for both Conception Group samples show a single distinct peak at ca. 595 Ma.

Arc-platform transition

The sample of the Cuckold Formation is dominated (85%; 68 of 80) by zircons that fall within one broad nearly unimodal peak Neoproterozoic peak at ca. 620 Ma that spans 60 m.y. between 590-650 Ma. On the cumulative probability plot, there is a minor peak at 565 Ma that consists of 8 zircons that range from 550-569 Ma; the four remaining analyses comprise 5% of the total population and yielded older ages between 666-687 Ma. The zircon signature of the Cuckold Formation is almost identical to the Crown Hill

Formation; the latter is characterized by a continuous cluster of zircons (85%; 81 of 95) between 590-650 Ma and minor components between 556-575 Ma (7 analyses) and 663-671 Ma (4 analyses). These components are separated by a gap of ca. 60 m.y. from older Neoproterozoic zircons of three concordant analyses at 734 ± 11, 736 ± 10, and 756 ± 7 Ma. Although comprising less than 2% of the total, two analyses indicate the presence of Mesoproterozoic (1338 ± 17 Ma) and Paleoproterozoic (2137 ± 21 Ma) components.

Platform

Detrital zircons analysis of the Random Formation yielded ages from 85 zircons, of which 79 or 93% cluster in the range from 590-650 Ma. A slightly younger grouping (four analyses) is separated by a ca. 20 m.y. gap from the dominant group and contains latest Neoproterozoic to earliest Paleozoic zircons between 560-539 Ma. Of the remaining two analyses, one concordant analysis is Neoproterozoic at 718 ± 34 Ma and an age of 1633 ± 16 Ma indicates the presence of a Paleoproterozoic zircon component. The cumulative probability plot of the Random Formation is characterized by a near-unimodal population that has a discrete relative peak at ca. 620 Ma.

Zircons from the Redmans Formation consist mainly of colourless and brown prismatic grains of variable size. Both colour types range from pristine to strongly pitted, and several grains have visible core and overgrowth components. A total of seventy-five grains representing the entire range of zircon morphologies in the sample were analysed. The data show one major cluster (50%; 37 of 75) from 550-680 Ma that peak on the cumulative probability plot at ca. 620 Ma. A Cambrian component is recognized in two analyses of 504 ± 8 and 534 ± 6 Ma; three older Neoproterozoic zircons yielded ages of

779 ± 30, 770 ± 15 and 975 ± 5 Ma. In contrast to all underlying samples from Avalonia in Newfoundland, the Redmans Formation contains a greater abundance of older pre-Neoproterozoic zircons; 21% of analyses (16 of 75) yielded Mesoproterozoic ages between 1036 ± 14 Ma and 1594 ± 24 Ma. Fourteen individual zircons define a cluster of Paleoproterozoic ages that range from 1670 ± 4 to 2235 ± 5 Ma. Finally, a single discordant analysis suggests the presence of an Archean zircon component at ca. 2.7 Ga.

DISCUSSION

Provenance

The new U-Pb geochronological data from detrital zircons from Neoproterozoic-early Paleozoic rocks from Avalonia in Newfoundland demonstrate the temporal controls on zircon heterogeneity in the various sampled stratigraphic successions. The data allow for the deduction of the changing tectonic regimes as the varied provenance can be correlated with discrete sources including contemporaneously generated Avalonian crust and older Gondwanan cratonic crustal sources.

The sedimentary rocks from the main arc phase contain a majority of zircons that fall in the ca. 570-620 Ma range which corresponds to the period of main phase of magmatic activity in the adjacent Neoproterozoic Avalonian arc. The Conception Group is therefore interpreted to contain a significant detrital component generated by erosion of coeval igneous rocks formed in these arc sequences which include the Harbour Main and Marystown groups. The lack of zircons in the range ca. 650-660 Ma and 700-720 Ma in both samples reflects relative periods of little magmatic activity in the early phase of Avalonian arc volcanism; the minor occurrence of ca. 730 Ma zircons in the Briscal

Formation, however, indicates that parts of the early arc was sourced as these ages correspond to volcanism in the Chapel Cove arc (Israel, 1998).

These data indicate that the Conception Group was principally derived from the underlying volcanic main phase arc. The detrital zircon ages are consistent with petrography and chemical composition of the detrital phases that indicate turbidite deposition in submarine fans adjacent to an active evolved magmatic arc (Dec *et al.*, 1992). The zircons are probably first cycle detritus because of the relatively short amount of time between their igneous crystallization and time of deposition. The very high rate of sedimentation, abundant pyroclastic and epiclastic detritus, deep-water environment (Williams and King, 1979; O'Brien *et al.*, 1996), sedimentation coeval with arc magmatism and detrital zircon ages that are roughly synchronous with the age of deposition all suggest that deposition of these main arc sequences occurred in an active tectonic environment.

The detrital zircon populations in the arc-platform transition (Cuckold and Crown Hill formations) yielded fewer zircons in the 570-600 Ma range and instead are dominated by a group of older zircons between 600-650 Ma. Vestiges of these 600-650 Ma rocks are exposed throughout Avalonia in Newfoundland and include the Holyrood and Simmons Brook intrusive suites and Connaigre Bay and Love Cove groups. A minor cluster of older Neoproterozoic zircons between 660-680 Ma and ca. 730 Ma can be attributed to erosion of the underlying early arc sequences (Furby's Cove intrusive suite, Tickle Point Formation, and Hawke Hill tuff) of Avalonia. Such derivation is consistent with facies trends and paleocurrents (O'Brien *et al.*, 1995). The change from siliceous volcaniclastic rocks of the Conception Group to overlying molasse-like red-beds of the

Signal Hill and Musgravetown groups represents a transition from deep water turbidite deposition to subaerial fluvial and alluvial plain conditions. The overall coarsening- and thickening-upwards sequences of the Cuckold and Crown Hill formations (King, 1990) indicate that deposition occurred in tectonically active fault-bounded basins controlled by major uplift of the underlying arc sequences during the latest Neoproterozoic Avalonian Orogeny (Hughes, 1970).

The detrital zircon populations in the Random Formation are particularly similar to those in the underlying Crown Hill Formation (600-650 Ma) and both contain Paleoproterozoic zircons. These data may indicate either a shared protolith and/or the presence of recycled components of the Crown Hill Formation in the Random Formation. The mineralogical and texturally mature quartzarenites, relatively high (up to 25 percent) plagioclase content and abundance of detrital muscovite argue against significant sediment recycling and suggest derivation from a proximal orogenic source area where detritus was not transported long distances prior to deposition (Jenness, 1963). The most likely provenance for the zircons in the Random Formation is the same Avalonian arc-related calc-alkaline plutonic suites as the underlying arc-transition sequences. Stratigraphic variations, however, suggest a change in the depositional environment of the Random Formation. The quartzarenites and interbedded fine-grained siltstones are interpreted to be subtidal sand shoals and intertidal mud flats formed on a macrotidal coastline adjacent to a broad continental shelf or in a large coastal embayment during marine transgression (Hiscott, 1982). Early Cambrian transgressive quartz-rich sandstone sequences are present throughout Avalonia in Massachusetts, Maritime Canada, Wales and England (Landing, 1996) and were deposited on shallow, wide, shelf platforms during eustatic sea level rise (Sloss, 1963).

Similar to the Random Formation, quartzarenites of the Redmans Formation contain a dominant late Neoproterozoic population (ca. 620 Ma) and suggest direct derivation from the arc plutonic suites. Less prominent groupings of zircons between 665-685 Ma and 700-760 Ma are interpreted to have been derived from the early arc sequences, the Furby's Cove intrusive suite/Tickle Point Formation and Burin Group, respectively. In contrast to other sequences in Avalonia, the Redmans Formation, however, also contains a much wider range of significantly older detrital zircon populations. The pronounced cluster of continuous ages between 1.0-1.6 Ga, together with Paleoproterozoic and Archean components, suggest a significant difference in provenance from the other Avalonian rocks analyzed in this study.

The presence of zircons with Mesoproterozoic ages, mainly in the Redmans Formation (but an accessory component in other units) is consistent with the existence of a Mesoproterozoic (ca. 1.0-1.6 Ga) crustal component in the basement of Avalonia. Although no exposed basement is present anywhere in Avalonia, Sm-Nd (Kerr *et al*., 1994; Murphy *et al*., 1996) and Pb (Ayuso *et al*., 1996) isotopic data indicate that the Avalonian magmatic arcs formed upon a dominantly ca. 1.0-1.2 Ga basement with a minor component of older ca. 1.6 Ga crust. Paleoproterozoic and Archean age grains in the Redmans Formation could also be derived from a local Avalonian basement source as rare ca. 2.0 and 2.4 Ga xenocrystic zircons are reported from Avalonian plutonic rocks in the Mira terrane (Bevier *et al*., 1990) and New England (Zartman and Hermes, 1987).

Source craton

Zircons from sedimentary units in Avalonia show a wide age spectrum with well defined Archean, Paleoproterozoic and late Neoproterozoic (Ediacaran) ages. Age patterns of detrital zircon data from main arc and transition samples in Avalonia are dominated by a unimodal population of Neoproterozoic zircons that almost certainly were locally-derived from the underlying/adjacent arc sequences of Avalonia and deposited as first cycle sediments. In contrast, the sequences from the platform contain significant quantities of Mesoproterozoic (1.0-1.6 Ga), Paleoproterozoic (1.6-2.3 Ga) and minor Archean (ca. 2.7 Ga) components. Although some of these zircons could have been derived from the underlying sequences as second-generation recycled zircons, the large population of zircons and absence of isotopic and geologic data for an older basement component in the underlying units, however, suggest that the Meso- and Paleoproterozoic and Archean zircons in the platform sequences were probably derived as first-cycle detritus from the basement or from a crustal source that was external to Avalonia.

The Ediacaran zircons provide no paleogeographical information as they overlap the known age range of underlying Avalonian igneous rocks. The older U-Pb detrital zircon ages however, can be compared to potential source cratons that are characterized by Archean to early Neoproterozoic tectonothermal activity. The detrital zircon population data presented herein to some extent match the age of tectonothermal events in Laurentia, Baltica and Gondwana; hence these cratons are potential sources for the zircons in the rocks of Avalonia.

Although Laurentia and Baltica have comparable geological histories during the Proterozoic, which suggest evolution as a single cratonic nuclei following the amalgamation of Archean cratons between 1.8-1.9 Ga (Hoffman, 1988; Gower *et al*., 1990), geological, lithological, faunal, paleomagnetic and isotopic evidence indicate that Avalonia is a distinct terrane exotic to Laurentia (Williams, 1964; Williams and Hatcher, 1983; Landing, 1996; Murphy and Nance, 1989; O'Brien *et al*., 1996; Hibbard *et al*., 2007 and references therein). The detrital zircon data also refute an eastern Laurentian-Baltica source because the analyzed rocks in Avalonia contain zircons with ages of 2.0-2.4 Ga and 620-750 Ma, which corresponds to major Paleoproterozoic (2.0-2.4 Ga) and Neoproterozoic tectonic and crust forming events that are noticeably absent from the geological record of eastern Laurentian and Baltica (Gower *et al*. 1990; Wardle *et al*., 2002). These ages are however compatible with a Gondwanan provenance.

The Paleoproterozoic and Archean detrital zircons match the age signatures of rocks found along the Neoproterozoic-early Paleozoic West African and Amazonian margins of Gondwana. However, the presence of Meosproterozoic-early Neoproterozoic grains in Avalonia is incompatible with a West African source as the latter contains only minor occurrences of Mesoproterozoic (ca. 1000 Ma) magmatism (de Witt, 2005) and no record of any tectonothermal events between 1.1 Ga and 2.0 Ga (Rocci *et al*., 1991). The data are compatible with an Amazonian provenance. Mesoproterozoic and Paleoproterozoic rocks are present along the Amazonian margin of Gondwana (Figure 3.8) and correlate with the Sunsás–Aguapeí (0.9-1.2 Ga), Rondônia-San Ignacio (1.2-1.4 Ga), Rio Negro-Jurena (1.5-1.75 Ga), and Trans-Amazonian (1.9-2.2 Ga) orogenic belts located along the periphery of the Archean (2.6-3.2 Ga) Amazon craton (Bettencourt *et al*., 1999; Sadowski and Bettencourt, 1996; Dall'Agnol *et al*., 1999). An Avalonia-Amazonia link is also consistent with Nd isotope (Murphy *et al*., 1996), xenocrystic zircon (Zartman and Hermes, 1987; Bevier and Barr, 1990), faunal and stratigraphic (Landing, 1996) data that are incompatible with a West African source for Avalonia.

Timing of rifting

Current paleotectonic models suggest that Avalonia formed along the Neoproterozoic margin of Gondwana and accreted to Ganderia/Laurentia in the Late Silurian-Early Devonian during the Acadian Orogeny (van Staal, 2007). Opening of the Rheic Ocean separating Avalonia from Gondwana is therefore constrained to a period between the Neoproterozoic-Silurian. However, there is considerable debate regarding the timing and extent of rifting of Avalonia within this period. A Neoproterozoic age of separation was proposed by Landing (1996; 2005) based on contrasting Cambrian faunal assemblages and platform sequences between Newfoundland and Morocco and interpretation of the Cambrian-Ordovician Gander Group as a slope and rise prism of the Avalonia microcontinent. A Neoproterozoic timing of separation of Avalonia from Gondwana is however, inconsistent with a wide range of paleomagnetic, faunal, isotopic and geological arguments (O'Brien *et al*., 1996; van Staal *et al*., 1998) as it relies on a pre-rifting connection to West Africa and interpretation of Avalonia and Ganderia as a single tectonic entity. As discussed above Avalonia is interpreted to have formed along the Amazonian margin of Gondwana and an Avalonia-Ganderia connection is not likely because even though Ganderia and Avalonia have similar arc-dominated Neoproterozoic basement rocks, they have very distinct magmatic, depositional and tectonothermal histories (O'Brien *et al*., 1996; van Staal *et al*., 1998; Hibbard *et al*., 2007) and were therefore almost certainly tectonically decoupled and separated in the early Paleozoic.

However, a younger age of separation during the Early Ordovician is supported by subsidence analysis (Prigmore *et al*., 1997), comparable faunal assemblages until the Tremadoc (Cocks and Fortey, 1990; Fortey and Cocks, 2003) and paleomagnetic data that indicate Avalonia resided at high southerly latitude near Gondwana from the Middle Cambrian to the end of the Early Ordovician (van der Voo and Johnson, 1985; Hodych and Buchan, 1998; MacNiocaill, 2000; Hamilton and Murphy, 2004). The zircon data presented herein are compatible with a younger timing of separation of Avalonia from Gondwana that occurred in the Early Ordovician (Figure 3.9). The absence of significant quantities of Mesoproterozoic, Paleoproterozoic and Archean zircons in Ediacaran-Early Cambrian sequences of Avalonia suggest that zircons of these ages found in Ordovician rocks of the platform represent first-cycle detritus derived directly from Amazonia rather than second generation recycled zircons from underlying sequences. This interpretation requires that Avalonia lay adjacent to Gondwana throughout the Cambrian until deposition of the Redmans Formation in the Early Ordovician.

Abundant Middle Cambrian to Middle Ordovician rift-related volcanic rocks in Newfoundland and Wales are generally considered to be related to Avalonia's rifting and departure from Gondwana (van Staal *et al*., 1998). The separation of Avalonia was followed by widespread Arenig subsidence recorded in the Stiperstone Quartzite of Avalonia in England and the Armorican Quartzite of Cadomia in Brittany, interpreted to reflect the rift-drift transition of the Rheic Ocean (van Staal *et al*., 1998; Nance *et al*., 2002; Murphy *et al*., 2006). A similar model of protracted, multiple phases of Neoproterozoic rift-related magmatism followed by later development of a Paleozoic rift-drift transition was proposed for opening of the Iapetus Ocean (Williams and Hiscott, 1987; Cawood *et al*., 2001; Waldron and van Staal, 2001).

SUMMARY AND CONCLUSIONS

Avalonia comprises a sequence of late Neoproterozoic volcano-sedimentary sequences that are overlain by a Cambrian-Ordovician shale-rich platformal sedimentary succession. U-Pb ages of detrital zircons from Neoproterozoic rocks of the type area of Avalonia in eastern Newfoundland are dominated by Ediacaran populations with ages between 620 and 580 Ma that are interpreted to be derived from the underlying volcanic-plutonic rocks of the main Avalonian arc. These rocks are inferred to have accumulated as a series of submarine fans in restricted fault-bounded, arc-adjacent basins that grade upwards into terrestrial siliciclastic rocks deposited under subaerial fluviatile conditions without a significant change in provenance. Early Paleozoic platform units show an overall up-section increase in Meso- and Paleoproterozoic and Archean zircons that are inconsistent with recycling from underlying Neoproterozoic rocks. The range of detrital zircon ages, combined with isotopic and sedimentological data argue against Avalonia being proximal to West Africa and suggest that the former originated along the periphery of Amazonia. The rapid influx of Mesoproterozoic and older detritus in the upper sequences of the Avalonian platform suggest a major change in tectonic regime to expose older material that is temporally consistent with Avalonian basement. This striking change in provenance is interpreted to be related to rifting and ensuing separation of Avalonia from Gondwana during the Early Ordovician opening of the Rheic Ocean.

There is close correspondence between lithology, depositional age and detrital zircon signatures of the Redmans Formation and Armorican Quartzite (Ranger *et al*., 1984; Fernández-Suárez *et al*., 2002) and therefore I propose that the Redmans Formation represents the rift-drift transition of the Rheic Ocean. Interpretation of the Redmans Formation as the Rheic rift-drift transition imposes important constraints on the paleotectonic evolution of Avalonia and opening of the Rheic Ocean. The most significant implication of this observation is the implied connection between Avalonia and the peri-Gondwanan block of Cadomia in the early Paleozoic. In this model, Avalonia and Cadomia represent two different terranes with distinct basement rocks and contrasting Neoproterozoic histories (Samson and D'Lemos, 1998; Murphy *et al*., 2000; Samson *et al*., 2005) albeit from the same craton. Both terranes formed independent of one another on the Amazonian margin and were juxtaposed along a Neoproterozoic suture, prior to the Early Ordovician opening of the Rheic Ocean (Murphy *et al*., 2006). Available data suggest that assembly of the Avalonian and Cadomian microplates was accomplished by margin-parallel strike-slip activity due to the complex interaction of a continental margin transform system with a subduction zone as a result of ridge-trench collision (Keppie *et al*., 2000; Nance *et al*., 2002). If this hypothesis is correct, the site of late Cambrian rifting and subsequent Early Ordovician opening of the Rheic Ocean occurred along the Neoproterozoic suture zone between Avalonia and Cadomia, a model first proposed by Murphy *et al*. (2006).

REFERENCES

Anderson, M.M, Bruckner, W.D., King, A.F., and Maher, J.B.
1975. The late Proterozoic "H.D. Lilly Unconformity" at Red Head, northeastern Avalon Peninsula, Newfoundland. American Journal of Science, 275, p. 1012-1027.

Ayuso, R.A., Barr, S.M., and Longstaffe, F.J.
1996. Pb and O isotopic constraints on the source of granitic rocks from Cape Breton Island, Nova Scotia, Canada. American Journal of Science, 296, p. 789-817.

Barr, S.M., Davis, D.W., Kamo. S., and White, C.E.
2003. Significance of U–Pb detrital zircon ages in quartzite from peri-Gondwanan terranes, New Brunswick and Nova Scotia, Canada. Precambrian Research, 126, p. 123-145.

Benus, A.P.
1988. Sedimentological context of a deep-water Ediacaran fauna (Mistaken Point, Avalon Zone, eastern Newfoundland). *In:* Landing, E., *et al*. (*eds.*), Trace fossils, small shelly fossils and the Precambrian-Cambrian boundary: New York State Museum and Geological Survey, Bulletin 463, p. 8-9.

Bettencourt, J.S., Tosdal, R.M., Leite, W.B., and Payolla, B.L.
1999. Mesoproterozoic rapakivi granites of the Rondônia Tin Province, southwestern border of the Amazon Craton, Brazil. Reconnaissance U-Pb geochronology and regional implications. Precambrian Research, 95, p. 41-67.

Bevier, M.L., and Barr, S.M.
1990. U–Pb age constraints on the stratigraphy and tectonic history of the Avalon terrane, New Brunswick, Canada. Journal of Geology, 58, p. 53-63.

Brenchley, P.J., Pickerill, R.K., and Stromberg, S.G.
1993. The role of wave reworking on the architecture of storm sandstone facies, Bell Island Group (Lower Ordovician), eastern Newfoundland. Sedimentology, 40, p. 359-382

Calon, T.
2001. Late Precambrian sedimentation and related orogenesis of the Avalon Peninsula, eastern Avalon Zone, Newfoundland. *In:* GAC-MAC Field Trip A9/B8. St. John’s, Newfoundland, Canada.

Cawood, P.A. and Nemchin, A.A.
2001. Paleogeographic development of the east Laurentian margin constrained by U/Pb dating of detrital zircon in the Newfoundland Appalachians. Geological Society of America Bulletin, 113, p. 1234-1246.

Cawood, P.A., McCausland, P.J.A., and Dunning, G.R.
2001. Opening Iapetus: Constraints from the Laurentian margin in Newfoundland. Geological Society of America Bulletin, 113, p. 443-453.

Cawood, P.A., Nemchin, A.A., Smith, M. and Loewy, S.
2003. Source of the Dalradian Supergroup constrained by U–Pb dating of detrital zircon and implications for the East Laurentian margin. Journal of the Geological Society, London, 160, p. 231-246.

Cocks, L.R.M. and Fortey, R.A.
1990. Biogeography of Ordovician and Silurian faunas. *In:* W.S. McKerrow and C.R. Scotese (*eds.*), Paleozoic Paleogeography and Biogeography. Geological Society Memoir, 12, p. 97-104.

Cocks, L.R.M. and Torsvik, T.H.
2002. Earth geography from 500 to 400 million years ago. A faunal and palaeomagnetic review. Journal of the Geological Society of London, 159, p. 631-644.

Cox, R.A., Wilton, D.H.C., and Košler, J.
2003. Laser-ablation U-Th-Pb in situ dating of allanite and zircon: an example from the October Harbour granite, central coastal Labrador, Canada. The Canadian Mineralogist, 41, p. 273-291

Dalziel, I.W.D.
1994. Precambrian Scotland as a Laurentia-Gondwana link—Origin and significance of cratonic promontories. Geology, 22, p. 589–592
1997. Neoproterozoic-Paleozoic geography and tectonics; review, hypothesis, environmental speculation. Geological Society of America Bulletin, 109, p. 16-42.

Dall'Agnol, R., Costi, H.T., Leite, A.A., Magalhaes, M.S., Teixeira, N.P.
1999. Rapakivi granites from Brazil and adjacent areas. Precambrian Research. 95, p. 9-39.

Davis, D.W.
2002. U-Pb geochronology of Archean metasediments in the Pontiac and Abitibi subprovinces, Quebec, constraints on timing, provenance and regional tectonics. Precambrian Research, 115, p. 97-117.

DeGraaff-Surpless, K., Mahoney, J.B., Wooden, J.L., and McWilliams, M.O.
2003. Lithofacies control in detrital zircon provenance studies: Insights from the Cretaceous Methow basin, southern Canadian Cordillera. Geological Society of America Bulletin, 115, p. 899-915.

de Wit, M.J., Bowring, S., Dudas, F., and Kamga, G.
2005. The great Neoproterozoic central Saharan Arc and the amalgamation of the North African Shield. Geolgoical Association of Canada, Abstracts with programs.

Fernández-Suárez, J., Gutiérrez-Alonso, G., and Jeffries, T.E.
2002. The importance of along-margin terrane transport in northern Gondwana: Insights from detrital zircon parentage in Neoproterozoic rocks from Iberia and Brittany. Earth and Planetary Science Letters, 204, p. 75–88.

Fortey, R.A. and Cocks, L.R.M.
2003. Palaeontological evidence bearing on global Ordovician-Silurian continental reconstructions. Earth Science Reviews, 61, p. 245-307.

Gower, C.F., Ryan, A.B. & Rivers, T.
1990. Mid-Proterozoic Laurentia-Baltica: an overview of its geological evolution and a summary of the contributions made by this volume. *In:* Gower, C.F., Rivers, T. & Ryan, A.B. (*eds.*), Mid-Proterozoic Laurentia-Baltica, Geological Association of Canada Special Paper, 38, p. 1-20.

Greenough, J.G. and Papezik, V.S.
1986. Acado-Baltic volcanism in eastern North America and western Europe: Implications for Cambrian tectonism. Maritime Sediments and Atlantic Geology, 22, p. 240-251.

Hamilton, M.A. and Murphy, J.B.
2004. Tectonic significance of a Llanvirn age for the Dunn Point volcanic rocks, Avalon terrane, Nova Scotia, Canada: implications for the evolution of the Iapetus and Rheic Oceans. Tectonophysics, 379, p. 199-209.

Hibbard, J.P., van Staal. C.R., and Miller, B.V.
2007: Links between Carolinia, Avalonia, and Ganderia in the Appalachian peri-Gondwanan Realm. Geological Society of America Special Paper.

Hiscott, R.N.
1982. Tidal deposits of the Lower Cambrian Random Formation, eastern Newfoundland: facies and paleoenvironments. Canadian Journal of Earth Sciences, 19, p. 2028-2042.

Hodych, J.P. and Buchan, K.L.
1998. Palaeomagnetism of the ca. 440 Ma Cape St Mary's sills of the Avalon Peninsula of Newfoundland: implications for Iapetus Ocean closure. Geophysical Journal International, 135, p. 155-164.

Hoffman, P.F.
1988. United Plates of America, the birth of a craton - Early Proterozoic assembly and growth of Laurentia. Annual review of earth and planetary sciences, 16, p. 543-603.

1991. Did the breakout of Laurentia turn Gondwanaland inside out?, Science, 252, p. 1409–1412.

Hughes, C.J.
1970. The Late Precambrian Avalonian Orogeny in Avalon, southeast Newfoundland. American Journal of Science, 269, p. 183-190.

Jaffey, A.H., Flynn, K.F., Glendenin, L.E., Bentley, W.C., and Essling, A.M.
1971. Precision measurement of half-lives and specific activities of 235U and 238U. Phys. Rev. C4, p. 1889–1906.

Kerr, A., Jenner, G.A., and Fryer, B.J.
1995. Sm-Nd isotopic geochemistry of Precambrian to Paleozoic granitoid suites and the deep-crustal structure of the southeast margin of the Newfoundland Appalachians. Canadian Journal of Earth Sciences, 32, p. 224-245.

King, A.F.
1990. Geology of the St. John's area. Geological Survey Branch, Dept. of Mines and Energy, Government of Newfoundland and Labrador, Report 90-2, 88 p.

Košler, J., Fonneland, H.C., Sylvester, P., Tubrett, M., and Pedersen, R.B.
2002. U-Pb dating of detrital zircons for sediment provenance studies - a comparison of laser ablation ICPMS and SIMS techniques. Chemical Geology, 182, p. 605-618.

Krogh, T.E.
1973. A low contamination method for hydrothermal decomposition of zircon and extraction of U and Pb for isotopic age determinations. Geochimica et Cosmochimica Acta, 37, p. 485-494.
1982. Improved accuracy of U–Pb zircon ages by the creation of a more concordant system using an air abrasion technique. Geochimica et Cosmochimica Acta, 46, p. 637-649.

Krogh, T.E., Strong, D.F., O'Brien, S.J., and Papezik, V.
1988. Precise U-Pb dates from zircons in the Avalon terrane of Newfoundland: Canadian Journal of Earth Sciences, 25, p. 442-453.

Israel, S.A.
1998. Geochronological, structural and stratigraphic investigation of a precambrian unconformity between the Harbour Main Group and Conception Group, east coast Holyrood Bay, Avalon Peninsula, Newfoundland. B.Sc. (Hons.) thesis, Memorial University of Newfoundland, 78 p.

Landing, E.
1996. Avalon: Insular continent by the latest Precambrian. *In:* Nance, R.D. and Thompson, M.D. (*eds.*) Avalonian and Related Peri-Gondwanan

Terranes of the Circum-North Atlantic. Geological Society of America, Special Paper, 304, p. 29-63.
2005. Early Paleozoic Avalon–Gondwana unity: an obituary—response to "Palaeontological evidence bearing on global Ordovician–Silurian continental reconstructions" by R.A. Fortey and L.R.M. Cocks. Earth Science Reviews, 69, p. 169-175.

Ludwig, K. R.
1999. Isoplot/Ex 2.01: a Geochronological Toolkit for Microsoft Excel. Berkeley Geochronology Center, Berkeley, CA.

MacNiocaill, C.
2000. A new Silurian paleolatitude for eastern Avalonia and evidence for crustal rotations in the Avalonian margin of southwestern Ireland: Geophysical Journal International, 141, p. 661-671.

McKerrow,W. S., Scotese, C. R., and Brasier, M. D.
1992. Early Cambrian continental reconstructions: Geological Society of London Journal, 149, p. 599-606.

Mezger, K. and Krögstad, E.J.
1997. Interpretation of discordant U-Pb zircon ages, an evaluation: Journal of Metamorphic Geology, 15, p. 127-140.

Murphy, J.B., Keppie, J.D., Dostal, J., and Cousins, B.L.
1996. Repeated late Neoproterozoic –Silurian lower crustal melting beneath the Antigonish Highlands, Nova Scotia: Nd isotopic evidence and tectonic interpretations. *In:* Nance, R.D. and Thompson, M.D. (*eds.*) Avalonian and Related Peri-Gondwanan Terranes of the Circum-North Atlantic. Geological Society of America,Special Paper, 304, p. 109-120.

Murphy, J.B., Keppie, J.D., Dostal, J., and Nance, R.D.
1999. Neoproterozoic–early Paleozoic evolution of Avalonia. *In:* Ramos, V.A., Keppie, J.D. (*eds.*), Laurentia–Gondwana Connections Before Pangea. Geological Society of America, Special Paper, 336, p. 253-266.

Murphy, J.B., Fernandez-Suarez, J., Jeffries, T.E., and Strachan, R.A.
2004. U–Pb (LA–ICP-MS) dating of detrital zircons from Cambrian clastic rocks in Avalonia: erosion of a Neoproterozoic arc along the northern Gondwanan margin. Journal of the Geological Society, London, 161, p. 243-254.

Murphy, J.B., Gutierrez-Alonso, G., Nance, R.D., Fernandez-Suarez, J., Keppie, J.D., Quesada, C., Strachan, R.A., and Dostal, J.
2006. Origin of the Rheic Ocean: Rifting along a Neoproterozoic suture? Geology, 34, p. 325-328.

Myrow, P.M. and Hiscott, R.N.
1993. Depositional history and sequence stratigraphy of the Precambrian–Cambrian boundary stratotype section, Chapel Island Formation, southeast Newfoundland. Paleogeography. Paleoclimatology. Paleoecology, 104, p. 13-35.

Myrow, P.M., and Kaufman, A.J.
1999. A newly discovered cap carbonate above Varanger-age glacial deposits in Newfoundland, Canada. Journal of Sedimentary Research, 69, p. 784-793.

Nance, R.D., Murphy, J.B., and Keppie, J.D.
2002. A Cordilleran model for the evolution of Avalonia. Tectonophysics, 352, p. 11-31.

Narbonne, G.M. and Gehling, J.G.
2003. Life After Snowball: The Oldest Complex Ediacaran Fossils. Geology, 31, p. 27-30.

O'Brien, S.J., O'Brien, B.H., Dunning, G.R., and Tucker, R.D.
1996. Late Neoproterozoic Avalonian and related peri-Gondwanan rocks of the Newfoundland Appalachians. *In:* Nance, R.D. & Thompson, M.D. (*eds.*) Avalonian and Related Peri-Gondwanan Terranes of the Circum-North Atlantic. Geological Society of America, Special Paper, 304, p. 9-28.

O'Brien, S.J., Dunning, G.R., Dube, B., O'Driscoll, C.F., Sparkes, B., Israel, S., and Ketchum, J.
2001. New insights into the Neoproterozoic geology of the central Avalon Peninsula (parts of NTS map areas 1N/6, 1N/7 and 1N/3), eastern Newfoundland. Government of Newfoundland and Labrador, Department of Mines and Energy, Geological Survey, Current Research, Report 2001-1, p. 169-189.

O'Brien, S.J., O'Driscoll, C.F., Greene, B.A., Tucker, R.D.
1995. Pre-carboniferous geology of the Connaigre Peninsula and the adjacent coast of Fortune Bay, southern Newfoundland. Government of Newfoundland and Labrador, Department of Mines and Energy, Geological Survey, Current Research, Report 95-1, p. 267-298.

O'Brien, S.J. and King, A.F.
2005. Late Neoproterzoic (Ediacaran) stratigraphy of Avalon Zone sedimentary rocks, Bonavista Peninsula, Newfoundland. Government of Newfoundland and Labrador, Department of Natural Resources, Geological Survey, Current Research, Report 06-1, p. 101-114.

Pollock, J.C., Wilton, D.H.C., van Staal, C.R., and Morrissey, K.D.
2007. U-Pb detrital zircon geochronological constraints on the Early Silurian collision of Ganderia and Laurentia along the Dog Bay Line: The terminal Iapetan suture in the Newfoundland Appalachians. American Journal of Science, 307, p. 399-433.

Prigmore, J.K., Butler, A.J., and Woodcock, N.H.
1997. Rifting during separation of eastern Avalonia from Gondwana; evidence from subsidence analysis. Geology, 25, p. 203-206.

Ranger, M.J., Pickerill, R.K., and Fillion, D.
1984. Lithostratigraphy of the Cambrian?-Lower Ordovician Bell Island and Wabana groups of Bell, Little Bell, and Kellys islands, Conception Bay, eastern Newfoundland. Canadian Journal of Earth Sciences, 21, p. 1245-1261.

Rice, T.G.
1996. Structure of the Flat Rock thrust zone, Avalon Peninsula, Newfoundland Appalachians. Unpublished B.Sc. (Hons.) thesis, Memorial University of Newfoundland, St. John's, Newfoundland, 117 p.

Rocci, G., Bronner, G., and Deschamps, M.
1991. Crystalline basement of the West African craton. *In:* Dallmeyer, R.D. and Lecorche, J.P., (*eds.*) The West African orogens and circum-Atlantic correlatives: Heidelberg, Germany, Springer-Verlag, p. 31–61.

Sadowski, G.R. and Bettencourt, J.S.
1996. Mesoproterozoic tectonic correlations between eastern Laurentia and the western border of the Amazon craton: Precambrian Research, 76, p. 213–227.

Samson, S.D. and D'Lemos, R.S.
1998. U–Pb geochronology and Sm–Nd isotopic composition of Proterozoic gneisses, Channel Islands, UK. Journal of the Geological Society, London, 155, p. 609–618.

Samson, S.D., D'Lemos, R.S., Miller, B.V. and Hamilton, M.A.
2005. Neoproterozoic paleogeography of the Cadomia and Avalon terranes: constraints from detrital zircon U-Pb ages. Journal of the Geological Society of London, 162, p. 65-71.

Sircombe K., Bleeker, W., and Stern, R.
2001. Detrital zircon geochronology and grain-size analysis of a ~2800 Ma Mesoarchean proto-cratonic cover succession, Slave Province, Canada. Earth and Planetary Science Letters, 189, p. 207-220.

Sloss, L. L.
1963. Sequences in the cratonic interior of North America: Geological Society of America Bulletin, 74, p. 93-114.

Strong, D.F. and Dostal, J.
1980. Dynamic melting of Proterozoic upper mantle: Evidence from rare earth elements in oceanic crust of Eastern Newfoundland. Contribributions to Mineralogy and Petrology, 72, p. 165-173.

Swinden, H.S. and Hunt, P.A.
1991. A U-Pb zircon age from the Connaigre Bay Group, southwestern Avalon Zone, Newfoundland: Implications for regional correlations and metallogenesis. *In:* Radiometric Age and Isotopic Studies, Report 4, Geological Survey of Canada, 90-2, p. 3-10.

Thompson, M.D. and Bowring, S.A.
2000. Age of the Squantum “tillite”, Boston Basin, Massachusetts: U–Pb zircon constraints on terminal Neoproterozoic glaciation. American Journal of Science, 300, p. 630–655.

Torsvik, T.H., Smethurst, M.A., Meert, J.G., Van der Voo, R., McKerrow, W.S., Brasier, M.D., Sturt, B.A., and Walderhaug, H.J.
1996. Continental break-up and collision in the Neoproterozoic—a tale of Baltica and Laurentia. Earth Science Reviews. 40, p. 229–258.

van der Voo, R. and Johnson, R.J.E.
1985. Paleomagnetism of the Dunn Point Formation (Nova Scotia): high paleolatitudes for the Avalon terrane in the Late Ordovician, Geophysical Research Letters, 12, p. 337-340.

Van Ingen, G.
1914. Cambrian and Ordovician faunas of south-eastern Newfoundland. Bulletin of the Geological Society of America, 25, p. 138

van Staal, C.R., Dewey, J.F., MacNiocaill, C., and McKerrow, W.S.
1998. The Cambrian–Silurian tectonic evolution of the northern Appalachians and British Caledonides: history of a complex west and southwest Pacific-type segment of Iapetus. *In:* Blundell, D.J., Scott, A.C. (*eds.*), Lyell: The Past is the Key to the Present. Geological Society of London, Special Publication, 143, p. 199–242.

Waldron, J.F. and van Staal., C.R.
2001. Taconian orogeny and the accretion of the Dashwoods block: A peri-Laurentian microcontinent in the Iapetus Ocean. Geology, 29, p. 811-814.

Wardle, R.J., Gower, C.F., James, D.T., St-Onge, M.R., Scott, D.J., Garde, A.A., Culshaw, N.G., van Gool, J.A.M., Connelly, J.N., Perreault, S., and Hall, J.
2002. Correlation chart of the Proterozoic assembly of the northeastern Canadian - Greenland Shield, Canadian Journal of Earth Sciences, 39, p. 895.

Williams, H., and King, A.F.
1979. Trepassey Map Area, Newfoundland: Geological Survey of Canada Memoir 389, 24 p.

Williams, H., O'Brien, S.J., King, A.F., and Anderson, M.M.
1985. Avalon zone—Newfoundland. *In:* Williams, H. (*ed*.), Geology of the Appalachian-Caledonian orogen in Canada and Greenland. Boulder, Colorado, Geological Society of America, Geology of North America, F-1, p. 226–237.

Williams, H. and Hiscott, R.N.
1987. Definition of the Iapetus rift-drift transition in western Newfoundland. Geology, 15, p. 1044-1047.

Zartman, O. and Hermes, D.
1987. Archean inheritance in zircon from late Paleozoic granites from the Avalon zone of southeastern New England: an African connection. Earth and Planetary Science Letters, 82, p. 305-315.

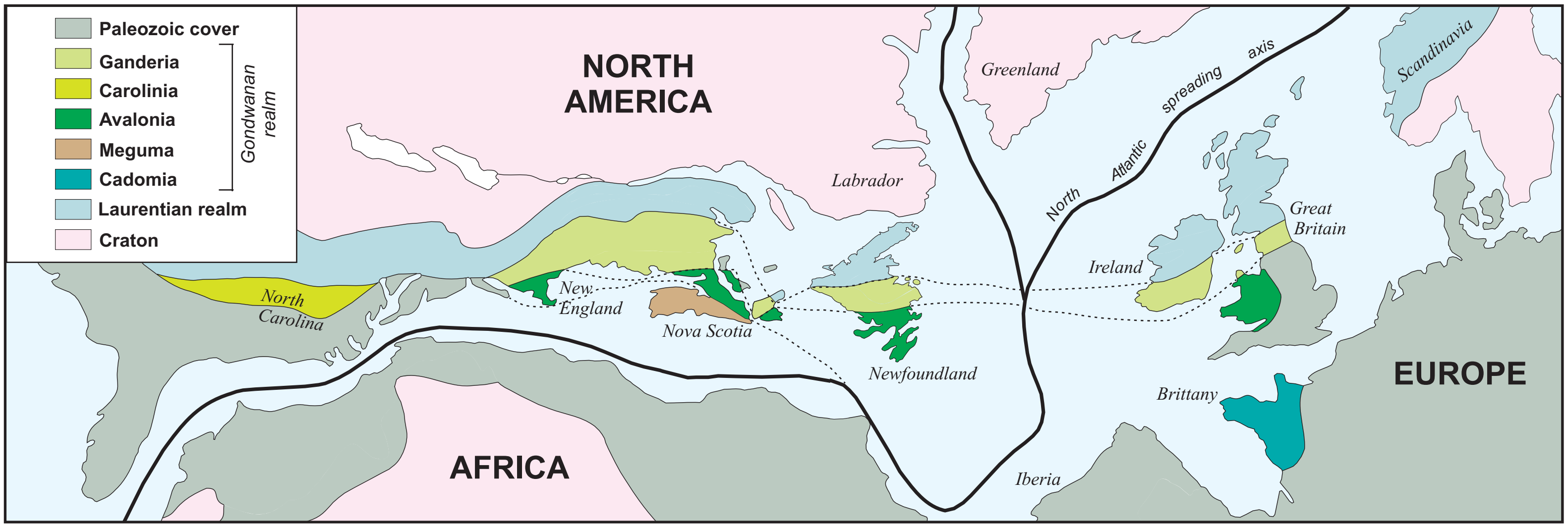

Figure 3.1. Early Mesozoic restoration of the North Atlantic region and Appalachian-Caledonian orogen (modified after Williams, 1984; Nance *et al*., 2002; Hibbard *et al*., 2007).

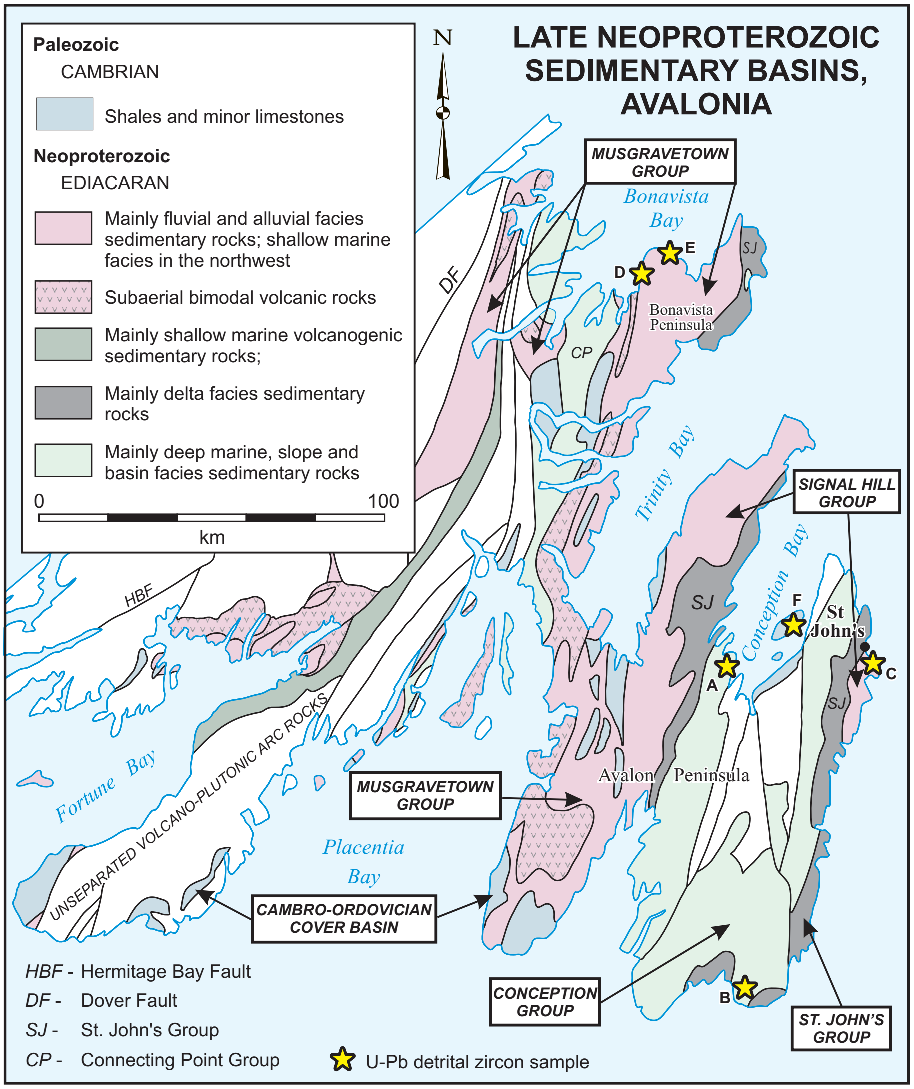

Figure 3.2. Regional distribution of late Neoproterozoic sedimentary rocks of Avalonia in eastern Newfoundland (modified after O'Brien and King, 2005).

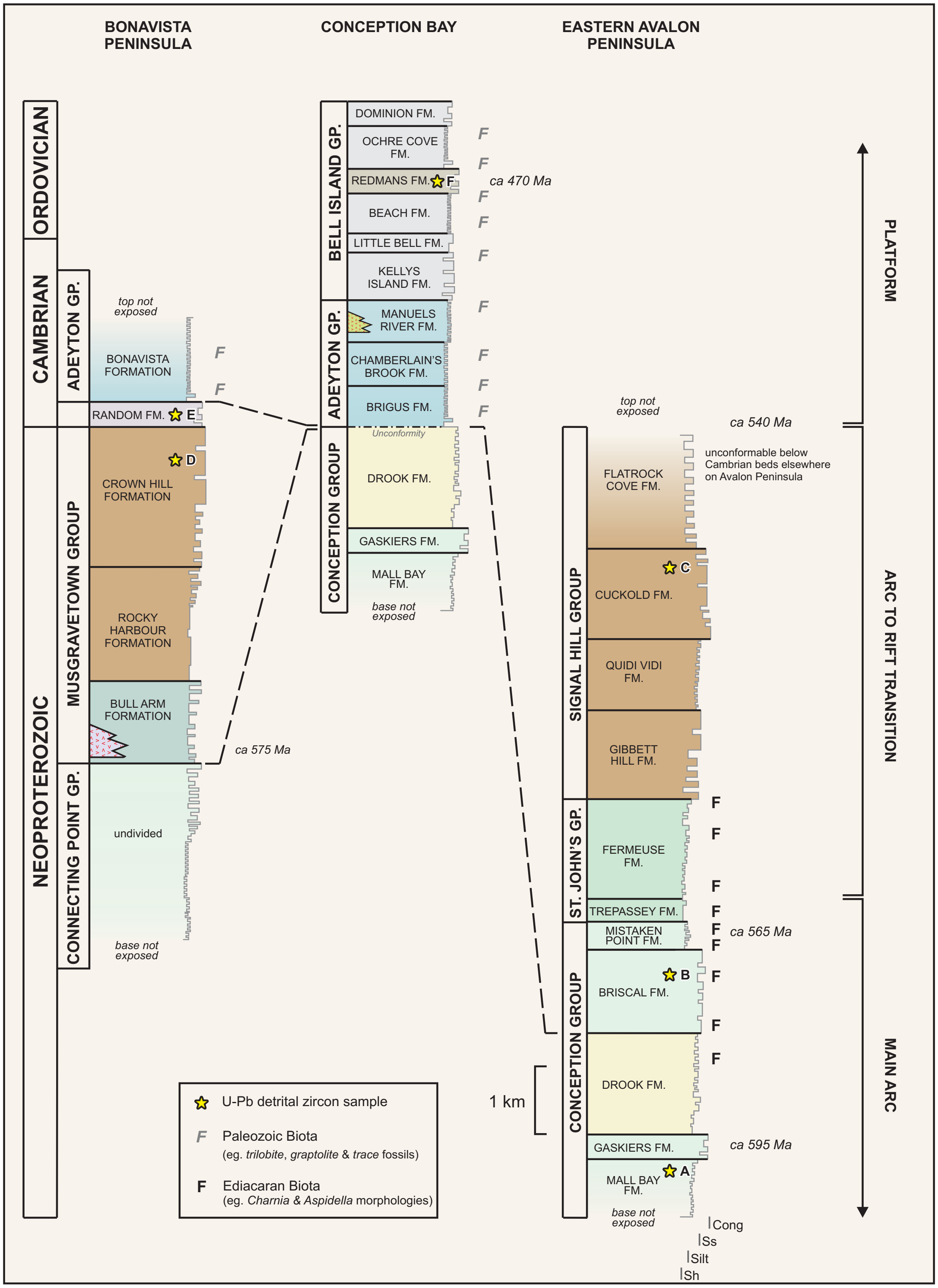

Figure 3.3. Composite stratigraphic section of Neoproterozoic-early Paleozoic sedimentary sequences of Avalonia (modified after O'Brien and King, 2005).

Figure 3.4. Representative samples for detrital zircon analysis: (A) Mall Bay Formation; (B) Briscal Formation; (C) Cuckold Formation; (D) Crown Hill Formation; (E) Random Formation; (F) Redmans Formation.

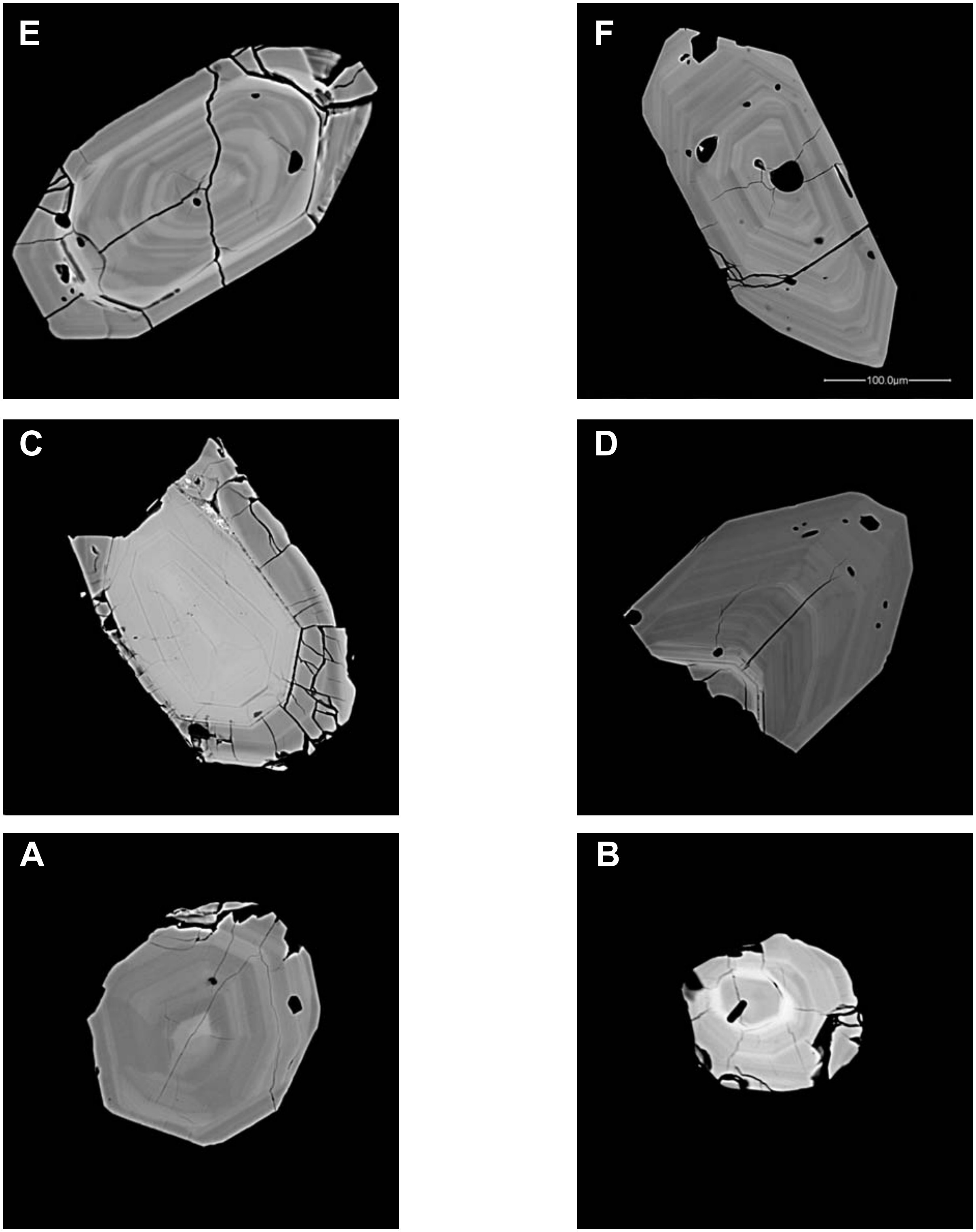

Figure 3.5. Back-scatter electron scanning electron microscope images of typical zircons: (A) Mall Bay Formation; (B) Briscal Formation; (C) Cuckold Formation; (D) Crown Hill Formation; (E) Random Formation; (F) Redmans Formation.

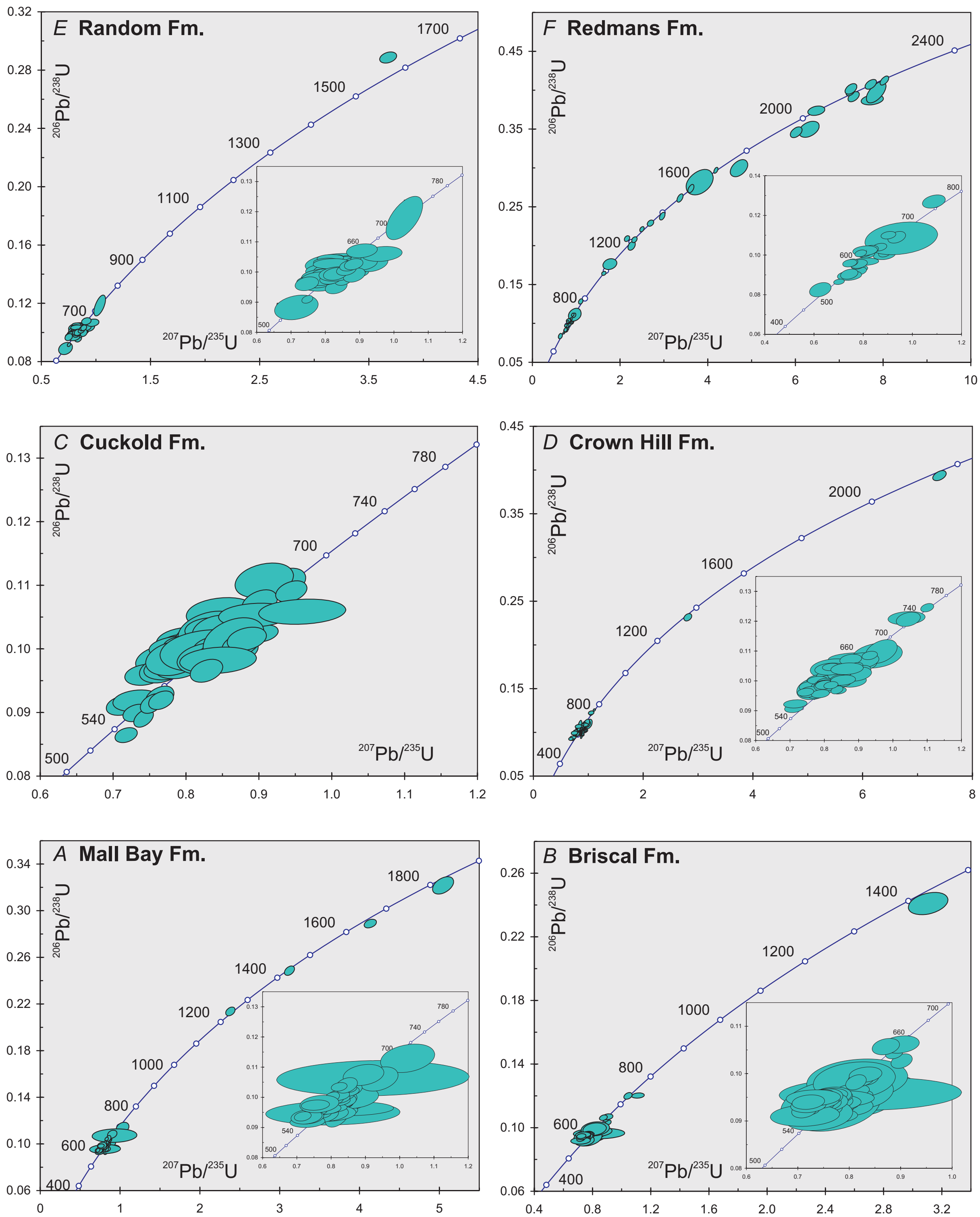

Figure 3.6. U-Pb Concordia diagrams of dated samples; ellipses are 1σ uncertainties.

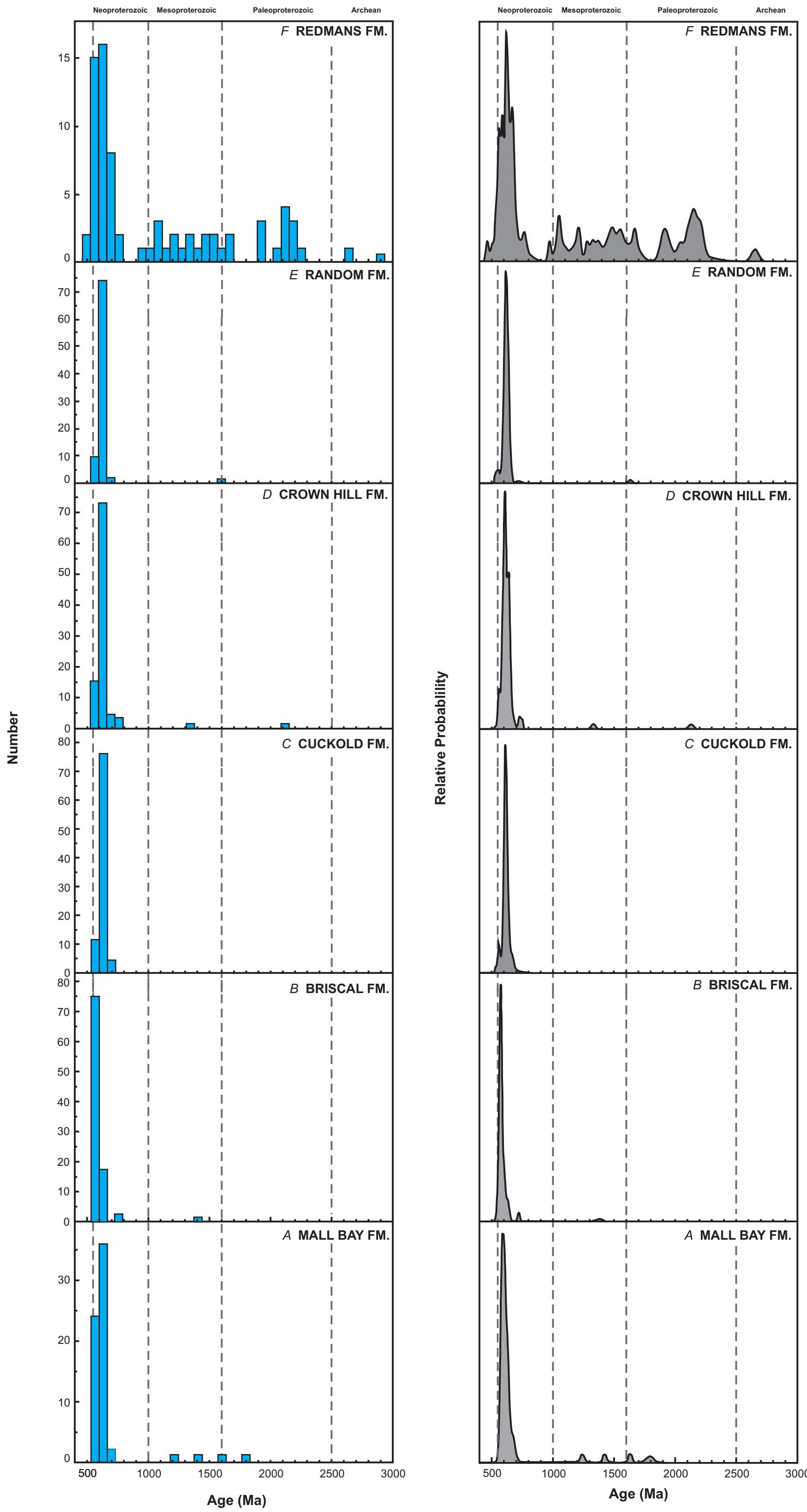

Figure 3.7. Gaussian cumulative probability curves for analyzed samples. Only analyses within +0.15/-0.10 concordance are plotted.

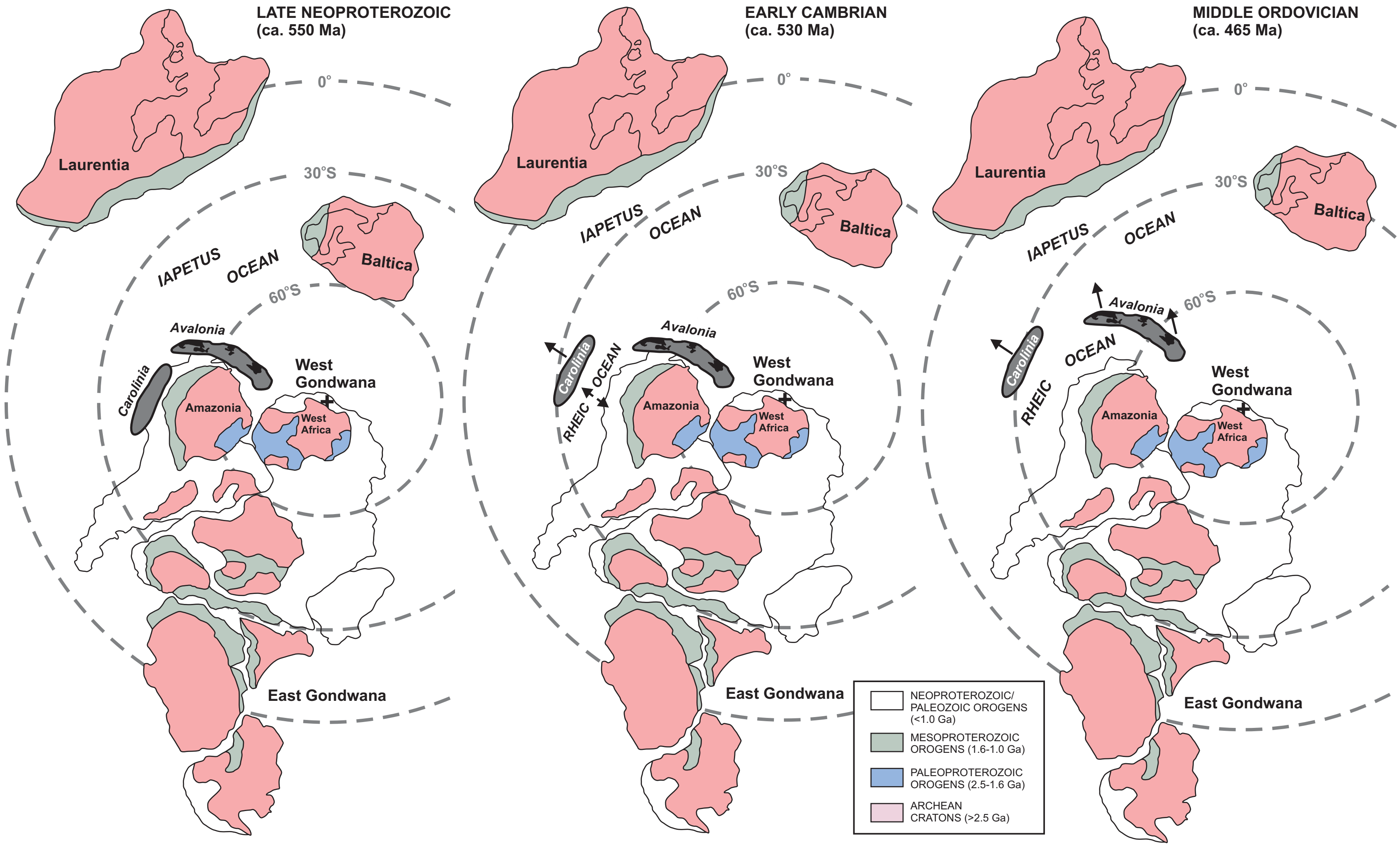

Figure 3.8. Late Neoproterozoic-early Paleozoic paleomagnetically controlled paleogeographic continental reconstructions of the southern hemisphere of Torsvik *et al*. (1996). Position of Avalonia and Carolinia from detrital zircon data. Relative position of Gondwana and Laurentia and age provinces from Hoffman (1991), Hodych *et al*. (2003), and Murphy *et al*. (2004).

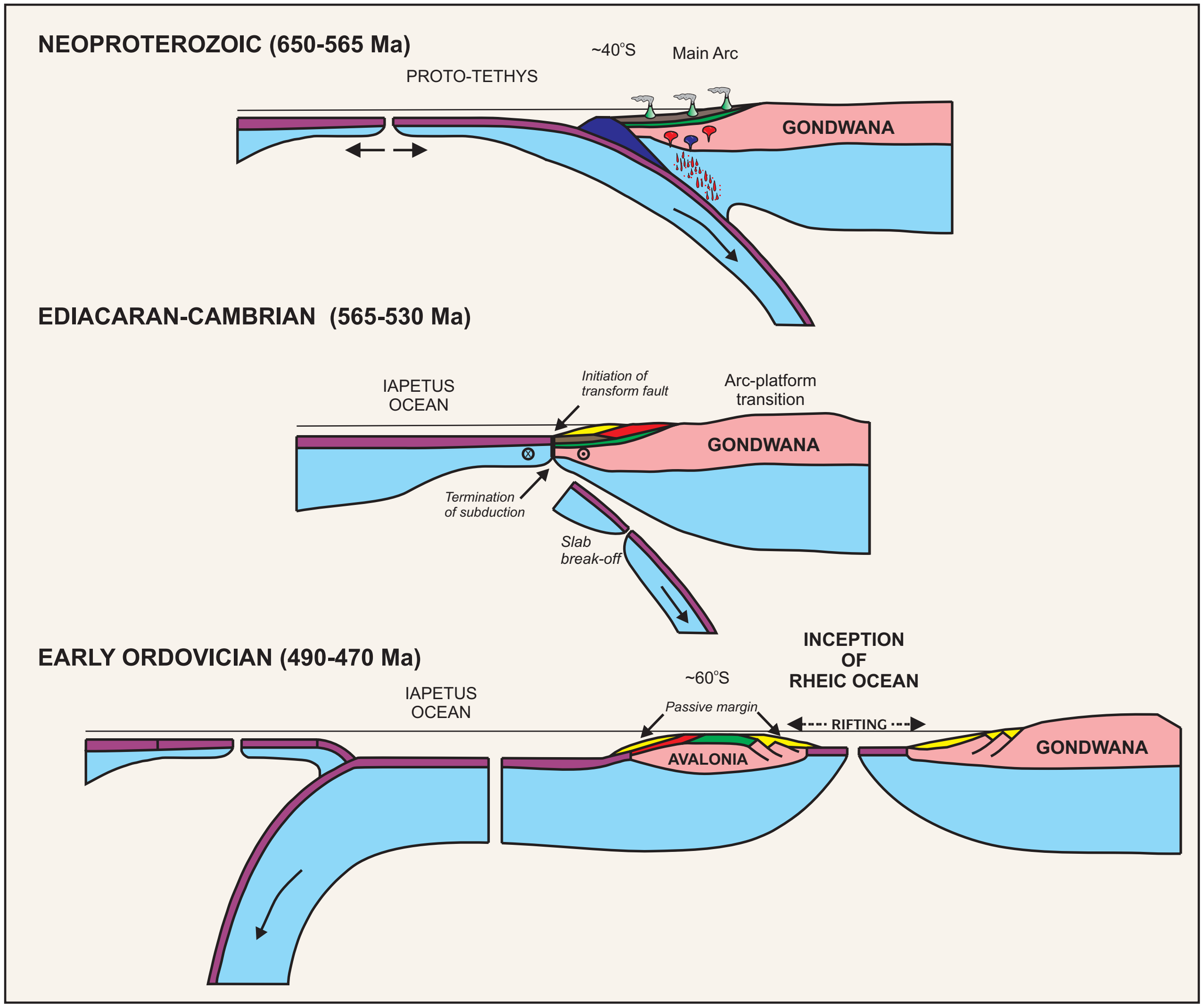

Figure 3.9. Late Neoproterozoic-early Paleozoic tectonic evolution of Avalonia and the west Gondwanan margin.

Table 3.1. U-Pb isotopic data of LAM ICP-MS analysis of detrital zircons.

MALL BAY FORMATION (340182E, 5253361N - Zone 22 NAD 1927)

	CONCORDIA COLUMNS						2 σ %		2 σ %	AGES Ma						
					I N T	E R	C E	P T	V A	L U	E S					
file	**207/235**	**7/5 err**	**206/238**	**6/8 err**	**Rho**	**207/206 c**	**7/6 err**	**207/206 m**	**7/6 err**	**7/5 age**	**1σ**	**6/8 age**	**1σ**	**7/6 age**	**1σ**	**Concordance**
jl21B03	0.7650	0.0467	0.0976	0.0024	0.20	0.0568	0.0037	0.0572	0.0009	576.9	26.8	600.4	14.1	499.8	33.3	120
jl21B04	0.7418	0.0236	0.0943	0.0014	0.23	0.0571	0.0020	0.0582	0.0004	563.5	13.7	580.9	8.2	535.7	16.8	108
jl21B07	2.3772	0.0483	0.2129	0.0031	0.36	0.0810	0.0020	0.0817	0.0003	1235.8	14.5	1244.5	16.5	1237.6	6.3	101
jl21B08	0.7304	0.0421	0.0917	0.0016	0.15	0.0578	0.0035	0.0575	0.0008	556.8	24.7	565.6	9.2	509.1	29.6	111
jl21B100	0.9697	0.1627	0.0998	0.0039	0.12	0.0704	0.0121	0.0687	0.0037	688.3	83.9	613.5	23.1	888.5	111.7	69
jl21B102	0.8288	0.0398	0.0953	0.0016	0.17	0.0631	0.0032	0.0628	0.0008	613.0	22.1	586.7	9.4	702.7	27.3	83
jl21B105	0.7167	0.0204	0.0935	0.0013	0.24	0.0556	0.0018	0.0558	0.0004	548.7	12.0	576.2	7.6	443.3	15.0	130
jl21B106	0.8189	0.0298	0.0939	0.0032	0.47	0.0633	0.0032	0.0627	0.0006	607.4	16.6	578.4	19.1	697.5	21.1	83
jl21B109	0.8049	0.0316	0.0941	0.0014	0.18	0.0620	0.0026	0.0621	0.0006	599.6	17.8	579.9	8.0	676.8	20.5	86
jl21B110	0.8511	0.0251	0.1018	0.0014	0.23	0.0606	0.0020	0.0609	0.0005	625.3	13.8	625.2	8.1	634.5	16.1	99
jl21B112	0.8486	0.1093	0.0961	0.0019	0.08	0.0641	0.0084	0.0667	0.0020	623.9	60.0	591.3	11.3	829.9	62.0	71
jl21B120	0.7808	0.0234	0.0957	0.0014	0.24	0.0592	0.0020	0.0590	0.0004	586.0	13.4	589.2	8.0	568.8	16.3	104
jl21B121	0.8944	0.0490	0.1073	0.0029	0.24	0.0605	0.0037	0.0613	0.0007	648.8	26.2	657.0	16.8	650.2	23.0	101
jl21B122	0.7338	0.0364	0.0933	0.0018	0.20	0.0571	0.0030	0.0574	0.0007	558.8	21.3	574.9	10.9	506.1	25.5	114
jl21B125	0.8640	0.0278	0.0976	0.0015	0.24	0.0642	0.0023	0.0642	0.0006	632.3	15.2	600.4	8.7	747.9	19.8	80
jl21B126	0.8649	0.0206	0.1025	0.0016	0.33	0.0612	0.0017	0.0615	0.0003	632.8	11.2	628.9	9.4	656.5	12.2	96
jl21B129	0.8438	0.0195	0.1005	0.0012	0.26	0.0609	0.0016	0.0606	0.0004	621.2	10.7	617.2	7.1	626.0	13.0	99
jl21B13	0.8000	0.0264	0.0962	0.0014	0.23	0.0603	0.0022	0.0601	0.0006	596.8	14.9	591.9	8.4	607.2	21.8	97
jl21B130	5.0506	0.1097	0.3213	0.0061	0.44	0.1140	0.0033	0.1122	0.0005	1827.9	18.4	1795.9	29.8	1835.5	8.6	98
jl21B132	0.9715	0.0341	0.1055	0.0031	0.42	0.0668	0.0031	0.0669	0.0008	689.3	17.5	646.3	18.3	833.7	24.9	78
jl21B133	3.1219	0.0515	0.2479	0.0034	0.41	0.0913	0.0020	0.0910	0.0002	1438.1	12.7	1427.7	17.4	1446.4	4.7	99
jl21B134	0.7532	0.0338	0.0973	0.0014	0.16	0.0562	0.0027	0.0565	0.0006	570.1	19.6	598.4	8.4	471.8	22.6	127
jl21B135	0.8703	0.0554	0.0997	0.0029	0.23	0.0633	0.0044	0.0631	0.0010	635.7	30.1	612.8	17.3	713.1	34.4	86
jl21B136	0.9216	0.0328	0.1004	0.0018	0.26	0.0666	0.0027	0.0664	0.0005	663.2	17.4	616.8	10.7	820.2	14.6	75
jl21B139	0.8108	0.0109	0.0958	0.0009	0.34	0.0614	0.0010	0.0611	0.0003	602.9	6.1	589.6	5.2	642.5	8.9	92
jl21B14	0.9312	0.0262	0.0971	0.0011	0.21	0.0696	0.0021	0.0700	0.0006	668.3	13.8	597.3	6.7	927.3	16.8	64
jl21B140	0.9928	0.0247	0.1053	0.0012	0.23	0.0684	0.0019	0.0682	0.0005	700.1	12.6	645.5	6.9	874.4	15.1	74
jl21B141	0.8023	0.0179	0.0999	0.0014	0.32	0.0582	0.0015	0.0581	0.0003	598.1	10.1	613.9	8.3	534.6	10.1	115
jl21B143	0.8142	0.0212	0.0943	0.0014	0.29	0.0626	0.0019	0.0620	0.0004	604.8	11.9	580.7	8.4	674.7	14.5	86
jl21B145	0.9393	0.0458	0.1059	0.0033	0.32	0.0643	0.0037	0.0626	0.0012	672.5	24.0	649.1	19.3	694.5	41.5	93
jl21B146	0.8638	0.0334	0.0982	0.0013	0.17	0.0638	0.0026	0.0635	0.0007	632.2	18.2	604.1	7.6	725.9	24.3	83
jl21B147	0.7561	0.0263	0.0952	0.0012	0.19	0.0576	0.0021	0.0567	0.0006	571.8	15.2	586.5	7.3	478.0	22.4	123
jl21B148	0.8049	0.1607	0.0946	0.0032	0.09	0.0617	0.0125	0.0625	0.0032	599.6	90.4	582.9	19.1	692.8	108.5	84
jl21B15	0.7821	0.0378	0.0960	0.0015	0.17	0.0591	0.0030	0.0589	0.0010	586.7	21.6	591.0	9.1	562.6	35.7	105
jl21B16	0.7804	0.0332	0.0941	0.0021	0.26	0.0601	0.0029	0.0606	0.0006	585.7	18.9	579.7	12.4	626.7	20.9	93
jl21B17	0.8232	0.0192	0.1033	0.0012	0.24	0.0578	0.0015	0.0584	0.0004	609.8	10.7	633.9	6.8	543.7	15.6	117
jl21B18	0.8197	0.0257	0.0974	0.0013	0.21	0.0610	0.0021	0.0613	0.0005	607.9	14.3	599.3	7.5	650.6	16.2	92
jl21B24	0.9705	0.0253	0.1023	0.0015	0.28	0.0688	0.0021	0.0682	0.0004	688.7	13.0	627.8	8.9	875.5	12.9	72

Table 3.1. (continued)

jl21B25	0.8580	0.0138	0.1027	0.0010	0.30	0.0606	0.0011	0.0606	0.0002	629.1	7.5	630.2	5.7	624.6	8.1	101
jl21B26	0.8211	0.0269	0.1005	0.0014	0.21	0.0592	0.0021	0.0596	0.0005	608.6	15.0	617.4	8.3	588.1	19.1	105
jl21B28	0.8589	0.0269	0.0951	0.0016	0.26	0.0655	0.0023	0.0664	0.0006	629.5	14.7	585.5	9.3	819.9	17.5	71
jl21B30	0.8526	0.0144	0.1035	0.0010	0.28	0.0598	0.0012	0.0595	0.0003	626.1	7.9	634.7	5.7	585.8	9.9	108
jl21B35	0.8210	0.0321	0.0952	0.0012	0.17	0.0625	0.0026	0.0632	0.0007	608.6	17.9	586.4	7.2	713.9	23.4	82
jl21B37	0.8322	0.0158	0.1004	0.0012	0.31	0.0601	0.0013	0.0598	0.0003	614.8	8.8	616.9	7.0	597.0	11.4	103
jl21B38	0.9306	0.0261	0.1012	0.0021	0.37	0.0667	0.0023	0.0662	0.0006	667.9	13.7	621.2	12.4	811.6	19.7	77
jl21B39	0.8444	0.0263	0.1038	0.0021	0.33	0.0590	0.0022	0.0592	0.0004	621.6	14.5	636.9	12.3	575.4	13.8	111
jl21B40	0.9587	0.0380	0.0979	0.0015	0.19	0.0710	0.0030	0.0703	0.0009	682.6	19.7	602.0	8.8	937.0	27.3	64
jl21B41	0.8309	0.0191	0.0932	0.0013	0.31	0.0646	0.0017	0.0646	0.0003	614.1	10.6	574.6	7.8	761.9	10.5	75
jl21B46	0.8010	0.0582	0.0945	0.0021	0.15	0.0615	0.0047	0.0631	0.0013	597.4	32.8	582.1	12.5	710.0	42.4	82
jl21B49	0.8447	0.0211	0.0985	0.0018	0.37	0.0622	0.0019	0.0615	0.0004	621.7	11.6	605.3	10.6	657.3	15.5	92
jl21B50	0.7277	0.0371	0.0934	0.0020	0.21	0.0565	0.0031	0.0575	0.0007	555.2	21.8	575.3	11.6	511.6	27.5	112
jl21B52	0.7903	0.0461	0.0963	0.0014	0.12	0.0595	0.0036	0.0587	0.0010	591.3	26.2	593.0	8.2	557.2	38.0	106
jl21B57	0.8097	0.0211	0.0990	0.0013	0.26	0.0593	0.0017	0.0599	0.0005	602.3	11.8	608.6	7.8	599.9	19.1	101
jl21B58	0.8796	0.0391	0.0982	0.0016	0.19	0.0650	0.0031	0.0652	0.0007	640.8	21.1	603.7	9.7	781.5	21.7	77
jl21B62	0.8679	0.0343	0.0985	0.0013	0.17	0.0639	0.0027	0.0634	0.0006	634.4	18.6	605.8	7.7	723.3	21.5	84
jl21B66	4.1363	0.0627	0.2885	0.0030	0.34	0.1040	0.0019	0.1027	0.0004	1661.5	12.4	1634.2	15.0	1674.4	7.8	98
jl21B69	0.8471	0.0233	0.0990	0.0018	0.34	0.0620	0.0021	0.0611	0.0004	623.0	12.8	608.8	10.8	644.5	13.3	94
jl21B73	0.8003	0.0408	0.0944	0.0020	0.21	0.0615	0.0034	0.0599	0.0009	597.0	23.0	581.8	11.9	599.1	34.3	97
jl21B77	0.9283	0.0426	0.0978	0.0023	0.26	0.0689	0.0036	0.0687	0.0011	666.8	22.4	601.3	13.5	889.8	32.3	68
jl21B79	0.8180	0.0303	0.0995	0.0014	0.19	0.0596	0.0024	0.0584	0.0008	607.0	16.9	611.3	8.2	544.6	28.9	112
jl21B80	1.0189	0.0431	0.1114	0.0020	0.21	0.0663	0.0030	0.0636	0.0010	713.4	21.7	681.1	11.3	729.9	33.4	93
jl21B81	0.8477	0.0143	0.0977	0.0012	0.35	0.0629	0.0013	0.0626	0.0004	623.4	7.8	601.1	6.8	695.2	12.1	86
jl21B82	0.8265	0.0378	0.0987	0.0020	0.22	0.0608	0.0030	0.0593	0.0010	611.7	21.0	606.6	11.6	576.4	35.7	105
jl21B83	0.7715	0.0238	0.0943	0.0012	0.21	0.0593	0.0020	0.0592	0.0005	580.6	13.7	581.1	7.3	573.0	19.2	101
jl21B88	0.9929	0.0425	0.1038	0.0025	0.28	0.0694	0.0034	0.0702	0.0011	700.2	21.6	636.8	14.4	934.6	32.5	68
jl21B89	0.9218	0.2300	0.1062	0.0048	0.09	0.0630	0.0160	0.0611	0.0055	663.3	121.5	650.7	28.0	643.5	193.0	101
jl21B93	0.7883	0.0179	0.0978	0.0011	0.24	0.0584	0.0015	0.0582	0.0003	590.2	10.2	601.6	6.3	536.9	13.2	112
jl21B94	1.0233	0.0651	0.1128	0.0039	0.27	0.0658	0.0048	0.0651	0.0014	715.6	32.7	689.1	22.5	777.5	43.7	89
jl21B98	0.8131	0.0349	0.0986	0.0014	0.17	0.0598	0.0027	0.0599	0.0007	604.2	19.5	606.3	8.3	601.1	24.8	101

Table 3.1. (continued)

BRISCAL FORMATION (329354E, 5179113N)

	CONCORDIA COLUMNS						2 σ %		2 σ %	AGES Ma						
					I N T E R C E P T V A L U E S											
file	**207/235**	**7/5 err**	**206/238**	**6/8 err**	**Rho**	**207/206 c**	**7/6 err**	**207/206 m**	**7/6 err**	**7/5 age**	**1σ**	**6/8 age**	**1σ**	**7/6 age**	**1σ**	**Concordance**
jl20A123	0.8335	0.0485	0.0946	0.0030	0.27	0.0639	0.0042	0.0598	0.0015	615.5	26.8	582.9	17.6	597.6	55.4	98
jl20A72	0.8410	0.1454	0.0956	0.0028	0.09	0.0638	0.0112	0.0598	0.0034	619.7	80.2	588.8	16.7	595.0	121.9	99
jl20A22	0.8411	0.0368	0.0957	0.0025	0.30	0.0637	0.0033	0.0589	0.0006	619.8	20.3	589.4	14.8	561.6	23.3	105
jl20A128	0.8064	0.0329	0.0928	0.0015	0.20	0.0630	0.0028	0.0588	0.0007	600.4	18.5	572.4	8.8	558.4	24.4	103
jl20A130	1.1088	0.0360	0.1196	0.0013	0.17	0.0672	0.0023	0.0639	0.0007	757.6	17.3	728.2	7.5	738.6	22.9	99
jl20A16	0.9021	0.0172	0.1026	0.0013	0.32	0.0638	0.0014	0.0612	0.0004	652.8	9.2	629.6	7.4	646.7	13.1	97
jl20A107	0.8181	0.0228	0.0954	0.0009	0.17	0.0622	0.0018	0.0594	0.0007	607.0	12.8	587.2	5.4	581.8	24.2	101
jl20A09	3.1078	0.1118	0.2407	0.0058	0.33	0.0936	0.0040	0.0912	0.0004	1434.6	27.6	1390.3	29.9	1450.5	9.1	96
jl20A122	0.8058	0.0294	0.0945	0.0011	0.16	0.0618	0.0024	0.0599	0.0005	600.1	16.5	582.2	6.4	599.5	19.4	97
jl20A112	0.8321	0.0803	0.0970	0.0027	0.14	0.0622	0.0062	0.0601	0.0018	614.8	44.5	596.5	15.8	606.5	64.9	98
jl20A99	0.7821	0.0198	0.0927	0.0013	0.28	0.0612	0.0018	0.0597	0.0005	586.7	11.3	571.2	7.7	591.9	17.2	97
jl20A102	0.7804	0.0244	0.0927	0.0014	0.25	0.0611	0.0021	0.0587	0.0005	585.7	13.9	571.5	8.5	556.9	18.0	103
jl20A93	0.7817	0.0165	0.0929	0.0010	0.25	0.0610	0.0014	0.0596	0.0003	586.4	9.4	572.5	5.8	590.0	11.1	97
jl20A113	0.7860	0.0292	0.0936	0.0014	0.21	0.0609	0.0024	0.0594	0.0006	588.9	16.6	577.0	8.5	581.7	20.2	99
jl20A137	0.7857	0.0196	0.0938	0.0014	0.30	0.0607	0.0018	0.0597	0.0004	588.7	11.1	578.1	8.4	592.2	15.9	98
jl20A18	0.8395	0.0147	0.0989	0.0011	0.33	0.0615	0.0013	0.0605	0.0002	618.9	8.1	608.1	6.7	621.9	8.4	98
jl20A139	0.7842	0.0185	0.0940	0.0015	0.33	0.0605	0.0017	0.0599	0.0003	587.9	10.5	579.1	8.6	600.8	10.2	96
jl20A97	0.7766	0.0245	0.0933	0.0015	0.25	0.0604	0.0021	0.0594	0.0004	583.6	14.0	575.0	8.8	581.3	16.4	99
jl20A13	0.8063	0.0269	0.0963	0.0012	0.18	0.0607	0.0022	0.0595	0.0008	600.4	15.1	592.8	6.8	586.0	30.3	101
jl20A64	0.7480	0.0560	0.0910	0.0015	0.11	0.0596	0.0046	0.0591	0.0013	567.1	32.5	561.3	8.6	572.4	46.0	98
jl20A05	0.7847	0.0525	0.0946	0.0014	0.11	0.0602	0.0041	0.0594	0.0012	588.2	29.8	582.6	8.3	581.7	44.1	100
jl20A134	0.8874	0.0140	0.1042	0.0010	0.29	0.0617	0.0011	0.0605	0.0004	645.0	7.5	639.2	5.6	622.5	12.5	103
jl20A110	0.7456	0.0281	0.0910	0.0017	0.25	0.0594	0.0025	0.0594	0.0005	565.6	16.4	561.2	10.3	581.4	18.0	97
jl20A59	0.8340	0.0158	0.0996	0.0011	0.29	0.0607	0.0013	0.0610	0.0003	615.8	8.7	612.0	6.3	638.1	10.6	96
jl20A33	0.7720	0.0418	0.0937	0.0014	0.14	0.0597	0.0034	0.0592	0.0009	580.9	23.9	577.6	8.2	574.2	32.5	101
jl20A116	0.8233	0.0212	0.0988	0.0014	0.27	0.0604	0.0018	0.0610	0.0005	609.9	11.8	607.5	7.9	640.6	17.8	95
jl20A23	0.8316	0.0263	0.0997	0.0013	0.21	0.0605	0.0021	0.0605	0.0004	614.5	14.6	612.8	7.8	619.9	15.6	99
jl20A55	0.7630	0.0794	0.0932	0.0044	0.23	0.0594	0.0068	0.0589	0.0012	575.7	45.7	574.2	26.2	563.0	43.5	102
jl20A83	0.9001	0.0297	0.1061	0.0015	0.22	0.0615	0.0022	0.0614	0.0006	651.8	15.9	650.1	8.8	654.3	20.9	99
jl20A131	0.8130	0.0164	0.0981	0.0013	0.33	0.0601	0.0015	0.0605	0.0004	604.1	9.2	603.3	7.8	622.1	15.4	97
jl20A143	0.7795	0.0184	0.0950	0.0014	0.31	0.0595	0.0017	0.0601	0.0004	585.2	10.5	584.9	8.2	605.6	14.7	97
jl20A106	0.7681	0.0321	0.0939	0.0015	0.19	0.0593	0.0027	0.0589	0.0006	578.7	18.4	578.5	8.7	563.4	22.8	103
jl20A58	0.7394	0.0550	0.0911	0.0027	0.20	0.0589	0.0047	0.0597	0.0009	562.0	32.1	562.1	15.8	593.9	31.1	95
jl20A34	0.8154	0.0807	0.0986	0.0037	0.19	0.0600	0.0063	0.0599	0.0015	605.5	45.1	606.1	21.5	601.1	53.4	101
jl20A109	0.7651	0.0145	0.0941	0.0010	0.27	0.0590	0.0013	0.0597	0.0003	577.0	8.4	579.5	5.7	591.3	10.7	98
jl20A03	0.7492	0.0252	0.0925	0.0012	0.19	0.0587	0.0021	0.0586	0.0005	567.8	14.6	570.5	7.0	553.0	17.8	103
jl20A108	0.8098	0.0655	0.0984	0.0033	0.20	0.0597	0.0052	0.0595	0.0012	602.4	36.8	605.2	19.1	586.5	43.2	103
jl20A132	0.7479	0.0319	0.0924	0.0016	0.21	0.0587	0.0027	0.0591	0.0009	567.0	18.5	569.9	9.6	571.0	32.5	100

Table 3.1. (continued)

jl20A24	1.0389	0.0235	0.1194	0.0017	0.32	0.0631	0.0017	0.0630	0.0005	723.4	11.7	727.2	10.0	708.0	16.3	103
jl20A47	0.7598	0.0174	0.0938	0.0011	0.27	0.0587	0.0015	0.0588	0.0004	573.9	10.1	578.0	6.8	560.3	13.7	103
jl20A27	0.7704	0.0294	0.0950	0.0013	0.17	0.0588	0.0024	0.0593	0.0007	580.0	16.9	585.1	7.4	577.4	24.7	101
jl20A119	0.7646	0.0327	0.0952	0.0015	0.19	0.0583	0.0027	0.0577	0.0007	576.7	18.8	586.1	9.1	516.9	25.4	113
jl20A84	0.7438	0.0157	0.0931	0.0010	0.26	0.0579	0.0014	0.0581	0.0003	564.6	9.2	573.9	6.1	535.3	10.7	107
jl20A140	0.8712	0.0220	0.1057	0.0014	0.26	0.0598	0.0017	0.0596	0.0003	636.2	12.0	647.5	8.3	590.8	12.0	110
jl20A142	0.7626	0.0282	0.0954	0.0011	0.16	0.0580	0.0022	0.0589	0.0006	575.5	16.2	587.5	6.7	564.3	23.1	104
jl20A78	0.7390	0.0377	0.0931	0.0017	0.18	0.0576	0.0031	0.0581	0.0007	561.8	22.0	574.0	9.9	533.7	26.3	108
jl20A65	0.7440	0.0436	0.0938	0.0019	0.17	0.0575	0.0036	0.0574	0.0010	564.8	25.4	577.9	10.9	508.0	37.1	114
jl20A77	0.7406	0.0358	0.0936	0.0015	0.17	0.0574	0.0029	0.0576	0.0008	562.8	20.9	576.8	9.1	514.9	29.2	112
jl20A150	0.7516	0.0292	0.0949	0.0015	0.21	0.0575	0.0024	0.0574	0.0006	569.1	17.0	584.2	9.1	508.6	22.4	115
jl20A39	0.7377	0.0287	0.0935	0.0014	0.20	0.0572	0.0024	0.0575	0.0007	561.0	16.7	576.2	8.4	509.4	25.2	113
jl20A95	0.7135	0.0553	0.0911	0.0019	0.13	0.0568	0.0046	0.0577	0.0013	546.8	32.8	561.8	11.1	518.5	49.1	108
jl20A75	0.7229	0.0155	0.0922	0.0008	0.21	0.0569	0.0013	0.0572	0.0003	552.4	9.1	568.5	4.9	498.0	11.8	114
jl20A121	0.7461	0.0177	0.0946	0.0012	0.26	0.0572	0.0015	0.0600	0.0005	566.0	10.3	582.7	6.8	604.4	16.9	96
jl20A141	0.7364	0.0227	0.0938	0.0011	0.20	0.0570	0.0019	0.0600	0.0005	560.3	13.3	577.8	6.7	604.0	17.5	96
jl20A04	0.7436	0.0237	0.0951	0.0012	0.20	0.0567	0.0019	0.0589	0.0005	564.5	13.8	585.6	7.3	563.2	18.9	104
jl20A85	0.7336	0.0384	0.0941	0.0014	0.14	0.0565	0.0031	0.0588	0.0010	558.7	22.5	579.9	8.3	559.8	36.9	104
jl20A100	0.7190	0.0183	0.0928	0.0010	0.22	0.0562	0.0016	0.0565	0.0004	550.1	10.8	571.9	6.1	472.5	16.2	121
jl20A74	0.7122	0.0200	0.0921	0.0013	0.25	0.0561	0.0018	0.0557	0.0004	546.1	11.9	568.2	7.7	441.6	17.5	129
jl20A56	0.7201	0.0283	0.0932	0.0012	0.17	0.0561	0.0023	0.0564	0.0006	550.7	16.7	574.1	7.2	469.3	21.6	122
jl20A52	0.7388	0.0195	0.0951	0.0011	0.21	0.0563	0.0016	0.0564	0.0004	561.7	11.4	585.8	6.2	469.2	16.3	125
jl20A149	0.7299	0.0434	0.0948	0.0014	0.12	0.0558	0.0034	0.0562	0.0011	556.5	25.5	583.9	8.3	460.4	44.2	127
jl20A36	0.7202	0.0260	0.0939	0.0013	0.19	0.0556	0.0021	0.0553	0.0005	550.8	15.3	578.6	7.4	425.6	20.7	136

Table 3.1. (continued)

CUCKOLD FORMATION (377852E, 5264479N)

CONCORDIA COLUMNS							2 σ %		2 σ %	AGES Ma						
I N T E R C E P T V A L U E S																
file	207/235	7/5 err	206/238	6/8 err	Rho	207/206 c	7/6 err	207/206 m	7/6 err	7/5 age	1σ	6/8 age	1σ	7/6 age	1σ	Concordance
jl24b03	0.8110	0.0193	0.0988	0.0015	0.32	0.0595	0.0017	0.0586	0.0003	603.0	10.8	607.5	8.8	551.6	11.6	110
jl24b04	0.8069	0.0212	0.0983	0.0014	0.27	0.0595	0.0018	0.0580	0.0004	600.7	11.9	604.7	8.2	531.3	15.6	114
jl24b06	0.8308	0.0278	0.0996	0.0019	0.29	0.0605	0.0023	0.0601	0.0005	614.1	15.4	612.3	11.4	605.8	17.7	101
jl24b07	0.8093	0.0268	0.0980	0.0018	0.28	0.0599	0.0023	0.0593	0.0005	602.1	15.0	602.7	10.5	579.7	17.0	104
jl24b09	0.9595	0.0492	0.1057	0.0017	0.15	0.0658	0.0035	0.0621	0.0008	683.0	25.5	647.9	9.6	678.1	26.2	96
jl24b102	0.8917	0.0175	0.0999	0.0015	0.38	0.0648	0.0016	0.0612	0.0004	647.3	9.4	613.6	8.8	646.8	13.4	95
jl24b104	0.8944	0.0410	0.1052	0.0016	0.16	0.0617	0.0030	0.0619	0.0009	648.7	22.0	644.6	9.1	669.8	32.3	96
jl24b105	0.8947	0.0404	0.0997	0.0024	0.26	0.0651	0.0033	0.0652	0.0009	648.9	21.7	612.6	14.0	806.3	27.7	76
jl24b106	0.8190	0.0228	0.1014	0.0015	0.27	0.0586	0.0019	0.0593	0.0003	607.5	12.7	622.6	9.0	576.4	12.9	108
jl24b107	0.8048	0.0238	0.0999	0.0014	0.23	0.0584	0.0019	0.0581	0.0005	599.5	13.4	613.7	8.1	531.9	17.1	115
jl24b108	0.9067	0.0162	0.1023	0.0011	0.30	0.0643	0.0013	0.0600	0.0004	655.3	8.6	627.8	6.4	602.1	11.6	104
jl24b109	0.7964	0.0203	0.0985	0.0011	0.23	0.0586	0.0016	0.0590	0.0004	594.8	11.5	605.7	6.7	567.8	15.8	107
jl24b112	0.8649	0.0341	0.1013	0.0028	0.35	0.0619	0.0030	0.0621	0.0008	632.8	18.6	622.2	16.3	679.2	25.8	92
jl24b113	0.9011	0.0199	0.1071	0.0016	0.35	0.0610	0.0016	0.0613	0.0003	652.3	10.7	656.0	9.6	650.3	10.4	101
jl24b114	0.7835	0.0325	0.0984	0.0023	0.28	0.0577	0.0027	0.0600	0.0005	587.5	18.5	605.1	13.2	603.2	20.5	100
jl24b115	0.8255	0.0173	0.1018	0.0013	0.31	0.0588	0.0015	0.0595	0.0004	611.1	9.6	624.9	7.8	585.4	13.1	107
jl24b117	0.8327	0.0250	0.1021	0.0018	0.30	0.0591	0.0021	0.0596	0.0006	615.1	13.8	626.7	10.6	589.2	21.1	106
jl24b118	0.8624	0.0172	0.1028	0.0012	0.30	0.0608	0.0014	0.0599	0.0004	631.4	9.4	630.8	7.1	600.5	12.8	105
jl24b119	0.8783	0.0125	0.1003	0.0012	0.40	0.0635	0.0012	0.0613	0.0003	640.1	6.8	616.3	6.8	649.8	10.5	95
jl24b122	0.8014	0.0171	0.0983	0.0013	0.30	0.0591	0.0015	0.0588	0.0003	597.6	9.6	604.4	7.4	561.1	11.9	108
jl24b123	0.8358	0.0119	0.1022	0.0009	0.31	0.0593	0.0010	0.0600	0.0003	616.8	6.6	627.2	5.3	603.3	10.2	104
jl24b124	0.8441	0.0128	0.1011	0.0012	0.39	0.0605	0.0012	0.0611	0.0003	621.4	7.0	621.1	7.0	642.4	9.2	97
jl24b125	0.8007	0.0262	0.1006	0.0012	0.18	0.0577	0.0020	0.0594	0.0005	597.2	14.8	617.7	6.9	582.9	19.8	106
jl24b126	0.8275	0.0268	0.1012	0.0019	0.29	0.0593	0.0022	0.0598	0.0006	612.2	14.9	621.6	11.0	595.1	20.6	104
jl24b127	0.8304	0.0179	0.1000	0.0014	0.33	0.0602	0.0016	0.0610	0.0003	613.8	9.9	614.2	8.5	640.4	10.2	96
jl24b128	0.8257	0.0504	0.0996	0.0027	0.22	0.0601	0.0040	0.0608	0.0010	611.2	28.0	612.0	15.9	632.2	35.6	97
jl24b13	0.7173	0.0127	0.0863	0.0010	0.32	0.0603	0.0013	0.0592	0.0003	549.0	7.5	533.5	5.8	573.3	12.8	93
jl24b133	0.8152	0.0248	0.1018	0.0016	0.26	0.0581	0.0020	0.0586	0.0005	605.4	13.9	625.1	9.3	552.8	16.8	113
jl24b135	0.8325	0.0363	0.1026	0.0026	0.29	0.0588	0.0030	0.0594	0.0008	615.0	20.1	629.8	15.2	580.5	28.6	108
jl24b136	0.8283	0.0178	0.0980	0.0014	0.32	0.0613	0.0016	0.0614	0.0003	612.7	9.9	602.8	8.0	651.6	10.3	93
jl24b138	0.8271	0.0191	0.1021	0.0011	0.23	0.0587	0.0015	0.0594	0.0004	612.0	10.6	627.0	6.4	582.1	14.6	108
jl24b139	0.8640	0.0211	0.1017	0.0018	0.37	0.0616	0.0019	0.0616	0.0004	632.3	11.5	624.3	10.7	660.1	14.1	95
jl24b14	0.8388	0.0193	0.0991	0.0015	0.33	0.0614	0.0017	0.0613	0.0003	618.5	10.7	609.4	8.9	651.0	10.3	94
jl24b140	0.9897	0.2128	0.1126	0.0069	0.14	0.0638	0.0143	0.0614	0.0030	698.6	108.6	687.8	40.2	653.2	95.0	105
jl24b141	0.8025	0.0143	0.0990	0.0011	0.32	0.0588	0.0012	0.0594	0.0002	598.3	8.1	608.5	6.6	583.2	8.3	104
jl24b145	0.8222	0.0215	0.0999	0.0013	0.25	0.0597	0.0018	0.0601	0.0004	609.3	12.0	614.1	7.8	606.9	15.8	101
jl24b146	0.8316	0.0148	0.1011	0.0011	0.31	0.0597	0.0013	0.0599	0.0003	614.5	8.2	620.6	6.6	599.1	9.9	104
jl24b147	0.7885	0.0256	0.0970	0.0015	0.24	0.0590	0.0021	0.0594	0.0005	590.3	14.5	596.6	8.8	580.3	19.5	103

Table 3.1. (continued)

jl24b148	0.8108	0.0262	0.0990	0.0019	0.30	0.0594	0.0022	0.0596	0.0005	602.9	14.7	608.4	11.3	588.7	17.6	103
jl24b150	0.7730	0.0260	0.0968	0.0015	0.23	0.0579	0.0021	0.0585	0.0005	581.5	14.9	595.4	8.7	549.9	17.6	108
jl24b17	0.8658	0.0186	0.0971	0.0017	0.40	0.0646	0.0018	0.0640	0.0006	633.3	10.1	597.6	9.9	766.8	19.3	78
jl24b22	0.9485	0.0289	0.1040	0.0017	0.27	0.0662	0.0023	0.0648	0.0005	677.3	15.1	637.7	9.9	794.8	17.0	80
jl24b23	0.7913	0.0260	0.0993	0.0017	0.26	0.0578	0.0021	0.0599	0.0004	591.9	14.7	610.5	9.8	599.0	16.9	102
jl24b26	0.8275	0.0240	0.1031	0.0014	0.23	0.0582	0.0019	0.0602	0.0004	612.2	13.3	632.4	8.2	611.9	15.2	103
jl24b28	0.9390	0.0179	0.1037	0.0016	0.41	0.0657	0.0016	0.0617	0.0004	672.4	9.4	636.2	9.4	664.5	11.8	96
jl24b29	0.8095	0.0179	0.0998	0.0014	0.31	0.0588	0.0015	0.0600	0.0004	602.2	10.0	613.1	8.0	603.0	14.6	102
jl24b33	0.8343	0.0219	0.0993	0.0016	0.30	0.0609	0.0019	0.0602	0.0004	616.0	12.1	610.6	9.3	612.1	14.0	100
jl24b38	0.9070	0.0328	0.1107	0.0023	0.28	0.0594	0.0025	0.0614	0.0005	655.5	17.4	676.5	13.1	652.5	20.6	104
jl24b44	0.8314	0.0257	0.1004	0.0014	0.23	0.0601	0.0020	0.0599	0.0005	614.4	14.3	616.5	8.3	599.6	17.4	103
jl24b45	0.8509	0.0178	0.1007	0.0016	0.39	0.0613	0.0016	0.0605	0.0003	625.2	9.8	618.5	9.5	621.0	10.4	100
jl24b46	0.9355	0.0233	0.1103	0.0018	0.33	0.0615	0.0018	0.0604	0.0003	670.5	12.2	674.7	10.5	617.2	12.3	109
jl24b48	0.8076	0.0285	0.0995	0.0015	0.22	0.0588	0.0023	0.0603	0.0004	601.1	16.0	611.7	9.1	613.1	15.8	100
jl24b49	0.8268	0.0214	0.1013	0.0014	0.27	0.0592	0.0017	0.0595	0.0003	611.8	11.9	622.2	8.3	583.6	12.0	107
jl24b53	0.8831	0.0222	0.1015	0.0015	0.29	0.0631	0.0018	0.0625	0.0005	642.6	12.0	622.9	8.7	692.7	15.4	90
jl24b55	0.9446	0.0177	0.1089	0.0014	0.34	0.0629	0.0014	0.0621	0.0003	675.3	9.2	666.3	7.9	677.5	9.9	98
jl24b56	0.8426	0.0209	0.1011	0.0012	0.25	0.0605	0.0017	0.0600	0.0004	620.6	11.5	620.8	7.3	604.5	12.8	103
jl24b57	0.7299	0.0141	0.0898	0.0011	0.32	0.0590	0.0014	0.0591	0.0003	556.5	8.3	554.2	6.6	569.6	9.7	97
jl24b58	0.9182	0.0288	0.1023	0.0019	0.29	0.0651	0.0024	0.0619	0.0006	661.4	15.3	628.0	11.0	669.3	22.1	94
jl24b59	0.8275	0.0184	0.0964	0.0015	0.34	0.0623	0.0017	0.0621	0.0017	612.2	10.2	593.3	8.6	676.8	10.2	88
jl24b64	0.8804	0.0132	0.1036	0.0011	0.34	0.0616	0.0011	0.0611	0.0003	641.2	7.1	635.4	6.2	643.4	11.1	99
jl24b65	0.8321	0.0364	0.0984	0.0021	0.24	0.0613	0.0030	0.0609	0.0008	614.8	20.2	604.9	12.3	637.1	30.0	95
jl24b66	0.8145	0.0212	0.0988	0.0015	0.29	0.0598	0.0018	0.0586	0.0004	605.0	11.9	607.5	8.8	553.8	14.9	110
jl24b67	0.8647	0.0280	0.0996	0.0018	0.28	0.0630	0.0023	0.0610	0.0005	632.7	15.3	612.0	10.6	640.9	18.1	95
jl24b69	0.7653	0.0245	0.0965	0.0017	0.27	0.0575	0.0021	0.0580	0.0004	577.1	14.1	594.1	9.8	527.9	15.8	113
jl24b74	0.7966	0.0203	0.0998	0.0014	0.27	0.0579	0.0017	0.0598	0.0004	594.9	11.4	613.0	8.1	595.9	15.0	103
jl24b75	0.8376	0.0242	0.1029	0.0019	0.31	0.0591	0.0020	0.0609	0.0004	617.8	13.4	631.2	10.8	636.3	13.1	99
jl24b76	0.7752	0.0167	0.0977	0.0014	0.32	0.0575	0.0015	0.0596	0.0003	582.7	9.6	600.9	8.0	590.3	12.0	102
jl24b79	0.8429	0.0174	0.0990	0.0011	0.26	0.0617	0.0014	0.0610	0.0004	620.8	9.6	608.7	6.2	638.3	13.5	95
jl24b82	0.7970	0.0154	0.0996	0.0010	0.27	0.0580	0.0013	0.0596	0.0003	595.2	8.7	612.0	6.1	588.9	10.8	104
jl24b83	0.7652	0.0140	0.0918	0.0012	0.35	0.0605	0.0013	0.0603	0.0002	577.0	8.0	565.9	6.9	615.2	7.8	92
jl24b84	0.8318	0.0215	0.1013	0.0015	0.29	0.0596	0.0018	0.0598	0.0003	614.6	11.9	621.9	8.8	595.3	11.4	104
jl24b85	0.7521	0.0128	0.0912	0.0013	0.41	0.0598	0.0013	0.0598	0.0002	569.5	7.4	562.8	7.5	594.6	5.7	95
jl24b86	0.8672	0.0147	0.1005	0.0013	0.39	0.0626	0.0014	0.0621	0.0003	634.0	8.0	617.4	7.8	677.8	11.3	91
jl24b88	0.8479	0.0279	0.0997	0.0012	0.18	0.0617	0.0022	0.0612	0.0006	623.5	15.4	612.9	6.8	645.4	21.4	95
jl24b89	0.8435	0.0432	0.0980	0.0017	0.17	0.0624	0.0034	0.0620	0.0009	621.1	23.8	602.9	9.9	672.7	32.4	90
jl24b92	0.7307	0.0259	0.0917	0.0014	0.21	0.0578	0.0022	0.0585	0.0006	557.0	15.2	565.5	8.1	547.2	23.1	103
jl24b93	0.7409	0.0111	0.0889	0.0012	0.44	0.0604	0.0012	0.0592	0.0002	562.9	6.5	549.1	6.9	574.1	7.4	96
jl24b97	0.7635	0.0159	0.0923	0.0014	0.36	0.0600	0.0015	0.0599	0.0003	576.0	9.1	568.9	8.2	598.7	9.8	95
jl24b99	0.7952	0.0254	0.0995	0.0013	0.20	0.0579	0.0020	0.0596	0.0005	594.1	14.4	611.7	7.6	587.4	18.8	104

Table 3.1. (continued)

CROWN HILL FORMATION (316980E, 5384472N)

CONCORDIA COLUMNS						2 σ %		2 σ %		AGES Ma						
I N T E R C E P T V A L U E S																
file	207/235	7/5 err	206/238	6/8 err	Rho	207/206 c	7/6 err	207/206 m	7/6 err	7/5 age	1σ	6/8 age	1σ	7/6 age	1σ	Concordance
jl19a03	0.8258	0.0286	0.0982	0.0013	0.19	0.0613	0.0009	6.93	2.66	611.3	15.9	603.8	7.7	650.7	30.0	93
jl19a04	0.8011	0.0295	0.0980	0.0015	0.20	0.0617	0.0005	7.37	3.00	597.4	16.6	602.8	8.6	665.1	16.6	91
jl19a05	0.8985	0.0177	0.1063	0.0011	0.27	0.0594	0.0005	3.94	2.12	650.9	9.5	651.4	6.6	582.3	17.4	112
jl19a06	0.8104	0.0491	0.1055	0.0019	0.15	0.0628	0.0007	12.12	3.67	602.7	27.5	646.6	11.3	701.4	24.7	92
jl19a07	0.8298	0.0359	0.1005	0.0015	0.17	0.0613	0.0054	8.66	3.03	613.5	19.9	617.4	8.9	648.2	188.1	95
jl19a08	0.7975	0.0215	0.1004	0.0012	0.23	0.0610	0.0005	5.39	2.44	595.4	12.1	616.9	7.2	640.9	16.4	96
jl19a09	0.6680	0.0333	0.0912	0.0013	0.15	0.0626	0.0008	9.97	2.95	519.5	20.3	562.7	7.9	693.8	26.5	81
jl19a101	0.8515	0.0198	0.1039	0.0012	0.25	0.0606	0.0004	4.66	2.30	625.5	10.9	637.2	7.0	625.5	13.9	102
jl19a102	0.9127	0.0151	0.1052	0.0012	0.34	0.0614	0.0004	3.30	2.25	658.5	8.0	644.9	6.9	653.3	13.2	99
jl19a103	1.1006	0.0158	0.1244	0.0012	0.33	0.0645	0.0003	2.87	1.87	753.6	7.6	756.0	6.7	759.3	10.5	100
jl19a104	0.9204	0.0126	0.1054	0.0011	0.39	0.0614	0.0003	2.73	2.13	662.6	6.6	646.2	6.6	651.9	11.2	99
jl19a106	0.7739	0.0192	0.0954	0.0012	0.26	0.0599	0.0004	4.96	2.55	582.0	11.0	587.3	7.1	598.4	15.9	98
jl19a107	0.8933	0.0208	0.1027	0.0017	0.36	0.0611	0.0003	4.67	3.36	648.2	11.2	629.9	10.1	642.8	11.4	98
jl19a108	0.8058	0.0222	0.0988	0.0015	0.28	0.0603	0.0004	5.52	3.04	600.1	12.5	607.5	8.8	614.7	14.8	99
jl19a109	0.8231	0.0531	0.1040	0.0027	0.20	0.0616	0.0007	12.89	5.13	609.8	29.6	637.8	15.6	660.5	22.9	97
jl19a110	0.9662	0.0384	0.1098	0.0033	0.37	0.0623	0.0007	7.94	5.94	686.5	19.8	671.3	18.9	683.2	22.7	98
jl19a113	0.7885	0.0328	0.1002	0.0016	0.19	0.0617	0.0005	8.33	3.13	590.3	18.6	615.4	9.2	663.3	17.6	93
jl19a114	0.9335	0.0159	0.1054	0.0012	0.34	0.0619	0.0004	3.40	2.31	669.4	8.3	645.7	7.1	670.8	15.1	96
jl19a115	0.8788	0.0218	0.1050	0.0016	0.30	0.0619	0.0004	4.96	2.95	640.4	11.8	643.8	9.0	671.9	12.2	96
jl19a116	0.8998	0.0291	0.1029	0.0017	0.25	0.0614	0.0005	6.48	3.29	651.6	15.6	631.6	9.9	654.1	17.0	97
jl19a117	0.7572	0.0254	0.0980	0.0014	0.21	0.0610	0.0006	6.70	2.77	572.4	14.7	602.9	8.0	639.6	20.7	94
jl19a12	0.9542	0.0601	0.1084	0.0035	0.25	0.0619	0.0003	12.59	6.41	680.3	31.2	663.6	20.2	669.4	9.9	99
jl19a120	1.0010	0.0513	0.1084	0.0044	0.39	0.0640	0.0005	10.26	8.04	704.3	26.0	663.5	25.3	742.5	17.5	89
jl19a121	0.8153	0.0334	0.1047	0.0014	0.17	0.0621	0.0005	8.19	2.74	605.4	18.7	641.7	8.4	678.4	18.6	95
jl19a122	0.8395	0.0298	0.1017	0.0017	0.24	0.0629	0.0005	7.09	3.41	618.8	16.4	624.2	10.1	705.9	18.4	88
jl19a123	0.8821	0.0332	0.0997	0.0016	0.21	0.0604	0.0008	7.52	3.23	642.1	17.9	612.7	9.5	618.3	28.5	99
jl19a126	0.8615	0.0155	0.1003	0.0010	0.29	0.0612	0.0003	3.61	2.09	630.9	8.5	616.4	6.1	646.6	9.3	95
jl19a127	0.7854	0.0204	0.0980	0.0014	0.27	0.0605	0.0004	5.20	2.77	588.6	11.6	602.8	8.0	622.9	15.6	97
jl19a129	0.8332	0.0472	0.1055	0.0017	0.15	0.0664	0.0008	11.34	3.30	615.4	26.2	646.7	10.1	819.0	23.9	79
jl19a13	0.8750	0.0254	0.1033	0.0016	0.26	0.0625	0.0006	5.80	3.03	638.3	13.7	633.8	9.1	691.9	18.8	92
jl19a130	1.0454	0.0289	0.1206	0.0020	0.30	0.0646	0.0004	5.54	3.27	726.6	14.4	733.8	11.3	762.6	12.3	96
jl19a132	0.8430	0.0321	0.1028	0.0021	0.27	0.0630	0.0005	7.61	4.11	620.8	17.7	630.7	12.3	706.8	18.5	89
jl19a135	0.8767	0.0263	0.1070	0.0015	0.23	0.0650	0.0006	5.99	2.77	639.2	14.2	655.6	8.6	775.1	19.7	85
jl19a136	0.8072	0.0273	0.1003	0.0014	0.20	0.0611	0.0006	6.76	2.73	600.9	15.3	616.1	8.0	642.8	22.7	96
jl19a137	0.7104	0.0223	0.0907	0.0012	0.22	0.0606	0.0005	6.27	2.71	545.0	13.2	559.7	7.3	624.2	18.2	90
jl19a14	0.9283	0.0174	0.1005	0.0011	0.29	0.0647	0.0005	3.74	2.19	666.7	9.1	617.5	6.4	765.9	16.7	81
jl19a140	0.8475	0.0165	0.0964	0.0015	0.39	0.0605	0.0005	3.90	3.05	623.3	9.1	593.1	8.6	622.8	19.0	95
jl19a141	0.8630	0.0165	0.0997	0.0015	0.38	0.0600	0.0005	3.82	2.92	631.7	9.0	612.9	8.5	601.9	17.5	102

Table 3.1. (continued)

jl19a142	0.8223	0.0159	0.0984	0.0014	0.36	0.0601	0.0003	3.86	2.75	609.3	8.9	605.2	7.9	608.1	11.3	100
jl19a144	0.8451	0.0247	0.1059	0.0013	0.20	0.0608	0.0005	5.84	2.39	622.0	13.6	649.1	7.4	633.5	18.2	102
jl19a146	0.8227	0.0777	0.1234	0.0019	0.08	0.0673	0.0013	18.89	3.11	609.6	43.3	750.0	11.0	847.0	41.6	89
jl19a15	0.9135	0.0127	0.1047	0.0013	0.44	0.0615	0.0002	2.77	2.45	658.9	6.7	641.8	7.5	658.3	6.8	97
jl19a16	0.9325	0.0188	0.1084	0.0012	0.26	0.0625	0.0005	4.02	2.13	668.9	9.9	663.4	6.7	690.9	16.4	96
jl19a17	0.9076	0.0232	0.1035	0.0013	0.24	0.0617	0.0005	5.11	2.50	655.8	12.3	635.1	7.6	665.3	17.5	95
jl19a21	0.7860	0.0253	0.0996	0.0013	0.21	0.0604	0.0005	6.44	2.69	588.9	14.4	612.0	7.9	619.3	17.1	99
jl19a23	0.7796	0.0240	0.1001	0.0010	0.17	0.0632	0.0006	6.17	2.09	585.2	13.7	615.1	6.1	714.0	20.7	86
jl19a24	0.8365	0.0217	0.1020	0.0014	0.26	0.0619	0.0006	5.19	2.67	617.2	12.0	626.3	8.0	671.3	20.5	93
jl19a25	0.7150	0.0281	0.0921	0.0011	0.16	0.0644	0.0007	7.87	2.46	547.7	16.7	568.1	6.7	754.9	22.3	75
jl19a26	0.8067	0.0184	0.0985	0.0011	0.25	0.0616	0.0005	4.56	2.30	600.6	10.3	605.7	6.7	659.4	18.2	92
jl19a27	0.9776	0.0201	0.1052	0.0013	0.31	0.0637	0.0006	4.12	2.52	692.3	10.3	644.8	7.7	732.7	18.8	88
jl19a29	7.4092	0.0994	0.3931	0.0047	0.44	0.1335	0.0003	2.68	2.38	2162.1	12.0	2137.0	21.7	2144.2	4.4	100
jl19a32	0.8944	0.0355	0.1021	0.0019	0.24	0.0616	0.0007	7.94	3.80	648.7	19.0	626.9	11.4	660.3	22.6	95
jl19a34	0.7976	0.0207	0.0966	0.0012	0.25	0.0612	0.0004	5.18	2.58	595.5	11.7	594.2	7.3	646.1	14.2	92
jl19a36	0.9004	0.0732	0.1072	0.0018	0.10	0.0659	0.0008	16.25	3.37	652.0	39.1	656.2	10.5	804.4	26.9	82
jl19a37	0.8008	0.0210	0.0981	0.0010	0.19	0.0623	0.0005	5.24	2.04	597.3	11.8	603.3	5.9	684.5	16.6	88
jl19a38	0.8383	0.0133	0.0996	0.0009	0.29	0.0605	0.0004	3.18	1.85	618.2	7.4	612.0	5.4	619.8	13.4	99
jl19a42	0.8007	0.0200	0.0993	0.0011	0.23	0.0594	0.0004	5.00	2.27	597.2	11.3	610.5	6.6	582.6	15.7	105
jl19a43	0.7015	0.0321	0.0912	0.0015	0.17	0.0632	0.0008	9.16	3.19	539.7	19.2	562.7	8.6	714.9	26.8	79
jl19a44	0.8279	0.0176	0.0991	0.0011	0.26	0.0614	0.0004	4.26	2.22	612.5	9.8	609.4	6.5	653.8	14.6	93
jl19a45	0.8055	0.0297	0.0986	0.0013	0.17	0.0616	0.0005	7.37	2.58	599.9	16.7	606.4	7.5	660.5	18.3	92
jl19a46	1.0102	0.0288	0.1068	0.0011	0.18	0.0654	0.0007	5.70	2.08	709.0	14.5	654.4	6.5	786.1	22.4	83
jl19a47	0.7535	0.0226	0.0961	0.0015	0.26	0.0602	0.0004	5.99	3.13	570.3	13.1	591.5	8.9	609.3	16.0	97
jl19a48	0.8177	0.0375	0.1038	0.0017	0.18	0.0625	0.0010	9.17	3.22	606.8	20.9	636.8	9.8	691.0	34.9	92
jl19a51	0.8054	0.0292	0.0983	0.0016	0.22	0.0610	0.0006	7.25	3.21	599.9	16.4	604.4	9.3	639.3	19.5	95
jl19a52	1.0402	0.0444	0.1210	0.0018	0.18	0.0656	0.0007	8.54	3.01	724.0	22.1	736.1	10.5	792.6	21.2	93
jl19a53	0.8901	0.0189	0.0968	0.0012	0.30	0.0629	0.0005	4.24	2.53	646.4	10.1	595.6	7.2	704.9	17.7	84
jl19a54	0.7880	0.0215	0.0955	0.0011	0.22	0.0611	0.0005	5.47	2.38	590.0	12.2	588.1	6.7	642.2	19.2	92
jl19a55	0.8433	0.0169	0.0966	0.0009	0.24	0.0602	0.0005	4.02	1.95	621.0	9.3	594.2	5.5	611.6	17.9	97
jl19a57	0.8066	0.0172	0.0984	0.0010	0.24	0.0612	0.0004	4.27	2.02	600.6	9.7	605.3	5.8	644.8	12.9	94
jl19a58	0.7585	0.0347	0.1000	0.0013	0.14	0.0639	0.0008	9.14	2.64	573.1	20.0	614.5	7.7	737.0	26.3	83
jl19a59	0.8585	0.0178	0.1024	0.0011	0.25	0.0612	0.0005	4.14	2.06	629.3	9.7	628.2	6.2	647.9	16.8	97
jl19a62	0.8190	0.0206	0.1045	0.0010	0.19	0.0620	0.0006	5.02	1.93	607.5	11.5	640.8	5.9	675.2	20.8	95
jl19a64	0.7723	0.0438	0.0974	0.0031	0.28	0.0605	0.0009	11.35	6.41	581.1	25.1	599.0	18.3	621.7	33.4	96
jl19a65	0.7445	0.0196	0.0961	0.0011	0.21	0.0601	0.0004	5.26	2.24	565.0	11.4	591.4	6.3	607.9	15.2	97
jl19a66	0.8367	0.0145	0.0968	0.0011	0.33	0.0599	0.0004	3.47	2.31	617.3	8.0	595.7	6.6	601.0	14.1	99
jl19a67	0.9217	0.0267	0.1008	0.0013	0.22	0.0646	0.0006	5.78	2.54	663.3	14.1	619.0	7.5	762.8	20.5	81
jl19a69	0.8929	0.0162	0.1048	0.0010	0.28	0.0590	0.0004	3.63	2.00	647.9	8.7	642.3	6.1	567.2	16.6	113
jl19a70	0.6918	0.0309	0.0960	0.0019	0.22	0.0597	0.0007	8.94	4.02	533.9	18.6	591.2	11.3	593.7	26.3	100
jl19a72	0.8021	0.0235	0.0985	0.0012	0.22	0.0614	0.0005	5.87	2.53	598.0	13.3	605.7	7.3	653.8	18.1	93
jl19a73	0.9500	0.0271	0.1008	0.0014	0.24	0.0633	0.0008	5.70	2.68	678.1	14.1	618.9	7.9	719.4	26.2	86
jl19a74	0.8415	0.0204	0.1004	0.0013	0.26	0.0628	0.0005	4.84	2.49	620.0	11.2	616.9	7.3	701.9	17.1	88
jl19a75	0.7683	0.1145	0.1187	0.0031	0.09	0.0682	0.0013	29.80	5.14	578.8	65.7	723.2	17.6	874.4	40.0	83
jl19a81	0.6705	0.0342	0.0935	0.0014	0.15	0.0613	0.0008	10.20	3.05	521.0	20.8	576.2	8.4	649.8	27.3	89

Table 3.1. (continued)

jl19a82	0.8660	0.0390	0.1040	0.0016	0.17	0.0631	0.0007	9.00	3.09	633.4	21.2	637.6	9.4	711.9	22.1	90
jl19a83	0.7558	0.0294	0.1061	0.0015	0.18	0.0590	0.0007	7.77	2.85	571.6	17.0	650.2	8.8	568.4	24.3	114
jl19a88	0.8543	0.0300	0.1001	0.0014	0.20	0.0604	0.0007	7.02	2.76	627.0	16.4	615.0	8.1	616.5	24.1	100
jl19a91	0.8655	0.0131	0.0934	0.0014	0.50	0.0622	0.0005	3.03	3.04	633.1	7.1	575.5	8.4	680.5	16.1	85
jl19a92	0.8187	0.0172	0.0984	0.0010	0.24	0.0612	0.0005	4.20	2.05	607.3	9.6	605.1	5.9	647.9	16.5	93
jl19a94	0.8011	0.0259	0.1020	0.0008	0.13	0.0636	0.0006	6.47	1.65	597.5	14.6	626.2	4.9	729.1	19.1	86
jl19a96	0.8938	0.0172	0.1020	0.0012	0.30	0.0611	0.0005	3.84	2.34	648.4	9.2	626.2	7.0	642.8	17.1	97
jl19a97	2.8091	0.0577	0.2307	0.0033	0.34	0.0875	0.0005	4.11	2.83	1358.0	15.4	1338.1	17.1	1370.7	12.0	98

Table 3.1. (continued)

RANDOM FORMATION (321822E, 5386410N)

	CONCORDIA COLUMNS					2 σ %		2 σ %		AGES Ma						
						I N T E R C E P T		V A L U E S								
file	207/235	7/5 err	206/238	6/8 err	Rho	207/206 c	7/6 err	207/206 m	7/6 err	7/5 age	1σ	6/8 age	1σ	7/6 age	1σ	Concordance
jl18b44	0.8159	0.0221	0.1013	0.0013	0.23	0.0584	0.0017	0.0596	0.0004	605.7	12.4	622.0	7.5	588.1	14.5	106
jl18b43	0.8215	0.0233	0.1022	0.0017	0.29	0.0583	0.0019	0.0597	0.0004	608.9	13.0	627.2	9.8	594.4	14.3	106
jl18b46	0.7147	0.0524	0.0881	0.0034	0.26	0.0588	0.0049	0.0577	0.0022	547.5	31.0	544.3	19.9	517.5	85.3	105
jl17A18	0.7943	0.0260	0.0999	0.0018	0.27	0.0577	0.0021	0.0595	0.0005	593.6	14.7	614.0	10.4	583.9	21.8	105
jl18b07	0.8196	0.0198	0.1013	0.0012	0.24	0.0587	0.0016	0.0597	0.0004	607.8	11.1	622.0	7.0	591.9	14.0	105
jl17A71	0.8416	0.0827	0.1024	0.0030	0.15	0.0596	0.0061	0.0599	0.0017	620.0	45.6	628.5	17.4	599.0	64.3	105
jl17A16	0.8022	0.0504	0.0990	0.0021	0.17	0.0588	0.0039	0.0594	0.0010	598.1	28.4	608.4	12.1	581.0	39.4	105
jl18b36	0.7801	0.0269	0.1001	0.0016	0.23	0.0565	0.0021	0.0596	0.0005	585.6	15.4	614.8	9.2	587.5	20.5	105
jl17A48	0.8210	0.0411	0.0998	0.0020	0.20	0.0596	0.0032	0.0596	0.0010	608.6	22.9	613.4	11.4	588.6	37.5	104
jl17A06	0.8012	0.0308	0.1015	0.0014	0.18	0.0572	0.0023	0.0599	0.0006	597.5	17.3	623.4	8.2	599.6	26.7	104
jl17A67	0.7927	0.0418	0.1004	0.0018	0.17	0.0573	0.0032	0.0597	0.0009	592.7	23.7	616.6	10.4	593.8	35.8	104
jl18b26	3.6788	0.0639	0.2884	0.0031	0.31	0.0925	0.0019	0.0975	0.0004	1566.8	13.9	1633.3	15.6	1576.0	7.9	104
jl17A54	0.8552	0.0517	0.1019	0.0019	0.16	0.0609	0.0039	0.0600	0.0011	627.5	28.3	625.4	11.3	603.7	39.0	104
jl17A88	0.8178	0.0246	0.1006	0.0023	0.37	0.0590	0.0022	0.0599	0.0005	606.8	13.8	617.7	13.3	600.1	17.4	103
jl17A52	0.7766	0.0408	0.0979	0.0023	0.23	0.0575	0.0033	0.0595	0.0008	583.6	23.3	602.0	13.7	585.3	30.7	103
jl17A44	0.9136	0.0295	0.1007	0.0015	0.24	0.0658	0.0024	0.0599	0.0007	658.9	15.7	618.4	9.0	601.4	22.6	103
jl17A73	0.8007	0.0297	0.1003	0.0016	0.22	0.0579	0.0023	0.0599	0.0006	597.2	16.7	616.4	9.4	600.3	23.9	103
jl17A31	0.7990	0.0565	0.0985	0.0021	0.15	0.0589	0.0043	0.0596	0.0010	596.3	31.9	605.4	12.1	590.3	41.3	103
jl17A83	0.8365	0.0238	0.0985	0.0016	0.29	0.0616	0.0020	0.0597	0.0005	617.2	13.2	605.4	9.5	591.5	16.2	102
jl17A45	0.8559	0.0187	0.0990	0.0011	0.26	0.0627	0.0015	0.0598	0.0004	627.9	10.2	608.8	6.7	595.6	14.5	102
jl17A30	0.7618	0.0375	0.0968	0.0015	0.16	0.0571	0.0030	0.0594	0.0008	575.0	21.6	595.7	9.1	582.9	31.7	102
jl18b12	0.7774	0.0294	0.1008	0.0015	0.20	0.0559	0.0023	0.0601	0.0005	584.0	16.8	619.1	9.0	605.8	17.6	102
jl17A37	0.8766	0.0271	0.1002	0.0016	0.27	0.0635	0.0022	0.0600	0.0005	639.2	14.7	615.4	9.7	603.7	16.7	102
jl18b22	0.7888	0.0262	0.0990	0.0016	0.24	0.0578	0.0021	0.0599	0.0005	590.5	14.9	608.3	9.4	600.4	20.1	101
jl17A29	0.8419	0.0205	0.0977	0.0012	0.25	0.0625	0.0017	0.0617	0.0004	620.2	11.3	601.0	6.9	664.8	13.5	90
jl17A15	0.7791	0.0345	0.0965	0.0015	0.18	0.0586	0.0028	0.0596	0.0006	585.0	19.7	593.8	9.0	588.7	24.4	101
jl17A19	0.8311	0.0263	0.0949	0.0018	0.31	0.0635	0.0024	0.0623	0.0005	614.2	14.6	584.2	10.8	685.4	19.8	85
jl18b25	0.8319	0.0261	0.1057	0.0017	0.26	0.0571	0.0020	0.0611	0.0003	614.6	14.5	647.5	9.9	642.5	13.0	101
jl17A26	0.8935	0.0275	0.0997	0.0014	0.23	0.0650	0.0022	0.0642	0.0006	648.2	14.7	612.6	8.3	749.4	20.7	82
jl17A10	0.7881	0.0479	0.0977	0.0019	0.16	0.0585	0.0037	0.0599	0.0010	590.1	27.2	600.8	11.1	600.7	41.2	100
jl18b09	0.8584	0.0256	0.1035	0.0015	0.24	0.0601	0.0020	0.0609	0.0005	629.2	14.0	634.9	8.6	636.3	18.5	100
jl17A47	0.8518	0.0199	0.0971	0.0014	0.30	0.0636	0.0017	0.0632	0.0003	625.6	10.9	597.4	8.1	715.2	11.3	84
jl17A35	0.8585	0.0511	0.1004	0.0019	0.16	0.0620	0.0039	0.0604	0.0009	629.3	27.9	616.6	11.0	619.6	33.5	100
jl17A34	0.7887	0.0477	0.0960	0.0020	0.17	0.0596	0.0038	0.0598	0.0008	590.4	27.1	590.8	11.9	596.5	31.5	99
jl18b49	0.8330	0.0169	0.1042	0.0012	0.27	0.0580	0.0013	0.0592	0.0003	615.3	9.4	638.8	6.8	573.7	12.8	111
jl17A74	0.8496	0.0288	0.1028	0.0018	0.26	0.0599	0.0023	0.0610	0.0005	624.4	15.8	630.9	10.5	637.8	16.1	99
jl18b14	0.8142	0.0318	0.1045	0.0010	0.12	0.0565	0.0023	0.0592	0.0007	604.8	17.8	640.6	5.8	575.9	26.0	111
jl17A76	1.0305	0.0437	0.1178	0.0059	0.59	0.0634	0.0042	0.0636	0.0014	719.2	21.9	718.1	34.1	727.8	51.6	99

Table 3.1. (continued)

jl18b15	0.8510	0.0256	0.1009	0.0017	0.29	0.0612	0.0021	0.0607	0.0004	625.2	14.0	619.6	10.2	629.0	12.7	99
jl18b28	0.8217	0.0179	0.1013	0.0013	0.29	0.0588	0.0015	0.0598	0.0003	609.0	10.0	622.3	7.4	596.0	10.8	104
jl17A58	0.8262	0.0257	0.0991	0.0014	0.22	0.0604	0.0021	0.0604	0.0005	611.5	14.3	609.4	8.0	619.6	17.3	98
jl17A81	0.9134	0.0311	0.1028	0.0018	0.26	0.0645	0.0025	0.0631	0.0006	658.9	16.5	630.7	10.7	712.5	19.7	89
jl17A63	0.8143	0.0258	0.0977	0.0015	0.24	0.0605	0.0021	0.0603	0.0005	604.9	14.4	600.6	8.8	613.1	17.5	98
jl18b13	0.8035	0.0314	0.1033	0.0010	0.13	0.0564	0.0023	0.0592	0.0006	598.8	17.7	633.5	5.9	575.5	24.9	110
jl18b05	0.8189	0.0448	0.1026	0.0014	0.12	0.0579	0.0033	0.0611	0.0008	607.4	25.0	629.7	8.1	643.5	30.6	98
jl17A57	0.8313	0.0416	0.0992	0.0020	0.20	0.0608	0.0033	0.0606	0.0010	614.3	23.1	609.8	11.6	625.6	34.7	97
jl17A84	0.7454	0.0281	0.0960	0.0019	0.26	0.0563	0.0024	0.0591	0.0006	565.6	16.4	590.7	11.0	571.5	23.2	103
jl18b45	0.8893	0.0131	0.1045	0.0012	0.40	0.0617	0.0012	0.0616	0.0003	646.0	7.1	640.8	7.2	660.1	10.5	97
jl17A43	0.8841	0.0264	0.0988	0.0019	0.33	0.0649	0.0023	0.0636	0.0005	643.2	14.2	607.5	11.4	729.8	19.4	83
jl17A85	0.8286	0.0283	0.0993	0.0017	0.25	0.0605	0.0023	0.0607	0.0006	612.8	15.7	610.1	10.1	629.7	20.7	97
jl17A17	0.8725	0.0196	0.0985	0.0015	0.33	0.0642	0.0017	0.0606	0.0004	636.9	10.6	605.9	8.5	626.8	12.6	97
jl18b27	0.7772	0.0200	0.1001	0.0014	0.26	0.0563	0.0016	0.0610	0.0003	583.9	11.4	615.1	8.0	639.4	12.3	96
jl18b03	0.7470	0.0133	0.0908	0.0011	0.33	0.0597	0.0013	0.0595	0.0003	566.5	7.7	560.2	6.3	584.3	10.3	96
jl18b33	0.8461	0.0205	0.1035	0.0012	0.25	0.0593	0.0016	0.0617	0.0004	622.5	11.3	634.8	7.2	662.5	13.4	96
jl17A46	0.9651	0.0481	0.1059	0.0020	0.19	0.0661	0.0035	0.0621	0.0007	685.9	24.9	648.8	11.9	678.7	22.2	96
jl17A62	0.7645	0.0463	0.1004	0.0018	0.15	0.0552	0.0035	0.0612	0.0009	576.6	26.6	617.0	10.8	645.4	34.3	96
jl17A38	0.9064	0.0372	0.1069	0.0019	0.22	0.0615	0.0027	0.0623	0.0006	655.1	19.8	654.9	11.0	685.5	23.6	96
jl17A56	0.8610	0.0234	0.1006	0.0015	0.28	0.0621	0.0019	0.0612	0.0006	630.7	12.8	617.7	9.0	647.3	19.3	95
jl18b35	0.8690	0.0227	0.1020	0.0015	0.27	0.0618	0.0018	0.0615	0.0004	635.0	12.3	626.0	8.5	656.3	14.0	95
jl18b06	0.8822	0.0223	0.1025	0.0015	0.29	0.0624	0.0018	0.0616	0.0004	642.2	12.0	628.8	8.9	660.3	13.6	95
jl17A09	0.9059	0.0217	0.1007	0.0015	0.31	0.0652	0.0018	0.0613	0.0004	654.9	11.6	618.5	8.6	650.3	14.8	95
jl17A21	0.9188	0.0227	0.1062	0.0017	0.33	0.0628	0.0019	0.0624	0.0004	661.7	12.0	650.4	10.1	687.9	13.9	95
jl17A70	0.7862	0.0346	0.1006	0.0016	0.18	0.0567	0.0026	0.0618	0.0007	589.0	19.7	617.7	9.1	666.7	27.3	93
jl18b50	0.8475	0.0294	0.0977	0.0019	0.28	0.0629	0.0025	0.0625	0.0007	623.3	16.1	601.1	11.1	691.2	23.1	87
jl17A80	0.7151	0.0249	0.0873	0.0017	0.29	0.0594	0.0024	0.0606	0.0006	547.7	14.7	539.4	10.3	626.3	22.6	86
jl18b21	0.9233	0.0330	0.1044	0.0021	0.28	0.0641	0.0026	0.0641	0.0006	664.1	17.4	640.4	12.3	745.0	19.7	86
jl17A82	0.8661	0.0412	0.1001	0.0021	0.22	0.0628	0.0033	0.0635	0.0009	633.5	22.4	614.8	12.5	724.1	29.9	85
jl17A25	0.9899	0.0377	0.1036	0.0021	0.27	0.0693	0.0030	0.0644	0.0007	698.6	19.2	635.5	12.4	753.8	21.5	84
jl17A05	0.9489	0.0282	0.1000	0.0015	0.25	0.0688	0.0023	0.0638	0.0005	677.5	14.7	614.4	8.9	734.3	17.3	84
jl17A65	0.8984	0.0261	0.0998	0.0018	0.32	0.0653	0.0022	0.0639	0.0006	650.9	13.9	613.1	10.8	738.1	18.6	83
jl18b08	0.9430	0.0351	0.1035	0.0017	0.22	0.0661	0.0027	0.0652	0.0008	674.4	18.4	635.0	9.9	780.9	26.1	81
jl17A64	0.8416	0.0189	0.0957	0.0016	0.36	0.0638	0.0018	0.0635	0.0003	620.0	10.4	589.3	9.2	725.4	11.6	81
jl17A55	0.9075	0.0216	0.1024	0.0013	0.28	0.0643	0.0018	0.0651	0.0005	655.8	11.5	628.4	7.9	776.5	16.8	81
jl17A49	0.9205	0.0289	0.0981	0.0021	0.33	0.0681	0.0026	0.0641	0.0006	662.6	15.3	603.0	12.1	746.4	20.3	81
jl17A53	0.9014	0.0320	0.1002	0.0017	0.23	0.0652	0.0026	0.0647	0.0007	652.5	17.1	615.8	9.8	765.6	21.3	80
jl17A75	0.8924	0.0193	0.0999	0.0013	0.30	0.0648	0.0016	0.0649	0.0004	647.6	10.3	614.0	7.5	771.8	12.6	80
jl18b34	0.9708	0.0151	0.1039	0.0008	0.26	0.0678	0.0012	0.0676	0.0003	688.9	7.8	637.1	5.0	855.4	9.4	74
jl17A12	0.8199	0.0320	0.0894	0.0021	0.30	0.0665	0.0030	0.0642	0.0005	608.0	17.9	552.2	12.6	746.6	17.4	74
jl18b37	0.9283	0.0217	0.0993	0.0015	0.32	0.0678	0.0019	0.0676	0.0005	666.8	11.4	610.2	8.7	854.8	15.5	71

Table 3.1. (continued)

REDMANS FORMATION (365459E, 5379562N)

	CONCORDIA COLUMNS					2 σ %	2 σ %		2 σ %	AGES Ma						
					INTERCEPT VALUES											
file	**207/235**	**7/5 err**	**206/238**	**6/8 err**	**Rho**	**207/235**	**206/238**	**207/206 m**	**7/6 err**	**7/5 age**	**1σ**	**6/8 age**	**1σ**	**7/6 age**	**1σ**	**Concordance**
jl26A148	4.2402	0.2173	0.2447	0.0033	0.13	10.25	2.73	0.1248	0.0021	1681.8	42.1	1411.3	17.3	2026.0	29.9	70
jl26A135	4.3303	0.5317	0.2489	0.0055	0.09	24.55	4.41	0.1151	0.0033	1699.2	101.3	1432.9	28.3	1880.7	51.9	76
jl26A036	4.7078	0.1703	0.2693	0.0041	0.21	7.24	3.06	0.1240	0.0012	1768.6	30.3	1537.5	21.0	2013.9	17.1	76
jl26A141	5.2635	1.6991	0.2880	0.0863	0.46	64.56	59.97	0.1291	0.0019	1863.0	275.4	1631.3	432.1	2085.6	25.6	78
jl26A097	13.4589	1.0983	0.4520	0.0286	0.39	16.32	12.64	0.2130	0.0024	2712.4	77.1	2404.2	126.8	2928.3	18.2	82
jl26A079	0.8755	0.0875	0.0918	0.0015	0.08	19.99	3.20	0.0702	0.0020	638.6	47.4	566.3	8.7	935.1	59.6	61
jl26A041	8.9828	0.1820	0.3829	0.0050	0.32	4.05	2.60	0.1648	0.0012	2336.3	18.5	2089.7	23.2	2505.6	12.0	83
jl26A158	0.9234	0.0652	0.0971	0.0044	0.32	14.12	9.08	0.0687	0.0009	664.2	34.4	597.6	25.9	890.1	27.5	67
jl26A024	1.3046	0.2329	0.1257	0.0110	0.24	35.70	17.47	0.0792	0.0011	847.8	102.6	763.2	62.9	1176.7	28.1	65
jl26A152	1.0719	0.0318	0.1093	0.0028	0.44	5.93	5.19	0.0709	0.0007	739.7	15.6	668.7	16.5	955.2	21.0	70
jl26A156	1.0475	0.0750	0.1077	0.0086	0.56	14.31	16.05	0.0698	0.0020	727.7	37.2	659.1	50.3	922.9	58.8	71
jl26A157	9.6241	0.7422	0.4021	0.0279	0.45	15.42	13.90	0.1700	0.0062	2399.5	70.9	2178.8	128.5	2557.2	60.9	85
jl26A139	4.3917	0.2301	0.2742	0.0139	0.48	10.48	10.12	0.1108	0.0006	1710.8	43.3	1562.2	70.2	1812.0	9.9	86
jl26A037	6.9317	0.1795	0.3489	0.0092	0.51	5.18	5.26	0.1411	0.0008	2102.7	23.0	1929.5	43.8	2241.2	9.6	86
jl26A089	1.0890	0.1229	0.1127	0.0100	0.39	22.57	17.74	0.0687	0.0029	748.0	59.7	688.3	57.9	890.6	87.3	77
jl26A076	3.5686	0.2391	0.2480	0.0182	0.55	13.40	14.65	0.1043	0.0037	1542.6	53.1	1428.2	93.8	1702.3	64.6	84
jl26A003	0.9616	0.0676	0.1034	0.0036	0.25	14.06	7.05	0.0648	0.0011	684.1	35.0	634.1	21.3	766.3	37.2	83
jl26A116	2.2165	0.0969	0.1860	0.0048	0.29	8.74	5.14	0.0869	0.0007	1186.3	30.6	1099.8	26.0	1359.3	14.8	81
jl26A017	3.5965	0.1116	0.2539	0.0066	0.42	6.20	5.20	0.0999	0.0003	1548.8	24.6	1458.7	33.9	1622.5	5.4	90
jl26A137	0.8315	0.0755	0.0940	0.0066	0.38	18.15	13.96	0.0643	0.0018	614.5	41.8	579.1	38.7	751.1	58.1	77
jl26A168	4.7042	0.1640	0.2987	0.0090	0.43	6.97	6.00	0.1139	0.0005	1768.0	29.2	1685.0	44.5	1862.2	8.7	90
jl26A109	0.8857	0.0372	0.1000	0.0021	0.24	8.41	4.12	0.0602	0.0007	644.0	20.1	614.1	12.1	610.9	24.3	101
jl26A031	6.3093	0.1897	0.3488	0.0084	0.40	6.01	4.82	0.1303	0.0005	2019.8	26.3	1928.8	40.2	2101.9	6.3	92
jl26A077	7.7516	0.2076	0.3868	0.0055	0.26	5.36	2.82	0.1368	0.0014	2202.6	24.1	2108.2	25.4	2186.7	16.7	96
jl26A004	0.9798	0.0873	0.1089	0.0031	0.16	17.82	5.66	0.0620	0.0016	693.5	44.8	666.5	17.9	673.5	53.1	99
jl26A092	0.8891	0.0215	0.1011	0.0018	0.38	4.85	3.65	0.0613	0.0004	645.9	11.6	620.7	10.8	648.0	14.3	96
jl26A066	0.7949	0.0194	0.0928	0.0014	0.30	4.89	2.92	0.0631	0.0005	594.0	11.0	572.1	8.0	711.8	16.0	80
jl26A118	0.7831	0.0247	0.0917	0.0017	0.29	6.32	3.70	0.0594	0.0005	587.2	14.1	565.7	10.0	580.7	16.4	97
jl26A102	6.0112	0.1104	0.3450	0.0056	0.44	3.67	3.25	0.1261	0.0004	1977.5	16.0	1910.9	26.9	2043.7	5.2	94
jl26A115	0.9180	0.0545	0.1045	0.0028	0.22	11.87	5.33	0.0612	0.0009	661.3	28.9	640.6	16.3	645.7	30.1	99
jl26A099	13.8057	0.1769	0.5098	0.0071	0.54	2.56	2.79	0.1947	0.0004	2736.5	12.1	2655.7	30.3	2782.2	3.4	95
jl26A043	0.9912	0.0481	0.1112	0.0031	0.29	9.71	5.64	0.0646	0.0006	699.3	24.5	679.4	18.2	762.0	20.4	89
jl26A126	0.9976	0.0284	0.1117	0.0018	0.28	5.70	3.15	0.0618	0.0005	702.6	14.5	682.8	10.2	666.6	16.0	102
jl26A068	7.8403	0.1829	0.3968	0.0111	0.60	4.67	5.62	0.1427	0.0008	2212.8	21.0	2154.2	51.4	2260.6	10.2	95
jl26A107	0.9368	0.0914	0.1069	0.0045	0.21	19.51	8.36	0.0610	0.0017	671.2	47.9	654.6	26.0	637.9	55.3	103
jl26A136	2.2497	0.0690	0.1987	0.0047	0.38	6.14	4.70	0.0789	0.0005	1196.7	21.6	1168.5	25.1	1170.9	11.4	100
jl26A065	0.7437	0.0407	0.0894	0.0020	0.20	10.94	4.46	0.0593	0.0010	564.6	23.7	552.1	11.8	577.0	35.1	96
jl26A132	2.9513	0.0555	0.2368	0.0042	0.47	3.76	3.57	0.0892	0.0003	1395.2	14.3	1370.2	22.0	1408.6	7.5	97

Table 3.1. (continued)

jl26A172	0.7428	0.0291	0.0902	0.0021	0.29	7.84	4.58	0.0595	0.0006	564.0	17.0	556.7	12.2	586.1	19.9	95
jl26A086	0.8820	0.0170	0.1033	0.0018	0.45	3.86	3.49	0.0617	0.0004	642.1	9.2	633.9	10.5	662.0	14.3	96
jl26A014	0.9545	0.1213	0.1099	0.0068	0.24	25.41	12.37	0.0616	0.0034	680.5	63.0	672.0	39.5	660.9	117.7	102
jl26A046	0.7012	0.0180	0.0863	0.0011	0.26	5.15	2.66	0.0587	0.0004	539.5	10.8	533.5	6.8	556.3	14.8	96
jl26A155	0.9367	0.0297	0.1088	0.0024	0.35	6.35	4.45	0.0627	0.0006	671.2	15.6	665.9	14.1	698.1	21.2	95
jl26A122	2.3171	0.0482	0.2064	0.0033	0.38	4.16	3.18	0.0806	0.0004	1217.5	14.8	1209.8	17.5	1211.2	9.8	100
jl26A100	8.0273	0.0822	0.4118	0.0047	0.56	2.05	2.29	0.1406	0.0004	2234.1	9.2	2223.0	21.5	2234.2	4.3	100
jl26A075	0.7782	0.0231	0.0946	0.0016	0.29	5.94	3.47	0.0591	0.0005	584.4	13.2	582.8	9.7	570.5	18.3	102
jl26A166	3.3537	0.0563	0.2602	0.0045	0.52	3.36	3.48	0.0924	0.0003	1493.7	13.1	1491.0	23.1	1474.7	5.6	101
jl26A111	1.6124	0.0402	0.1632	0.0022	0.27	4.99	2.65	0.0706	0.0005	975.0	15.6	974.6	12.0	945.5	13.6	103
jl26A138	2.6846	0.0597	0.2279	0.0033	0.33	4.45	2.94	0.0842	0.0004	1324.2	16.4	1323.7	17.6	1297.5	9.6	102
jl26A167	6.4697	0.1577	0.3729	0.0049	0.27	4.88	2.65	0.1265	0.0008	2041.8	21.4	2042.9	23.2	2049.9	11.2	100
jl26A151	3.8037	0.2516	0.2806	0.0135	0.36	13.23	9.63	0.1002	0.0015	1593.5	53.2	1594.5	68.0	1628.6	27.7	98
jl26A146	7.7160	0.1030	0.4068	0.0053	0.48	2.67	2.59	0.1367	0.0004	2198.5	12.0	2200.3	24.1	2185.5	4.7	101
jl26A121	0.7814	0.0285	0.0953	0.0019	0.27	7.30	3.92	0.0602	0.0007	586.3	16.3	587.1	11.0	610.9	24.3	96
jl26A140	4.1778	0.0423	0.2961	0.0030	0.50	2.02	2.04	0.1006	0.0002	1669.7	8.3	1672.1	15.0	1634.6	4.1	102
jl26A145	3.6043	0.0591	0.2725	0.0043	0.48	3.28	3.17	0.0951	0.0003	1550.5	13.0	1553.6	21.9	1530.9	5.6	101
jl26A130	0.8667	0.0241	0.1038	0.0016	0.28	5.56	3.09	0.0600	0.0004	633.8	13.1	636.6	9.4	603.9	15.9	105
jl26A080	7.2498	0.0750	0.3969	0.0039	0.47	2.07	1.94	0.1319	0.0004	2142.7	9.2	2154.7	17.8	2123.7	5.1	101
jl26A161	1.7974	0.0393	0.1774	0.0026	0.34	4.37	2.95	0.0732	0.0004	1044.5	14.2	1052.8	14.3	1019.8	10.8	103
jl26A147	1.7922	0.0393	0.1772	0.0031	0.40	4.39	3.55	0.0730	0.0004	1042.6	14.3	1051.7	17.2	1015.2	10.7	104
jl26A030	1.7531	0.1308	0.1749	0.0057	0.22	14.92	6.57	0.0748	0.0019	1028.3	48.2	1039.0	31.5	1061.8	52.8	98
jl26A085	2.4854	0.0393	0.2199	0.0028	0.40	3.16	2.52	0.0810	0.0004	1267.8	11.4	1281.2	14.6	1220.8	9.8	105
jl26A159	7.2611	0.1129	0.4012	0.0056	0.45	3.11	2.77	0.1302	0.0004	2144.0	13.9	2174.4	25.6	2100.8	5.8	104
jl26A069	0.8145	0.0266	0.1002	0.0016	0.24	6.54	3.10	0.0602	0.0007	605.0	14.9	615.5	9.1	610.9	24.3	101
jl26A071	0.8268	0.0290	0.1023	0.0020	0.27	7.02	3.83	0.0583	0.0004	611.9	16.1	628.0	11.4	541.8	15.4	116
jl26A129	0.9028	0.0248	0.1098	0.0016	0.26	5.50	2.85	0.0593	0.0004	653.2	13.2	671.9	9.1	578.1	15.2	116
jl26A169	1.0879	0.0384	0.1269	0.0027	0.31	7.06	4.32	0.0609	0.0009	747.5	18.7	770.0	15.7	636.1	33.0	121
jl26A008	0.6247	0.0360	0.0823	0.0030	0.31	11.52	7.17	0.0544	0.0008	492.8	22.5	509.6	17.6	388.3	32.8	131
jl26A105	0.8047	0.0279	0.1012	0.0019	0.28	6.93	3.84	0.0597	0.0005	599.5	15.7	621.3	11.4	592.5	18.2	105
jl26A091	0.7523	0.0215	0.0960	0.0016	0.28	5.70	3.25	0.0565	0.0004	569.6	12.4	590.6	9.2	470.8	13.8	125
jl26A150	0.7453	0.0238	0.0957	0.0016	0.26	6.39	3.29	0.0572	0.0005	565.5	13.9	589.3	9.3	499.5	20.9	118
jl26A020	0.8072	0.0413	0.1020	0.0020	0.19	10.24	3.95	0.0600	0.0004	600.9	23.2	626.2	11.8	603.9	15.9	104
jl26A067	2.1455	0.0509	0.2078	0.0031	0.31	4.74	2.96	0.0754	0.0004	1163.6	16.4	1217.3	16.4	1078.8	11.2	113
jl26A117	0.7894	0.0196	0.1006	0.0015	0.29	4.97	2.88	0.0575	0.0003	590.8	11.1	618.1	8.5	511.5	12.6	121
jl26A087	0.7762	0.0202	0.1002	0.0012	0.24	5.20	2.46	0.0576	0.0003	583.3	11.5	615.5	7.2	515.5	12.6	119
jl26A029	0.8431	0.0710	0.1075	0.0022	0.12	16.84	4.11	0.0607	0.0006	620.9	39.1	658.1	12.9	629.3	19.9	105
jl26A127	0.5734	0.5769	0.1054	0.0050	0.02	201.23	9.47	0.0593	0.0077	460.2	372.3	646.0	29.1	576.6	281.1	112

FUTURE RESEARCH

This dissertation presents the results of an integrated geochronological, geochemical and radiogenic isotopic study of the Neoproterozoic-early Paleozoic rocks from North Carolinia and Newfoundland. I conclude with a summary of some of the problems that remain unresolved and possible suggestions for future work in the peri-Gondwanan crustal blocks of Carolinia and Avalonia:

1. What is the relationship of the Redmans Formation to other Ordovician quartzite units elsewhere in Avalonia and Cadomia? Specifically, the Stiperstone quartzite in England and the Armorican quartzite in Iberia. Do each of these units record subsidence associated with formation of the Rheic Ocean? Do they each have similar detrital zircon age spectra and source cratons?
2. What is the source of the Gaskiers Formation? The adjoining units analyzed in this study contain only locally-derived detritus from the underlying volcanic-plutonic sequences. The glacially-influenced diamictite sequences of the Gaskiers Formation contain a variety of dropstones and striated and faceted clasts that attest to a glacial origin and are interpreted to possibly be related to a Neoproterozoic “Snowball Earth.” Does the detrital zircon signature of the Gaskiers Formation reflect this exotic provenance for the unit?
3. What is the age of the Aaron Formation? Detrital zircon data indicate a ca. 30 m.y. hiatus between eruption of the Hyco Formation and deposition of the Aaron Formation, what is the nature of the relationship between these units? What is the source of the quartzitic clasts in the Aaron Formation?
4. Are the units of the Albemarle Group a continuous stratigraphic sequence? The minimum ages of some units of the Albemarle Group are still unconstrained. Careful stratigraphic studies of the group should be directed at solving this problem.

5. Interpretation of the nature of the mantle source of the Stony Mountain gabbro is limited by using a single (Sm-Nd) isotope system. Are the N-MORB-OIB mixed signatures reflected in other radiogenic isotopes (e.g. Pb and Rb-Sr)?
6. What is the precise age of the Stony Mountain gabbro and thus, timing of rifting of Carolinia?
7. What is the nature of the basement to the Albemarle sequence? Previous workers have suggested the presence of a Mesoproterozoic basement to Carolinia (e.g., Mueller *et al*., 1996) yet the Nd isotope data provide strong evidence against an isotopically evolved continental basement.

- Endispiece -

View looking east from Signal Hill of Fort Amherst and Cape Spear, the most easterly point in North America.

"WE'RE ONLY IMMORTAL - FOR A LIMITED TIME"

-Neil Peart-